Impact of viral vectors on vaccine design: IL-13Rα2 in DC regulation

Sreeja Roy

A thesis submitted for the degree of Doctor of Philosophy

The Australian National University

December 2019

Australian National University

The Molecular Mucosal Vaccine Immunology Group,
The John Curtin School of Medical Research,
The Australian National University
Canberra, Australia

Statement

I declare that all data presented in this thesis were obtained from my own experiments, unless otherwise mentioned in respective publications, under the supervision of A/Prof. Charani Ranasinghe. I certify that this work contains no material which has been accepted for the award for any other degree or diploma in any university.

Sreeja Roy

Sreeja Roy

Acknowledgements

Firstly, I want to wholeheartedly thank my family, especially my **parents** for being the wind beneath my wings and for their constant financial and emotional support whenever I was in dire need of it.

Secondly, I want to extend my immense gratitude towards my supervisor **Assoc. Prof. Charani Ranasinghe** for all her valuable input and advice for my experiments, journal articles and thesis writing, as well as her life lessons which, I believe has equipped me for my future endeavors. I also want to thank my co-supervisors **Prof. Anthony Kelleher and Dr. MeeLing Munier (UNSW)** for all their feedback and insight into my understanding of cytokine signalling.

I want to thank all the Ranasinghe group members I have known or worked with, past and present, each of whom have individually contributed towards my work. Especially, **Dr. Zheyi Li (Jerry), Mr. Irwan Jaeson and Ms Shaaerah Mahboob** for their important contributions to parts of this thesis. A special thanks to Jerry for being there like a big brother whenever I needed help. **Dr. Mayank Khanna** for being my partner in crime, **Mr. Lachlan Deimel (Lachie)**, for always being there as a friend and all the support I have received, **Ho-Ying Liu (Sally)** for performing some of the *in vitro* experiments. I want to thank **Dr. Shubhanshi Trivedi** for her help with Fluidigm experiments and **Dr. Danushka Wijesundara** for his insightful advice. Finally, all my friends and colleagues in the John Curtin School, especially Ms. Yoshika Janabala, Dr. Sofia Omari and Dr. Racheal Aye for all the hugs and support.

A big thank you to **The Imaging and Cytometry Facility,** ACRF Biomolecular Resource Facility, especially, Mr. Michael Devoy for all his help on single cell sorting, Dr. Peter Milburn for providing support for qPCR and Fluidigm experiments and Ms. Cathy Gillespie for training me in Confocal microscopy and being there when dendritic cells were being tricky to handle.

Lastly, I want to thank the **Australian Phenomics Facility** for providing the mice for all my experiments, especially Mr. Anthony Barker who has relentlessly worked with me to keep fueling my experimental requirements. Lastly, I want to extend my deepest gratitude to all those mice who gave their precious lives for my research.

Publications relevant to thesis

1. **Roy, S.,** Liu, HY., Jaeson, M.I., Deimel, L.P., and Ranasinghe, C. Unique IL-13Rα2/STAT3 mediated IL-13 regulation detected in lung conventional dendritic cells, 24 h post viral vector vaccination. *Scientific Reports* 2020.

   This work is presented in Chapter 4

2. **Roy, S.,** Jaeson, M.I., Li, Z., Mahboob, S., Jackson, R.J., Grubor-Bauk, B., Wijesundara, D.K., Gowans E.J., and Ranasinghe, C. Viral vector and route of administration determine the ILC and DC profiles responsible for downstream vaccine-specific immune outcomes. *Vaccine* 2019.

   This work is presented in Chapter 3

3. **Roy, S.,** Li, Z., and Ranasinghe C. Differential IL-13 receptor regulation on lung dendritic cells likely governs the unique poxviral vector-specific immune outcomes. *(2019, submitted).*

   This work is presented in Chapter 5

Other publications

1. Ranasinghe, C.**, Roy, S**., Li, Z., Khanna, M., and Jackson, R.J. IL-4 and IL-13 receptors. Published In: Encyclopedia of Signaling Molecules, 2nd Edition. Springer publication, edited by Sangdun Choi (2018) (Invited book chapter) https://doi.org/10.1007/978-3-319-67199-4.

2. Hamid, M.A.*, Jackson, J.R.*, **Roy, S***, Khanna, M., and Ranasinghe, C. Unexpected Involvement of IL-13 Signalling via a STAT6 Independent Mechanism, During IgG2a Development Following Viral Vaccination. *Eur J Immunol.* 2018

   * Authors contributed equally to the work.

3. Jaeson, M.I., **Roy, S.,** Mahboob, S., Li, Z., and Ranasinghe, C. Novel regulation mechanisms of type 2 innate lymphoid cells following mucosal versus systemic viral vector vaccination: Role of STAT3, STAT6, TGF-b1 and IFN-γR. *(Manuscript in preparation).*

Conference presentations

1. **Roy, S**., Jaeson, M.I., Mahboob, S., and Jackson, R.J. ILC and DC profiles at the lung mucosae influence vaccine specific immune outcomes 24 h post vaccination.

   International Congress of Mucosal Immunology (2019). (Oral presentation).

2. **Roy, S**., Li, Z., Jackson, R.J., Mahboob, S., Wijesundara, D.K., Gowans, E., and Ranasinghe, C. IL-13Rα2 is crucial for DC subset activation following viral vector vaccination.

   Australian Society for HIV, Viral Hepatitis and Sexual Health Medicine. (Oral presentation).

3. **Roy, S**., Jaeson, M.I., Mahboob, S., and Ranasinghe, C. IL-13Rα2 is crucial for differential DC subset activation following viral vector vaccination.

   Canberra Health Annual Research Meeting. (Oral presentation).

Abstract

Studies in our laboratory have established that the route of vaccination, viral vector and the cytokine milieu, specifically IL-13 can critically impact the vaccine-specific adaptive immune outcomes. Recent efforts in understanding which cells at the vaccination site produced IL-13 revealed that innate lymphoid cells (ILC)2 were the major source of this cytokine at the vaccination site 24h post delivery. Knowing that manipulating IL-13 levels at the vaccination site also significantly altered resident lung dendritic cell (DC) recruitment, this study focused on dissecting the underlying mechanisms by which ILCs and DCs regulated vaccine-specific immunity at the lung mucosae following intranasal vaccination.

Poxviral and non-poxviral vaccine vectors induced uniquely different ILC-derived cytokine and DC profiles at the lung mucosae, 24 h post vaccination. For example, rFPV priming known to induce high avidity T cells, exhibited low ILC2-derived IL-13, high ILC1/ILC3-derived IFN-γ and enhanced recruitment of CD11b^{+} CD103^{-} conventional DCs (cDC). Whereas, rMVA, rVV and Influenza A vector priming, linked to low avidity T cells, induced opposing ILC-derived cytokine profiles, together with enhanced CD11b^{-} CD103^{+} cross-presenting DCs and reduced cDCs. Interestingly, Rhinovirus (RV) and Adenovius type 5 (Ad5) vectors, also showed different ILC-derived cytokine profiles and predominant recruitment of CD11b^{-} B220^{+} plasmacytoid DCs (pDC). Knowing that cDCs are associated with high avidity CD8 T cell priming and pDCs are involved in antibody differentiation, these findings showed that vaccine derived early ILC/DC profiles directly impact the downstream adaptive immune outcomes.

When trying to unravel how IL-13 signalling modulated these vaccine-specific adaptive immune outcomes, unlike IL-13Rα1, IL-13Rα2 was found to be the major sensor and regulator of early IL-13 mediated DC activity. For the first time a dual role of IL-13Rα2 was unraveled on lung cDC, where low IL-13 was associated with IL-13Rα2 signalling via STAT3 activating TGF-β1, whilst, high IL-13 triggered sequestration by the same receptor. Interestingly, in this study differential IL-13 receptor mediated STAT3/STAT6 paradigms were observed, regulated collaboratively or independently by TGF-β1 and IFN-γ. Low IL-13 driven early IL-13Rα2/STAT3 responses were regulated primarily by TGF-β1, whereas, high IL-13 driven IL-13Rα1/STAT6 responses were associated with IFN-γR expression bias. Moreover, inherent properties of viral vaccine vectors (host tropism, replication status and presence or absence of immunomodulatory genes), were also found to significantly alter the IL-4/IL-13 receptor regulation on lung DCs, in a time dependent manner. Specifically, the generation of a balanced adaptive immune outcome was associated with early regulation of IL-13Rα2, succeeded by IL-13Rα1/ IL-4Rα on lung DCs, as observed with rFPV vaccination unlike the other poxviral vectors tested.

Collectively, findings of this thesis for the first time demonstrated the importance of understanding the mechanisms of IL-13 mediated DC regulation, at the vaccination site. Therefore, knowing these innate mechanisms associated with ILC/DC regulation may help design more efficacious vaccines and therapeutics against IL-13 related disease conditions.

Abbreviations

HIV	Human immunodeficiency virus
DC	Dendritic cell
PAMPs	Pathogen associated molecular patterns
PRRs	Pattern recognition receptors
TLRs	Toll-like receptors
NLRs	NOD-like receptors
MALT	Mucosa-associated lymphoid tissue
NALT	Nasal-associated lymphoid tissue
BALT	Bronchus-associated lymphoid tissue
GALT	Gut-associated lymphoid tissue
HEV	High endothelial venules
ILC	Innate lymphoid cell
Ig	Immunoglobulin
NK	Natural killer
APC	Antigen presenting cell
Batf3	Basic Leucine Zipper ATF-Like Transcription Factor 3
ID2	Inhibitor of DNA binding 2
IRF8	Interferon regulatory factor 8
cDC	Conventional dendritic cell
pDC	Plasmacytoid dendritic cell
moDC	Monocyte-derived dendritic cell
MHC	Major histocompatibility complex
MAdCAM-1	mucosal addressin cell adhesion molecule-1
VCAM-1	Vascular cell adhesion protein-1

HSV	Herpes simplex virus
RSV	Respiratory Syncytial Virus
i.n.	Intranasal
i.m.	Intramuscular
i.p.	Intraperitoneal
IL	Interleukin
IL-1βR	Interleukin-1 beta receptor
IFN	Interferon
ADCC	Antibody dependent cellular cytotoxicity
VEGF	Vascular endothelial growth factor
IRAK	Interleukin-1 receptor associated kinase
TNF	Tumor necrosis factor
TRAF	Tumor necrosis factor receptor associated factor 6
NFκB	Nuclear factor kappa-light-chain-enhancer of activated B cells
IBD	Inflammatory bowel disease
rFPV	Recombinant fowlpox virus
rMVA	Recombinant modified vaccinia ankara
VACV	Vaccinia virus
rVV	Recombinant vaccinia virus
NYVAC	Copenhagen derived New York vaccinia virus
CVA	Chorioallantoic vaccinia ankara
rRV	Recombinant human rhinovirus
rAd5	Recombinant Adenovirus 5
rTV	Recombinant tiantan vaccinia virus
JAK	Janus kinase

STAT	Signal transducer and activator of transcription
TSLPR	Thymic stromal lymphopoietin protein receptor
IL-18bp	Interleukin 18 binding protein
TYK	Tyrosine kinase
AP-1	Activation protein-1

Table of contents

Chapter 1

General Introduction

1.1 The immune system

The immune system is mainly comprised of two compartments, the innate and the adaptive systems. The innate immune system contains physical, chemical barriers, and immune cells which serve as the first line of defence against invading pathogens. Skin and mucous membranes are strategically placed externally on the body to prevent entry of pathogens or toxins [1], whereas mucus, digestive enzymes, antimicrobial peptides and complement proteins have the ability to prevent microbes from establishing infection [2]. Whilst innate immune system initiates non-pathogen-specific defence, the adaptive immune system (comprising of specialized cells such as lymphocytes), initiates pathogen-specific or antigen-specific memory T and B cell immunity.

1.2 Innate immune cells

Cells of the innate immune system can be of both haematopoietic as well as non-haematopoietic origin. Haematopoietic cells include mast cells, macrophages, neutrophils, eosinophils, natural killer (NK) cells, NKT cells, innate lymphoid cells (ILCs) and dendritic cells (DCs). Non-haematopoietic immune cells comprise of epithelial cells on various tissues like the skin and the gastrointestinal tract [3]. Innate immune cells use germline-encoded broadly specific pattern recognition receptors (PRRs) such as Toll-like receptors (TLRs) and NOD-Like receptors (NLRs) to recognize conserved and invariant surface molecules called pathogen associated molecular patterns (PAMPs) on pathogens [4-6], and activation of these cells can induce various inflammatory immune responses. Cells such as macrophages, neutrophils and DCs can employ phagocytosis by which pathogen-derived particles are engulfed by phagocytes to cause degradation and antigen processing and subsequent presentation to T and B lymphocytes [7]. Other

cells such as NK cells can also employ cytotoxic lytic granules to kill recognized pathogens or infected target cells [8]. Most PRR activated innate immune cells also lead to secretion of pro-inflammatory cytokines/ chemokines and antimicrobial proteins to orchestrate the local and systemic inflammatory responses such as recruitment of macrophages to secrete antimicrobial proteins and peptides or activate complement factors for opsonization of the pathogen [5]. These innate immune responses perform as the first line of defence and also subsequent activation of the adaptive immune system.

1.3 Mucosal immune system

The mucosal immune system is comprised of sensory organs (eyes, nose, mouth and throat), lungs, gastrointestinal tract, genito-rectal tract **(Figure 1.1)** and is the first line of defence against pathogens. The mucosal immune system can employ both physical barriers and specialized immune responses to combat infection. Mucous produced by mucosal epithelial cells forms a protective layer, whilst epithelial cilia use beating movement to prevent pathogen infection [9,10]. Chemical agents such as defensins and antimicrobial peptides are also secreted by the mucosal epithelium to degrade pathogenic particles [9,11,12]. Interestingly, according to the site of pathogen encounter the immunity generated at the local and distal mucosal compartments can be vastly different (eg. nasal vs oral or rectal) [13].

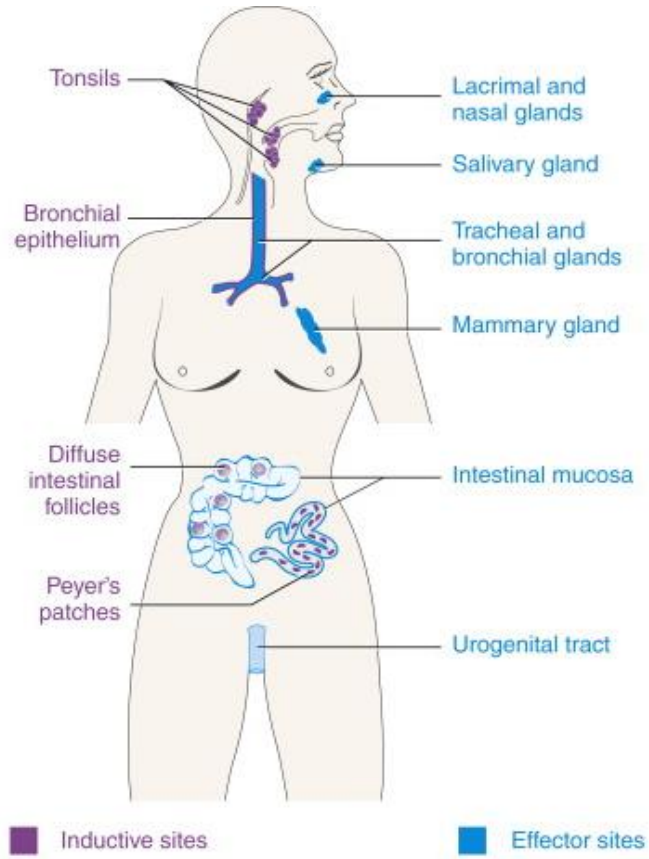

Figure 1.1. The common mucosal immune system. The common mucosal immune system is distributed across several organs including eyes, nose, mouth, lungs, gut and the uro-genital tract. This system is comprised of epithelial cells, commensal microbes as well the innate and adaptive immune cells which are further divided into inductive and effector sites. In the inductive sites, antigens are encountered by antigen presenting cells like DCs, which process and present antigens to naïve lymphocytes. Whilst, immune responses mediated by activated and mature lymphocytes migrate to effector sites to combat infection. *(Mak, Saunders and Jett. Primer to the immune response. 2nd edition. 2014).*

The mucosal immune system is perceived as a holistic global organ called the common mucosal immune system containing a complex network of epithelial cells, innate and adaptive immune cells including an extensive microbiota. The mucosa-associated lymphoid tissue (MALT) is mainly comprised of the nasal-associated lymphoid tissue (NALT), bronchus-associated lymphoid tissue (BALT), gut-associated lymphoid tissue (GALT), and the uro-genital-associated lymphoid tissue [9,14]. Functionally, MALT is divided into inductive sites, comprising of naïve lymphocytes and antigen presenting cells and effector sites, which consists of activated T and B cells. Principally the inductive sites, such as Peyer's patches in the gut, are fortified by specialised epithelial cells called microfold (M) cells, unique to mucosal surfaces. M cells have a unique ability to uptake and transport pathogen-derived antigens from the apical surface to the basolateral surface of the epithelium causing antigen uptake by antigen presenting cells (APCs), specifically DCs **(Figure 1.2)**, which then present antigen to naïve lymphocytes at the inductive sites. Activated DCs can also migrate to draining lymph nodes, initiate activation and migration of lymphocytes to effector sites (such as lamina propria in the gut) via lymph vessels to initiate pathogen clearance **(Figure 1.2)** [15-17].

In the context of lungs, antigenic exposure triggers tertiary lymphoid tissue organized into inducible bronchus-associated lymohid tissue (iBALT) **(Figure 1.3).** iBALT is commonly formed in the lower airway lung parenchyma, specifically areas underlying the bronchial epithelium [18,19]. Similar to conventional secondary lymphoid structures, iBALT is also compartmentalized into distinct B and T cell follicles where lymphocyte differentiation and maturation occur [20]. However, interestingly, unlike in rats, iBALT areas in

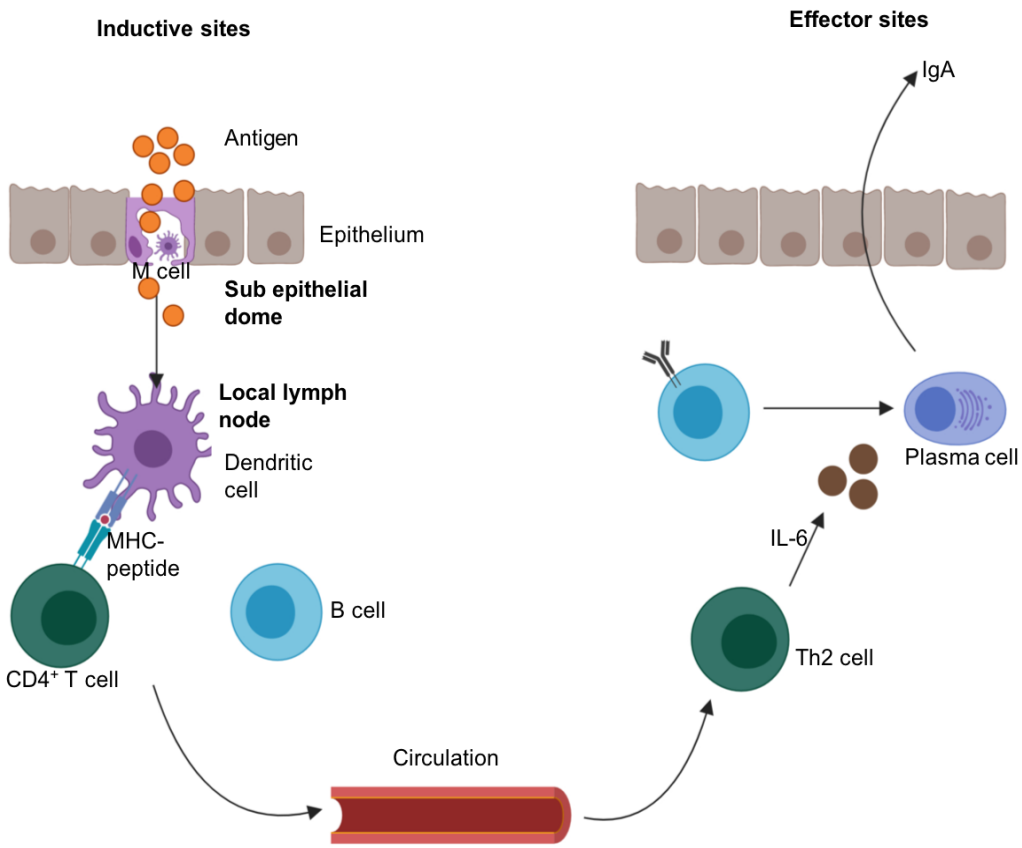

Figure 1.2. Mucosa-associated lymophoid tissue (MALT) structure and function. MALT consists of inductive sites (left), organised into the overlying epithelium containing specialised M cells which transport antigen to the subepithelial dome, where DCs perform antigen uptake and migrate to the local draining lymph nodes. Here, naïve T and B cells are primed by DCs, following which differentiated lymphocytes migrate to effector sites to perform effector functions such as secretion of IgA antibodies to the lumen *(Kiyono et al. Nat Rev. Immunol 2004).*

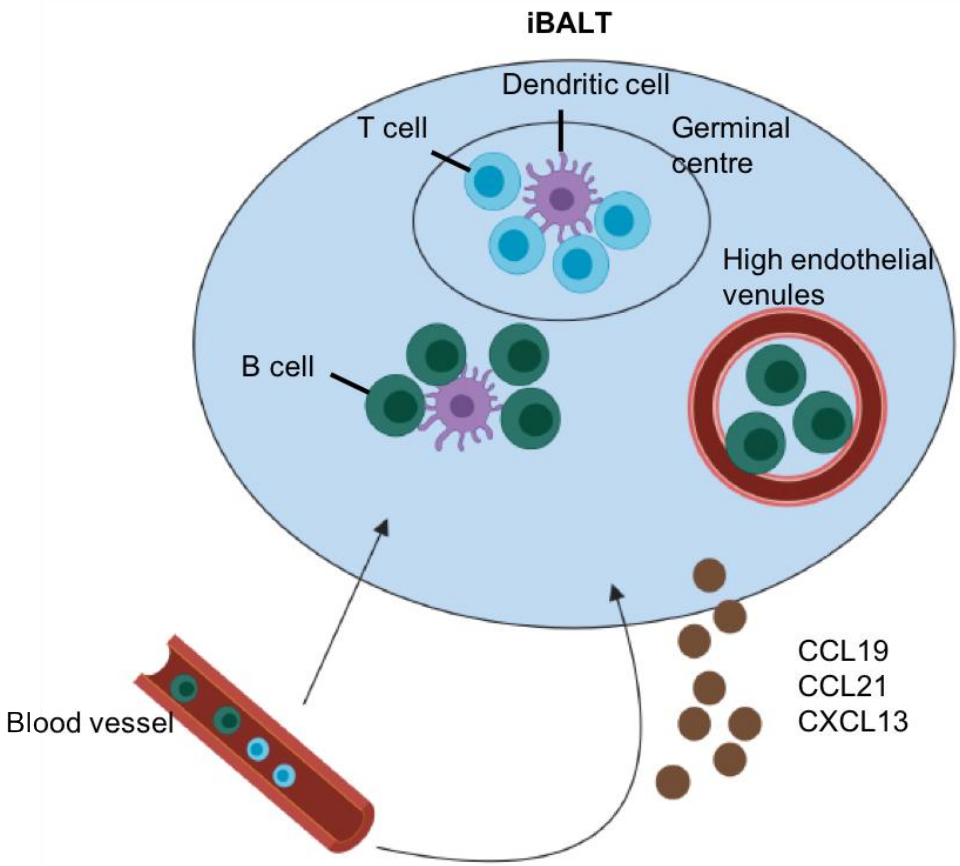

Figure 1.3. inducible Bronchus-associated lymphoid tissue (iBALT). iBALT is commonly induced in lung parenchyma upon infection or inflammation. The secondary structure is infiltrated by various immune cells like DCs, T and B cells, which in turn are organised in germinal centres where secondary reactions are mediated by follicular DCs for further maturation of lymphocytes. The iBALT is maintained by CCL19, CCL21 and CXCL13, produced by fibroblasts, vascular endothelial cells and lymphatic endothelial cells *(Hirahara et al. Front Immunol. 2019).*

humans and mice rarely exhibit presence of M cells [21,22]. In these areas, lymphocyte trafficking majorly occurs via the lymphatics. Specifically, antigen uptake and transport of naïve lymphocytes into iBALT from the blood compartment is carried out by the afferent lymphatics, especially the high endothelial venules (HEVs) [23,24]. Transport of antigen expressing DCs as well as primed T and B cells into the circulation is performed by the efferent lymphatics [25,26].

1.4. Dendritic cells

Dendritic cells are professional APCs, which play a central role in linking the innate and adaptive arms of the immune system by activating pathogen-specific adaptive immune responses. Immature or semi-mature DCs are strategically located at the first line of defence (skin, lungs, gut, genito-rectal tract and all mucous membranes) as well as the circulatory system [27]. Pathogen encounter activates immature DCs to take-up/process antigens and migrate to the respective lymphoid tissues (e.g. Gut-associated DC to mesenteric lymph nodes, lung-associated DCs to mediastinal lymph nodes). Mature DCs then present processed antigens to $CD8^+$ or $CD4^+$ T cells via the Major Histocompatibility Complex MHC-I or MHC-II respectively [28-30]. The cytokines and chemokines expressed by the different DCs, macrophages and other innate immune cells govern T cell polarization and differentiation. For example, in general IL-12 and IFN-γ have been established to polarize the type I (Th1) phenotype; IL-4 and IL-13 are associated with type II (Th2) responses [31-34] and IL-6 and TGF-β1 are known to induce Th17 cell differentiation [35]. Interestingly, DCs can have both myeloid or lymphoid origins, which lead to two principle populations of DCs, classical or conventional DCs (cDCs) and plasmacytoid DCs (pDCs) **(Figure 1.4)**

[36]. cDCs are further classified into migratory DCs such as Langerhans cells, dermal DCs and resident DCs which perform antigen uptake either from the periphery or the lymph nodes and present antigens in the draining lymph nodes [37]. Whilst, pDCs retain an immature phenotype at steady-state which upon activation can induce inflammatory factors including type 1 interferons (IFN) [38,39].

1.4.1 Mucosal dendritic cells

Mucosal DCs are found either in MALTs or in the mucosal surfaces [40-45]. These DCs also have the unique ability to directly sample antigens by extending dendrites through the epithelium [46] or indirectly via M cells, goblet cells or in some cases via neonatal Fc receptors [47-49]. DCs in the mucosae are mainly classified into two groups non-migratory DCs which are tissue resident, or migratory DCs which sample antigens and migrate to the draining lymph nodes [50,51]. For example, in one of the most studied mucosal organs, the small intestine, tissue resident DCs co-expressing CX3CR1 and CD11b sample local circulatory or luminal antigens to activate intraepithelial lymphocytes. Whilst migratory $CD11b^{low}$ $CD103^{+}$ $CD8^{+}$ or $CD11b^{+}$ $CD103^{+}$ DCs are responsible for generation of other T cell responses like differentiation of Th1 immunity and activation of regulatory T cells respectively. Other major DC subsets found in the small intestine include $TLR5^{+}$ DCs which activate Th1 and Th17 cells, and plasmacytoid DCs (pDCs) both of which generate IgA responses [52]. Mucosal DCs have the unique ability to imprint T cells with tissue-specific homing markers. Specifically, during T cell priming, mucosal dendritic cells induce tissue-specific 'homing markers' (for example $\alpha4\beta7$ and CCR9 for gut homing [53] and CCR5, CXCR3, $\alpha4\beta1$ and CCR4 for lung homing [54-56]) on T cells [24,57,58].

These T cell homing markers (integrins and chemokines) have the unique ability to bind to their tissue-specific ligands/adhesion molecules expressed on mucosal sites to initiate tissue-specific homing of effector and memory T cells. For example, $\alpha4\beta7$ can bind to mucosal addressin cell adhesion molecule-1 (MAdCAM-1) present in gut, whereas, $\alpha4\beta1$, can bind to VCAM-1 in lung or BALT [55,59]. More and more studies are showing that when designing vaccines against chronic mucosal pathogens such as HIV, TB or chlamydia, it is imperative to induce effective mucosal T cell homing to the site of first pathogen encounter [60-66]. Hence, different routes of mucosal delivery are now being considered, when designing vaccines against these pathogens.

1.4.2 Lung-specific dendritic cells: role in infection and immunity

Four major DC subsets are found in the murine lung namely, $CD11b^-$ $CD103^+$ cross-presenting DCs, $CD11b^+$ $CD103^-$ conventional DCs (cDCs), (both of which constitute phagocytic classical DCs), plasmacytoid DCs (pDCs) and inflammatory monocyte-derived DCs (moDCs) **(Figure 1.5)** [67-70]. For many years, immune activation and virus-specific DC activity have been studied using many viruses, such as Influenza, Herpes Simplex virus 1, Respiratory Syncytial Virus (RSV) and poxviruses [71,72]. Interestingly, the precise roles of different DC subsets following different viral infections still remain controversial.

1.4.2.1 Cross-presenting DCs

Two major cross-presenting DCs, namely $CD11b^-$ $CD103^+$ and $CD11b^-$ $CD8\alpha^+$, are found in mouse lung, which share common developmental origins as well as functions. Both these DCs require Batf3 (Basic Leucine Zipper ATF-Like Transcription Factor 3), ID2 (Inhibitor of DNA Binding 2), IRF8 (Interferon

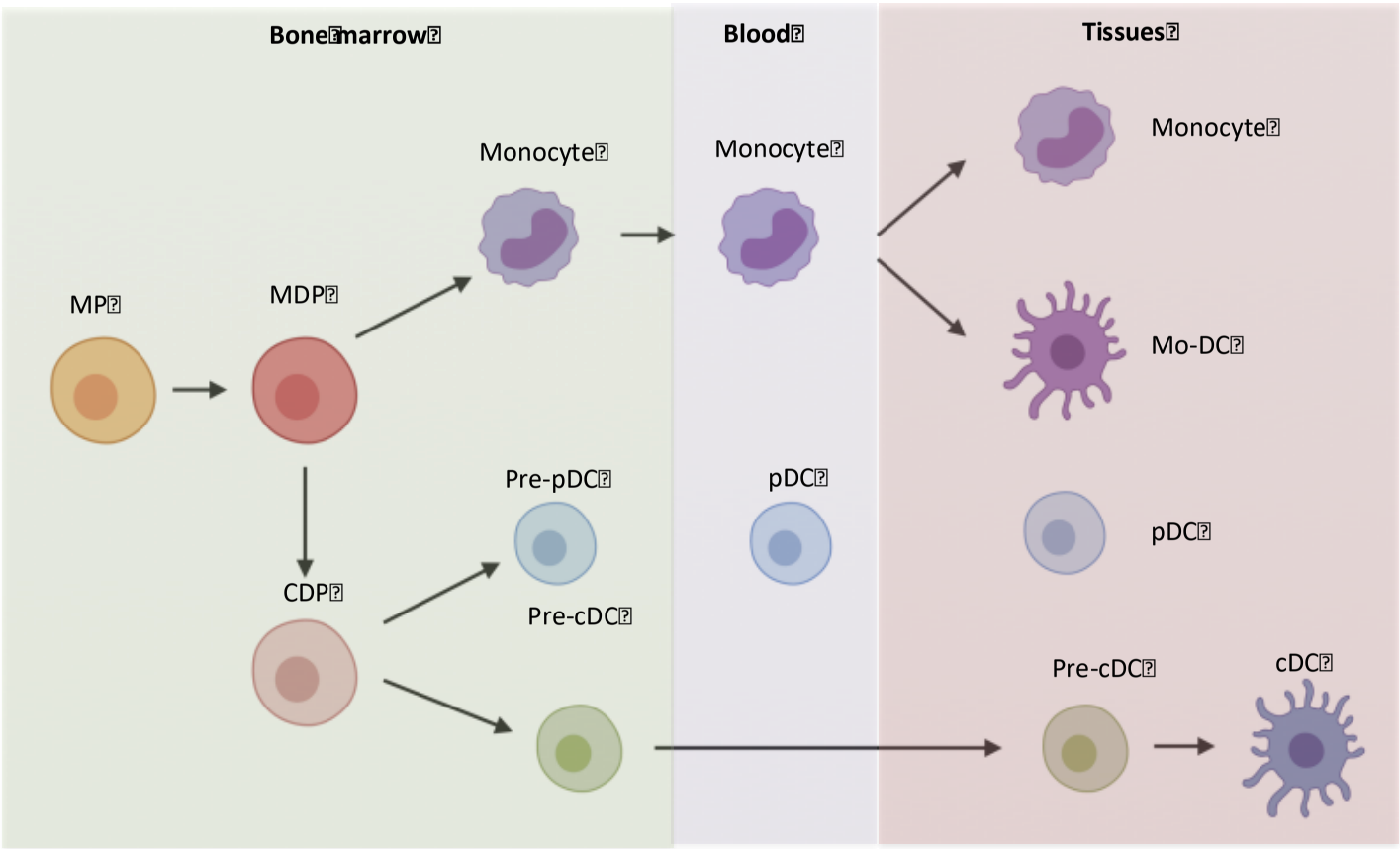
Bone marrow
Blood
Tissues
Monocyte
Monocyte
Monocyte
MP
MDP
Mo-DC
Pre-pDC
pDC
pDC
CDP
Pre-cDC
Pre-cDC
cDC

Figure 1.4. Dendritic cell development. During hematopoiesis, commom myeloid progenitor (MP) differentiates into common macrophage-dendritic cell-restricted precursor (MDP). Monocytes and common dendritic cell progenitor (CDP) develop from MDP. During inflammation, monocytes differentiate into monocyte-derived DCs (mo-DC). CDP also differentiates into either Pre-plasmacytoid DC (Pre-pDC) or Pre-classical DC (Pre-cDC) which differentiate into pDCs and cDCs respectively. (*Adapted from Cybulsky et al. Circulation Research 2016).*

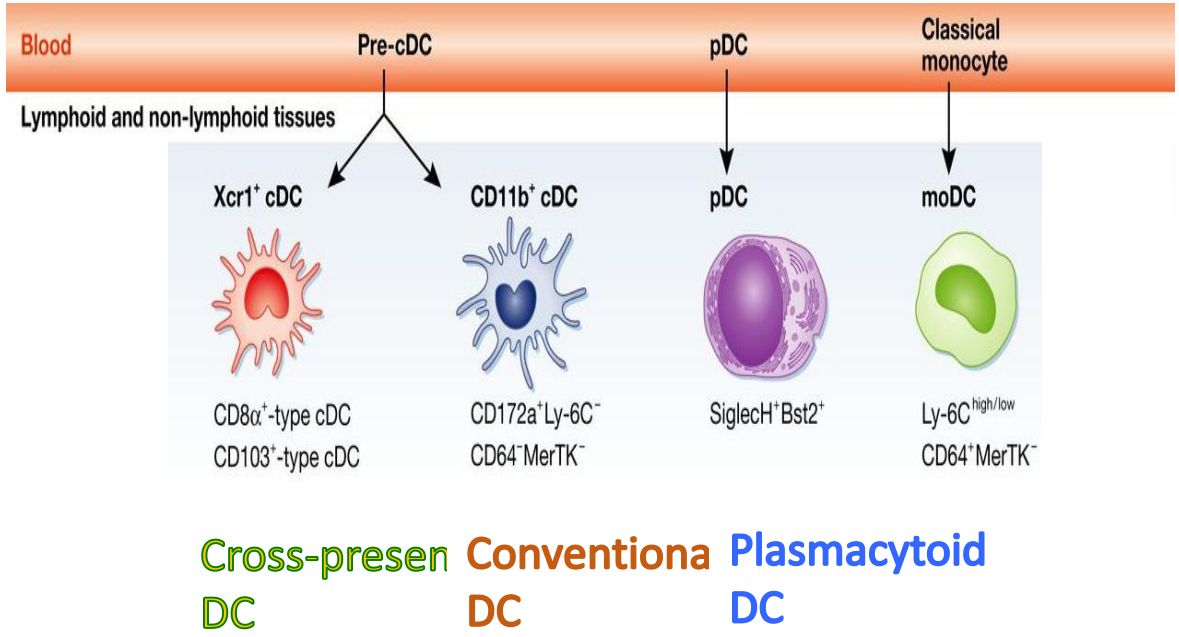

Figure 1.5. Lung dendritic cell subsets. There are four major lung DC subsets found in mouse. Among the resident lung DC populations are the CD103$^+$ cross presenting DCs, which have been shown to generate low avidity CD8$^+$ T cells; conventional CD11b$^+$ DCs (cDCs) have been associated with activation of high avidity CD8$^+$ T cells. Plamacytoid DCs (pDCs) are key inducers of type I interferons and in turn are responsible for B cell differentiation. Monocyte-derived DCs (moDCs) migrate to the lung following infection *(Dalod et al. EMBO J. 2014).*

Regulatory Factor 8) for activation [73], and functionally, have the unique ability to present exogenous antigens (normally presented via MHC-II molecules) to $CD8^+$ T cells via MHC-I molecules [74]. Specifically, in the context of acute viral infections such as Influenza and vaccinia virus infections, cross-presenting DCs have shown to efficiently activate cytotoxic $CD8^+$ T cells, essential for viral clearance [69,75-77]. However, these two cross-presenting DCs, have unique structural and functional features. Specifically, $CD11b^-$ $CD103^+$ cross-presenting DCs, more predominant in the lung, reside at the lung interface and sample exogenous antigens [78], as well as have the ability to process large quantities of apoptotic cells [79,80]. In contrast, $CD11b^-$ $CD8\alpha^+$ cross-presenting DCs, which are lymph node resident [73], have the ability to extend dendrites to sample antigens from lymphatics or the blood compartment and also acquire transferred antigens from $CD11b^-$ $CD103^+$ DCs at the draining lymph nodes using a process known as cross-dressing [81-83].

1.4.2.2 Conventional DCs

$CD11b^+$ $CD103^-$ cDCs are normally located in the lung parenchyma, below the basement membrane. At steady state, compared to cross-presenting DCs, fewer cDCs are found in the lung tissue. Developmentally, $CD11b^+$ $CD103^-$ cDCs are a heterogenous population, activated by major transcription factors IRF2 and IRF4 [74]. In addition to enhanced expression of MHC-II, CD11c and CD11b, cDCs have also been shown to express CD24 and CD86 in mice [84,85]. Despite having some overlapping functions with other classical DCs, some functions are unique to lung cDCs. Specifically, after resolution of respiratory viral infections, cDCs perform maintenance of iBALT function [86]. Furthermore, cDCs are more adept at processing and presenting soluble antigens compared to other classical DCs [87].

Upon antigen uptake, cDCs majorly express antigens via MHC-II to $CD4^+$ T cells [88], although in some cases such as severe Influenza infection, $CD11b^+$ cDCs have also been shown to potentiate $CD8^+$ T cells [89 90].

1.4.2.3 Plasmacytoid DCs

pDCs, upon activation, infiltrate into the lung tissues and are distributed in the lung airways. In contrast to classical DCs, pDCs are pre-DCs and do not exhibit the classical 'DC form'. pDCs specifically express TLR7 and TLR9 molecules, responding to a defined repertoire of PAMP signals. In addition to expressing low or no CD11b, pDCs also express surface markers B220, Ly6c, siglec-H along with low MHC-II in mice. pDCs are activated by transcription factors E2-2 (belonging to the E protein family) and IRF8 [70,91-93]. Unique pDC properties include secretion of type I Interferons, specifically IFN-α in the context of Influenza and RSV infection [94-96]. Type I IFN production by pDCs have also shown to activate virus mediated B cell differentiation and hence development of antibody responses [97]. Studies using systemic Herpes Symplex Virus (HSV) infection have shown that in addition to being interferon producers, pDCs are important activators of NK cells and $CD8^+$ T cells [98].

Unlike in acute viral infection, in the context of recombinant viral vector-based vaccination, $CD11b^-$ $CD103^+$ cross-presenting DCs have been associated with induction of low avidity vaccine-specific $CD8^+$ T cells whereas $CD11b^+$ $CD103^-$ cDCs have been associated with high avidity T cell immunity [99]. Knowing that pDCs are associated with effective antibody responses [97], understanding the regulation of these three lung DC subsets at the lung mucosae (vaccination site) immediately post intranasal vaccination forms the basis of this thesis.

1.5 Importance of Mucosal vaccination

It is now well established that the route of vaccination can significantly influence the resulting local and distal immune responses. Both systemic and mucosal vaccination have been historically used against mucosal pathogens [100]. Interestingly, although systemic vaccination can induce effective immunity at the blood compartment, it has shown to be ineffective at inducing long lasting mucosal immunity [101]. For example, intramuscular vaccination has shown to promote mucosal immunity against certain mucosal pathogens such as Bovine respiratory syncytial virus, bovine rotavirus and H5N1 [102-105], but have elicited poor immune outcomes against chronic mucosal pathogens such as HIV-1, tuberculosis and chlamydia [102]. This has been mainly associated with poor T cell homing to the mucosae post systemic delivery, where the pathogen is first encountered [53,106]. Thus, vaccine strategies that can induce immunity at the local and distal mucosae are important for control of these infections, specifically strategies that can induce effective long lasting mucosal T cell immunity as well as IgA responses [107-111]. Different mucosal routes of vaccination for example intranasal, oral, intrarectal, intravaginal and intraocular have shown to induce immunity at different local and distal mucosae. Specifically, intranasal (i.n.) vaccination has been more successful at generating immunity in the upper respiratory tract, gut, as well as the genito-rectal mucosae [112-114] **(Figure 1.6a)**. Whereas, oral vaccination has shown to induce immunity in the salivary glands, mammary glands, gut mucosae and in some instances at the rectal tract [113]. Vaginal vaccination has shown to induce immunity in the local mucosae, whereas, rectal vaccination has shown to induce immunity at the local rectal as well and the gastro-intestinal mucosae [115-117]**.** It is

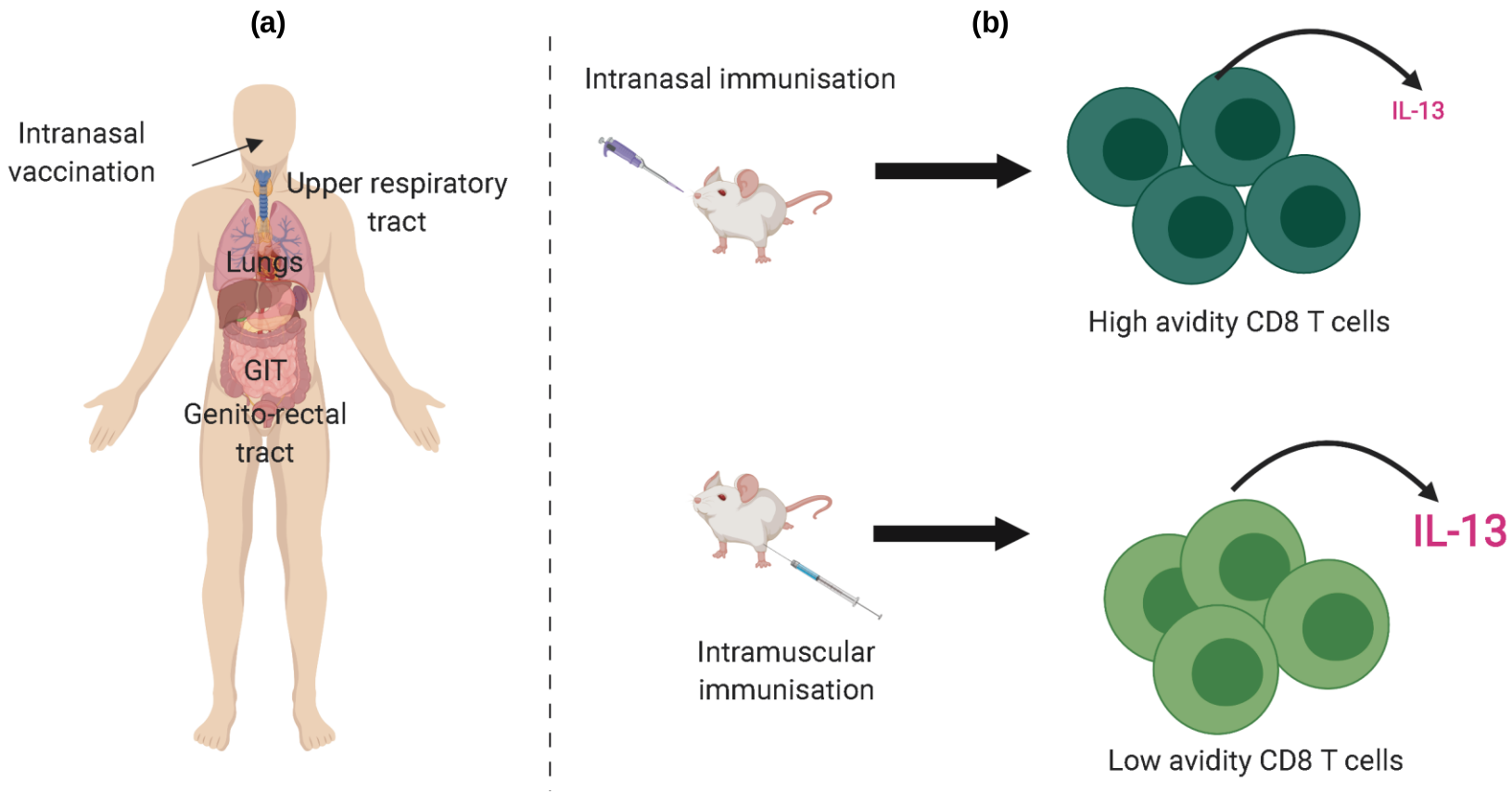
(a)
Intranasal vaccination
Upper respiratory tract
Lungs
GIT
Genito-rectal tract
(b)
Intranasal immunisation
IL-13
High avidity CD8 T cells
Intramuscular immunisation
IL-13
Low avidity CD8 T cells

Figure 1.6. Mucosal versus systemic vaccination schematic. It is now well established that mucosal, specifically intranasal route of vaccination induce immunity in local and distal mucosal sites as well as systemic compartments. Additionally mouse studies have shown that intranasal administration of viral vector-based vaccine can induce high avidity $CD8^+$ T cells, associated with low IL-13 production. In contrast, systemic viral vector-based vaccination has shown to induce low $CD8^+$ T cell avidity, associated with enhanced IL-13 production *(Belyakov et al. 1998, Belyakov et al. 2001, Ranasinghe et al. 2006, Ranasinghe et al. 2007, Ranasinghe et al. 2009)*.

now well established that these differential immune responses are mainly governed by the activation of unique tissue-specific mucosal DCs promoting tissue-specific T cell and B cell homing [24,57,58].

1.5.1 HIV vaccines and mucosal immunity

In the context of HIV, despite being a disease of the mucosae, no mucosal HIV vaccine strategy has yet been tested in humans. All the systemic vaccination approaches tested in human clinical trials have yielded poor outcomes [118-121], except the RV144 trial showing marginal efficacy with 31.2 % protection [121]. Over two decades of work in animal models (both in mice and macaques) have shown that HIV mucosal vaccination strategies can induce promising long lasting protective immunity [122-124]. Studies by Belyakov *et al*. and studies in our laboratory have shown that intrarectal vaccination approaches can induce effective HIV-specific cytotoxic $CD8^+$ T cells at the mucosae both in mice and non-human primates, and established the importance of mucosal cytotoxic $CD8^+$ T cells in prevention of viral dissemination and protection against HIV [102,107,125-129]. Several decades of work, trying to understand why systemic vaccines were failing in clinical trials, Ranasinghe *et al.* were the first to show that, compared to a purely systemic approach, a purely mucosal or mucosal/systemic prime-boost vaccination regimen (i.n./i.m. prime poxviral vector-based HIV vaccine approach) can induce high avidity HIV-specific T cell immunity [130]. They showed that these responses were mainly associated with the expression of IL-4/IL-13 by cytotoxic $CD8^+$ T cells, where systemic vaccination was shown to induce elevated IL-4/ IL-13 production compared to mucosal delivery [130-132] **(Figure 1.6b)**. Recent studies in the laboratory have shown that, HIV vaccines that transiently block IL-4/IL-13 activity at the vaccination site can lead to high avidity/poly-functional cytotoxic T

cells in murine and macaque models [122-124] (Li *et al.* in preparation). Moreover, in addition to the route of delivery and cytokine cell milieu in a prime-boost vaccine modality, the choice of vaccine vector, specifically the priming vector was also shown to significantly impact avidity/poly-functionality of T cells [131,133]. Thus, understanding how these factors (specifically, IL-3 levels and viral vectors) influence adaptive immune outcomes at the innate immune level forms the basis of this thesis.

1.6 Viral vectors: poxviral vector-based vaccines

For many decades, viral vectors such as poxviruses have been promising vaccine delivery vehicles [134-140]. Their unique ability to contain large amounts of foreign genetic material without loss of viral function or host cell infectivity, and the ability to express these genes/antigens at high concentrations, enabling the induction of robust pathogen-specific cellular and humoral responses, have made these vectors popular vaccine candidates, specifically in prime-boost vaccine modalities [99,121,130,141-145].

1.6.1 Recombinant vaccinia virus-vectored vaccines

Vaccinia virus (VACV) has been the most studied poxvirus in the context of vaccine design. Historically, several VACV strains have been used as smallpox vaccines, which ultimately lead to smallpox eradication [146-148 149-151]. Different VACV strains with improved safety, reduced pathogenicity and high immunogenicity have been used as recombinant vaccines for pathogens, for which effective vaccine strategies are not yet available, for example HIV-1, hepatitis, tuberculosis and malaria [152-157]. In the context of HIV-1, recombinant Tiantan Vaccinia virus (rTV), Copenhagen derived New York Vaccinia Virus

(NYVAC) [158-162] and recombinant Modified Vaccinia Ankara (rMVA) have been tested in different prime-boost vaccine modalities (rDNA/viral; protein/viral; viral/protein). [148,163-166]. Mucosal delivery of rTV, NYVAC and rMVA have also been tested and have shown some promising mucosal HIV-specific T cell outcomes [128,162,167,168].

1.6.2 Recombinant MVA-based vaccines

MVA was first derived from the Chorioallantoic Vaccinia Ankara (CVA) strain after extensive serial passaging of the virus in cell culture [164,165]. The resultant MVA was known to be replication deficient and non-pathogenic in most mammalian cells rendering the virus extremely safe in humans as a vaccine vector [169,170]. Additionally, due to its intrinsic adjuvant abilities and capacity to induce robust cellular and humoral immune responses, recombinant MVA (rMVA) vector-based vaccines were extensively studied against many pathogens such as HIV-1, *Mycobacterium tuberculosis*, Malaria and Hepatitis B [148,154,171,172]. Interestingly, i.m. rDNA prime/i.m. rMVA booster vaccination strategies were one of the first to be tested against HIV. Although these vaccines were found to be effective in animals models [173-176], due to the poor uptake of rDNA, as well as inability to induce long lasting mucosal immunity [177,178], rDNA vaccine strategies resulted in poor immune outcomes in Phase I clinical trials, similar to other systemic rDNA-based vaccine strategies in the early 2000s [129,144,163,179-181]. In later studies, even though mucosal delivery of rMVA-based HIV vaccines has yielded some promising outcomes in mice and macaques [167,182], rMVA mucosal vaccine strategy has not yet been trialed in humans. Additionally, Esteban *et al*. were the first to design a range of rMVA deletions mutants, rendering the vaccine more effective and safe by removing vector-specific immune evasive genes [137], such

as IL-1β receptor, IL-18 binding protein, C6L (genes associated with type I IFN signaling), or F1L, (involved in apoptosis). Interestingly, these mutants were shown to induce HIV-specific immune outcomes in animal models compared to parental rMVA [183-186].

1.6.3 Recombinant avipoxvirus vector-based vaccines

Avipoxvirus vectors, such as canarypox and fowlpox, which cannot replicate in mammalian hosts, rendering them extremely safe in humans, have also been studied as recombinant vaccine vectors [187-189]. In the context of HIV vaccine design, recombinant canarypoxvirus (known as ALVAC,) and the close relative recombinant fowlpox virus (rFPV) vaccine strategies have been well studied [190-196]. Interestingly, the only HIV vaccine trial that have been partially successful in humans, the RV144 trial (31.2% reduction in HIV-1 infections in vaccine recipients), used an ALVAC prime followed by HIV gp120 protein booster strategy [121]. This partial protection was correlated with antibody dependent cell mediated cytotoxicity (ADCC) and HIV envelope-specific non-neutralizing antibody responses elicited by this vaccination approach [197-201]. This partial success renewed the interest in recombinant poxviral vector-based approaches as potential HIV vaccine candidates.

FPV was first used as a vaccine against fowlpox in chickens and was later used as a vehicle to deliver antigens against other poultry diseases such as avian influenza, Newcastle disease and infectious bronchitis [202]. Boyle *et al*. were the first to use rFPV vectors as a vaccine strategy against HIV [135,193,203]. The initial prime-boost vaccination strategy, using pure intramuscular (i.m.) rDNA prime/ rFPV booster, although showed promising immune outcomes in mice and

macaques [129,191,193,204,205], unfortunately failed in Phase I clinical trials [144]. However, these trials clearly established that rFPV was extremely safe in humans [144,204]. Later rDNA prime followed by rFPV co-expressing HIV antigens together with co-stimulatory molecules or cytokines including IFN-γ, IL-12, 4-1BBL), although were found to enhance immunogenicity/vaccine efficacy in murine and macaque models [131,206-213], co-expression of IFN-γ and IL-12 were later found to be ineffective in humans [204,214]. Interestingly, despite disappointing outcomes with i.m. rDNA/i.m. rFPV systemic vaccination strategy in human clinical trials [144], i.m. rDNA/i.n. or rectal rFPV strategies were found to induce better protective efficacy in non-human primates compared to pure systemic delivery [129]. These, together with later studies revealed that rFPV was an excellent mucosal delivery vector [131,205]. These studies also demonstrated that compared to rDNA/viral vector-based vaccine strategies viral/viral prime-boost modalities could induce better poly-functional long lasting T cell immunity [215-218]. Specifically, i.n. rFPV prime followed by i.m. rVV or rMVA booster strategies were shown to generate sustained mucosal and systemic HIV-specific high avidity/poly-functional $CD8^+$ T cells both in mice and macaques [123,130,131], unlike the inverse strategies [131,133] (Ranasinghe, personal communication) **(Figure 1.7)** eliciting, not only the route of delivery [130,131,205], but also the order in which these viral vectors are delivered in a prime-boost modality, played an important role in modulating the final vaccine-specific adaptive immune outcomes [133].

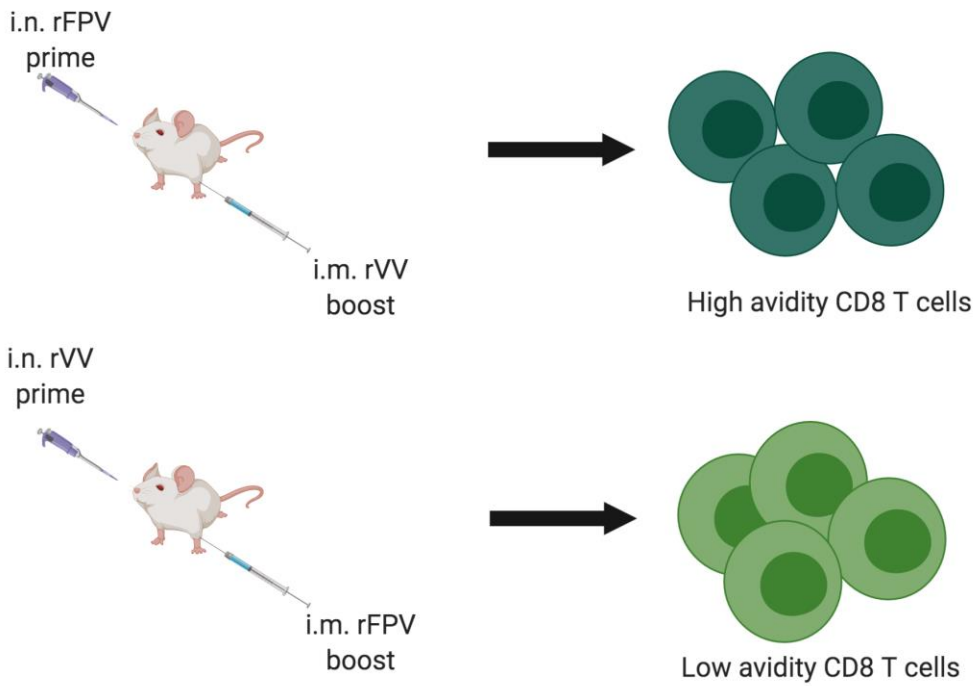

Figure 1.7. Order of administration of viral vaccine vector influences vaccine efficacy. In a heterologous prime boost modality, intranasal prime vaccination with rFPV followed by intramuscular booster with rMVA or rVV has shown to induce high avidity, polyfunctional $CD8^+$ T cells. In comparison, intranasal priming with rMVA or rVV followed by intramuscular rFPV booster has shown to generate lower avidity $CD8^+$ T cells *(Ranasinghe et al. 2006, Wijesundara et al. 2014, Ranasinghe, personal communication).*

1.7 Non-poxviral vector-based vaccines

Apart from poxviruses, many other viruses have also been used as vectors to deliver vaccine antigens. Among the non-poxvirus recombinant vector-based vaccines, Cytomegalovirus, Sendai virus, Lentiviruses, Polio-virus, different retroviruses, adenoviruses, Influenza virus, Human Rhinoviruses have been used in many major pre-clinical and clinical vaccine trials [136,138,219-222].

1.7.1 Recombinant Adenovirus vector-based vaccines

In the context of HIV vaccine design, several recombinant Adenovirus (Ad) vectors have also been found to induce high immunogenicity in animal models [140,219,222,223]. Recombinant Adenovirus serotype 5 (rAd5) was used in the STEP/ Phambili HIV clinical trials with great anticipation of success in 2008 [118,119]. Even though the vaccine strategy induced robust HIV-specific cellular and neutralizing antibody responses in mice and non-human primate models [224-227], Phase I STEP/Phambili trials had to be unexpectedly hauled due to vector-specific immunity in humans leading to increased HIV acquisition [118,228]. Since then, several other non-human related and modified rAd vectors, for example Ad26, Ad35 and Chimpanzee Ad vectors, have been tested [223,229,230]. In clinical trials, these modified rAd vectors have shown better safety profiles (reduced liver toxicity and anti-vector immunity) with promising cross-clade antibody responses [231]. Recent clinical trials by Barouch and colleagues using rAd26 HIV vaccination strategy in human clinical trials, although have shown ADCC and broad epitope-specific Env antibody responses, have shown limited breadth of HIV-specific T cell immunity [232,233]. Interestingly, using these rAd vectors, efforts are now being made to induce unique innate immune cell profiles to improve breadth and cross-

reactivity of T cell response as well as Env-specific neutralizing antibody responses [225,234-238].

1.7.2 Recombinant Influenza vector-based vaccines

Influenza A has a broad host range inducing immune responses in many different animals and known to induce both Th1 and Th2 immunity, essentially eliciting both cellular and humoral immunity [239]. Due to these properties, various live and inactivated recombinant Influenza A-based vaccine strategies have been tested against several pathogens, including HIV-1 [138,239-242]. Recombinant Influenza A expressing HIV Nef antigens used in an i.n. H1N1 prime/ i.n. H3N2 booster vaccination strategy in mice have shown to induce elevated Nef-specific systemic as well as mucosal $CD8^+$ T cells (in the genito-rectal nodes) [242]. Similarly, recombinant Influenza expressing HIV Env or Gag in a heterologous Influenza prime/ rVV booster modality have also shown enhanced antigen-specific $CD8^+$T cells both in mice and macaques [138,243,244]. Gherardi *et al*. have also shown that i.n. Influenza/i.n. or intraperitoneal (i.p.) rMVA or rVV booster strategy, can not only induce env-specific $CD8^+$ T cells expressing IFN-γ, but also env-specific IgG2a responses in mice [138]. Moreover, Tan *et al.* have shown that compared to i.n. rFPV/ i.n. Influenza HIV prime-boost vaccine strategy, the inverse strategy can induce low avidity mucosal and systemic HIV-specific $CD8^+$ T cells (Tan, Derose *et al.* personal communication), once again eliciting the importance of the choice of priming vector in prime-boost modalities.

1.7.3 Recombinant rhinovirus vector-based vaccines

Recently, recombinant human rhinovirus (rHRV)-based HIV prime-boost vaccine strategy was also tested in mice, specifically with the intention of inducing

effective immunity at the first line of defence at the genito-rectal and gut mucosae. [220]. i.n.rHRV/ i.m. rDNA booster vaccination strategy expressing HIV Gag and Tat antigens was shown to induce enhanced poly-functional Gag- and Tat-specific systemic and mucosal (mesenteric lymph nodes) $CD8^+$ T cell responses and also Tat-specific mucosal IgA and serum IgG antibodies in vaginal lavage and blood [220,245].

While the appetite to design new vaccine strategies using different recombinant viral vector-based vaccines are growing, how different recombinant viral vectors, expressing similar pathogen-specific genes/antigens induce vastly different adaptive immune outcomes still remains unanswered. Surprisingly, the mechanisms underpinning how these different vectors induce different vaccine-specific immune outcomes, especially at the innate immune level, still remains poorly characterised, which this forms the main basis of this thesis.

1.8. Role of cytokines in viral infection and immunity

Activation of TLRs following an infection commonly signal in Myd88 dependent or independent pathways to activate downstream elements such as the Interleukin-1 receptor associated kinase (IRAK), Tumor necrosis factor receptor associated factor 6 (TRAF6), Interferon regulatory factor (IRF) and/or nuclear factor kappa-light-chain-enhancer of activated B cells (NFκB), which in turn induce production of a plethora of pro-inflammatory cytokines such as type I IFN, Tumor necrosis factor (TNF)-α, Interleukin (IL)-1, IL-6, IL-8, depending on the pathogen encountered [246]. Whilst the IFNs employ direct antiviral activities such as inhibiting replication of the virus, enhancing lysis of infected cells or activation of other pro-inflammatory cells such as macrophages [247,248], TNFs can enhance

vascular adhesion of inflammatory cells to promote antiviral responses [249]. Furthermore, interleukins can promote both pro- and anti-inflammatory properties following binding specific receptors [250]. Traditionally, whilst Th1 immune responses have been responsible for defence against intracellular pathogens such as viruses and bacteria, Th2 responses have known to be associated with extracellular infections, such as, helminths and also parasitic infections. In addition to Th1 and Th2 immunity, Th17 cells are also known to secrete IL-17 and IL-22 in response to extracellular bacterial and fungal infections [251]. Individual roles as well as inter-regulation between Th1 and Th2 immunity has been well-documented in allergy/asthma, helminth infections as well as viral infections [252-263]. In the context of poxviral vector-based vaccination, IL-4 and IL-13 expression by antigen-specific $CD8^+$ T cells have been directly linked to T cell avidity and protective efficacy [122-124,130-132] (Li *et al*. in preparation).

1.8.1 IL-4 and IL-13 in disease and viral vector-based vaccine efficacy

Th2 cytokines IL-4 and IL-13 have been extensively studied in disorders involving Th2 immunity including inflammatory conditions such as allergy and asthma, fibrosis, atopic dermatitis, tumor progression as well as parasitic infections [255,257,264-269]. In the context of allergic asthma, although IL-4 and IL-13 have shown overlapping functions such as IgE associated pathogenesis and eosinophil recruitment to the lung parenchyma, the two cytokines have also been associated with unique functions. Over-expression of IL-4 associated humoral immunity has been linked to Th2 inflammation [256,270], whilst IL-13 mediated activation of fibroblasts, goblet cell differentiation, smooth muscle contraction, mucous production and bronchial hyperresponsiveness has been associated with airway hyperreactivity and pathogenesis in allergic asthma [254]. In the context of different

infections, IL-4 and IL-13 have also shown opposing as well as unique functions. For example, following *N. brasiliensis* infection, whilst IL-4 has been involved in promoting disease progression, IL-13 is essential for parasite clearance [259,271,272]. During, *Streptococcus* infection in mice, IL-4 has shown to exacerbate the bacterial infection [273]. Interestingly, during *Klebsiella pneumonia* infection, IL-13 has shown to promote host protection, whilst, in the context of *Chlamydia trachomatis* infection, IL-13 has been associated with susceptibility to infection [252,274-276]. Additionally, in acute and primary viral infections (Ectromelia virus and respiratory syncytial virus) IL-13 has been associated with improved antiviral immunity [263,277], whilst in the context of viral vector-based vaccination, presence of IL-4 and IL-13 have shown to dampen effective T cell immunity [131,132]. Interestingly, Ranasinghe *et al*. have shown that novel poxviral vector-based vaccines, that transiently inhibit IL-14 and/or IL-13 at the vaccination site can differentially regulate HIV-specific T and B cell immunity [122,124].

1.8.2 IL-4/IL-13 signalling

IL-4/ IL-13 functions via a common receptor system comprising of Type I (IL-4Rα/γc) and Type II (IL-4Rα/IL-13Rα1) receptor complexes **(Figure 1.8)** [278]. IL-4 binds IL-4Rα with high affinity, which heterodimerises with γc subunit and forms the Type I IL-4R complex. Membrane bound IL-13Rα1 is the low affinity receptor for IL-13 (Kd ~30 nM) which heterodimerises with IL-4Rα to form the high affinity functional Type II IL-4R complex [279]. Once activated, both IL-4R Type I and Type II complexes activate the JAK/STAT6 signalling pathway [280]. In allergic asthma, IL-4 type I and type II receptor complexes play a central role in

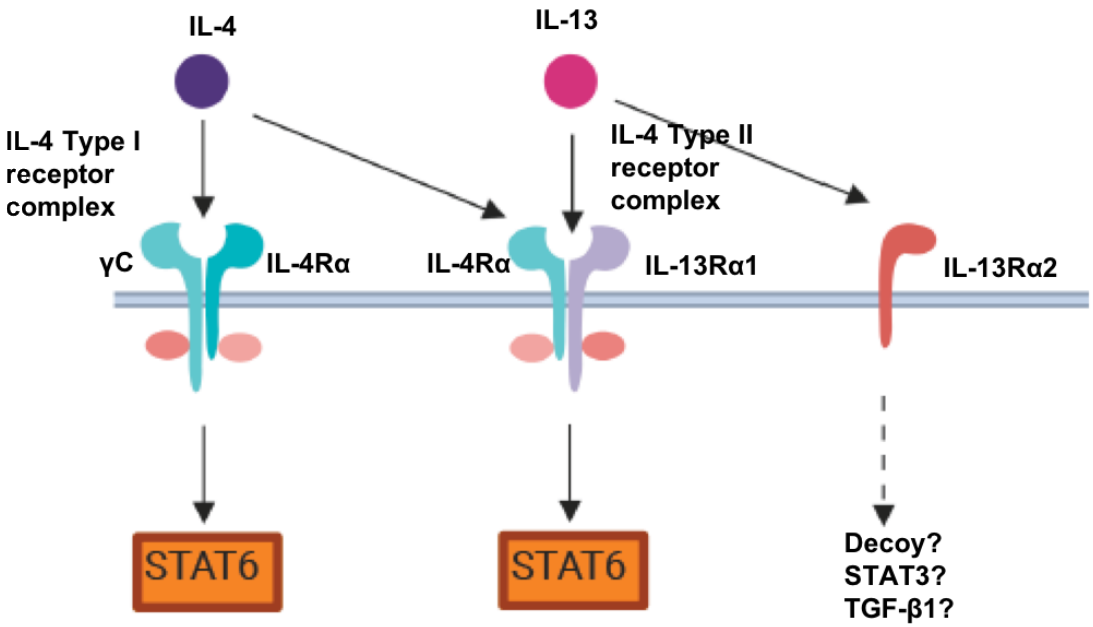

Figure 1.8. IL-4/IL-13 signalling. IL-4 binds to the high affinity receptor IL-4Rα which complexes with γC to form the IL-4 Type I receptor complex. IL-13 shares the IL-4 Type II receptor complex with IL-4, which is comprised of IL-4Rα and the IL-13 low affinity receptor IL-13Rα1. IL-13 alternatively can also bind with the high affinity receptor IL-13Rα2. Due to the lack of signalling motifs and a short cytoplasmic tail IL-13Rα2 has been long thought to be a decoy receptor for IL-13. However, in the context of human cancer and fibrosis IL-13Rα2 has shown to activate STAT3 as well as TGF-β1 *(Tabata et al. 2007, Rahaman et al. 2005, Fichtner-Feigl et al. 2006).*

promoting inflammation. Whilst IL-4Rα signalling activates Th2 responses via alternatively activated macrophages [281], IL-13Rα1 signalling mediates lung pathology by promoting lung fibrosis, mucous production and airway hypersensitivity [262,282]. In the context of eosinophilic esophagitis and cardiac homeostasis, the association of IL-13Rα1/IL-4Rα with STAT3 signalling has also been proposed [108,283].

IL-13Rα2 is the high affinity receptor for IL-13 (Kd ~440 pM), which exists as a membrane bound, as well as a soluble form **(Figure 1.8)**. Interestingly, IL-13Rα2 first discovered in mouse urine [284], was long thought to be a decoy receptor in mice, functioning to only sequester IL-13 from the milieu [285-287]. However, IL-13Rα2 is now known to be a functional receptor in humans and has been associated with certain cancers (of the brain, breasts, ovaries, liver) and disease conditions [288-292]. Hence, in the recent years IL-13Rα2 has been targeted as an anti-cancer treatment [293]. In the context of chronic inflammatory diseases such as inflammatory bowel disease (IBD), expression of IL-13Rα2 has been associated with disease promotion/progression [294], and up-regulation of IL-13Rα2 in the airway inflammation has also shown to negatively regulate IL-13 mediated pathogenicity in mice and humans [295,296]. Furthermore, in helminth infection (schistosomiasis), IL-13Rα2 expression has been linked to down-regulation of inflammation causing disease protection [297]. Although the exact mechanism is not well understood, studies have reported that IL-13Rα2 can signal via STAT3 [298,299]. Interestingly, other studies have also shown the association of IL-13Rα2 to downstream activation of transforming growth factor beta 1 (TGF-β1) [300,301]. Recent studies in our laboratory using poxviral vector-

based vaccination that transiently inhibited STAT6 and IL-13 activity at the vaccination site [122,124] have shown the involvement of an STAT6 independent pathway, (likely linked to IL-13Rα2 pathway), associated with antibody differentiation [122,302].

1.9 Impact of IL-13 levels on lung resident ILCs and DCs at the vaccination site

Over a decade of work in our laboratory using poxviral vector-based mucosal and systemic vaccine strategies, it was established that more than IL-4, IL-13 was detrimental for the induction of high avidity/poorly poly-functional HIV-specific T cells [130,132]. Subsequently, vaccines that co-expressed HIV antigens together with IL-4/IL-13 inhibitors were developed in the laboratory as described before, that transiently inhibited IL-4 and IL-13 activity at the vaccination site; namely, IL-4R antagonist and IL-13Rα2 adjuvanted vaccines. Specifically, IL-4R antagonist adjuvanted vaccine transiently inhibited IL-4/IL-13 signalling via STAT6 by binding IL-4Rα [122,123], whereas IL-13Rα2 adjuvanted vaccine transiently sequestered IL-13 at the vaccination site, reducing IL-13 activity [124] **(Figure 1.9)**. In an HIV i.n. rFPV/i.m. rMVA prime-boost modality both these vaccines were shown to induce high avidity poly-functional (ability to express IFN-γ, TNF-α and IL-2 and cytotoxic markers) mucosal and systemic T cells with better protective efficacy in both mice and macaques [122-124]. In addition to effective T cell immunity, unlike the IL-13Rα2 adjuvanted vaccine strategy, IL-4R antagonist adjuvanted HIV vaccine strategy was also shown to induce IgG1 and IgG2a antibodies in mice, showing that IL-13 was necessary for effective antibody differentiation [122,302]. Interestingly, presence of high avidity poly-functional T cells and effective antibody differentiation have been hallmarks of

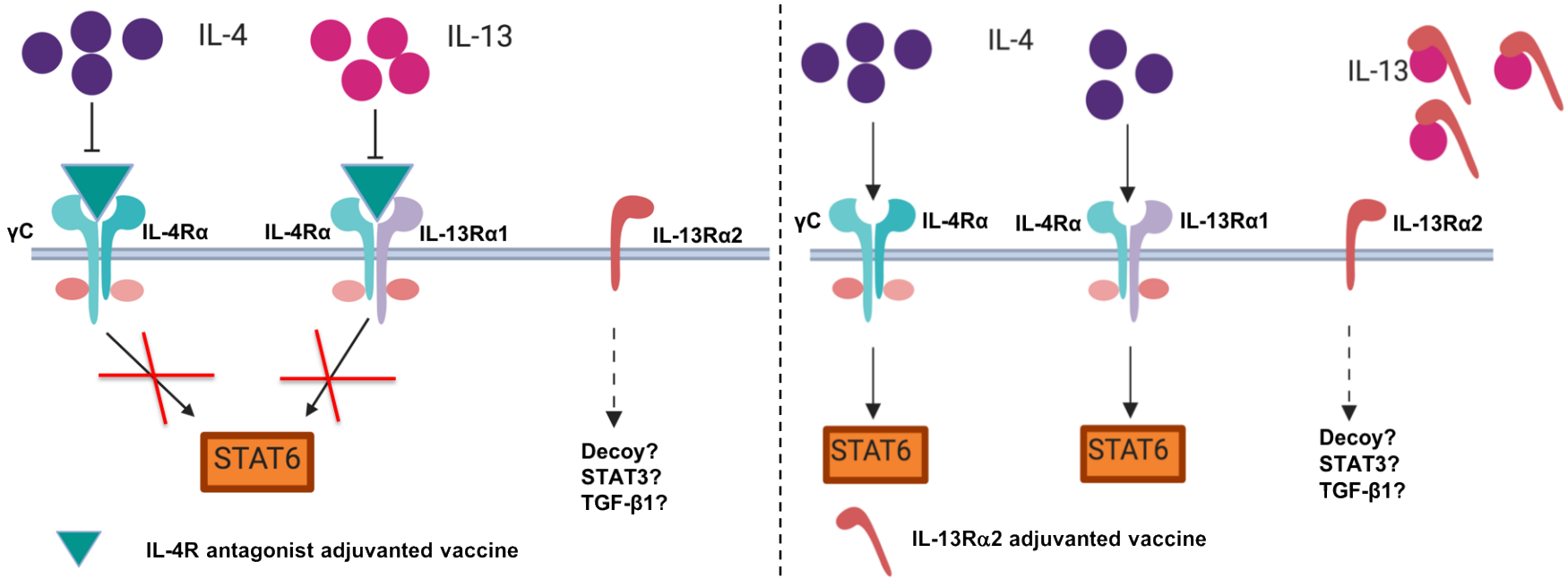

Figure 1.9. IL-4/IL-13 inhibitor HIV vaccines. IL-4R antagonist adjuvanted vaccine co-expressing mutant IL-4 (IL-4C118) with HIV antigens, binds IL-4Rα, transiently blocking IL-4/IL-13 signalling via STAT6 at the vaccination site. The IL-13Rα2 adjuvanted vaccine, co-expressing soluble IL-13Rα2 with HIV antigens, sequesters IL-13, transiently blocking IL-13 activity at the vaccination site. *(Ranasinghe et al. 2013, Jackson et al. 2014).*

protective immunity observed in a rare cohort of people who naturally control HIV infection, known as elite controllers [303-305].

Hence, when trying to unravel how these novel IL-4/IL-13 inhibitor viral vector-based vaccines modulated vaccine-specific immunity at the innate and adaptive compartments, recent studies for the first time demonstrated that, innate lymphoid cell type 2 (ILC2), were the major source of IL-13 at the vaccination site, post 24 h delivery [306] and ILC2-derived IL-13 also modulated the ILC1/ILC3-derived IFN-γ and IL-17 production at the vaccination site [306]. Using i.n. delivery of these novel vaccines it was also established that IL-13 levels at the lung mucosae could significantly alter the lung DC recruitment, 24 h post delivery (during the peak antigen expression) [99,307]. Specifically, transient inhibition of IL-13 enhanced recruitment of $CD11b^+$ cDCs to the lung mucosae, which was associated with high avidity T cell induction [99,124]. Moreover, adoptive transfer studies revealed that lung $CD103^+$ cross-presenting DCs were responsible for induction of low avidity CD8 T cells [99]. These studies clearly established that the level of IL-13 at the vaccination site as well as different DC subsets induce uniquely different downstream HIV-specific adaptive immune outcomes (specifically, IL-13 was detrimental for induction of high avidity poly-functional T cells, whereas IL-13 was necessary for effective antibody differentiation) **(Figure 1.10)**. However, whether different viral vectors induced different ILC2-derived IL-13 at the vaccination site that impacted the recruitment of different DC subsets were not established, which forms the basis of this study.

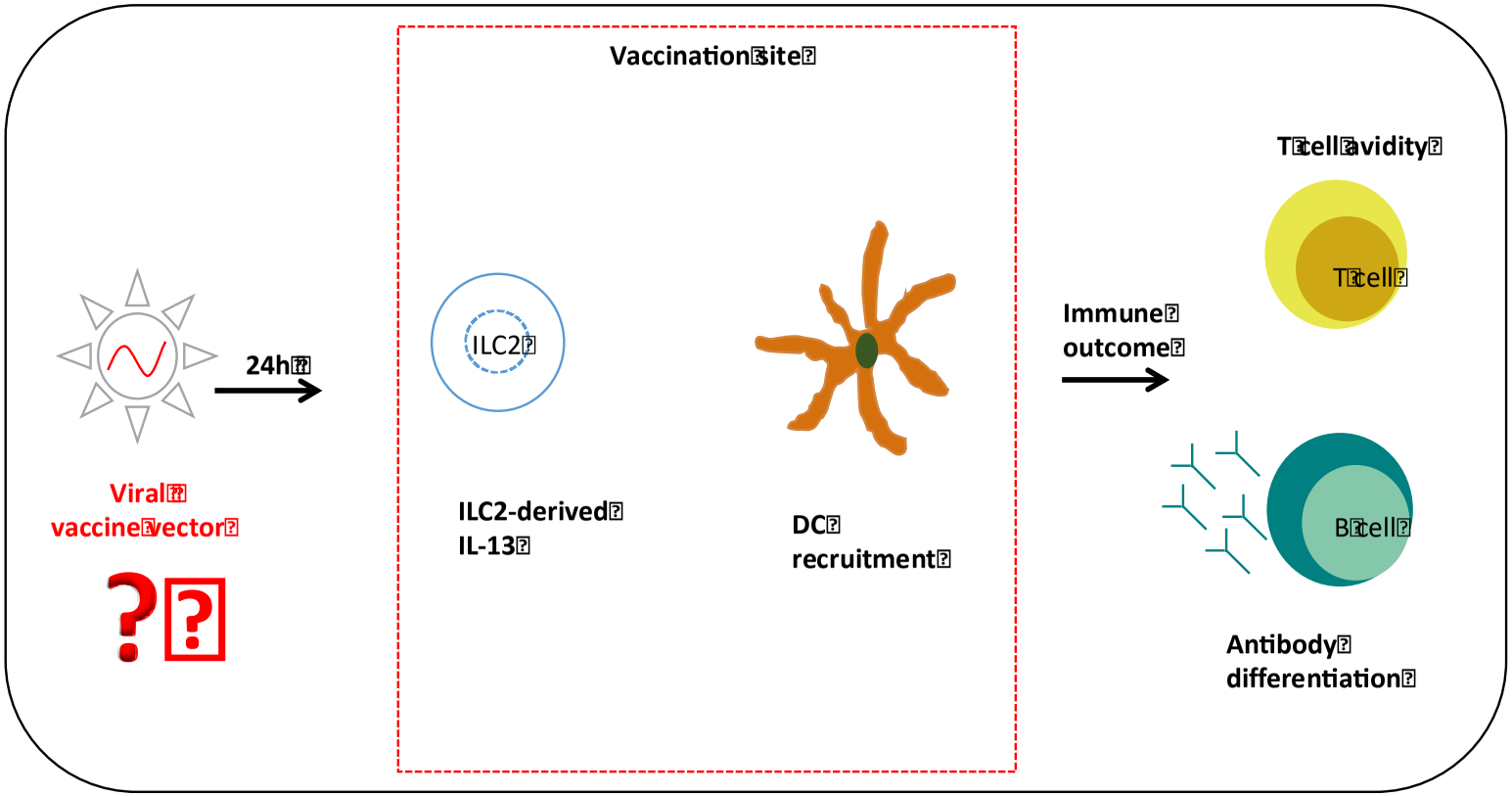
Vaccination site
24h
Viral vaccine vector
ILC2
ILC2-derived IL-13
DC recruitment
Immune outcome
T cell avidity
T cell
B cell
Antibody differentiation

Figure 1.10. Schematic scope of the thesis. Previous studies in the laboratory have shown that despite encoding similar immunogens, viral vectors used for vaccine delivery significantly influenced the quality of adaptive immune outcomes in an IL-13 dependent manner. Furthermore, recent studies have also shown that the ILC2 are the major source of IL-13 at the vaccination site. Modulating IL-13 levels at the vaccination site has also shown to influence the local cDC recruitment. Knowing that different lung DCs can differentially activate T cells, giving rise to vastly different immune outcomes, firstly, this thesis evaluated the ILC and DC profiles recruited following differential intranasal viral vector-based vaccination. Also knowing that IL-13 can impact DC recruitment, this thesis also focused on evaluating the effect of viral vector on the IL-13 receptor expression and regulation, which crucially mediates lung DC responses during the early stages of vaccination.

1.10 Scope of the thesis

1.10.1 Hypotheses

1. Different viral vector-based vaccines induce uniquely different adaptive immune outcomes by differential DC recruitment, mainly associated with ILC2-derived IL-13 levels at the vaccination site.
2. Level of IL-13 at the vaccination site differentially regulates IL-13Rα2 and IL-13Rα1 on lung cDCs, which is co-regulated by transcription factors STAT3 and STAT6.
3. Differential regulation of IL-4/IL-13 receptors on lung DCs 24-72 h post delivery, governs the unique vaccine-specific adaptive immune outcomes induced by different recombinant poxviral vector-based vaccines (expressing the same vaccine antigen).

1.10.2 Aims

1. Study the influence of lung ILC2-derived IL-13 levels on lung DC recruitment, 24 h post intranasal poxviral and non-poxviral vector-based vaccination.
2. Assess how IL-4/IL-13 receptors and related downstream molecules are regulated on lung cDCs 24 h post recombinant viral vector-based vaccination.
3. Using four different poxviral vector-based vaccines, assess how IL-4/IL-13 receptors are regulated on different lung DC subsets, 24 - 72 h post vaccination.

In this thesis, the results section is divided into three chapters:

Chapter 3: Recent studies by Li *et al,* using transient inhibition of IL-13 and STAT6 signalling at the vaccination site have shown that ILC2 were the major source of IL-13 at the vaccination site, 24 h post rFPV vaccination [306], responsible for modulating downstream adaptive immune outcomes both in mice and macaques (specifically modulating T cell avidity and B cell immunity) [122-124]. Trivedi *et al.* also showed that manipulating IL-13 levels at the vaccination site significantly altered resident lung cDC recruitment and downstream T cell outcomes [308]. Knowing that route of delivery and different viral vector-based vaccines can induce vastly different antigen-specific immune outcomes [130,131,133,308], this study attempted to dissect the underlying mechanisms by which innate immune cells, notably ILC and DC regulated vaccine-specific immune outcomes. Specifically, assess whether there was any association between the level of ILC2-derived IL-13 and the DCs recruited to the vaccination site, 24 h post delivery, using 7 different viral vector-based vaccines (4 poxviral and 3 non-poxviral).

Chapter 4: Knowing that IL-13 can promote chronic inflammatory conditions as well as certain infections [259,271,272], and studies in our laboratory have shown that IL-13 levels at the vaccination site can differentially regulate/recruit lung cDCs to the lung mucosae 24 h post vaccination [99], this study evaluated the mechanisms by which viral vector-induced ILC2-derived IL-13 levels regulate the lung cDC response following intranasal vaccination. Specifically, 24 h post intranasal poxviral vector-based vaccination, this study evaluated the expression of IL-4/IL-13 receptor and associated immunomodulatory molecules (STAT3, STAT6, TGF-β1 and IFN-γR) on lung cDCs.

Chapter 5: Dysregulation of IL-13 receptors have shown to promote several disease conditions associated with different IL-13 conditions. Whilst IL-13Rα1 is the low affinity receptor, IL-13Rα2 is the high affinity receptor for IL-13. Interestingly, under high IL-13 conditions, IL-13Rα1 has been central in mediating allergic asthma and chronic inflammation [262,282], and the lesser understood IL-13Rα2 has been deemed instrumental in promoting certain diseases conditions, [309-311]. In contrast, under low IL-13 conditions, IL-13Rα1 has also been shown to promote homeostasis and induce tissue repair [310,312]. Hence, these studies clearly demonstrate that IL-13 receptors can be differentially regulated under different IL-13 conditions. Therefore, given that post viral vector vaccination, level of IL-13 at the vaccination site were found to differentially regulate DC responses (chapters 3 & 4), in this chapter, regulatory patterns of IL-13Rα1 and IL-13Rα2 were evaluated on lung DCs, 24 to 72h post four different recombinant HIV poxviral vector-based vaccines (which were found to induce different ILC2-derived IL-13 levels at the vaccination site).

Chapter 2

General Materials[1]

[1] All methods used in the thesis have been mentioned in specific chapters which have been also compiled as journal articles.

Table 2.1 Medium

Name	Component	Company	Catalogue no.
Complete RPMI medium	RPMI 1640 (500ml) HI-FCS (35ml) 1M HEPES (10ml) Penicillin-Streptomycin (0.5ml) 100mM sodium pyruvate β-mercaptoethanol	Sigma GIBCO GIBCO JCSMR GIBCO GIBCO	R8758 10099-133 15630-080 N/A 11360070 M-6250
Complete Essential Medium (MEM)	MEM 5% (v/v) FCS 1mM HEPES 30ug/ml penicillin-G 50ug/ml streptomycin 50ug/ml neomycin	GIBCO/Sigma Invitrogen Invitrogen Sigma Sigma Sigma	M-4655 10437028 15630-080 021156065 S6501 N-6386
RPMI medium (wash medium)	RPMI 1640 (500ml) 10 mM HEPES	Sigma Invitrogen	R8758 15630-080

Table 2.2 Buffers and solutions

Name	Component	Company	Catalogue no.
Lung Digestion Buffer	1 ml Complete RPMI 1 mg/ml Collagenase	Sigma Sigma	R8758 C2139

	1.2 mg/ml Dispase 5 Units/ml DNase	GIBCO Calbiochem	17105-041 26095
Red Blood Cell Lysis Buffer (RBC-LB)	0.16 mM NH4Cl 0.17M Tris HCL (pH 7.6)	Sigma	A0171
FACS buffer	PBS 2% FCS	Sigma GIBCO	D8537-500ML 10099-133
Intracellular Fixation Buffer (IC-Fix)	IC-Fix	Biolegend	420801
Intracellular Permeabilisation buffer (IC-Perm)	10% 10X IC-PERM 90% dH_2O	eBioscience JCSMR	00-8333-56 N/A
Paraformaldehyde (PFA)	0.5% (w/v) PFA in PBS	Sigma	P-6148
Brefeldin A (BFA)	1:1000 working dilution in complete RPMI medium	eBioScience	00-4506-51
Phosphate Buffer Saline (PBS)	1X PBS	Sigma	D8537
Poly-L-Lysine solution	0.1% (w/v) in H_20	Sigma	P1274
Antifade Vectashield mounting medium for fluorescence with	10µl per slide	Vector Laboratories, USA	H-1200

4′,6-diamidino-2-phenylindole (DAPI)			
Antifade Vectashield mounting medium for fluorescence	10µl per slide	Vector Laboratories, USA	H-1000

Table 2.3 Anti-mouse antibodies used for flow cytometry

Antibody	**Fluorochrome**	**Working dilution**	**Company**	**Clone**
CD3	FITC	1:200	BioLegend	17A2
CD19	FITC	1:100	BioLegend	6D5
CD11b	FITC	1:200	BioLegend	M1/70
CD11c	FITC	1:100	BioLegend	N418
CD49b	FITC	1:200	BioLegend	HMα2
FcεRI	FITC	1:100	BioLegend	MAR-1
CD45	APC/Cy7	1:200	BioLegend	30-F11
ST2	PE	1:100	BioLegend	DIH9
IL-25R	APC	1:100	BioLegend	9B10
NKp46	Brilliant Violet 421	1:100	BioLegend	29A1.4
IFN-γ	Brillian Violet 510	1:100	BioLegend	XMG1.2
IL-17A	Alexa Fluor 700	1:100	BioLegend	TC11-18H10.1
IL-13	PE-eFLuor 610	1:100	eBioscience	eBio13A

TSLPR	APC	1:100	R&D	FAB5461A
MHC-II I-A^d	APC	1:1600	eBioscience	M5/114.15.2
CD11c	Biotin	1:200	BioLegend	N418
Streptavidin	Brilliant Violet 421	1:400	BioLegend	N/A
CD8	APC-eFluor780	1:300	eBiosceince	53-6.7
B220	PerCPCy5.5	1:300	eBioscience	RA3-6B2
CD11b	Alexa Fluor 700	1:300	BioLegend	M1170
CD103	FITC	1:200	eBioscience	2E7
7-amino-actinomycin D viability staining solution (7AAD)	N/A	1:100	BioLegend	N/A
IL-4Rα	PE	1:100	BioLegend	I015F8
IL-13Rα1	PE	1:100	eBioscience	13MOKA
IL-13Rα2	Biotin	1:100	R&D	110815
Streptavidin	PE	1:100	BioLegend	N/A
IFN-γRα	Biotin	1:400	BioLegend	2E2
Streptavidin	APC	1:100	BioLegend	N/A
γc	PE	1:100	BioLegend	TUGm2

p-Stat3	Biotin	1:100	Santa Cruz Biotechnology	Tyr 705
p-Stat6	Biotin	1:100	Santa Cruz Biotechnology	Tyr 641
TGF-β1	PE	1:100	BioLegend	Tw7-16B4
Fc block	N/A	1:200	BD Biosciences	2.4G2

Table 2.4 Viral vector based vaccines and doses used to immunize mice

Virus	**Dose (pfu/mouse)**	**Family**
Recombinant fowlpox virus expressing HIV-1 (rFPV)	2×10^7	Poxviridae
Recombinant Vaccinia Virus expressing HIV-1 (rVV)	2×10^7	Poxviridae
Recombinant Modified Vaccinia Ankara expressing HIV-1 (rMVA)	2×10^7	Poxviridae
IL-1βR deletion variant of rMVA expressing HIV-1 (rMVA-ΔIL-1βR)	2×10^7	Poxviridae
Influenza A vector	500	Orthomyxoviridae

Recombinant human Rhinovirus serotype 1A (RV)	$5x10^6$ $TCID_{50}$	Picornaviridae
Adenovirus 5 (Ad5)	2×10^7	Adenoviridae

Table 2.5 Reagents for Fluidigm 48.48 Biomark Assay

Preamplification mix (single cell) per reaction (5ul)	Cells Direct 2x reaction buffer	2.5 µL	Invitrogen
	SuperScript® III RT/Platinum® Taq Mix*	0.1 µL	Invitrogen
	0.2x pooled assays	1.25 µL	Invitrogen
	SUPERase• In™ RNase Inhibitor	0.05 µL	Invitrogen
	DEPC treated water	1.1 µL	Ambion
Preamplification mix (100 cell) per reaction (20 ul)	Cells Direct 2x reaction buffer	10 µL	Invitrogen
	SuperScript® III RT/Platinum® Taq Mix*	0.4 µL	Invitrogen

	0.2x pooled assays	0.5 µL per assay diluted in DEPC treated water in a total volume of 5 µL	Invitrogen
	SUPERase• In™ RNase Inhibitor	0.2 µL	Invitrogen
	DEPC treated water	4.4 µL	Ambion
Preamplification mix (100 cell) per reaction (25 ul)	Cells Direct 2x reaction buffer	12.5 µL	Invitrogen
	SuperScript® III RT/Platinum® Taq Mix*	0.5 µL	Invitrogen
	0.2x pooled assays	0.5 µL per assay diluted in DEPC treated water in a total volume of 6.25 µL	Invitrogen
	SUPERase• In™ RNase Inhibitor	0.25 µL	Invitrogen
	DEPC treated water	5.5 µL	Ambion
Taqman qPCR mix	20X Taqman	0.5 µL	Thermofisher

per reaction (10 µL)	gene expression assay		
	2X Taqman PCR universal mastermix	5 µL	Applied Biosystems
	Diluted cDNA template	1 µL	See section 2.3.5
	DEPC treated water	3.5 µL	Ambion
Fluidigm sample premix per inlet (5 µL)	2X Taqman PCR universal mastermix	2.5 µL	Applied Biosystems
	20X GE sample loading reagent	0.25 µL	Millennium Biosciences
	cDNA	2.25 µL	
Fluidigm assay premix per inlet (5 µL)	20X Taqman gene expression assay	2.5 µL	Thermofisher
	Assay loading reagent	2.5 µL	Millennium Biosciences

Table 2.6. Primer probe sets used for Fluidigm Biomark 48.48 gene expression assay

Gene symbol	Encoded protein	Assay ID	Reference sequence

Ifngr1	IFN-γ receptor subunit 1	Mm00599890_m1	NM_010511.2
Icos	Inducible T-cell costimulatory (ICOS)	Mm00497600_m1	NM_017480.2
Tgfb1	Transforming growth factor beta 1	Mm01178820_m1	NM_011577.2
Stat6	Signal transducer and activator (STAT) 6	Mm01160477_m1	NM_009284.2
Stat3	STAT3	Mm01219775_m1	NM_213660.3 NM_011486.5 NM_213659.3
Cd86	T-lymphocyte activation antigen	Mm00444543_m1	NM_019388.3
Siglech	Sialic acid binding Ig-like lectin H (SiglecH)	Mm00618627_m1	NM_178706.5 NM_001310738.1 NM_001310740.1
Rpl32	Ribosomal protein L32	Mm02528467_g1	NM_172086.2
Ywhas	Stratifin	Mm02524691_s1	NM_018754.2
Eef2	Eukaryote elongation factor 2	Mm01171435_gH	NM_007907.2

Chapter 3

Viral vector and route of administration determine the ILC and DC profiles responsible for downstream vaccine-specific immune outcomes2

This chapter is published as: ***Roy, S.,*** *Jaeson, M.I., Li, Z., Mahboob, S., Jackson, R.J., Grubor-Bauk, B., Wijesundara, D.K., Gowans E.J., and Ranasinghe, C. Viral vector and route of administration determine the ILC and DC profiles responsible for downstream vaccine-specific immune outcomes. Vaccine 2019.*

---

[2] The chapter related ILC experiments were performed by Ms. Shaaerah Mahboob, Mr. Irwan Jaeson and Dr. Zheyi Li.

3.1 Abstract

This study demonstrates that route and viral vector can significantly influence the innate lymphoid cells (ILC) and dendritic cells (DC) recruited to the vaccination site, 24 hours post delivery. Intranasal (i.n.) vaccination induced ST2/IL-33R$^+$ ILC2, whilst intramuscular (i.m.) induced IL-25R$^+$ and TSLPR$^+$ (Thymic stromal lymphopoietin protein receptor) ILC2 subsets. However, in muscle a novel ILC subset devoid of the known ILC2 markers (IL-25R$^-$ IL-33R$^-$ TSLPR$^-$) were found to express IL-13, unlike in lung. Different viral vectors also influenced the ILC-derived cytokines and the DC profiles at the respective vaccination sites. Both i.n. and i.m. recombinant fowlpox virus (rFPV) priming, which has been associated with induction of high avidity T cells and effective antibody differentiation exhibited low ILC2-derived IL-13, high NKp46$^+$ ILC1/ILC3 derived IFN-γ and low IL-17A, together with enhanced CD11b$^+$ CD103$^-$ conventional DCs (cDC). In contrast, recombinant Modified Vaccinia Ankara (rMVA) and Influenza A vector priming, which has been linked to low avidity T cells, induced opposing ILC derived-cytokine profiles and enhanced cross-presenting DCs. These observations suggested that the former ILC/DC profiles could be a predictor of a balanced cellular and humoral immune outcome. In addition, following i.n. delivery Rhinovirus (RV) and Adenovius type 5 (Ad5) vectors that induced elevated ILC2-derived IL-13, NKp46$^+$ ILC1/ILC3-derived-IFN-γ and no IL-17A, predominantly recruited CD11b$^-$ B220$^+$ plasmacytoid DCs (pDC). Knowing that pDC are involved in antibody differentiation, we postulate that i.n. priming with these vectors may favour induction of effective humoral immunity. Our data also revealed that vector-specific replication status and/or presence or absence of immune evasive genes can significantly alter the ILC and DC activity.

Collectively, our findings suggest that understanding the route- and vector-specific ILC and DC profiles at the vaccination site may help tailor/design more efficacious viral vector-based vaccines, according to the pathogen of interest.

3.2 Introduction

In the last two decades, inactivated, live attenuated, replication-competent or -defective viruses have been extensively tested as viral vector-based vaccines. Interestingly, poxviruses such as Modified Vaccinia Ankara (MVA), New York strain of vaccinia virus (NYVAC), which are attenuated versions of vaccinia virus (VV), and Avipoxvirus; canarypox and fowlpox (FPV) viruses, used in prime-boost modalities have yielded uniquely different immune outcomes, dependent upon the route of delivery and/or the vaccine vector combination [121,131,159,313]. For example, heterologous rFPV/rVV compared to rVV/rFPV vaccination has shown to induce highly poly-functional/ high avidity T cells [131,133,205,314], moreover, rMVA used as a booster, as opposed to a prime has shown to induce more effective T cell immunity [138,143,315]. Similarly, both replication-competent and -defective recombinant Adenovirus-based vaccines have also shown to induce T cell responses associated with immune protection in animal models [118,140,316]. Moreover, viruses such as, Influenza A, Human RV, Cytomegalovirus, and Vesicular stomatitis virus, have also been assessed as promising vaccine delivery vehicles [220,315,317,318]. In a recent prime-boost vaccination study, mucosal RV prime vaccination was shown to induce HIV-specific T cell responses associated with protection in mice [245]. To improve vaccine-specific immunity, variants of viral vectors, such as IL-1βR and/or IL18 binding protein (IL-18bp) deletion mutants of MVA and Adenoviral vectors have also been recently tested [229,319,320]. Despite the knowledge of different viral vector-based vaccines conferring different adaptive immune outcomes, the underlying innate immune mechanisms governing these processes at the vaccination site still remains

elusive, specifically the role of innate lymphoid cells (ILCs) and dendritic cells (DCs).

ILCs, although derived from a common progenitor are lineage negative in nature and according to the transcription factors, receptors and cytokines they express, are broadly classified into three main categories (ILC1, ILC2 and ILC3) [321]. ILC2, due to their ability to express IL-13, have been heavily studied under chronic inflammation, allergic asthma and helminth infections [322]. During intracellular pathogen infection, ILC1 have shown to express IFN-γ and tumour necrosis factor (TNF)-α [323], whilst during extracellular bacterial and fungal infections, ILC3 have been associated with interleukin (IL)-17A and IL-22 expression [324,325]. Although ILCs have three distinct phenotypes, studies have shown that they have the ability to interconvert between the phenotypes, according to the external stimuli, and thus thought to be highly plastic [326,327]. It is postulated that ILCs can polarize the immune response, according to the immune cell milieu or pathogen encountered, towards Th1, Th2 or Th17 immunity. However, the role of ILCs in viral vector-based vaccination is not well characterised.

DCs sample antigens at various body surfaces; skin, gastrointestinal tract and lungs, and are among the first line of defence against many pathogens. Based on the anatomical location and the invading pathogen, distinct DC subsets carry out differential functions [328]. For example; lung DCs have been extensively studied under respiratory infections. Lung conventional $CD11b^{+}$ $CD103^{-}$ DCs (cDCs) and cross-presenting $CD11b^{-}$ $CD103^{+}$ DCs have been associated with CD8 T cell priming [329,330]. Although conflicting evidence suggest that cDCs are

functionally more important in mounting an effective antiviral response [75,331], there is growing evidence to support the notion that the activity of a particular DC subset is determined by the specific infection. For example: control of acute influenza virus infection is associated with CD11b$^-$ CD103$^+$ DCs cross presentation to CD8 T cells [332], whilst, CD11b$^-$ CD8$^+$ DCs, which share a common developmental origin with CD11b$^-$ CD103$^+$ DCs, have been associated with activation of cytotoxic CD8 T cells against non-respiratory pathogens such as West Nile Virus [333]. In the context of respiratory syncytial virus (RSV) infection, CD11b$^+$ and CD103$^+$ DC subsets have been involved in antigen presentation to both CD4 and CD8 T cells [72]. In addition, during Influenza A infection, CD11b$^+$ DCs have also been associated with humoral immunity [86]. Furthermore, plasmacytoid DCs (pDCs) also have been associated with distinct functions during viral infections [334,335].

It is now well established that the route of delivery, cytokine milieu, viral vectors and the order in which they are administered can yield vastly different adaptive immune outcomes [128,131,133,205,336]. We have previously shown that i) IL-13, although detrimental for high avidity/poly-functional CD8 T cell immunity, was necessary for effective antibody differentiation [122,124,337]. ii) Using rFPV adjuvanted vaccines that transiently inhibited IL-13 activity at the vaccination site, we have recently established that ILC2 (not other lineage$^+$ cells) were the major source of IL-13 at the vaccination site 24 h post vaccination [338]. iii) Furthermore, using the same vaccines we have also shown that elevated IL-13 in the milieu recruited CD11b$^-$ CD103$^+$ cross-presenting DCs, associated with low avidity CD8 T cells [99,124]. Therefore, in this study to further understand which specific innate

immune cell subsets play a predominant role in shaping the downstream adaptive immune outcomes, replicating and non-replicating viral vectors were delivered intranasally and intramuscularly and subsequent ILC-derived cytokine profiles and DCs subsets were assessed 24 h post vaccination.

3.3 Materials and Methods

3.3.1 Mice.

Pathogen-free 6–8 weeks old female BALB/c mice were purchased from the Australian Phenomics Facility, The Australian National University. All animals were maintained, monitored daily and cervically dislocated at the endpoint according to the Australian NHMRC guidelines within the Australian Code of Practice for the Care and Use of Animals for Scientific Purposes and in accordance with guidelines approved by the ANU Animal Experimentation and Ethics Committee (AEEC), protocol number A2014/14 and A2017/15.

3.3.2 Viral vector-based Vaccines.

Recombinant FPV, VV and MVA expressing HIV antigens described previously were used in this study [190,338]. The rMVAΔIL-1βR was constructed and kindly provided by Dr. Jackson. Influenza A and Adenovirus 5 (Ad5) vectors were kindly provided by Prof. Arno Mullbacher, JCSMR, ANU. Recombinant Human Rhinovirus serotype 1A (RV) was kindly provided by Prof. Gowans and Dr. Wijesundara, Basil Hetzel Institute, University of Adelaide [220].

3.3.3 Immunisation.

BALB/c mice were intranasally or intramuscularly immunised with $1x10^7$ plaque forming units (pfu) of each of the poxviruses rFPV, rVV, rMVA, rMVA-ΔIL-1βR; $2x10^7$ pfu (i.n.) or $2.5x10^7$ pfu (i.m.) of Ad5, $5x10^6$ $TCID_{50}$ of RV or 500 pfu of Influenza A. Note that, doses used were comparable to those used in previous studies, optimal to induce adaptive immune outcomes. Mice were vaccinated with 10 µl per nostril (i.n.) or 50 µL per leg (i.m.) under mild isofluorane anaesthetic. rFPV, rVV, rMVA, rMVA-ΔIL-1βR were sonicated three times for 15 seconds on ice at 50% capacity using Branson Sonifier 450 immediately prior to vaccination.

3.3.4 Preparation of lung lymphocytes.

Lung tissues were collected 24 h post vaccination in complete RPMI for ILC studies as described previously [338]. For DC studies, lungs were harvested at 12, 24 and 48 hours post vaccination. Lung tissues were prepared as described previously [338]. Briefly, tissues were cut into small pieces, and enzymatically digested for 45 min at 37°C in digestion buffer containing 1 mg/ml collagenase (Sigma-Aldrich, St Louis, MO), 1.2 mg/ml Dispase (Gibco, Auckland, NZ), 5 Units/ml DNase (Calbiochem, La Jolla, CA) in complete RPMI. Samples were crushed and passed through a 100µm falcon cell strainer and resulting lung cell suspensions were then treated with red cell lysis buffer followed by extensive washing to remove the lysis buffer. Samples were then passed through gauze to remove debris, cells were re-suspended in complete RPMI, rested overnight at 37°C under 5% CO_2 as per our previous studies prior to staining [124,205].

3.3.5 Preparation of muscle lymphocytes.

Muscle tissues were harvested 24 h post vaccination in complete RPMI and prepared as previously indicated [338]. Briefly, tissues were, homogenised and enzymatically digested for 45 min at 37°C in a digestion buffer containing 2 mg/mL collagenase, 2.4 mg/mL dispase and 5 Units/mL of DNAse in complete RPMI. Subsequently, samples were very gently pushed through a 70 μM Falcon cell strainer, to avoid debris. Resulting cell suspension was then washed, resuspended in complete RPMI and rested overnight as per lung prior to staining [124,205]

3.3.6 Evaluation of lung and muscle ILCs using flow cytometry.

Monoclonal antibodies FITC-conjugated anti-mouse CD3 (T cells) clone 17A2, CD19 (B cells) clone 6D5, CD11b (macrophages and dendritic cells) clone M1/70, CD11c (dendritic cells) clone N418, CD49b (NK, NKT, T cells) clone HMα2, FcεRIα (Mast cells and Basophils) clone MAR-1 (all linage positive markers were selected as FITC), PE-conjugated anti-mouse ST2/IL-33R (clone DIH9), APC-conjugated IL-25R (clone 9B10), APC/Cy7-conjugated anti-mouse CD45 (clone 30-F11), Brilliant Violet 421-conjugated anti-mouse CD335 (NKp46) (clone 29A1.4), Brilliant Violet 510-conjugated anti-mouse IFN-γ (clone XMG1.2), Alexa Fluor 700-conjugated IL-17A (clone TC11-18H10.1) were obtained from BioLegend. PE-eFluor 610-conjugated anti-mouse IL-13 (clone eBio13A) was purchased from eBioscience and APC- conjugated anti-mouse TSLPR R&D systems. ILC2 and ILC1/3s were stained separately to avoid fluorochrome overlap. Specifically, FITC-conjugated lineage cocktail antibodies and APC/Cy7-conjugated anti-mouse CD45 were used in both ILC2 and ILC1/ILC3 staining. For lung and muscle ILC2 staining, PE-conjugated anti-mouse ST2/IL-33R, and PE-

eFluor 610-conjugated anti-mouse IL-13 were used and for muscle ILC2 staining, additionally APC-conjugated IL-25R and APC-conjugated anti-mouse TSLPR were used. Brilliant Violet 421-conjugated anti-mouse NKp46, Brilliant Violet 510-conjugated anti-mouse IFN-γ, Alexa Fluor 700-conjugated IL-17A were only used in ILC1/3s staining. Briefly, for intracellular staining, samples were treated with Brefeldin A for 5 hours, washed, cell surface staining was performed followed by and intracellular staining after fixing and permeabilising the cells as per our previous protocols[124]. Once the staining was completed all samples were fixed with 0.5% paraformaldehyde, 1.4 x 10^6 events from each lung sample were acquired and 3.0 x 10^6 events were acquired for muscle on a BD LSR Fortessa. Data were analysed using Tree Star FlowJo software (version 10.0.7) using gating strategies indicated in **Chapter 3 Appendix Figures 1 and 2.**

3.3.7 Evaluation of lung DCs using Flow cytometry.

2x10^6 cells were blocked with anti-mouse CD16/CD32 Fc Block antibody (BD Biosciences, USA) for 20 min at 4°C and cells were surface stained with APC conjugated MHCII I-Ad (e-Biosciences, USA), biotin conjugated CD11c (N418 clone, Biolegend, USA), followed by streptavidin Brilliant violet 421 (Biolegend, USA) and other DC markers CD8 APC-eFluor780 (53–6.7 clone, ebiosciences, USA), B220 PercpCy5.5 (RA3-6B2 clone, e-Biosciences, USA), CD11b AlexaFluor 700 (M1170 clone, Biolegend, USA) and CD103 FITC (2E7 clone, e-Biosciences, USA) for 30 min on ice. Cells were resuspended in PBS and analysed using BD LSRII flow cytometer Becton Dickinson, San Diego, CA). 5x10^5 events per sample were collected and results were analyzed using FlowJo software version 10.0.7, as described in **Figures 3.1 – 3.3.** Note that, live/dead

staining was also performed using viability dye 7-amino-actinomycin D (7-AAD Biolegend, USA) **(Figures 3.1).**

3.3.8 Statistical analysis.

Cytokine expression by ILCs was calculated as a percentage of the parent ILC subset**.** To depict the differences in IL-13 expression, following i.n. vs i.m. vaccinations, number of ILC2 expressing IL-13 were also back calculated to $CD45^+$ population and normalized to $1x10^6$. The muscle ILC2 subset percentages were calculated as (subset of interest/Lin^- population x 100%). The DC subsets were represented as a percentage of total MHC-II^+ $CD11c^+$ DCs. The *p*-values were calculated using two-tailed paired parametric student's t-test, unpaired parametric student's t-test or Ordinary One-way ANOVA with Tukey's multiple comparison post-test. All experiments were repeated minimum 2-3 times.

3.4 Results

3.4.1 Different viral vector-based vaccines can induce uniquely different ILC2-derived 13 profiles following intranasal and intramuscular vaccination.

BALB/c mice were vaccinated intranasally or intramuscularly with four different poxviral vectors rFPV, rMVA, rVV and rMVAΔIL-1βR and three non-poxviral vectors Influenza A, Human rhinovirus (RV) and Adenovirus type 5 (Ad5). Percentage of lung and muscle ILC2 and their corresponding IL-13 expression were assessed 24 h post vaccination. ILC2 were gated as $CD45^+$ FSC^{low}, SSC^{low}, $lineage^-$ ST2/IL-$33R^+$ cells for lung **(Chapter 3 Appendix Figure 1)** or $lineage^-$ IL-$25R^+$, $TSLPR^+$ and ST2/IL-$33R^+$ for

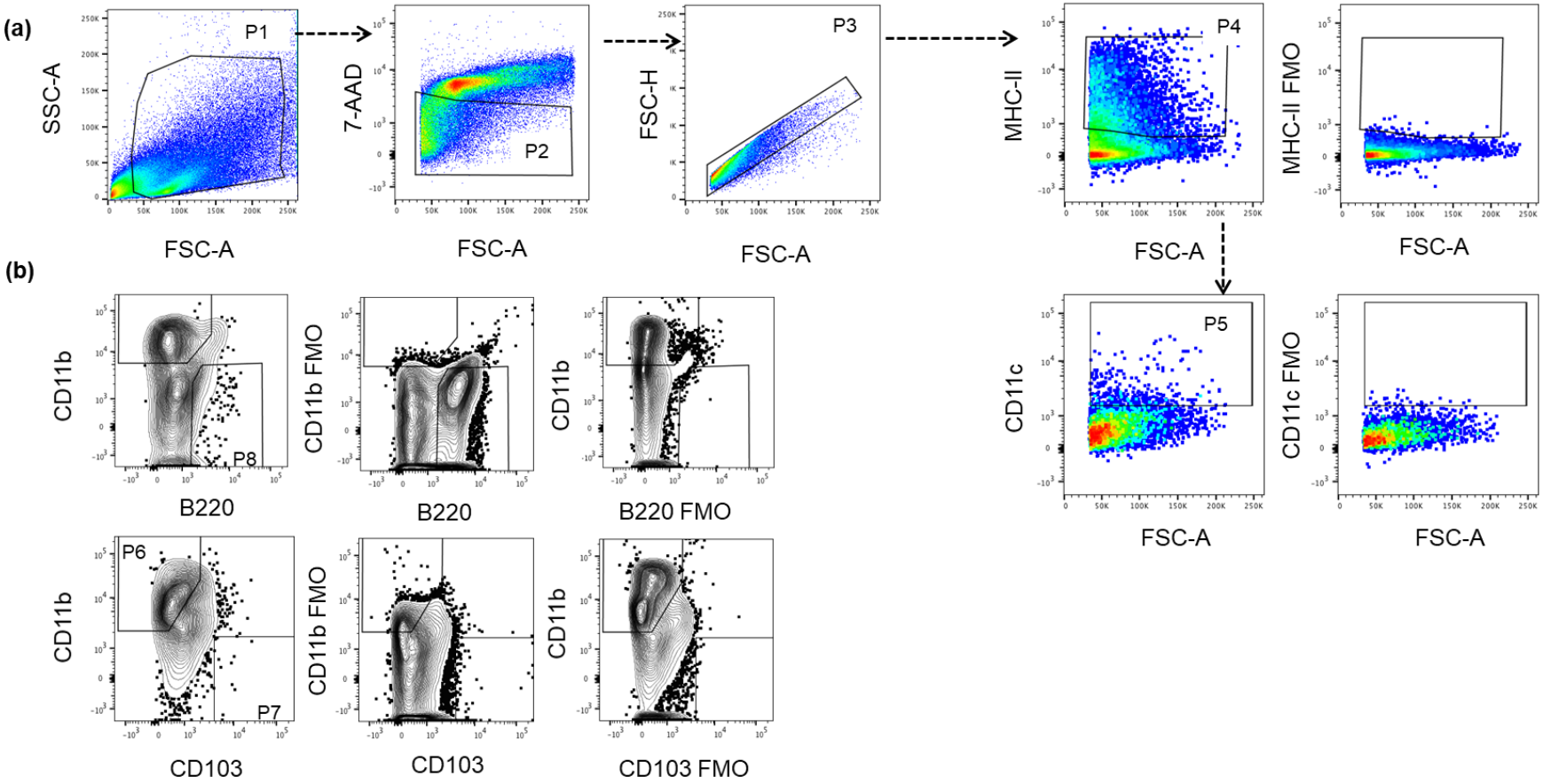
(a)
P1
SSC-A
FSC-A
P2
7-AAD
FSC-A
P3
FSC-H
FSC-A
P4
MHC-II
FSC-A
MHC-II FMO
FSC-A
P5
CD11c
FSC-A
CD11c FMO
FSC-A
(b)
P8
CD11b
B220
CD11b FMO
B220
CD11b
B220 FMO
P6
P7
CD11b
CD103
CD11b FMO
CD103
CD11b
CD103 FMO

Figure 3.1. Flow cytometry gating of DC subsets. Flow cytometry gating strategy used in evaluation of DC subsets in lung following i.n. immunisation. **(a)** Plots show cells pre-gated on cells (P1), viable cells (P2) gated on 7-AAD^{-} cells, followed by doublet exclusion (P3) based on forward scatter (FSC-H and FSC-A). Cells were then gated on MHC-II-I-Ad^{+} (P4) and analysed for CD11c expression compared to the FMO controls. **(b)** Total DCs (MHC-II-I-A^{d+} CD11c^{+} - P5) were further gated on CD11b^{+} CD103^{-} (P6), CD11b^{-} CD103^{+} (P7), CD11b^{-} B220^{+} (P8) DC subsets. Gates were placed compared to FMO controls for each indicated surface marker.

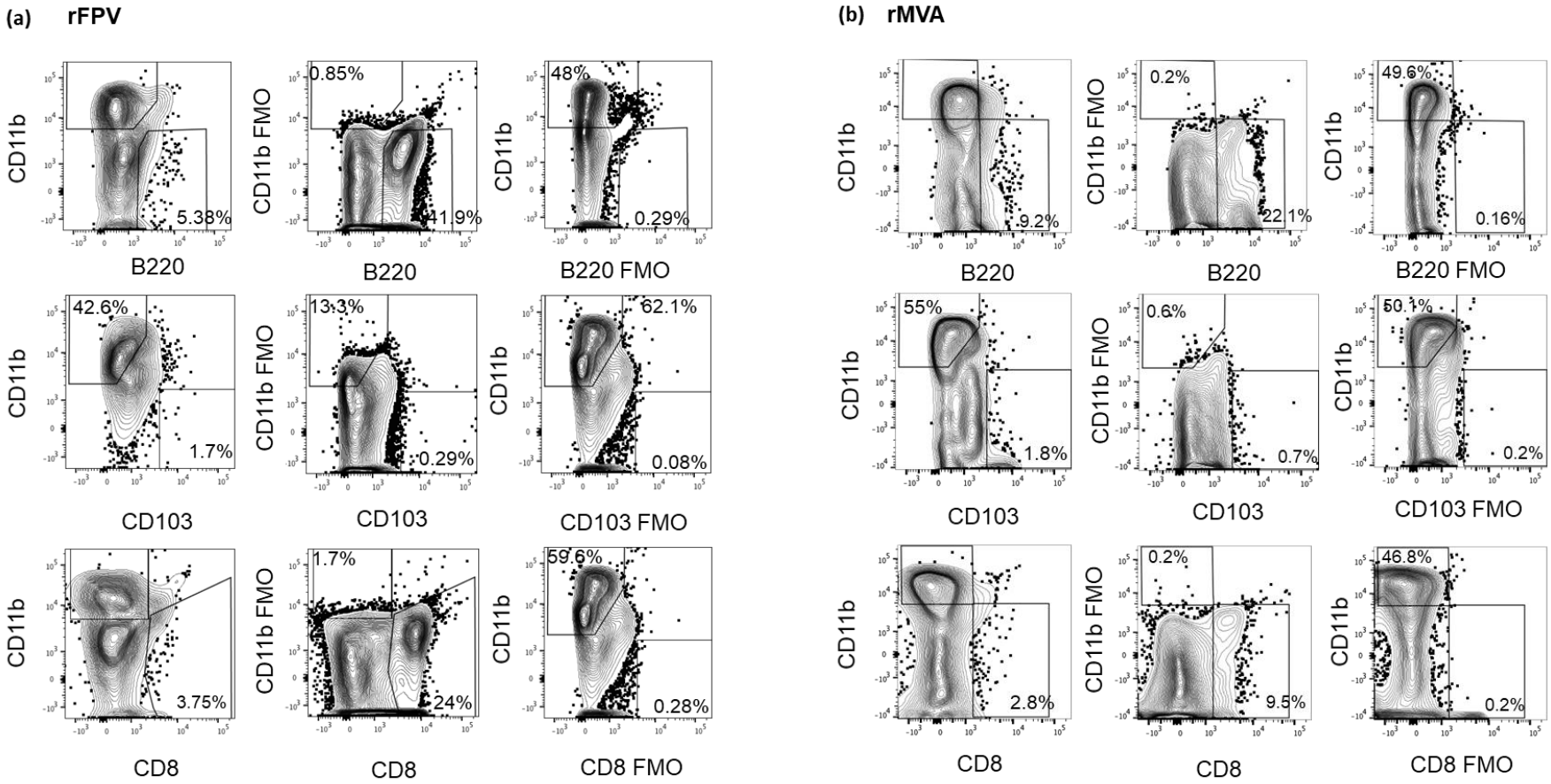
(a) rFPV
CD11b
B220
5.38%
CD11b FMO
B220
0.85%
41.9%
CD11b
B220 FMO
48%
0.29%
CD11b
CD103
42.6%
1.7%
CD11b FMO
CD103
13.3%
0.29%
CD11b
CD103 FMO
62.1%
0.08%
CD11b
CD8
3.75%
CD11b FMO
CD8
1.7%
24%
CD11b
CD8 FMO
59.6%
0.28%
(b) rMVA
CD11b
B220
9.2%
CD11b FMO
B220
0.2%
22.1%
CD11b
B220 FMO
49.6%
0.16%
CD11b
CD103
55%
1.8%
CD11b FMO
CD103
0.6%
0.7%
CD11b
CD103 FMO
50.1%
0.2%
CD11b
CD8
2.8%
CD11b FMO
CD8
0.2%
9.5%
CD11b
CD8 FMO
46.8%
0.2%

Figure 3.2. Viral vector-specific FMO applied to rFPV and rMVA vaccinated samples to gate on each DC subset. Representative FACS plots showing gated DC subsets compared to FMO controls specifically 24h post immunisation with (a) rFPV and (b) rMVA. Lungs were harvested from immunized BALB/c mice and DC subsets were evaluated by flow cytometry as per in Methods. Cells were pre-gated on total antigen-specific dendritic cells (MHC-II-I-Ad^{+} CD11c^{+}) followed by subsequent expression of lineage markers CD11b, CD103, B220 and CD8 determined by viral vector specific FMO controls to identify different lung DC subsets. Based on the similarity of fluorescence patterns of specific DC subsets, the FMO controls used for rFPV and rMVA were used for unimmunised, rMVAΔIL-1βR and rVV samples.

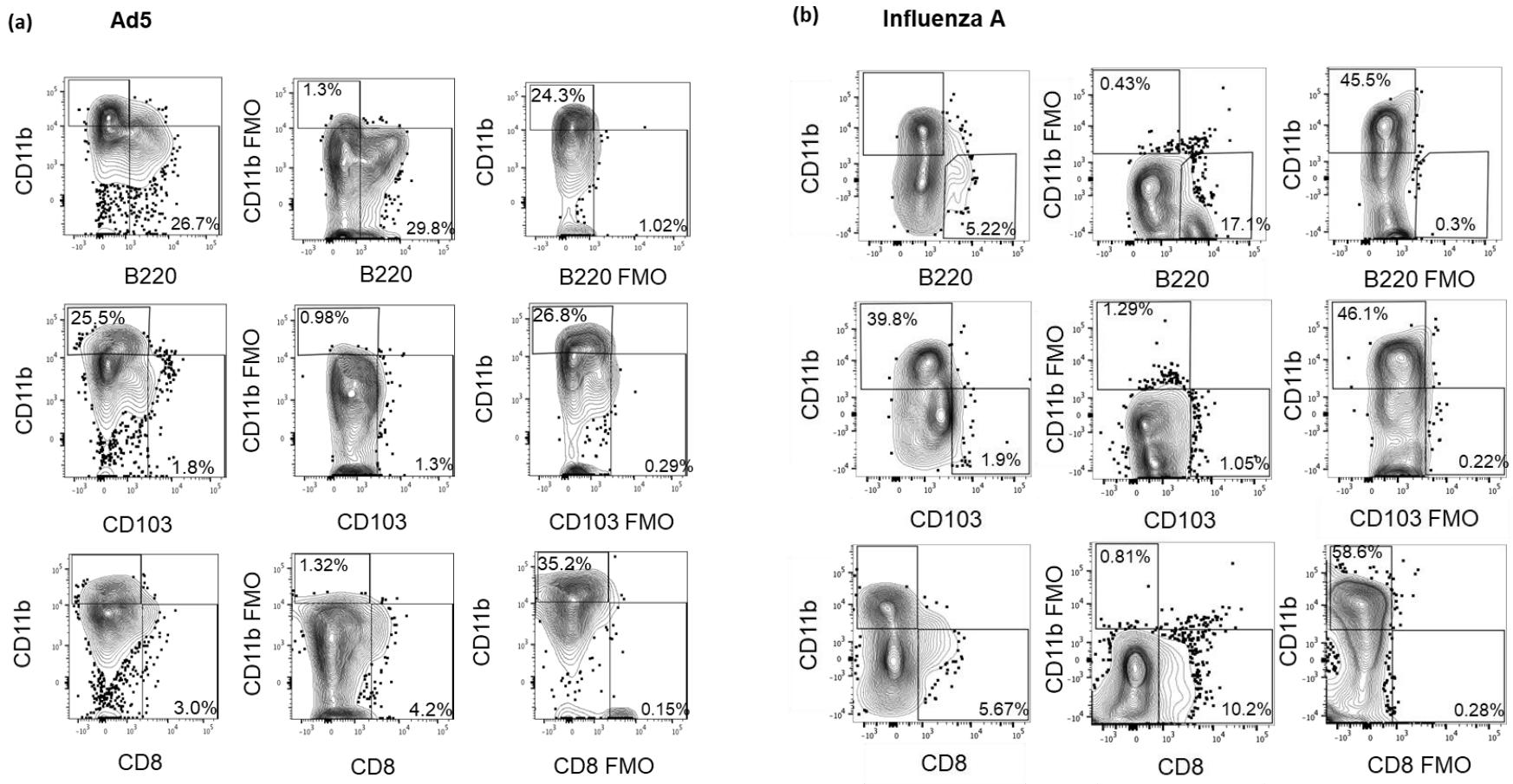
(a)
Ad5
CD11b
B220
26.7%
CD11b FMO
B220
1.3%
29.8%
CD11b
B220 FMO
24.3%
1.02%
CD11b
CD103
25.5%
1.8%
CD11b FMO
CD103
0.98%
1.3%
CD11b
CD103 FMO
26.8%
0.29%
CD11b
CD8
3.0%
CD11b FMO
CD8
1.32%
4.2%
CD11b
CD8 FMO
35.2%
0.15%
(b)
Influenza A
CD11b
B220
5.22%
CD11b FMO
B220
0.43%
17.1%
CD11b
B220 FMO
45.5%
0.3%
CD11b
CD103
39.8%
1.9%
CD11b FMO
CD103
1.29%
1.05%
CD11b
CD103 FMO
46.1%
0.22%
CD11b
CD8
5.67%
CD11b FMO
CD8
0.81%
10.2%
CD11b
CD8 FMO
58.6%
0.28%

Figure 3.3. Viral vector specific FMO showing Ad5 and Influenza A vaccinated group to gate on each DC subset. Representative FACS plots showing gated DC subsets compared to FMO controls specifically 24h post immunisation with **(a)** Ad5 and **(b)** Influenza A. Lungs were harvested from immunized BALB/c mice and DC subsets were evaluated by flow cytometry as per in Methods. Cells were pre-gated on total antigen-specific dendritic cells (MHC-II-I-Ad^{+} CD11c^{+}) followed by subsequent expression of lineage markers CD11b, CD103, B220 and CD8 determined by viral vector specific FMO controls to identify different lung DC subsets. Based on the similarity of fluorescence patterns, the FMO controls used for Ad5 were applied to the RV group.

muscle **(Chapter 3 Appendix Figure 2)**, as indicated in Materials and Methods and Li *et al* 2018 [338]. Among all the vectors tested, following i.n. delivery, Influenza A vector recruited the highest percentage of Lin$^-$ ST2/IL-33R$^+$ ILC2 to the vaccination site (lung mucosae). In contrast, RV and Ad5 recruited the lowest percentage of ILC2, which was much lower than unimmunized control (p=0.0014 *and* p=0.0011 respectively) **(Figures 3.4a and Chapter 3 Appendix Figure 3)**. However, despite this, RV and Ad5 expressed elevated IL-13 levels, which were similar to rMVA and Influenza A **(Figures 3.4b and c)**. Among the three poxviral vectors tested, the highest IL-13 level was detected in rMVA (rFPV vs rMVA p<0.0001, rMVAΔIL-1βR vs rMVA p<0.0001), whilst rMVAΔIL-1βR showed the lowest (rFPV vs rMVAΔIL-1βR p=0.4159) **(Figures 3.4b and c)**. It is also noteworthy that, all the vectors showed significantly elevated IL-13 expression by Lin$^-$ ST2/IL-33R$^+$ ILC2 compared to the unimmunized control (rFPV p=0.0028; rMVA p<0.0001*;* rMVAΔIL-1βR p=0.0412; Influenza A p<0.0001; RV p<0.0001; Ad5 p<0.0001) **(Figures 3.4a-c)**.

Following i.m. vaccination, mainly IL-25R$^+$ ILC2s and TSLPR$^+$ ILC2, ranging from 0.25% to 2% were detected. In the context of IL-25R$^+$ ILC2, rMVA and Ad5 vector vaccination showed significantly elevated numbers compared to unimmunised control (p=0.0183 *and* p=0.0178 respectively)**.** Furthermore, Ad5 vaccination also showed higher proportion of IL-25R$^+$ ILC2s compared to influenza A (p=0.0004) **(Chapter 3 Appendix Figure 4)**. Interestingly, rMVAΔIL-1βR (1.8% average) showed a significantly elevated proportion of TSLPR$^+$ ILC2 compared to rFPV and rMVA vaccination (p<0.0001 and p=0.0240 *respectively*) **(Chapter 3 Appendix Figure 4)**. Ad5 also showed elevated TSLPR$^+$ ILC2s compared to rFPV and influenza A vaccination (p=0.0103 and p=0.0006 *respectively*)

(Chapter 3 Appendix Figure 4). Following i.m. vaccination, similar to our previous studies extremely low or no ST2/IL-33R$^+$ ILC2 were detected with all vaccine groups tested **(Chapter 3 Appendix Figure 4)**.

Surprisingly, following i.m. delivery, canonical ILC2 subsets (IL-25R$^+$, TSLPR$^+$) were found to express marginal IL-13. In contrast, compared to the unimmunised control, a not yet defined ILC2 subset that lacked IL-25R, ST2/IL-33R and TSLPR were found to express IL-13 **(Chapter 3 Appendix Figures 5 and 6)**. Out of the vectors tested, Ad5 showed remarkably higher proportion (2 to 3-fold) of IL-25R$^-$ IL-33R$^-$ TSLPR$^-$ cells expressing IL-13 (p<0.0001) **(Chapter 3 Appendix Figure 5),** which was comparatively lower than i.n. Ad5 vaccination **(Figure 3.4b)**. It is noteworthy that, the ILC2-derived IL-13 expression by each vector was significantly higher following i.m. delivery compared to i.n. delivery. (Note that: The parent ILC2 population in the i.m. groups were much greater than the i.n. ST2$^+$/IL-33R$^+$ ILC2s. Thus, the difference in IL-13 expression by these two ILC subsets were also represented normalised to the CD45$^+$ subset, described in materials and methods (**Chapter 3 Appendix Figure 4d**).

3.4.2 Poxviral and non-poxviral vectors showed significantly different ILC1/ILC3- derived IFN-γ and IL-17A expression profiles.

Our recent intranasal rFPV vaccination studies have shown that the transient inhibition of ILC2-derived IL-13 at the vaccination site can directly impact the level of IFN-γ and IL-17A expression by NKp46$^+$ and NKp46$^-$ ILC1/ILC3s at the vaccination site 24h post vaccination 338. Hence, we next investigated the induction of IFN-γ and IL-17A expression by ILC1/ILC3s by different viral vaccine vectors as per indicated in Materials and Methods using flow cytometry gating

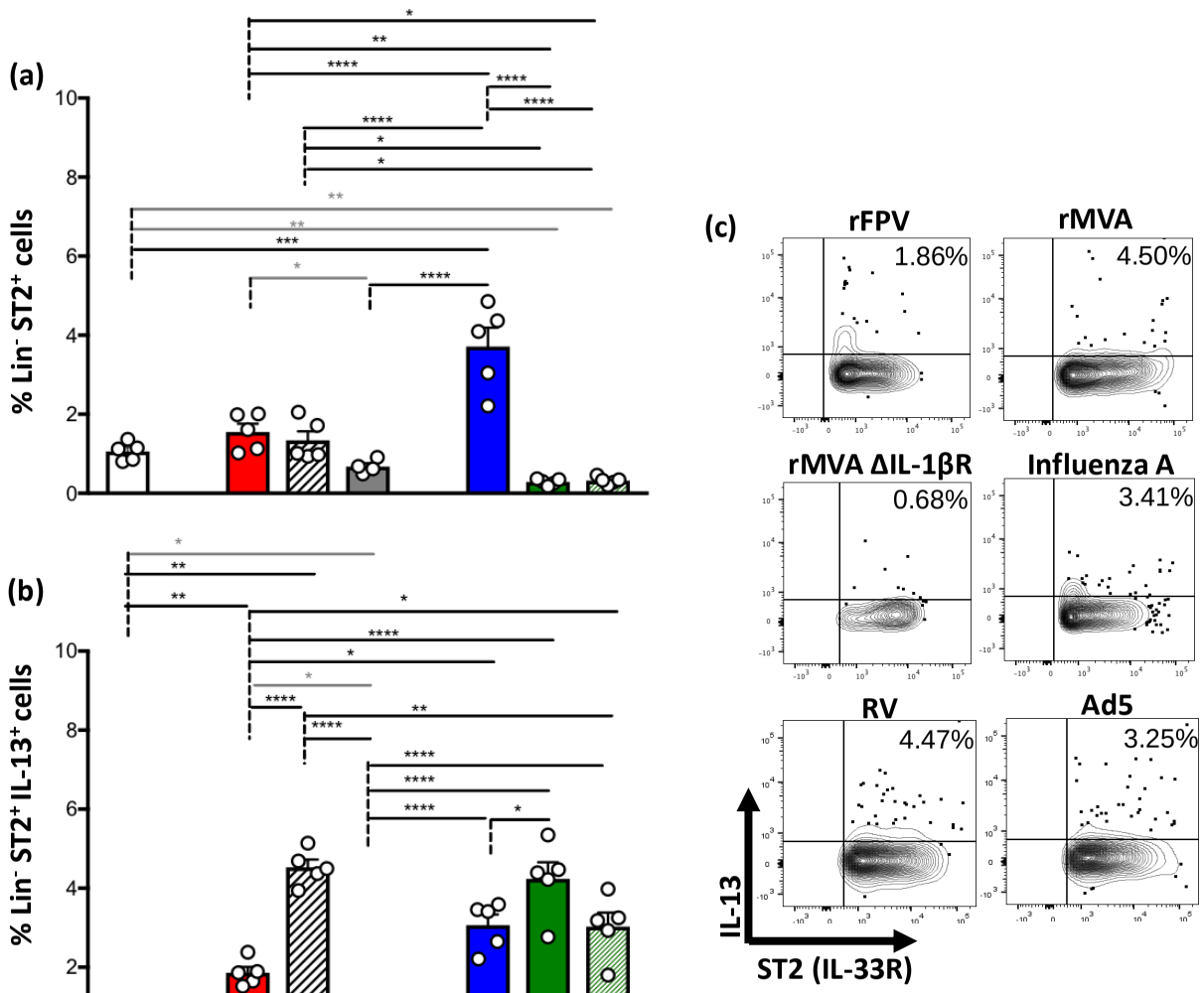
(a)
% Lin⁻ ST2⁺ cells
(b)
% Lin⁻ ST2⁺ IL-13⁺ cells
(c)
rFPV
1.86%
rMVA
4.50%
rMVA ΔIL-1βR
0.68%
Influenza A
3.41%
RV
4.47%
Ad5
3.25%
IL-13
ST2 (IL-33R)

Figure 3.4. Evaluation of lung ILC2 and corresponding IL-13 expression, following intranasal viral vaccination. BALB/c mice (n=5-9 per group) were i.n. or i.m. immunised with rFPV, rMVA, rMVAΔIL-1βR, Influenza A, RV or Ad5. 24 h post vaccination lungs were harvested and single cell suspensions were stained for ILC2s and their IL-13 expression and analysed using flow cytometry. Cells were pre-gated on $CD45^{+}$ FSC^{low} SSC^{low} cells using FlowJo software as described in Materials and Methods and **Chapter 3 Appendix Figures 1 and 2**. Lung ILC2 graphs show **(a)** the percentage of Lin^{-} ST2/IL-33R^{+} ILC2 and **(b)** IL-13 expression by Lin^{-} ST2/IL-33R^{+} ILC2. **(c)** Representative FACS plots show percentage of Lin^{-} ST2/IL-33R^{+} ILC2 expressing IL-13. Error bars represent Standard Error of mean (SEM) and *p* values were calculated using One-way ANOVA followed by Tukey's multiple comparison test for comparison between any two conditions (black lines). Statistical differences between specific pairs (such as unimmunized versus Ad5) were determined using paired student's t test (grey lines). **p*<0.05, ***p*<0.01, ****p*<0.001, *****p*<0.0001. Experiments with each vector were repeated minimum 2-3 times.

strategies described in Chapter 3 Appendix Figure 1. Following i.n. vaccination, although no significant differences in the percentages of NKp46$^+$ ILC1/ILC3s were detected compared to the unimmunized control (Figure 3.5a), compared to Influenza A, Ad5 showed significantly reduced numbers of NKp46$^+$ ILC1/ILC3s (p=0.042). Whist rMVAΔIL-1βR recruited NKp46$^+$ ILC1/ILC3s similar to rFPV, rMVA recruited significantly lower numbers of NKp46$^+$ ILC1/ILC3s compared to rFPV (*p*=0.036) (Figure 3.5a). In the context of IFN-γ expression by NKp46$^+$ ILC1/ILC3s, RV induced the highest (average 14.5%), followed by Ad5 (average 5%) and rFPV (average 2.9%) **(Figure 3.5b and c)**. Unlike rFPV, the deletion mutant rMVAΔIL-1βR and rMVA showed significantly lower IFN-γ expression (*p*=0.0187, and 0.0011 respectively), which was also lower than the unimmunized control (*p*=0.0086 respectively) **(Figure 3.5b and c)**. Expression of IFN-γ by Influenza A was similar to that of the unimmunized control.

Interestingly, following i.n. delivery 95-98% ILC1/ILC3s were found to be NKp46$^-$ **(Figure 3.6a).** Although there were no differences observed between the numbers of NKp46$^-$ ILC1/ILC3s recruited by any of poxvirus vectors **(Figure 3.6a)**, IFN-γ expression was vastly different. rFPV was amongst the highest inducers of IFN-γ expression by NKp46$^-$ ILCs **(Figure 3.6b and c)**, whilst showing modest IFN-γ expression also by NKp46$^+$ ILCs **(Figure 3.6b and c)**. Out of all the vaccine vectors tested, rMVAΔIL-1βR showed the lowest IFN-γ expression by NKp46$^-$ ILC1/ILC3s **(Figure 3.6b and c)**. Although Influenza A recruited significantly lower numbers of NKp46$^-$ ILC1/ILC3s compared to RV and Ad5 (*p*=0.0004, *p*<0.0001 respectively), it induced the highest IFN-γ expression among the non-poxviral vectors **(Figure 3.6b and c).** Interestingly, the IFN-γ expression by NKp46$^-$ ILC1/ILC3s was very similar between Influenza A and

rFPV vaccinated groups **(Figure 3.6b and c)**. It is noteworthy that, although the unimmunized control showed elevated NKp46$^-$ ILC1/ILC3 numbers, low or no expression of IFN-γ was observed **(Figures 3.6a-b and Chapter 3 Appendix Figure 3)**. Remarkably, rMVAΔIL-1βR induced the highest IL-17A expression by both NKp46$^+$ **(Figures 3.7a and c)** and NKp46$^-$ ILC1/ILC3 subsets **(Figures 3.7b and d)**. rMVA and Influenza A vectors induced modest IL-17A expression by both these subsets **(Figure 3.7)**, whilst rFPV, Ad5 and RV showed no IL-17A expression, similar to the unimmunized control **(Figures 3.7 and Chapter 3 Appendix Figure 3.**

Unlike i.n., following i.m. delivery, the proportion of NKp46$^+$ ILC1/ILC3 in the muscle was very minimal (0-0.8%) across all vaccine vectors **(Chapter 3 Appendix Figure 7a)**, with significant differences observed between rMVA compared to rFPV, rMVAΔIL-1βR and Ad5 (p=0.0087 p=0.0049, and p=0.0397 respectively). Additionally, only rFPV and Influenza A vaccinated groups showed any expression of IFN-γ by NKp46$^+$ ILC1/ILC3 **(Chapter 3 Appendix Figure 7b)**. Interestingly, IFN-γ expression by these subsets was much greater following i.m versus i.n. vaccination (rFPV i.m. ~12.06% i.n. 2.5% and influenza A i.m. ~4.67% i.n.~1.5%) **(Chapter 3 Appendix Figure 7b and 3.2)**. In the context of IL-17A expression by NKp46$^+$ ILC1/ILC3, only Influenza A vaccinated animals showed any significant expression (average 8.39%, p<0.0001 influenza A vs. all vaccine vectors) **(Chapter 3 Appendix Figure 7c)**. Of the poxviral vectors tested, rMVAΔIL-1βR vaccinated group also showed an increase in the proportion of NKp46$^+$ ILC1/ILC3 expressing IL-17A (average 0.89%) although not significant and was similar to what was observed with i.n. delivery (average 1.0%).

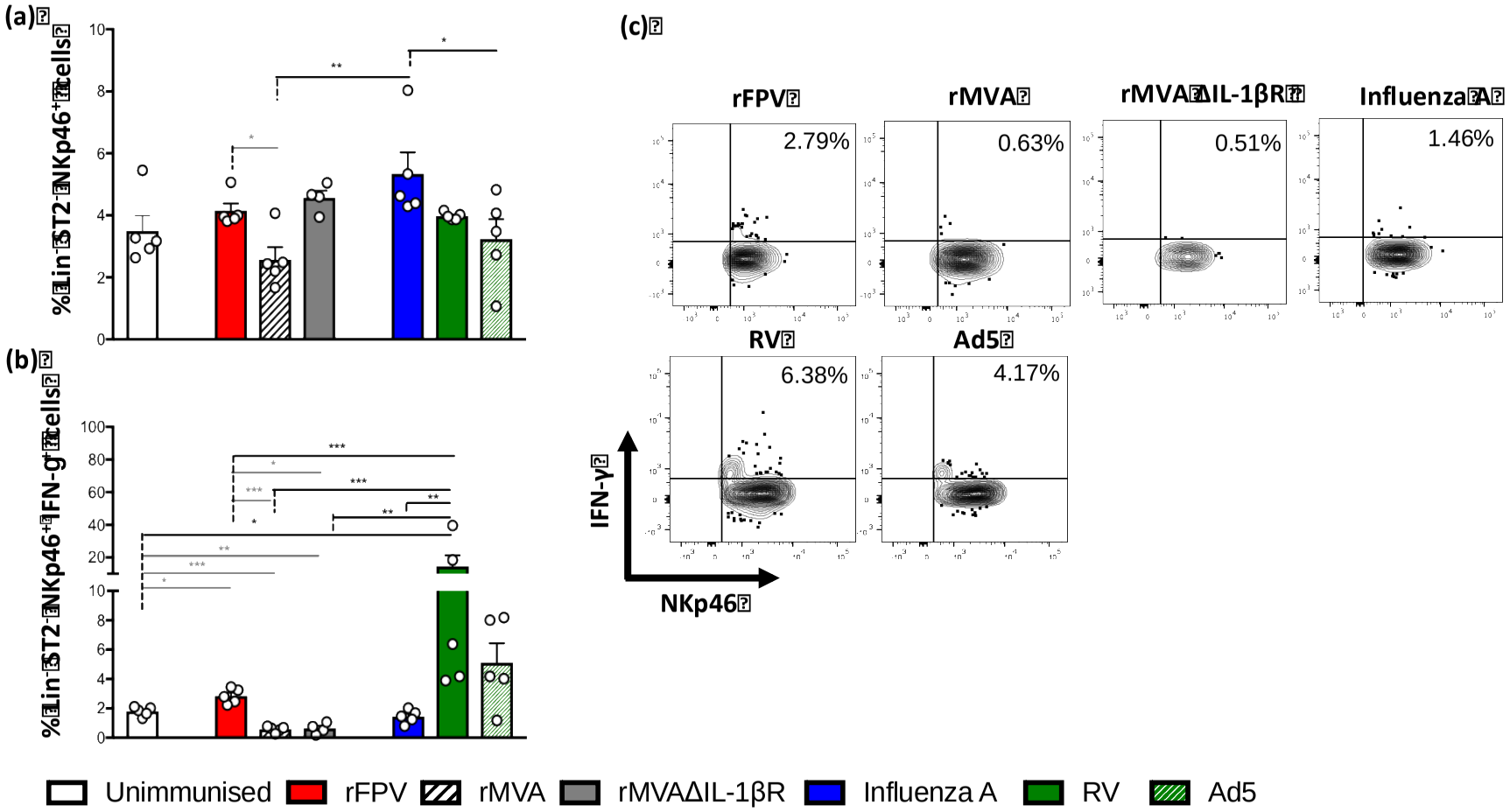
(a)
(b)
(c)
rFPV
rMVA
rMVAΔIL-1βR
Influenza A
RV
Ad5
2.79%
0.63%
0.51%
1.46%
6.38%
4.17%
IFN-γ
NKp46
Unimmunised
rFPV
rMVA
rMVAΔIL-1βR
Influenza A
RV
Ad5

Figure 3.5. Evaluation of lung Lin$^-$ ST2$^-$ NKp46$^+$ and corresponding IFN-γ expression following intranasal viral vector vaccination. BALB/c mice (n=5) were i.n. immunised with same vectors as per in **Figure 3.1**, stained for Lin$^-$ ST2/IL-33R$^-$ NKp46$^+$ cells and their corresponding IFN-γ expression. Cells were pre-gated on CD45$^+$ FSC^{low} SSC^{low} cells as described in Materials and Methods and **Chapter 3 Appendix Figure 1**. Graphs show percentage of **(a)** Lin$^-$ ST2/IL-33R$^-$ NKp46$^+$ ILC and **(b)** corresponding IFN-γ. **(c)** Representative FACS plots show IFN-γ expression by Lin$^-$ ST2/IL-33R$^-$ NKp46$^+$ ILCs. Error bars represent Standard Error of mean (SEM) and *p* values were calculated using One-way ANOVA followed by Tukey's multiple comparison test for comparison between any two conditions (black lines). Statistical differences between specific pairs (such as unimmunized versus rFPV) were determined using paired student's t test (grey lines). *$p<0.05$, **$p<0.01$, ***$p<0.001$, ****$p<0.0001$. Experiments for each group was repeated minimum 2-3 times.

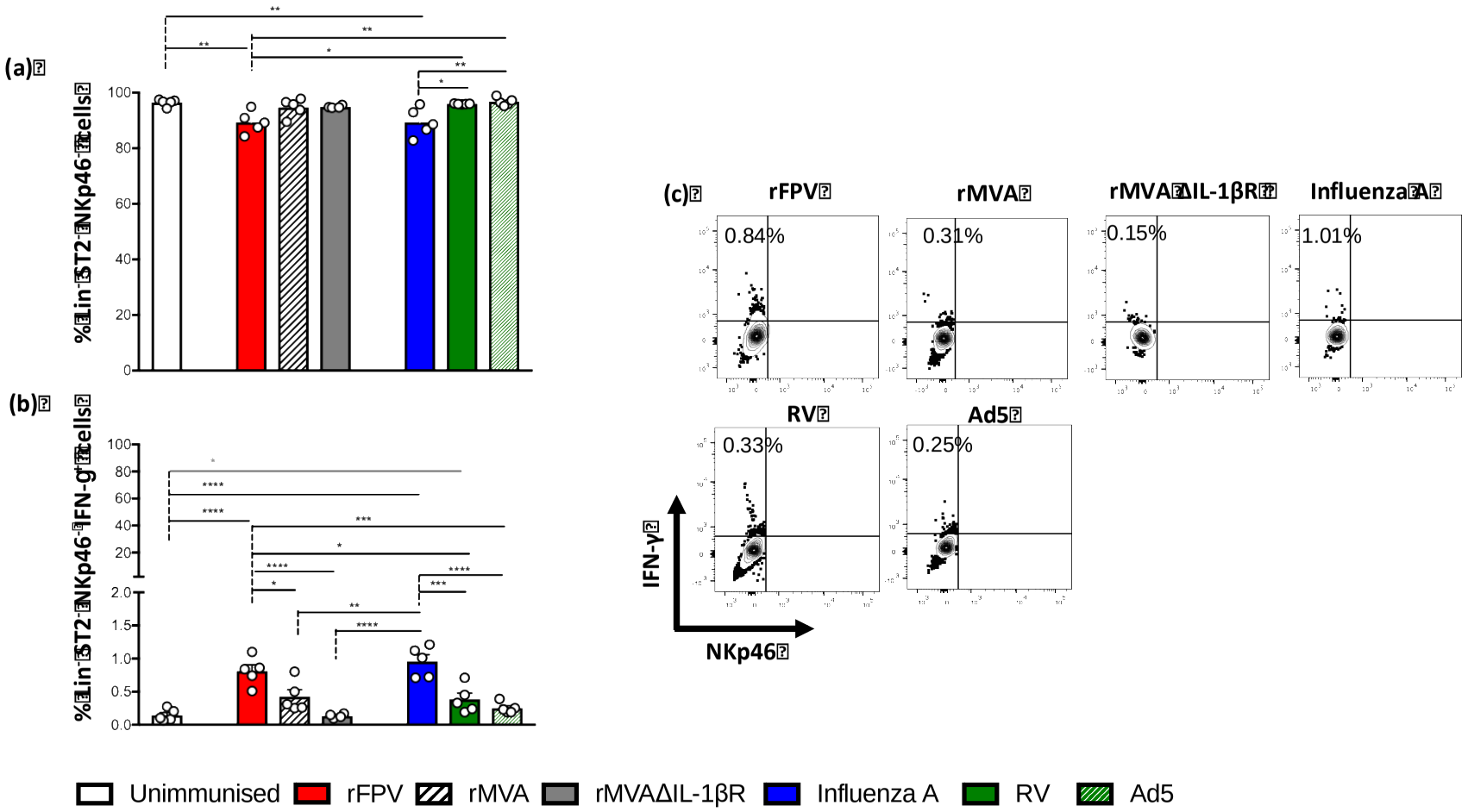
(a)
(b)
(c)
rFPV
rMVA
rMVAΔIL-1βR
Influenza A
RV
Ad5
0.84%
0.31%
0.15%
1.01%
0.33%
0.25%
IFN-γ
NKp46
Unimmunised
rFPV
rMVA
rMVAΔIL-1βR
Influenza A
RV
Ad5

Figure 3.6. Evaluation of lung Lin$^-$ ST2$^-$ NKp46$^-$ and corresponding IFN-γ expression following intranasal viral vector vaccination. BALB/c mice (n=5) were i.n. immunised with same vectors as per in **Figure 3.1**, stained for Lin$^-$ ST2/IL-33R$^-$ NKp46$^-$ cells and their corresponding IFN-γ expression. Cells were pre-gated on CD45$^+$ FSC^{low} SSC^{low} cells as described in Materials and Methods and **Chapter 3 Appendix Figure 1**. Graphs show percentage of **(a)** Lin$^-$ ST2/IL-33R$^-$ NKp46$^-$ ILC and **(b)** corresponding IFN-γ. **(c)** Representative FACS plots show IFN-γ expression by Lin$^-$ ST2/IL-33R$^-$ NKp46$^-$ ILCs. Error bars represent Standard Error of mean (SEM) and *p* values were calculated using One-way ANOVA followed by Tukey's multiple comparison test for comparison between any two conditions (black lines). Statistical differences between specific pairs (unimmunized versus RV) were determined using paired student's t test (grey lines). *$p<0.05$, **$p<0.01$, ***$p<0.001$, ****$p<0.0001$. Experiments for each group was repeated minimum 2-3 times.

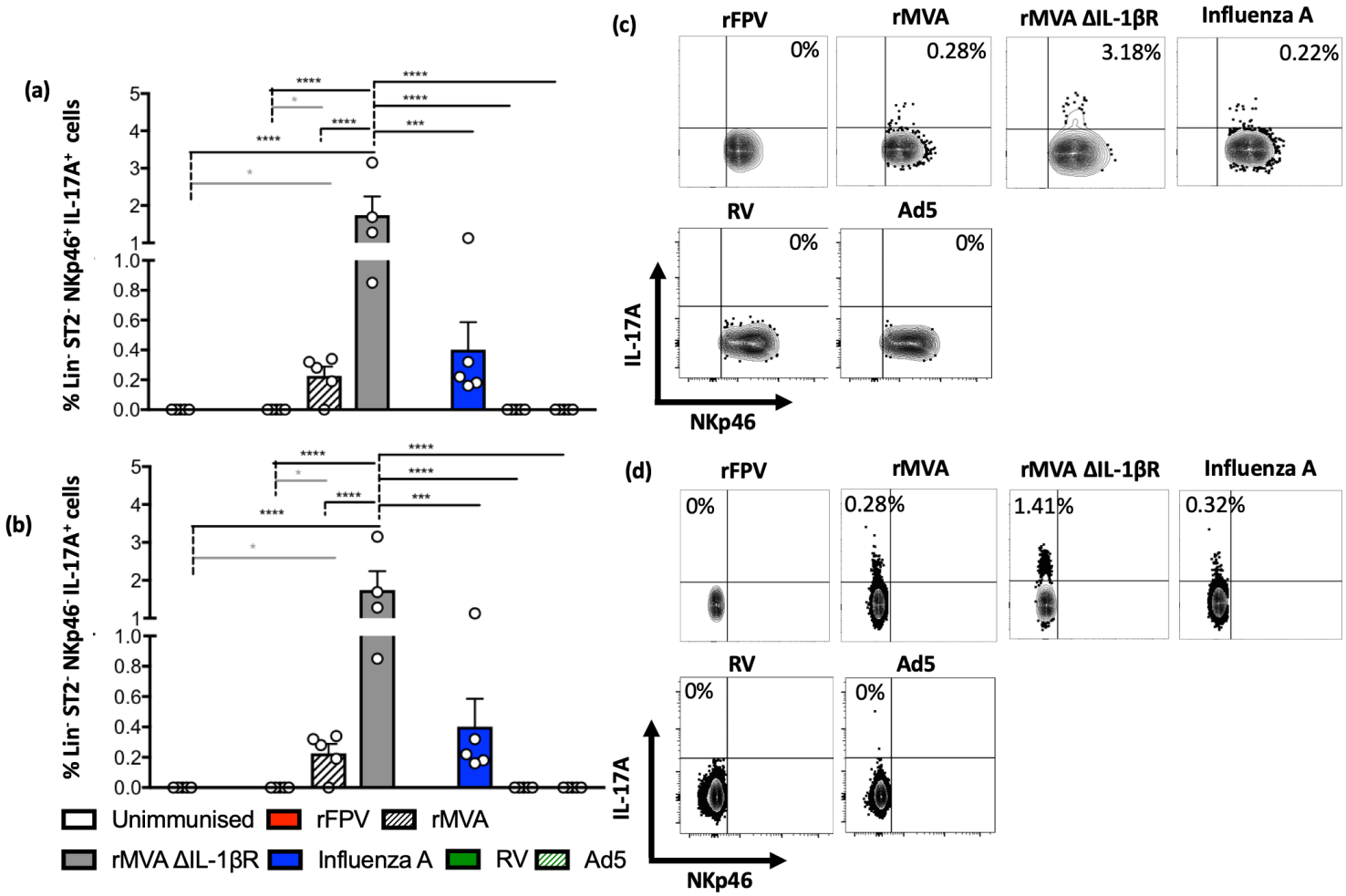
(a)
% Lin⁻ ST2⁻ NKp46⁺ IL-17A⁺ cells
(b)
% Lin⁻ ST2⁻ NKp46⁻ IL-17A⁺ cells
Unimmunised
rFPV
rMVA
rMVA ΔIL-1βR
Influenza A
RV
Ad5
(c)
rFPV
rMVA
rMVA ΔIL-1βR
Influenza A
0%
0.28%
3.18%
0.22%
RV
Ad5
0%
0%
IL-17A
NKp46
(d)
rFPV
rMVA
rMVA ΔIL-1βR
Influenza A
0%
0.28%
1.41%
0.32%
RV
Ad5
0%
0%
IL-17A
NKp46

Figure 3.7. Evaluation of IL-17A expression by lung Lin$^-$ ST2$^-$ NKp46$^+$ and Lin$^-$ ST2$^-$ NKp46$^-$ ILCs following intranasal viral vector vaccination. BALB/c mice (n=5) were i.n. immunised with same vectors as per in **Figure 3.1**, stained for Lin$^-$ ST2/IL-33R$^-$ NKp46$^+$ and Lin$^-$ ST2/IL-33R$^-$ NKp46$^+$ cells and their corresponding IL-17A expression. Cells were pre-gated on CD45$^+$ FSC^{low} SSC^{low} cells as described in Materials and Methods and **Chapter 3 Appendix Figure 1**. Graphs show percentage of IL-17A expression by **(a)** Lin$^-$ ST2/IL-33R$^-$ NKp46$^+$ and **(b)** Lin$^-$ ST2/IL-33R$^-$ NKp46$^-$ ILCs. Representative FACS plots show IL-17A expression by **(c)** Lin$^-$ ST2/IL-33R$^-$ NKp46$^+$ and **(d)** Lin$^-$ ST2/IL-33R$^-$ NKp46$^-$ ILCs. Error bars represent Standard Error of mean (SEM) and *p* values were calculated using One-way ANOVA followed by Tukey's multiple comparison test for comparison between any two conditions (black lines). Statistical differences between specific pairs (such as unimmunized versus rMVA) were determined using paired student's t test (grey lines). *$p<0.05$, **$p<0.01$, ***$p<0.001$, ****$p<0.0001$. Experiments for each group was repeated minimum 2-3 times.

Moreover, following i.m. delivery, different IFN-γ and IL-17A expression profiles were detected by NKp46$^-$ ILC1/ILC3 **(Chapter 3 Appendix Figure 7e and f)**. Unlike i.n. delivery, very low IFN-γ expression was detected following i.m. vaccination, and only influenza A (~0.01%) and Ad5 (~0.03%) showed any IFN-γ expression **(Chapter 3 Appendix Figure 7e and f)**. All vectors showed different NKp46$^-$ ILC1/ILC3-derived IL-17A expression profiles. Specifically, out of the vectors tested, Ad5 and rMVAΔIL-1βR showed the highest expression (~0.58% and ~0.84% respectively) **(Chapter 3 Appendix Figure 7f).** Interestingly, the NKp46- ILC1/ILC3-derived IL-17A expression by the rMVAΔIL-1βR group was significantly elevated compared to unimmunised, rFPV, rMVA and influenza A ($p<0.0001$, $p=0.0064$, $p<0.0001$, and $p<0.0001$ respectively) **(Chapter 3 Appendix Figures 6 and 7f)**. Whilst, Ad5 showed significant differences compared to unimmunised, rMVA, and influenza A vaccinated groups ($p=0.0048$, $p=0.0172$ and $p=0.0219$ respectively) **(Chapter 3 Appendix Figure 7e and f)**.

3.4.3 rFPV and rMVAΔIL-1βR lead to preferential recruitment of CD11b$^+$ CD103$^-$ conventional DCs to the lung mucosae, 24h post intranasal vaccination.

Our previous studies have shown that transient inhibition of IL-13 at the vaccination site can significantly modulate DC recruitment and resulting avidity of CD8$^+$ T cells, including B cell immunity [99,122,124]. Since we have shown that ILC2 are the major source of IL-13 at the vaccination site and this is also viral vector-dependent [338], in this study we have also assessed the influence of viral vector on lung DC recruitment 24h post i.n. vaccination as indicated in **Figures 31.-3.3**. In this study, four different lung DC subsets was assessed (CD11b$^+$ CD103$^-$ cDC, CD11b$^-$ CD103$^+$ cross-presenting DC, CD11b$^-$ CD8$^+$ cross-presenting DC and

CD11b$^-$ B220$^+$ pDC (not other immune cell infiltrates)). Percentage of each DC subset, for a given viral vector was calculated as a proportion of total MHC-II$^+$ CD11c$^+$ DCs, as described in Materials and Methods.

In agreement with Trivedi et al 2014, these studies also showed that rFPV recruited significantly elevated proportions of CD11b$^+$ CD103$^-$ cDCs compared to rMVA and rVV (p=0.0062, p=0.0322 respectively). Additionally, the deletion mutant rMVAΔIL-1βR recruited the highest percentage of CD11b$^+$ CD103$^-$ cDCs, whilst Ad5 recruited the lowest **(Figures 3.8a and b)**. Furthermore, CD11b$^+$ CD103$^-$ cDC recruitment by Influenza A was similar to that of rFPV, rMVA, rVV and RV **(Figures 3.8a and b)**. Compared to the unimmunized control, rFPV, rMVAΔIL-1βR and Influenza A showed significant elevated CD11b$^+$ CD103$^-$ cDC recruitment *(*p=0.0069*,* p<0.0001 and p=0.0077 respectively*)*.

3.4.4. Intranasal rVV vaccination recruited elevated numbers of CD11b$^-$ CD103$^+$ and CD11b$^-$ CD8$^+$ cross-presenting DCs to the lung mucosae 24 h post vaccination.

Unlike CD11b$^+$ CD103$^-$ cDC recruitment, rFPV induced significantly lower CD11b$^-$ CD103$^+$ cross-presenting DCs compared to that of the unimmunized control *(*p=0.0224), and these values were significantly lower than that of rVV, Influenza A and RV vectors (p<0.0001, p=0.0065 and p<0.0001 respectively) **(Figures 3.8a and c).** Interestingly, compared to all viral vectors tested, rVV recruited the highest percentage of CD11b$^-$ CD103$^+$ cross-presenting DCs to the lung mucosae 24 h post vaccination **(Figures 3.8a and c)**. Whilst, rFPV recruited the lowest number similar to rMVA, rMVAΔIL-1βR and Ad5 **(Figures 3.8a and c).** Furthermore, the proportion of CD11b$^-$ CD8$^+$ cross-presenting DCs recruited by

all the vaccine vectors showed a comparable profile to that of the CD11b$^-$ CD103$^+$ cross-presenting DCs, where rVV showed the highest proportion of CD11b$^-$ CD8$^+$ cross-presenting DCs **(Figures 3.8a,c, 3.9)**. It is noteworthy that the cross-presenting CD11b$^-$ CD103$^+$ DCs recruited by rVV, Influenza A and RV were significantly higher than unimmunized control (p<0.0001, p=0.0067 and p=0.0113 respectively) **(Figures 3.8a and c)**. Whereas, cross-presenting CD11b$^-$ CD8$^+$ DCs recruited by rVV and Influenza A although were significantly higher than unimmunized control (p<0.0001, p=0.0498 respectively), Ad5 recruitment was significantly lower (p=0.0164) **(Figures 3.9)**.

3.4.5. Compared to the other viral vectors, RV and Ad5 recruited elevated CD11b$^-$ B220$^+$ plasmacytoid DCs to the lung mucosae 24h post intranasal vaccination.

Next when the CD11b$^-$ B220$^+$ pDC recruitment profile was assessed, these DCs showed a unique profile compared to the other three DC subsets examined. At 24 h post vaccination, RV and Ad5 recruited the highest percentage of CD11b$^-$ B220$^+$ pDCs to the lung mucosae, whilst Influenza A, rFPV and rMVAΔIL-1βR showed the lowest **(Figure 3.10).** Among the poxviral vectors, rVV recruited the highest proportion of CD11b$^-$ B220$^+$ pDCs whilst rFPV recruited the lowest, and rMVA and rMVAΔIL-1βR showed a similar pDC profile. Compared to the unimmunised control, rVV, RV and Ad5 vectors showed significant differences in pDC recruitment 24h post vaccination (p=0.0025, p<0.0001 and p<0.0001 respectively) **(Figure 3.10).**

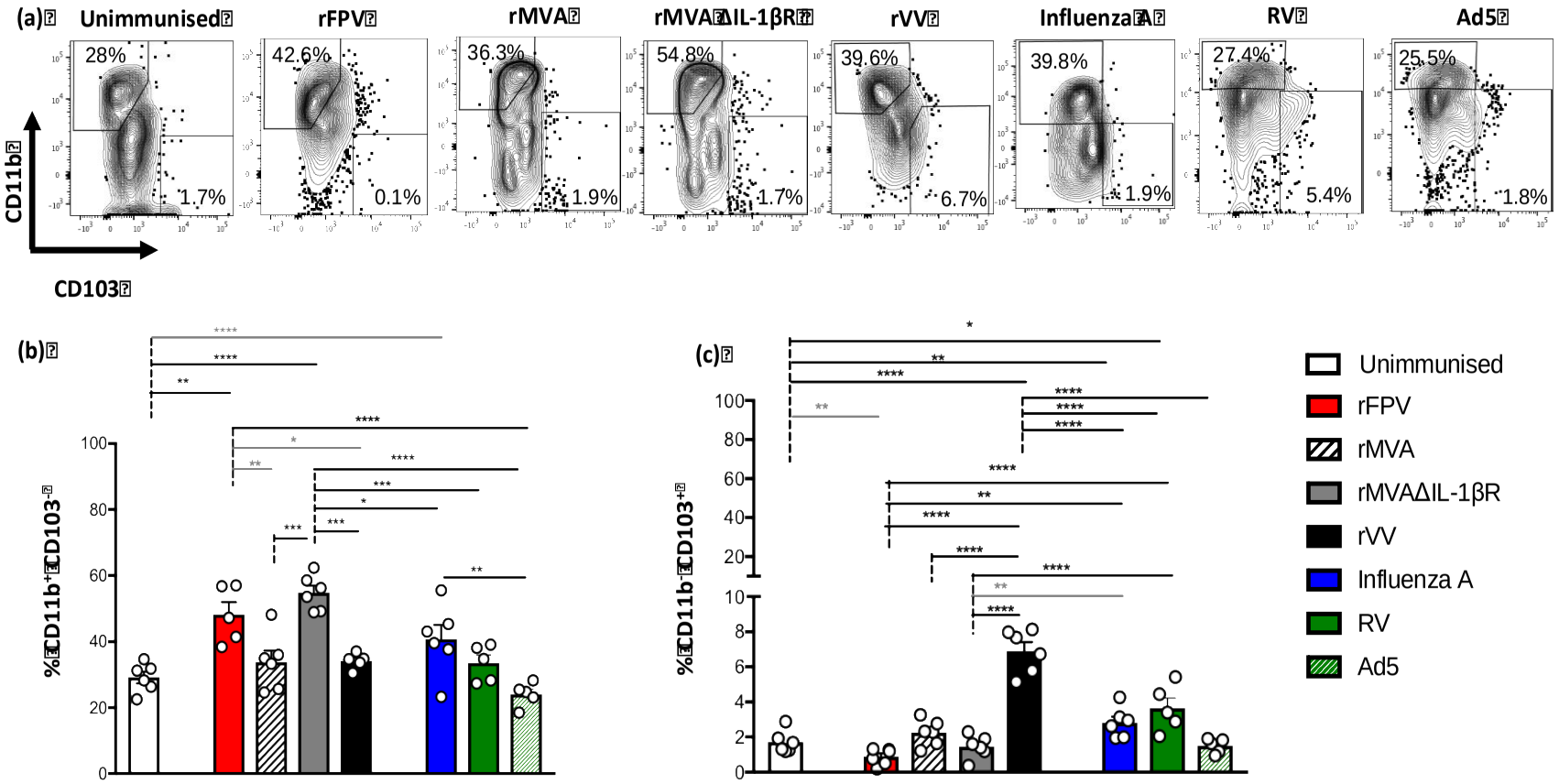
(a)
Unimmunised
rFPV
rMVA
rMVAΔIL-1βR
rVV
Influenza A
RV
Ad5
28%
1.7%
42.6%
0.1%
36.3%
1.9%
54.8%
1.7%
39.6%
6.7%
39.8%
1.9%
27.4%
5.4%
25.5%
1.8%
CD11b
CD103
(b)
%CD11b+CD103+
(c)
%CD11b-CD103+
Unimmunised
rFPV
rMVA
rMVAΔIL-1βR
rVV
Influenza A
RV
Ad5

Figure 3.8. Evaluation of CD11b$^+$ CD103$^-$ cDCs and CD11b$^-$ CD103$^+$ cross-presenting DCs following intranasal viral vector vaccination. BALB/c mice (n=5) were i.n. immunised with rFPV, rMVA, rMVAΔIL-1βR, rVV, Influenza A, RV or Ad5. 24 h post vaccination lungs were harvested single cell suspensions were prepared and stained for different DC subsets and analysed using flow cytometry as described in Materials and Methods. Cells were pre-gated on MHC-II$^+$ CD11c$^+$ cells using fluorescence minus one (FMO) controls for each virus as described in Materials and Methods and **Figures 3.1-3.3.** **(a)** Representative FACS plots show percentage of CD11b$^+$ CD103$^-$ DCs (gated top left) and CD11b$^+$ CD103$^-$ DCs (gated bottom right) recruited to lung mucosae. **(b)** Percentage of CD11b$^+$ CD103$^-$ DCs and **(c)** CD11b$^-$ CD103$^+$ DCs are shown as bar graphs, recruited by each vaccine vector. Percentages were calculated as a proportion of total MHC-II$^+$CD11c$^+$ DCs generated by each vector as indicated in Materials and Methods. Error bars represent Standard Error of mean (SEM) and *p* values were calculated using One-way ANOVA followed by Tukey's multiple comparison test for comparison between any two conditions (black lines). Statistical differences between specific pairs (such as unimmunized versus Influenza A) were determined using paired student's t test (grey lines). *$p<0.05$, **$p<0.01$, ***$p<0.001$, ****$p<0.0001$. Experiments with each vector were repeated minimum 2-3 times.

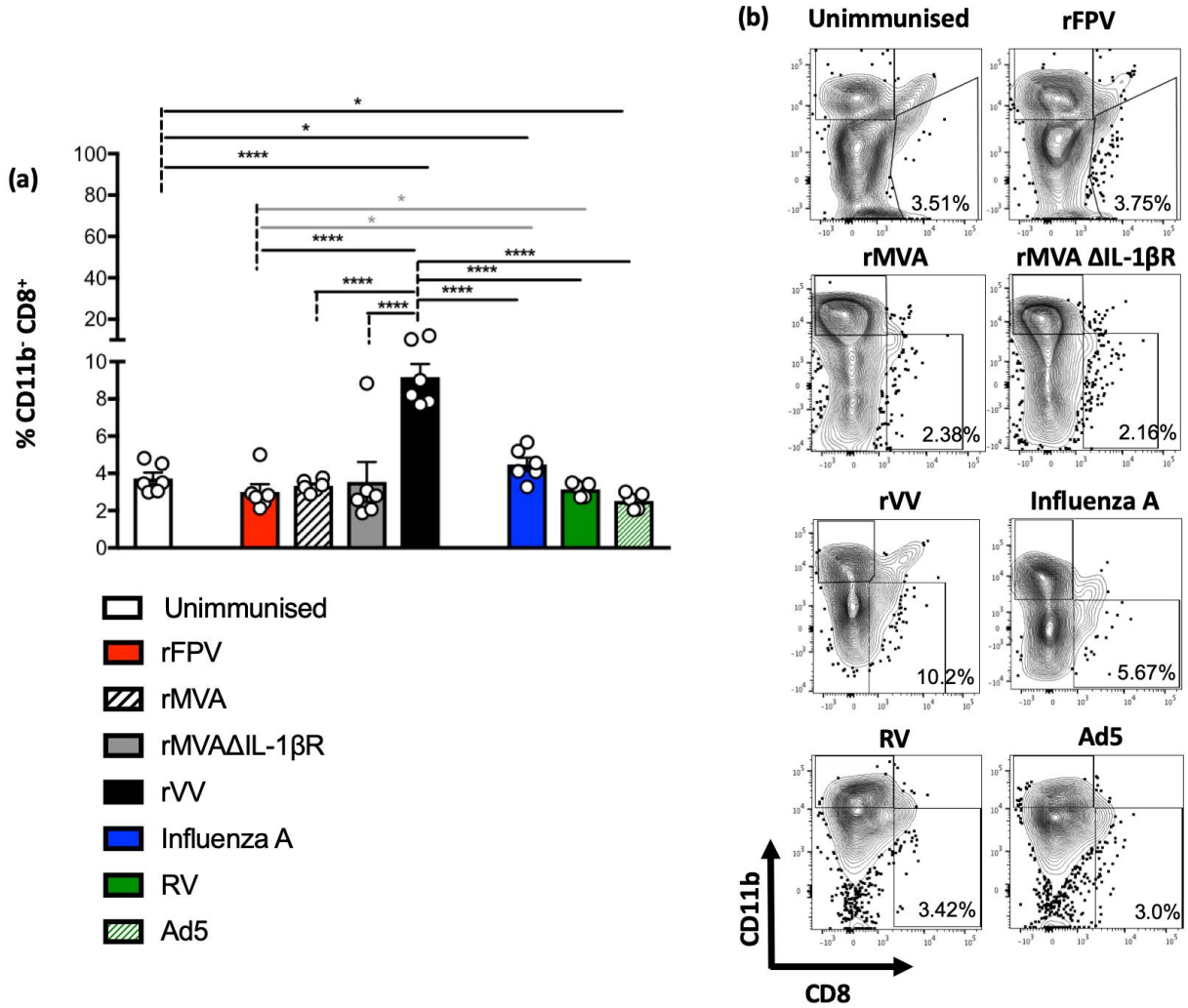
(a)
% CD11b⁻ CD8⁺
100
80
60
40
20
10
8
6
4
2
0
*
*
****
*
*
****
****
****
****
****
****
Unimmunised
rFPV
rMVA
rMVAΔIL-1βR
rVV
Influenza A
RV
Ad5
(b)
Unimmunised
rFPV
3.51%
3.75%
rMVA
rMVA ΔIL-1βR
2.38%
2.16%
rVV
Influenza A
10.2%
5.67%
RV
Ad5
3.42%
3.0%
CD11b
CD8

Figure 3.9. Evaluation of CD11b$^-$ CD8$^+$ cross-presenting DCs following intranasal viral vector vaccination. BALB/c mice (n=5) were i.n. immunised with same vectors as in **Figure 3.8** and lung cells were analysed using flow cytometry for DC subsets as per described in Materials and Methods. Cells were pre-gated on MHC-II$^+$ CD11c$^+$ cells using fluorescence minus one (FMO) controls as described in **Figures 3.1-3.3. (a)** Bar graphs and **(b)** representative FACS plots show percentage of CD11b$^-$ CD8$^+$ DCs recruited to the lung mucosae 24 h post vaccination with each viral vector compared to the unimmunized control. Percentages were calculated as a proportion of total MHC-II$^+$CD11c$^+$ DCs generated by each vector as indicated in Materials and Methods. Error bars represent Standard Error of mean (SEM) and *p* values were calculated using One-way ANOVA followed by Tukey's multiple comparison test for comparison between any two conditions (black lines). Statistical differences between specific pairs (such as rFPV versus RV) were determined using paired student's t test (grey lines). *$p<0.05$, **$p<0.01$, ***$p<0.001$, ****$p<0.0001$. Experiments with each vector were repeated minimum 2-3 times.

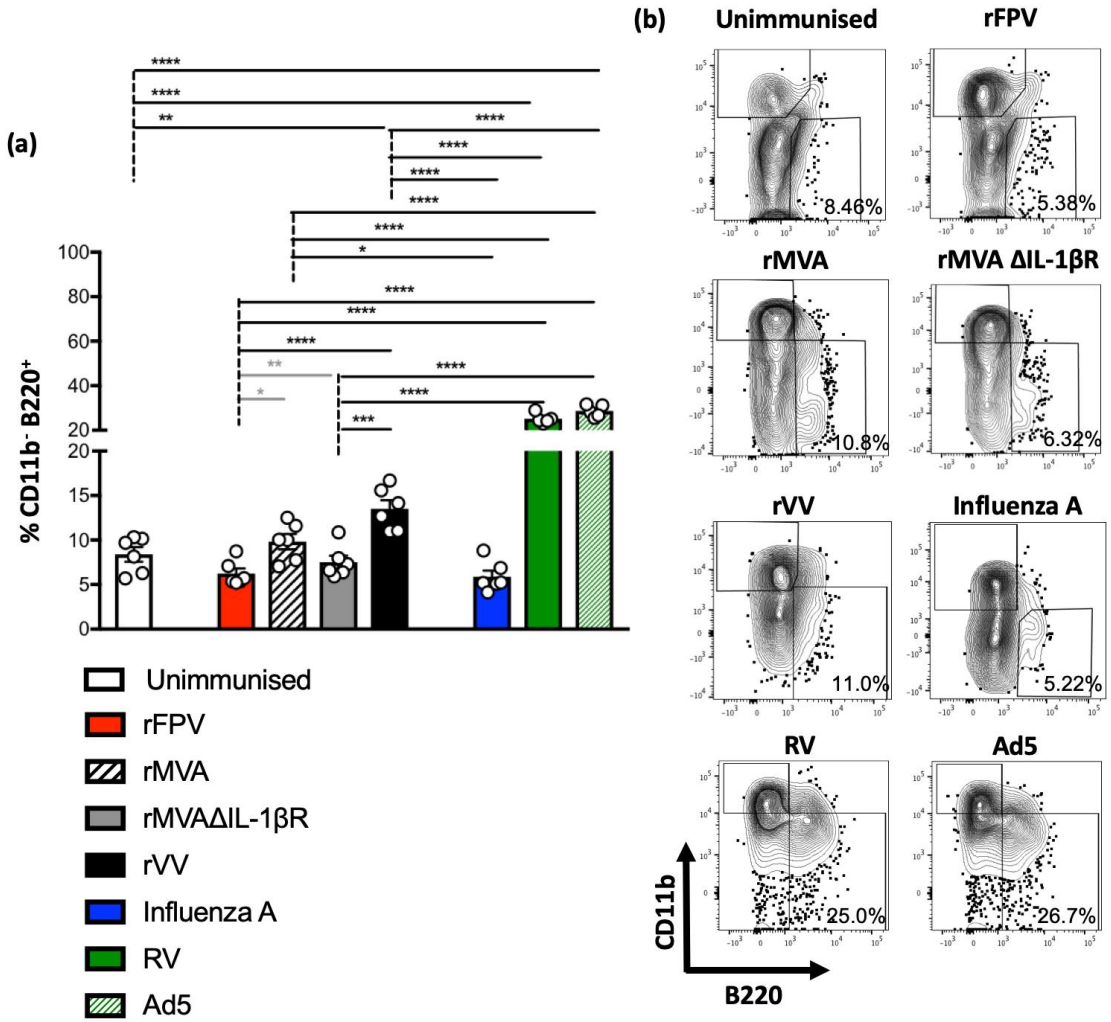
(a)
% CD11b- B220+
Unimmunised
rFPV
rMVA
rMVAΔIL-1βR
rVV
Influenza A
RV
Ad5
(b)
Unimmunised
rFPV
rMVA
rMVA ΔIL-1βR
rVV
Influenza A
RV
Ad5
8.46%
5.38%
10.8%
6.32%
11.0%
5.22%
25.0%
26.7%
CD11b
B220

Figure 3.10. Evaluation of CD11b$^-$ B220$^+$ plasmacytoid DCs following intranasal viral vector vaccination. BALB/c mice (n=5) were i.n. immunised with same vectors as in **Figure 3.8** and lung cells were analysed using flow cytometry for DC subsets as per described in Materials and Methods. Cells were pre-gated on MHC-II$^+$ CD11c$^+$ cells using fluorescence minus one (FMO) controls as described in **Figures 3.1-3.3. (a)** Bar graphs and **(b)** representative FACS plots show percentage of CD11b$^-$ B220$^+$ pDCs recruited to the lung mucosae 24 h post vaccination with each viral vector compared to the unimmunized control. Percentages were calculated as a proportion of total MHC-II$^+$CD11c$^+$ DCs generated by each vector as indicated in Materials and Methods. Error bars represent Standard Error of mean (SEM) and *p* values were calculated using One-way ANOVA followed by Tukey's multiple comparison test for comparison between any two conditions (black lines). Statistical differences between specific pairs (such as rFPV versus rMVA) were determined using paired student's t test (grey lines). *$p<0.05$, **$p<0.01$, ***$p<0.001$, ****$p<0.0001$. Experiments with each vector were repeated minimum 2-3 times.

3.4.6. Following intranasal vaccination different viral vectors showed different kinetic profiles 0 to 48h post vaccination.

Next, we also evaluated the DC recruitment kinetics 0 to 48 hours post vaccination. Distinct DC kinetic profiles for each of the vectors were detected over time. rFPV showed significant regulation of CD11b$^+$ CD103$^-$ cDCs, which was similar to the cDC profile induced by the rMVA deletion variant (rMVAΔIL-1βR), unlike the parental rMVA **(Figures 3.11a and 3.12a-b)**. The replication competent rVV showed regulation of all DC subsets, with significant modulation of cross-presenting DCs. Interestingly, cDC recruitment kinetics between rVV, rMVA and Influenza were very similar **(Figures 3.11b, 3.12a and c).** Ad5 recruited a pDC profile similar to RV and a CD11b$^-$ CD8$^+$ profile similar to rVV **(Figures 3.11b, c and 3.12d).**

3.5. Discussion

This study has clearly demonstrated that not only the route of vaccination, but also different viral vector-based vaccines can induce significantly different ILC subsets at the respective vaccination sites 24 h post delivery. In the context of ILC2, Lin$^-$ ST2/IL-33R$^+$ ILC2 were predominant in lung, whilst Lin$^-$ IL-25R$^+$ or/and Lin$^-$ TSLPR$^+$ ILC2 were found in muscle 24 h post viral vector vaccination. This was not entirely surprising as Lin$^-$ IL-25R$^+$ ILC2 has been associated with circulation [339,340], whilst Lin$^-$ TSLPR$^+$ ILC2 is known to be skin-resident [341]. Although, Lin$^-$ ST2/IL-33R$^+$ ILC2 was the major source of IL-13 in lung, Lin$^-$ IL-25R$^-$ TSLPR$^-$ ST2/IL-33R$^-$ ILC2s were the predominant source of IL-13 in muscle. Interestingly, recently we have also found that following viral vector vaccination IL-5 expression was specific to lung ILC2, not muscle (Jaeson *et al.* submitted), reaffirming that ILCs can be highly plastic under different conditions (specifically

chronic inflammatory conditions versus vaccination or infection) [326,342], and why different routes of delivery may yield uniquely different innate and adaptive immune outcomes.

In addition to ILC2, i.n. versus i.m. vaccinations induced different proportions of NKp46^{+} ILC1/ILC3s unlike NKp46^{-} ILC1/ILC3s. Specifically, significantly lower numbers of NKp46^{+} ILC1/ILC3s were detected in muscle compared to the lung (~ 1% vs 4-8%), confirming that circulatory ILC1/ILC3s are scarce as opposed to tissue resident ILCs [343]. Both NKp46^{+} and NKp46^{-} ILC1/ILC3s were able to express different levels of IFN-γ, that were vaccine route- and vector-dependent. Specifically, whilst both NKp46$^{+/-}$ ILC1/ILC3 subsets were able to express IFN-γ in lung, only the NKp46^{+} ILCs in muscle expressed IFN-γ, albeit by two vaccination groups, where the expression was in the order of rFPV > Influenza A. Moreover, muscle NKp46^{-} cells expressed extremely low IFN-γ following Influenza and Ad5 vaccination. Majority of i.m. delivered vectors induced elevated ILC2-driven IL-13 and minimal ILC1/ILC3-driven IFN-γ expression compared to i.n. delivery. Additionally, our previous studies with pox-viral vectors have shown that, compared to i.m., i.n. delivery can induce T cells of higher avidity, associated with low IL-13 at the vaccination site [205,314,338]. Furthermore, i.n. rFPV priming has shown to induce high avidity T cells compared to i.n. rVV and Influenza priming vaccination [131,133,344], (Tan, Derose *et al.* personal communication). In agreement with our current study, i.n. Ad5 vaccination has also shown comparable ILC2 gene expression profiles to i.n. rFPV, unlike i.m. Ad5 delivery (Jaeson *et al.* submitted). Taken together, these findings may explain why systemic vaccination with some viral vectors may lead to suboptimal antiviral immunity, compared to mucosal vaccination [133,314,345,346].

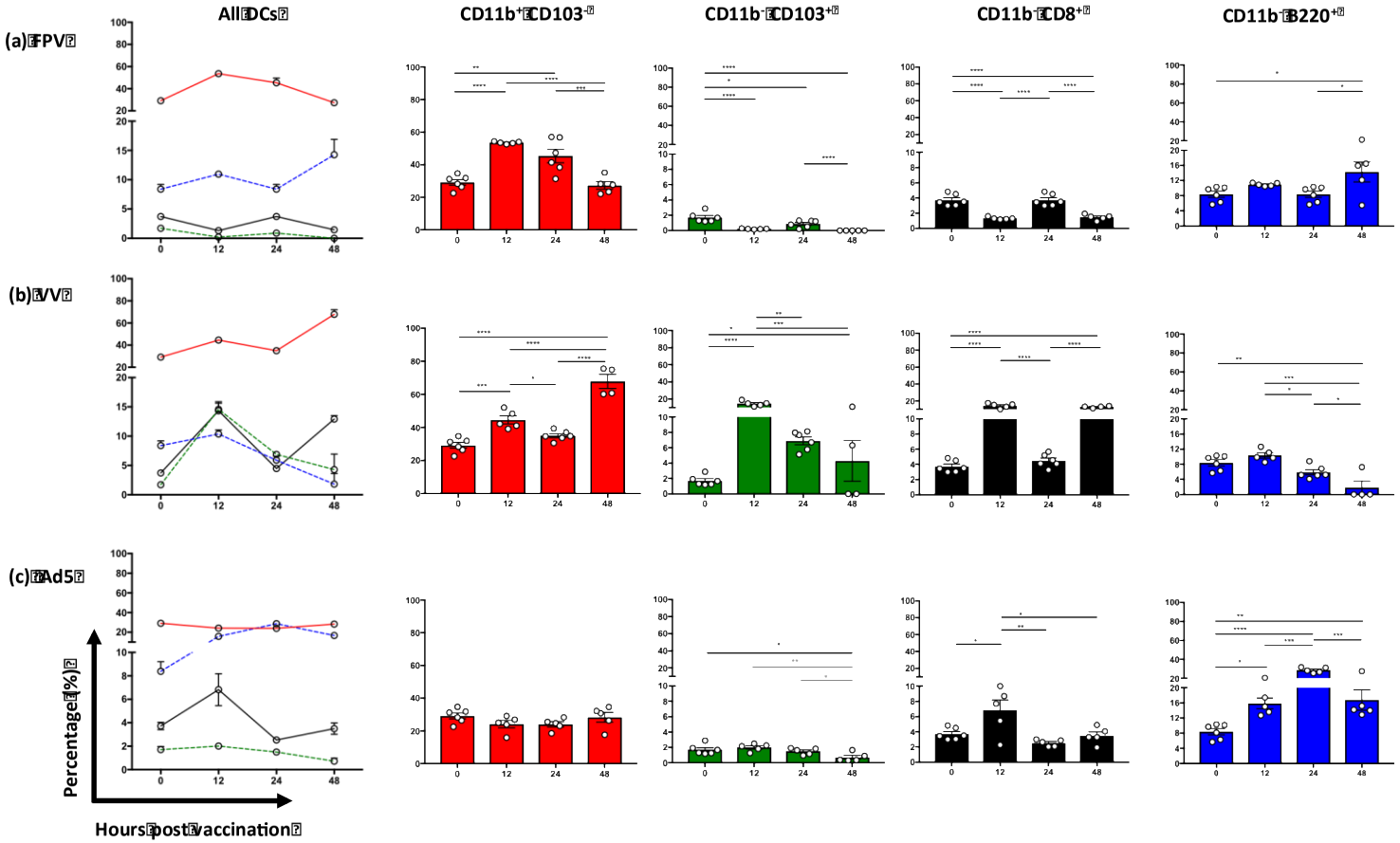
All DCs
CD11b+ CD103-
CD11b- CD103+
CD11b- CD8+
CD11b- B220+
(a) FPV
(b) I/V
(c) Ad5
Percentage (%)
Hours post vaccination

Figure. 3.11. DC kinetics following intranasal viral vector based vaccination 0-48h post vaccination with rFPV, rVV and Ad5. BALB/c mice (n=5) were i.n. immunised with rFPV, rVV and Ad5. Lungs were harvested at 12, 24 and 48 hours post vaccination and lung DC subsets and analysed using flow cytometry as described in Materials and Methods. Cells were pre-dated on MHC-II^{+} CD11c^{+} cells using fluorescence minus one (FMO) controls as described in **Figures 3.1-3.3.** Line graphs (left panel) and bar graphs (right four panels) show percentage of CD11b^{+} CD103^{-} DCs (red), CD11b^{-} CD103^{+} DCs (green), CD11b^{-} CD8^{+} DCs (black) and CD11b^{-} B220^{+} DCs (blue) recruited by **(a)** rFPV, **(b)** rVV and **(c)** Ad5 to the lung mucosae 0 to 48 hours post vaccination. Error bars represent Standard Error of mean (SEM) and *p* values were calculated using One-way ANOVA followed by Tukey's multiple comparison test for comparison between any two time points (black lines). Statistical differences between two specific time points were determined using paired student's t test (grey lines). *$p<0.05$, **$p<0.01$, ***$p<0.001$, ****$p<0.0001$. Experiments with each vector were repeated minimum 2-3 times

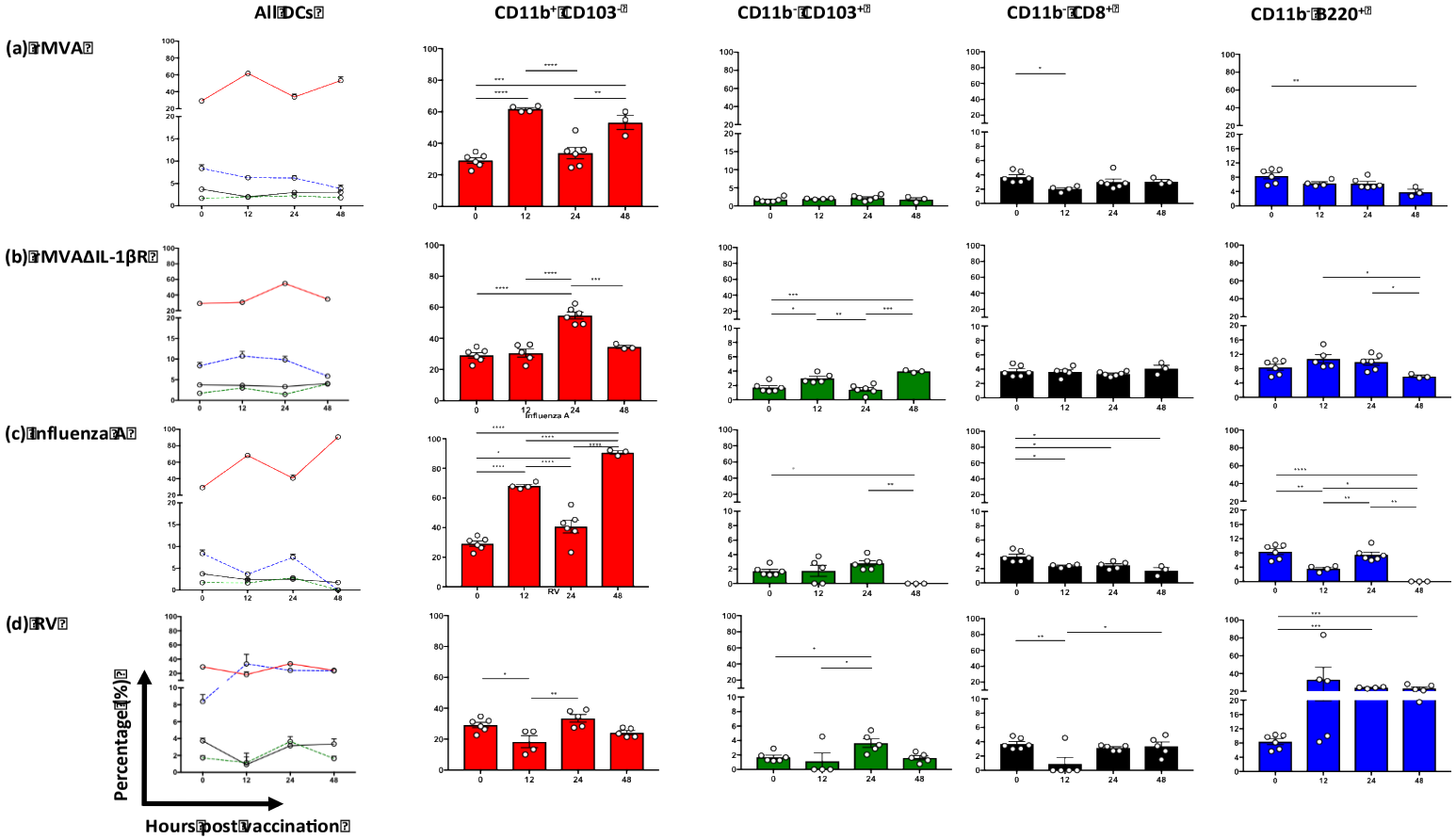
All DCs
CD11b+ CD103-
CD11b- CD103+
CD11b- CD8+
CD11b- B220+
(a) rMVA
(b) rMVAΔIL-1βR
(c) Influenza A
(d) RV
Influenza A
RV
Percentage (%)
Hours post vaccination

Figure. 3.12. DC kinetics following intranasal viral vector based vaccination 0-48h post vaccination with rMVA, rMVA-ΔIL-1βR, Influenza A and RV. BALB/c mice (n=5) were i.n. immunized with rMVA, rMVA-ΔIL-1βR, Influenza A and RV. DC subsets were analysed by flow cytometry from lungs harvested at 12, 24 and 48 hours post immunisation. Line graphs and histograms show percentage of $CD11b^{+}$ $CD103^{-}$ DCs (green), $CD11b^{-}$ $CD8^{+}$ DCs (black) and $CD11b^{-}$ $B220^{+}$ DCs (blue) recruited by **(a)** rMVA, **(b)** rMVA-ΔIL-1βR, **(c)** Influenza A and **(d)** RV to the lung mucosae. Experiments were repeated minimum two times. Error bars represent SEM and *p* values were calculated using One-way Anova followed by Tukey's multiple comparison test (black lines) and paired student's t test (grey lines). *p<0.05, **p<0.01, ***p<0.001, ****p<0.0001.

Besides the route of delivery, each viral vector also induced a uniquely different ILC2-driven IL-13 and ILC1/ILC3-driven IFN-γ expression profiles. Specifically, both i.n. and i.m. rFPV vaccination induced low ILC2-derived IL-13, and high NKp46^{+} or NKp46^{-} ILC1/ILC3-derived IFN-γ. In contrast, i.m. rMVA vaccination induced lower ILC2-derived IL-13 compared to i.n. delivery. Knowing that, low IL-13 is associated with improved T cell immunity, our current data may explain why previously rMVA has been found to be more efficacious as an i.m. delivery vector than a mucosal delivery vector [138,315]. Moreover, whilst i.n. delivery of rMVA, Influenza A, RV and Ad5 induced elevated ILC2-derived IL-13, the expression of IFN-γ was lower in NKp46^{+} ILC1/ILC3s following rMVA, Influenza A; and NKp46^{-} ILC1/ILC3s following RV and Ad5 vaccinations. Interestingly, we have previously shown that IL-4R antagonist adjuvanted vaccination that transiently inhibited IL-13 signalling via STAT6, induced low ILC2-derived IL-13 expression associated with elevated expression of NKp46^{-} ILC1/ILC3-derived IFN-γ [338]. Additionally, enhanced *IfngR* gene expression on ILC2 was also recently associated with low ILC2-derived IL-13 (Jaeson *et al.* submitted). Taken together, these observations suggest that enhanced ILC1/ILC3-derived IFN-γ expression regulates ILC2-derived IL-13 at the vaccination site, similar to the Th1/Th2 paradigm. Hence, we propose that ILC-derived IL-13 and IFN-γ balance at the vaccination site crucially impacts the downstream vaccine-specific immunity.

Different vectors also lead to differential expression of IL-17A by NKp46^{+} and NKp46^{-} ILC1/ILC3. Specifically, i.n. rMVA, rMVAΔIL-1βR and Influenza A vectors induced elevated IL-17A by both ILC1/ILC3 subsets at the lung mucosae 24h post vaccination. However, majority of the vectors induced different levels of IL-17A by NKp46^{-} ILC1/ILC3 subsets in the muscle. In asthma studies the

importance of maintaining IL-13 and IL-17 balance has been well documented [347]. Similarly, our vaccination studies have also shown that IL-13 can regulate IL-17A expression at the transcriptional and translational level, which plays an important role in determining the quality of T cell immunity [348]. Knowing that i) rVV and its derivatives (rMVA) perform better as a booster vaccine than a prime [133,138] ii) Influenza A prime yield poor adaptive immune outcomes (Tan, Derose *et al.* personal communication) [344] and iii) systemic Ad5 immunization have shown to induce less effective antiviral T cell responses [118,349-351], collectively our data suggest that the early onset of high ILC1/ILC3-derived IL-17A together with low IFN-γ and high ILC2-derived IL-13 could be detrimental for inducing effective cellular immunity.

Our study demonstrated that in addition to different ILC profiles, mucosal vaccination with different viral vectors yielded uniquely different lung DC profiles at the vaccination site 24 h post vaccination. We have previously shown that IL-13 levels at the vaccination site can significantly alter DC phenotype, specifically, inhibition of IL-13 can recruit elevated $CD11b^+$ $CD103^-$ cDCs associated with high avidity T cells [99]. This study further substantiated our previous findings of enhanced recruitment of $CD11b^+$ $CD103^-$ cDCs as opposed to $CD11b^-$ $CD103^+$ cross-presenting DCs following i.n. rFPV vaccination. Moreover, moderate proportions of $CD11b^-$ $B220^+$ pDCs were also observed with rFPV vaccination. pDCs are known to induce antibody differentiation via IFN-γ production [336] and their clustering with cDCs have shown to induce efficient T cell mediated antiviral immunity [335]. We have already established that rFPV priming can induce robust high avidity T cells and differentiated antibodies, involved in protective immunity against viral pathogens such as HIV [122,133]. Thus, our current findings suggest

that although in the context of certain viral vectors, the cDC/pDC balance may govern the quality of T and B cell immunity, replicating vectors such as Influenza A may employ other mechanisms (as Influenza A showed similar cDC/pDC profile to rFPV associated with poor quality T cells).

In contrast to rFPV vaccination, rMVA lead to elevated ILC2-derived IL-13, similar to rVV (data not shown), and both vectors significantly enhanced recruitment of $CD11b^{-}$ $CD103^{+}$ cross-presenting DCs to the lung mucosae, as shown previously [99]. This may explain why rMVA and rVV priming lead to low avidity T cells following recombinant HIV vaccination [131,133]. Moreover, intranasal Influenza A, RV and Ad5 vaccination which also lead to high ILC2-derived IL-13, preferentially induced $CD11b^{-}$ $CD103^{+}$ cross-presenting DCs as opposed to cDCs. In a prime-boost vaccine modality, recombinant Influenza A priming has shown to induce enhanced magnitude of vaccine-specific T cells, however, are of low avidity unlike rFPV priming (Tan, Derose *et al.* personal communication). Similarly, recombinant Ad5 vaccination has also shown to induce high magnitude of vaccine-specific CD8 T cells [140]. Therefore, these observations suggest that these vectors although lead to enhanced magnitude of vaccine-specific T cell immunity (IFN-γ production by T cells), may lead to low avidity T cells against chronic infections such as HIV-1. Despite low cDCs, Ad5 and RV exhibited a bias towards pDC recruitment. Knowing that pDC-driven IFN-γ can induce effective antibody responses, we postulate that Ad5- and RV-based vaccines could be more efficacious in inducing humoral immunity. Similar to $CD11b^{-}$ $CD103^{+}$ cross-presenting DCs, rVV additionally induced elevated $CD11b^{-}$ $CD8^{+}$ cross-presenting DCs to the lung mucosa. These observations suggested that, early induction of $CD11b^{-}$ $CD8^{+}$ cross-presenting DCs, could also be associated with

induction of low avidity T cells. However, in the context of some pathogens, (for example, *Leishmania*, and also some viruses, Influenza and HSV-1 infections), induction of cross-presenting DCs have been associated with protective immunity [330,352,353]. Thus, when designing recombinant viral vector-based vaccines, careful selection of the vector, according to the pathogen of interest may be of great importance.

rMVAΔIL-1βR is known to induce effective memory T cell responses compared to parental rMVA vaccination [354]. Unlike rMVA, rMVAΔIL-1βR induced low ILC2-derived IL-13 and elevated cDCs similar to rFPV, which has shown to induce high avidity T cells with better protective immunity. These findings indicated that removal of a single immune evasive gene from the viral vector can significantly alter the innate immune outcomes, specifically the ILCs and DCs, associated with effective protective immunity. However, compared to rFPV (which showed elevated IFN-γ and no IL-17A expression), rMVAΔIL-1βR vaccination induced suboptimal ILC1/ILC3-derived IFN-γ and high IL-17A expression at the vaccination site. It is well established that IFN-γ is crucial for antiviral immunity, and overexpression of IL-17A can lead to immune imbalance [355]. It is also known that viral IL-18bp neutralize host IL-18 and prevent IFN-γ production [356]. Thus, the residual IL-18bp in the rMVAΔIL-1βR vector could be responsible for the observed ILC1/ILC3-derived IFN-γ profile. Thus, we postulate that rMVA vector lacking both IL-1βR and IL-18bp genes may lead to ILC/DC profiles similar to rFPV and balanced T and B cell outcomes.

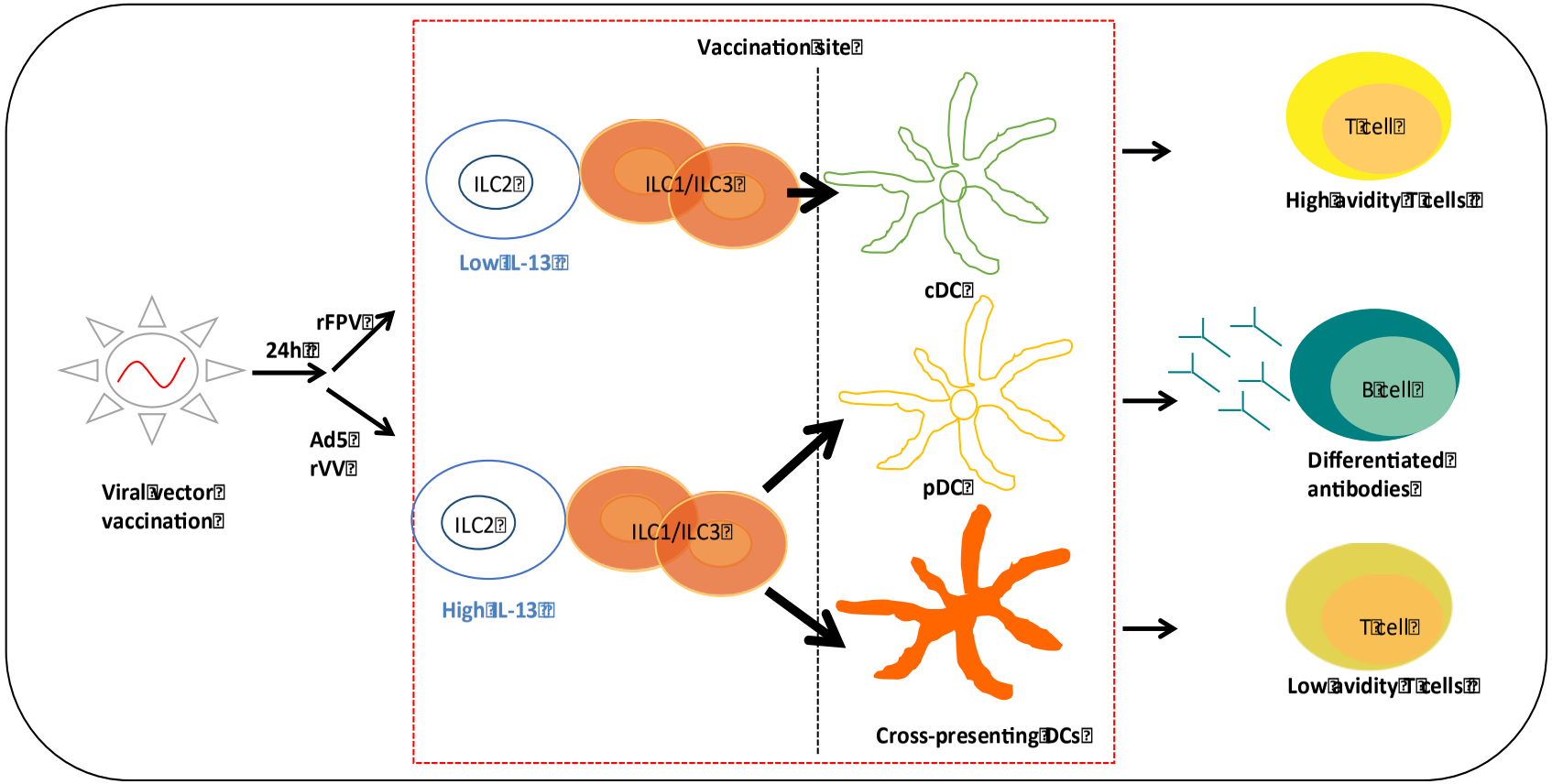
Vaccination site
ILC2
ILC1/ILC3
Low IL-13
cDC
rFPV
24h
Ad5
rVV
Viral vector
vaccination
ILC2
ILC1/ILC3
High IL-13
pDC
Cross-presenting DCs
T cell
High avidity T cells
B cell
Differentiated
antibodies
T cell
Low avidity T cells

Figure. 3.13. Graphical summary of ILC and DC cross-talk at the lung mucosae 24 h following viral vector vaccination. The viral vaccine vector administered determines the ILC2-derived IL-13 levels at the vaccination site. The subsequent level of IL-13 in the milieu significantly impacts the DC recruitment, where low IL-13 levels lead to preferential recruitment of cDCs and high IL-13 levels recruit cross-presenting DCs and/or pDCs. DC subsets recruited to the vaccination site ultimately determine the quality of vaccine- specific adaptive immune outcomes. Specifically, whilst cDCs generate high avidity CD8 T cells, cross presenting DCs prime low avidity CD8 T cells, pDCs could potentially yield effective antibody differentiation.

Furthermore, rVV, rMVA and rMVAΔIL-1βR data clearly demonstrated that the attenuation status of a viral vector and the presence or absence of virokines significantly modulated the ILC cytokine expression and DC profile. The rFPV and rMVAΔIL-1βR data indicated that viral vectors that do not interfere with the host immune system could be more efficacious at inducing vaccine-specific immunity in humans (e.g.- Avipoxvirus compared to Orthopoxvirus). These observations strongly highlight the notion that when designing viral vector-based vaccines, in addition to the safety and genetic stability, inherent properties of the viruses themselves need serious consideration (in this case, its replicative ability within the mammalian host).

We have previously shown that ILC2s are the only source of IL-13 at the vaccination site, 24 h post vaccination and IL-13 level in the milieu can crucially impact the DC recruitment at the lung mucosae [99,124,338]. Hence, collectively our findings suggest that, early ILC2-derived IL-13, together with ILC1/ILC3-derived IFN-γ and IL-17A, differentially impact DC recruitment/regulation at the vaccination site **(Figure 3.13)**, associated with adaptive immune outcomes and this warrants further investigation. Therefore, we postulate that i) following vaccination, ILC and DC profiles may act as predictors of downstream vaccine-specific immunity and ii) selection of viral vector according to the pathogen of interest (eg: virus, bacteria or parasites) may help tailor/design effective viral-vector based vaccines against chronic pathogens.

Chapter 4

Post viral vector-based vaccination IL-13Rα2 functions as a master sensor on conventional dendritic cells to regulate IL-13 in a STAT3 dependent manner. [3]

This work is now published as: ***Roy, S.,*** *Liu, HY., Jaeson, M.I., Deimel, L.P., and Ranasinghe, C. Unique IL-13Rα2/STAT3 mediated IL-13 regulation detected in lung conventional dendritic cells, 24 h post viral vector vaccination. Scientific Reports 2020.*

---

[3] Experiments related to Figures 4.14 and 4.15 were performed by Ho-Ying Liu; and 4.16 was performed by Lachlan Deimel.

4.1 Abstract

This study demonstrates that 24 h following viral vector-based vaccination IL-13Rα2 functions as a master sensor on conventional dendritic cells (cDCs), abetted by high protein stability coupled with minimal mRNA expression, to rapidly regulate DC mediated IL-13 responses at the lung mucosae, unlike IL-13Rα1. Under low IL-13, IL-13Rα2 performs as a primary signalling receptor, whilst under high IL-13, acts to sequester IL-13 to maintain homeostasis, both in a STAT3-dependent manner. Likewise, we show that viral vector-derived IL-13 levels at the vaccination site can induce differential STAT3/STAT6 paradigms in lung cDC, that can get regulated collaboratively or independently by TGF-β1 and IFN-γ. Specifically, low IL-13 responses associated with recombinant Fowlpox virus (rFPV) is regulated by early IL-13Rα2, correlated with STAT3/TGF-β1 expression. Whilst, high IL-13 responses, associated with recombinant Modified Vaccinia Ankara (rMVA) is regulated in an IL-13Rα1/STAT6 dependent manner associated with IFN-γR expression bias. Different viral vaccine vectors have previously been shown to induce unique adaptive immune outcomes. Taken together current observations suggest that IL-13Rα2-driven STAT3/STAT6 equilibrium at the cDC level may play an important role in governing the efficacy of vector-based vaccines. These new insights have high potential to be exploited to improve recombinant viral vector-based vaccine design, according to the pathogen of interest and/or therapies against IL-13 associated disease conditions.

4.2 Introduction

IL-13 and IL-4 share a common signalling receptor system and are known to have overlapping as well as distinct functions [278]. These two cytokines have been extensively studied under allergy, asthma, helminth and parasitic infections [309,357-359]. IL-13 is produced by various immune cell types, specifically innate lymphoid cells (ILC2s), CD4 and CD8 T cells [130,360] and can directly impact the function of eosinophils, basophils and dendritic cells (DCs) [361,362]. Recent allergy and asthma studies have shown that ILC2-derived IL-13 can stimulate the migration of lung DCs to promote Th2 immunity [363]. Interestingly, whilst overproduction of IL-13 is associated with tissue pathology [364], deficiency of IL-13 has been associated with increased susceptibility to certain skin cancers [365]. Moreover, mounting evidence has also suggested the importance of IL-13 regulation in infection and immunity.

We have previously demonstrated that the vaccine route, viral vector combination and cytokine milieu (level of IL-13) can significantly alter the adaptive immune outcomes [130,132,133]. Pox viral vector-based HIV vaccine strategies that transiently inhibited IL-13 activity at the vaccination site, can induce high avidity/poly-functional T cells both in mice and macaques [122-124] (Li *et. al* in preparation). Interestingly, 24h post delivery of these vaccines, whilst ILC2s were found to be the major source of IL-13 at the vaccination site [366], elevated recruitment of $CD11b^{+}$ $CD103^{-}$ conventional DCs (cDC) to the lung mucosae were associated with the observed adaptive immune outcomes [99]. Moreover, recently we have shown that different viral vector-based vaccines can induce unique ILC2-derived IL-13 profiles and recruitment of different DC subsets to the vaccination site, 24 h post delivery [367]. Specifically, i.n. rFPV vaccination associated with low ILC2-

derived IL-13 recruited CD11b$^+$ CD103$^-$ conventional DC (cDC) [99], whilst high/medium ILC2-derived IL-13 producers, rMVA and Ad5 vaccinations recruited enhanced cross-presenting DCs and plasmacytoid DCs (pDCs) to the lung mucosae, respectively. Using adoptive transfer of different DC subsets to the lung mucosae, we have also shown that cross-presenting DCs induced low avidity HIV-specific T cells, whilst cDC were associated with high avidity T cells [99]

IL-13 can bind to IL-13Rα1 with low affinity (K_D = 30 nM) and, heterodimerize with IL-4Rα subunit to form the Type II IL-4 receptor complex to activate downstream JAK1- or JAK2-/TYK2- induced STAT6 signalling [358]. Cheng *et al*. have also proposed that activation of IL-13Rα1/IL-4Rα could induce STAT3 signalling under certain IL-13 conditions [108] and a recent study has shown an association of IL-13Rα1 with STAT3 in relation to cardiac homeostasis [368]. Interestingly, IL-13Rα2, known to be the high affinity receptor for IL-13 (K_D = 440 pM) [278,369], initially thought to be a decoy receptor in mice has now been established as a functional receptor in humans [370]. Overexpression of IL-13Rα2 has been associated with various cancers and targeted as an anti-cancer therapeutic [291,293]. Although the exact signalling mechanism of IL-13Rα2 is not yet well-characterised, in malignant glioma, IL-13Rα2 has shown to regulate activation of STAT3 [299] and initiate signalling via activation protein 1 (AP-1). Furthermore IL-13Rα2 has also shown to induce transforming growth factor beta 1 (TGF-β1) under certain chronic infections and autoimmune disease conditions [309]. Recently, we have also shown that in the context of viral vector-based vaccination, the STAT6 independent pathway (likely associated with IL-13Rα2) was involved in antibody differentiation [302]. Therefore, knowing that both STAT3

and STAT6 are involved in IL-13 regulation and that IFN-γ can also modulate IL-13 activity [286,311,371], this study focused on deciphering the IL-13 signalling mechanisms lung cDCs employ under different IL-13 conditions (different viral vector-based vaccination conditions), to induce vastly different adaptive immune outcomes.

4.3 Materials and Methods

4.3.1 Mice.

Pathogen-free 6–8 weeks old female wild type BALB/c, IL-13$^{-/-}$ and STAT6$^{-/-}$ mice on a BALB/c background were purchased from the Australian Phenomics Facility, The Australian National University (ANU). All animals were maintained, monitored daily, euthanized by cervical dislocation and experiments were performed in accordance with the Australian NHMRC guidelines within the Australian Code of Practice for the Care and Use of Animals for Scientific Purposes and in accordance with guidelines approved by the ANU Animal Experimentation and Ethics Committee (AEEC), protocol number A2014/14 and A2017/15.

4.3.2 Immunisation.

BALB/c mice were intranasally immunised with 1 X 10^7 plaque forming units (pfu) of rFPV, rMVA, or 2 X 10^7 pfu of Ad5. Mice were vaccinated with a volume of 10 µl per nostril (total 20 µl) under mild isofluorane anaesthetic. rFPV and rMVA were sonicated thrice for 15 seconds in ice at 50% capacity using Branson Sonifier 450 immediately prior to vaccination.

4.3.3 Evaluation of lung DCs and IL-4/IL-13 and IFN-γ receptors using Flow cytometry.

Lung tissues were collected 24 h post vaccination as described in Li *et al.* 2018 [366]. 2 X 10^6 cells from each sample were blocked with anti-mouse CD16/CD32 antibody (BD Biosciences, USA) for 20 min at 4°C and cells were surface stained with APC-conjugated anti-mouse MHCII I-Ad (e-Biosciences, USA), biotin-conjugated anti- mouse CD11c (N418 clone, Biolegend, USA), followed by streptavidin Brilliant violet 421 (Biolegend, USA), anti-mouse CD11b AlexaFluor 700 (M1170 clone, Biolegend, USA) and anti-mouse CD103 FITC (2E7 clone, e-Biosciences, USA) for 30 min on ice as previously described in [367]. Cells were additionally extracellularly or intracellularly stained with anti-mouse IL-4Rα (CD124) PE (I015F8 clone, Biolegend, USA), anti-mouse IL-13Rα1 (CD213a) PE (13MOKA clone, e-Biosciences, USA), Biotin-conjugated anti-mouse IL-13Rα2 (110815 clone, R&D systems, USA), followed by streptavidin PE (Biolegend, USA), anti-mouse γc (CD132) PE (TUGm2 clone, Biolegend, USA) and biotin-conjugated anti-mouse IFN-γRa chain (CDw119) (2E2 clone, Biolegend, USA), followed by streptavidin PE (Biolegend, USA). For intracellular staining, cells were fixed using Fixation buffer (Biolegend, USA) for 10 minutes at 4°C followed by permeabilisation using 1x Intracellular staining permeabilisation wash buffer (Biolegend, USA) for 10 minutes at 4°C prior to intracellular staining. Cells were fixed using 1.5% paraformaldehyde followed by resuspension in PBS and analysed using BD LSRII flow cytometer Becton Dickinson, San Diego, CA). 5 x10^5 events per sample were acquired and results were analyzed using FlowJo software v10.0.7.

4.3.4 *In vitro* STAT3 and STAT6 inhibition assays.

Unimmunised BALB/c lung suspensions were treated with either 100 nM of small molecule STAT6 inhibitor (Axon Medchem) or 20 μM Stattic (small molecule STAT3 inhibitor) in PBS overnight followed by low (100 pg/ml) or high (10,000 pg/ml) IL-13 stimulation for 3 h or 0.5 h (as mentioned in specific figures) before evaluation of IL-4 and IL-13 receptor expression on lung DCs using flow cytometry as described above. Biologically relevant inhibitor concentrations were used in this study as reported previously [302,372].

4.3.5 Immunofluorescence assays.

Single cell suspensions of lungs were washed to remove media and blocked with anti-mouse CD16/CD32 Fc Block antibody (BD Biosciences, USA) for 20 min at 4°C and cells were surface stained with FITC- conjugated anti-mouse CD11c (N418 clone, Merck, Germany), anti-mouse IL-4Rα (CD124) PE (I015F8 clone, Biolegend), anti-mouse IL-13Rα1 (CD213a) PE (13MOKA clone, e-Biosciences, USA), Biotin-conjugated anti-mouse IL-13Rα2 (110815 clone, R&D systems, USA), followed by streptavidin APC (Biolegend, USA) and biotin-conjugated anti-mouse IFN-γRα chain (CDw119) (2E2 clone, Biolegend, USA), followed by streptavidin PE (Biolegend, USA). Cells were fixed using 1.5% Paraformaldehyde (Biolegend, USA) and suspension cells were centrifuged onto Poly-L-Lysin (Sigma, USA) coated glass cover slips. Cover slip containing cell pellet was covered with 10 μl of Antifade Vectashield mounting medium with or without 4′,6-diamidino-2-phenylindole (DAPI) from Vector Laboratories, USA and mounted onto a clean glass slide. Slides were imaged and analysed using Leica TCS SP5 confocal microscope (Leica, Germany) at 60x magnification. $DAPI^{low}$ $CD11c^{+}$ cells were identified as viable lung DCs for receptor expression. To quantify receptor co-expression, each $CD11c^{+}$ DC double positive for a given receptor

combination (IL-13Rα1 and IL-13Rα2, IL-4Rα and IL-13Rα2, or IL-13Rα2 and IFN-γR) was identified and quantified per imaged area as described in **Figure 4.1**. Proportion of each receptor combination was calculated as a percentage of the total number of viable DCs per imaged area. Data were represented as an average of 5 imaged areas from each experiment. To quantify IL-13/IL-4 receptor intensity, ImageJ software v 1.52e (for Windows) was used. During this process, $DAPI^{low}$ $CD11c^{+}$ cells expressing the receptor of interest were identified **(Figure 4.2)**. Next, each cell was identified as a region of interest (ROI) and the software generated integrated density of the ROI was used to calculate receptor intensity as; IL-13/IL-4 receptor intensity = (Integreated density of ROI/ Area of ROI).

4.3.6 cDC sorting for Fluidigm 48.48 Biomark and qPCR assays.

Single (n=48 per vaccine group) or 500 cDCs were sorted into 5 µl or 25 µl pre-amplification mixture respectively using a BD FACS Aria II cell sorter, using the gating strategy as described in **Figure 4.12**. The pre-amplification mixture contained 2x reaction buffer, SuperScript® III RT/Platinum® Taq Mix, 0.2x pooled assays, SUPERase• In™ RNase Inhibitor and DEPC treated water per well.

Sorted cDCs in pre-amplification mixture were centrifuged at 1454 x g to release mRNA as previously described [308]. The cDNA was synthesised using thermo-cycling program: 1x cycle of 50° C for 15 minutes, 95° C for 2 minutes followed by 14- 20 cycles (for single or 500 cells) of 95° C for 15 seconds and 60° C for 4 minutes, followed by storing samples at -20° C until use.

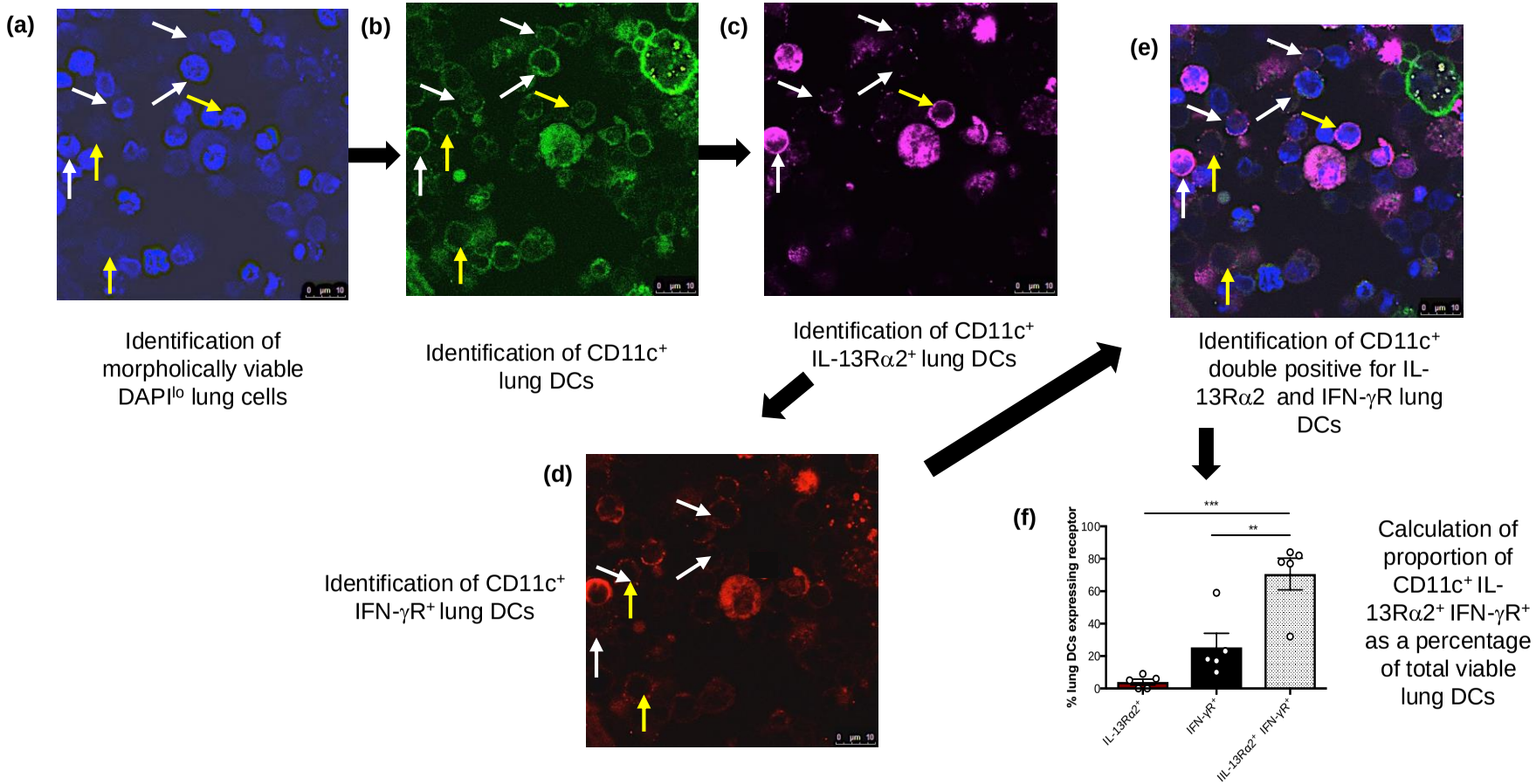
(a)
(b)
(c)
(d)
(e)
(f)
Identification of morpholically viable DAPI^{lo} lung cells
Identification of CD11c^{+} lung DCs
Identification of CD11c^{+} IL-13Rα2^{+} lung DCs
Identification of CD11c^{+} IFN-γR^{+} lung DCs
Identification of CD11c^{+} double positive for IL-13Rα2 and IFN-γR lung DCs
Calculation of proportion of CD11c^{+} IL-13Rα2^{+} IFN-γR^{+} as a percentage of total viable lung DCs
% lung DCs expressing receptor
100
80
60
40
20
0
***
**
IL-13Rα2^{+}
IFN-γR^{+}
IIL-13Rα2^{+} IFN-γR^{+}

Figure 4.1. IL-13Rα2 and IFN-γR co-expression and quantification strategy using confocal microscopy. (a) $DAPI^{low}$ cells were identified as viable lung cells followed by **(b)** $CD11c^{+}$ lung DCs, **(c)** IL-13R$\alpha 2^{+}$ lung DCs, **(d)** IFN-γR^{+} lung DCs and **(e)** cells double positive for IL-13Rα2 and IFN-γR. Yellow arrows indicate $DAPI^{low}$ $CD11c^{+}$ lung DCs expressing a single receptor and and white arrows indicate co-expression of both receptors. **(f)** Bar graph represents percentage of IL-13R$\alpha 2^{+}$, IFN-γR^{+} and IL-13R$\alpha 2^{+}$ IFN-γR^{+} lung $CD11c^{+}$ DCs calculated as a proportion of the total viable $DAPI^{low}$ $CD11c^{+}$ DCs from 5 imaged areas.

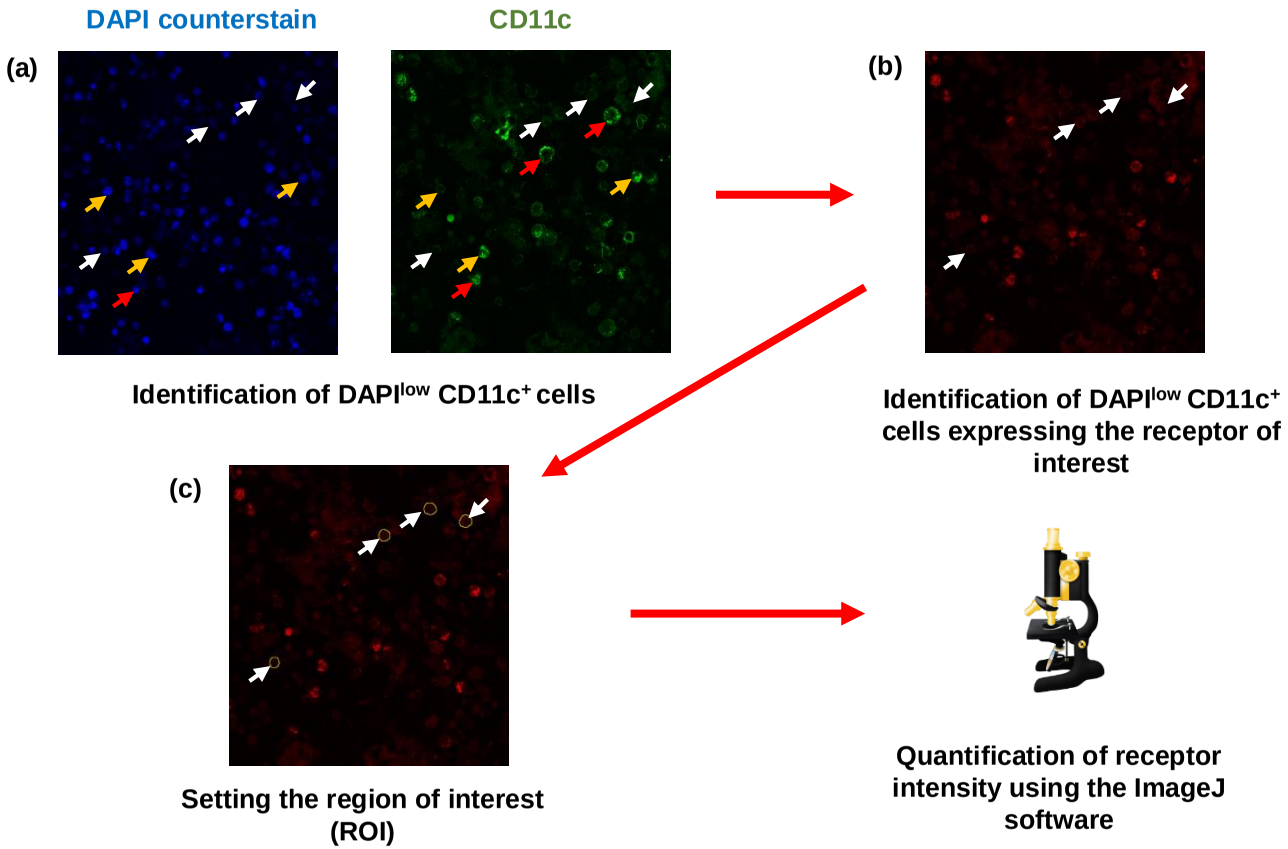
DAPI counterstain
CD11c
(a)
(b)
Identification of DAPI^{low} CD11c^{+} cells
Identification of DAPI^{low} CD11c^{+} cells expressing the receptor of interest
(c)
Setting the region of interest (ROI)
Quantification of receptor intensity using the ImageJ software

Figure 4.2. IL-13/ IL-4 receptor intensity quantification strategy using confocal microscopy. (a) White arrows indicate $DAPI^{low}$ $CD11c^{+}$ cells, red arrows and yellow arrows indicate apoptotic cells with unstructured cell membrane morphology and pre-apoptotic cells with high DAPI counterstaining respectively, which were not considered in this study. **(b)** White arrows indicate $DAPI^{low}$ $CD11c^{+}$ cells expressing the receptor of interest, **(c)** each cell of interest was identified by a region of interest (ROI) (yellow circle) (left) and measured the integrated density using the ImageJ software (right). Receptor intensity was calculated as: integrated density of ROI/ area of ROI.

4.3.7 Real-time quantitative PCR (RT-qPCR) analysis of IL-4/IL-13 receptors.

RT-qPCR for 500 cells was performed using TaqMan qPCR mix (containing 1 µL of each gene expression assay (primers listed in **Table 2.6**), 5 µL of 2X TaqMan Universal PCR master mix, 1 µL cDNA and 4.5 µL of DEPC treated water), using a 7900HT thermocycler program: 50°C for 2 minutes, 95°C for 10 minutes, and 45 cycles of 95°C for 15 seconds and 60°C for 1 minute. The targeted primer-probe FAM fluorescence was detected by normalising to ROX (6- carboxy-X-rhodamine) intensity. SDS 2.4 for Windows software was used to obtain the cycle threshold (Ct) values (ranging from 0 to 45) and the mRNA amplification profiles. Ct values were subject to quality control using SDS 2.4 analysis software where, 0 indicated a high expression and values closer to 45
indicated low expression levels.

4.3.8 Fluidigm 48.48 Biomark gene expression assay.

Fluidigm 48.48 gene expression assay was performed as previously described [308]. Briefly, prior to loading the integrated fluidic chip (IFC) (Fluidigm), the cDNA was diluted 1:1 cDNA:DEPC treated water. Following chip priming, 2.5µL of diluted cDNA (in DEPC water) and 0.25 µL of 20X GE Sample Loading Reagent was loaded onto the sample side of the chip. Subsequently, 2.5 µL of each gene expression assay **(Figure 4.3)** and 2.5 µL of 20X GE Assay Loading Reagent was loaded onto the assay side of the IFC. Next, the IFC was loaded onto the IFC Controller MX and gene expression assay was performed and analysed using the GE 48.48 Standard.pcl program on the Fluidigm Biomark™. The fluorescence values obtained from the Fluidigm Biomark™ were normalised to ROX (6- carboxy-X-rhodamine) intensity. Ct values (ranging from

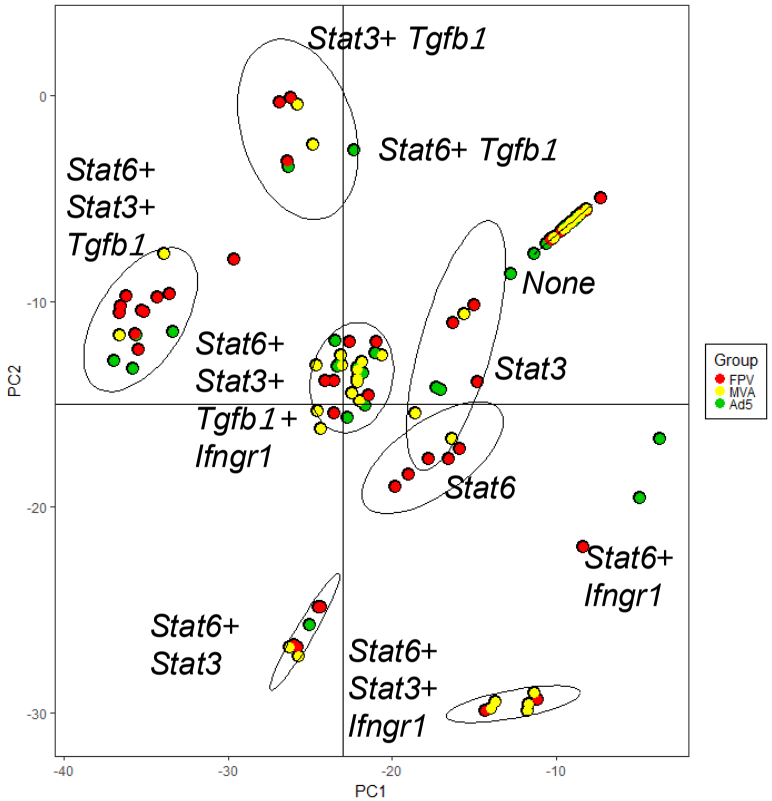

Figure 4.3. Evaluation of viral vector dependent *Stat3*, *Stat6*, *Tgfb1* and *Ifngr1* expression using PCA and K-means clustering. BALB/c mice (n=3 per group) were vaccinated with rFPV, rMVA or Ad5. 24 h post vaccination single cDCs were sorted from lung suspensions and Fluidigm 48.48 Biomark assay was performed as described in methods. Data indicate the different *Stat3, Stat6, Tgfb1* and *Ifngr1* gene co-expression profiles in cDCs relevant to each viral vector analysed using PCA and K-means clustering as described in the methods. Each point in the K-mean cluster analysis represents a single cell expressing genes within a cluster. These experiments were performed with 48 cDCs per vaccine group.

0 to 40) were subject to quality control using the Biomark Real-time qPCR analysis software where, 0 indicated a high expression and values closer to 40 indicated low expression levels. Binary analysis was performed to determine the proportion of cells expressing a certain gene using RStudio and Microsoft Excel 2016 software and analysed using GraphPad Prism 7.0.

4.3.9 Statistical analysis.

Lung MHC-II$^+$ CD11c$^+$ CD11b$^+$ CD103$^-$ cDC proportions were represented as a percentage of total MHC-II$^+$ CD11c$^+$ DCs and receptor proportions were calculated as a percentage of parent cDC population as described in [367]. The *p*-values were calculated using either two-tailed, paired parametric Student's t-test or Ordinary One-way ANOVA with Tukey's multiple comparison post-test. Gene expression was first analysed as percentage of cDCs expressing a gene of interest. For each gene of interest, the Ct value for the housekeeping gene (*I32*) was subtracted from each sample Ct value to determine ΔCt, and the gene expression level was calculated as 40–ΔCt or 45–ΔCt. All experiments were repeated minimum two times. Principal Component Analysis (PCA) was performed to analyse the relationship between the genes, using a correlation matrix created using Spearman's rho (ρ) as described previously [308]. To determine the co-expression profile with respect to only *Stat3, Stat6, tgfb1* and *Ifngr1*, following PCA, a k-means clustering algorithm using RStudio was used to identify clusters. To determine statistical significance with respect to co-expression studies, a Fisher's exact test was implemented with False Discovery Rate (FDR) correction.

4.4 Results

4.4.1 rFPV vaccination significantly up-regulated IL-13Rα2 expression on lung cDCs 24 h post i.n. vaccination

Knowing that rFPV priming, which induced low ILC2-derived IL-13 and CD11b$^+$ CD103$^-$ cDCs [367], was associated with high avidity T cells [99], this study aimed to unravel the underlying mechanisms by which IL-13 regulated cDC recruitment, following intranasal (i.n.) rFPV vaccination. Hence, IL-4/IL-13 receptor expression on lung cDCs (MHC-II$^+$ CD11c$^+$ CD11b$^+$ CD103$^-$) were evaluated 24 h post delivery using flow cytometry following gating strategy described in **Figure 4.4**. Data revealed that infiltrated lung cDCs in response to 24 h of i.n. rFPV vaccination exhibited significantly higher proportion of intracellular and extracellular expression of IL-13Rα2 compared to the unimmunised control (p<0.0001; **Figure 4.5a and b**). In the context of other IL-4/IL-13 associated receptors, IL-4Rα, IL-13Rα1 and γc were marginally or not expressed on cDCs **(**p<0.001; **Figure 4.5a and b)**. Upon vaccination although intracellular IL-13Rα1 expression was up-regulated compared to the unimmunised control (p=0.0019), no such difference was observed extracellularly **(Figure 4.5a and b)**. Moreover, unlike the other receptors, significantly higher IL-13Rα2 density was also observed on vaccinated lung cDCs compared to the unimmunized control (p=0.0006) **(Figure 4.5c and d)**. Note that to validate the specificity of IL-4/IL-13 receptor antibodies, expression of these receptors was assessed on several different immune cells as well as tissue types. Interestingly, elevated IL-13Rα2 expression was only observed on vaccinated lung DCs not splenic (systemic) DCs or other immune cells (CD4$^+$ T cells, CD8$^+$ T cells and B220$^+$ B cells) tested from both tissue types (**Figures 4.6 and 4.7**), indicating that the IL-13Rα2 expression pattern was lung DC-specific.

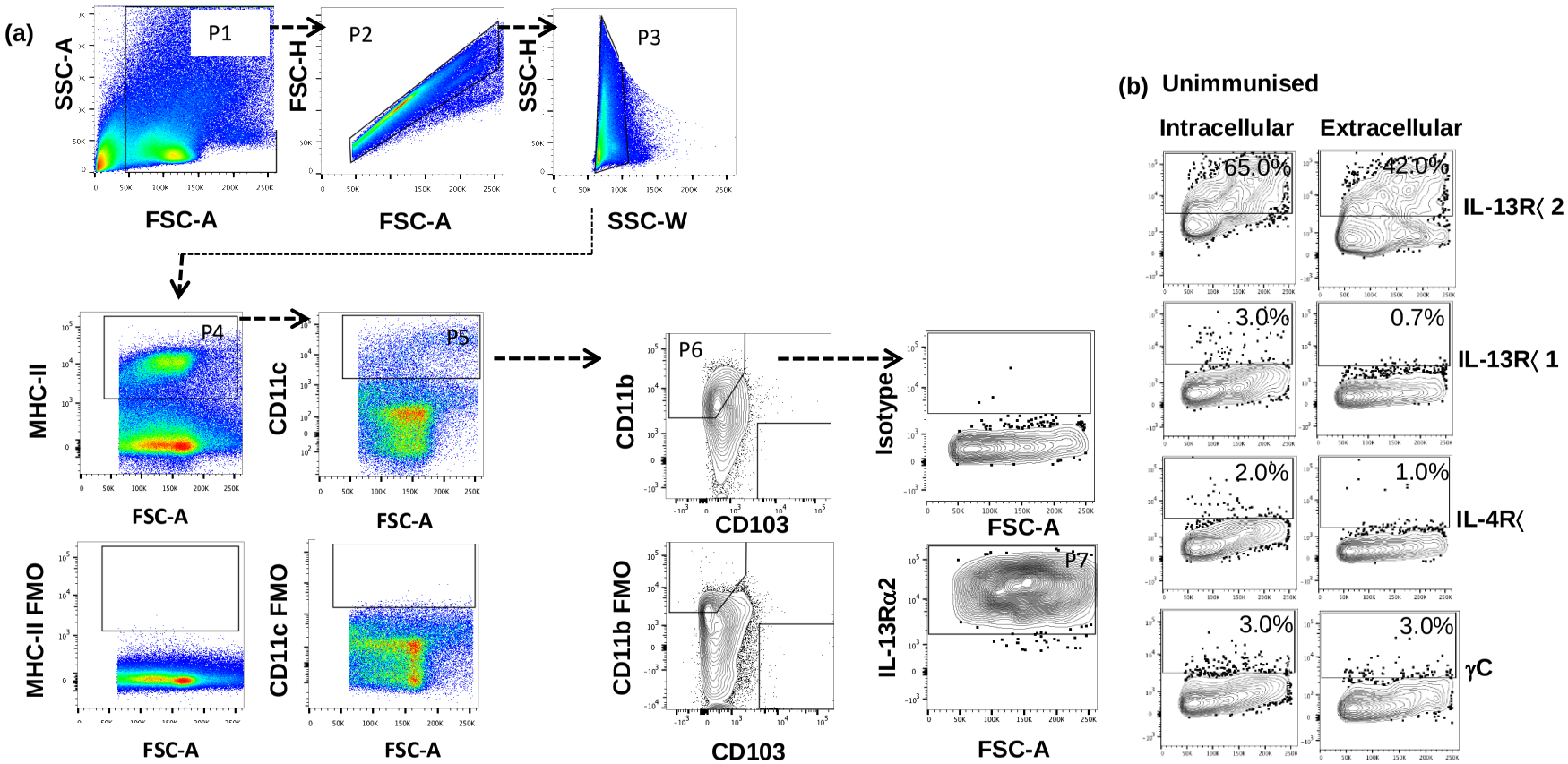
(a)
P1
SSC-A
FSC-A
P2
FSC-H
FSC-A
P3
SSC-H
SSC-W
P4
MHC-II
FSC-A
P5
CD11c
FSC-A
MHC-II FMO
FSC-A
CD11c FMO
FSC-A
P6
CD11b
CD103
CD11b FMO
CD103
Isotype
FSC-A
P7
IL-13Rα2
FSC-A
(b) Unimmunised
Intracellular
Extracellular
65.0%
42.0%
IL-13R⟨ 2
3.0%
0.7%
IL-13R⟨ 1
2.0%
1.0%
IL-4R⟨
3.0%
3.0%
γC

Figure 4.4. Flow cytometry gating for lung cDCs and IL-4/IL-13 receptors 24 h following i.n. rFPV immunisation. **(a)** Plots show viable cells (P1) after gating on single cells based on forward scatter (FSC-H and FSC-A; P2) and side scatter (SSC-H and SSC-W; P3) were then gated on MHC-II-I-Ad^{+} (P4) and analysed for CD11c expression compared to FMO controls. Total DCs (MHC-II-I-A^{d+} CD11c^{+} - P5) were further gated on CD11b^{+} CD103^{-} (P6) using appropriate FMO controls for each marker. (Note that to avoid breaking the CD11b population in half, the FMO was set to include CD11b^{low}, CD11b^{int} and CD11b^{hi} populations, even though IL-13Rα2 expression was mainly associated with CD11b^{int} and CD11b^{hi} populations). Receptor positive cells (P7) were gated based on isotype controls specific for the viral vector. **(b)** Representative flow cytometry plots show intracellular and extracellular IL-13Rα2, IL-13Rα1, IL-4Rα and γc expressions on lung cDCs from unimmunised BALB/c mice.

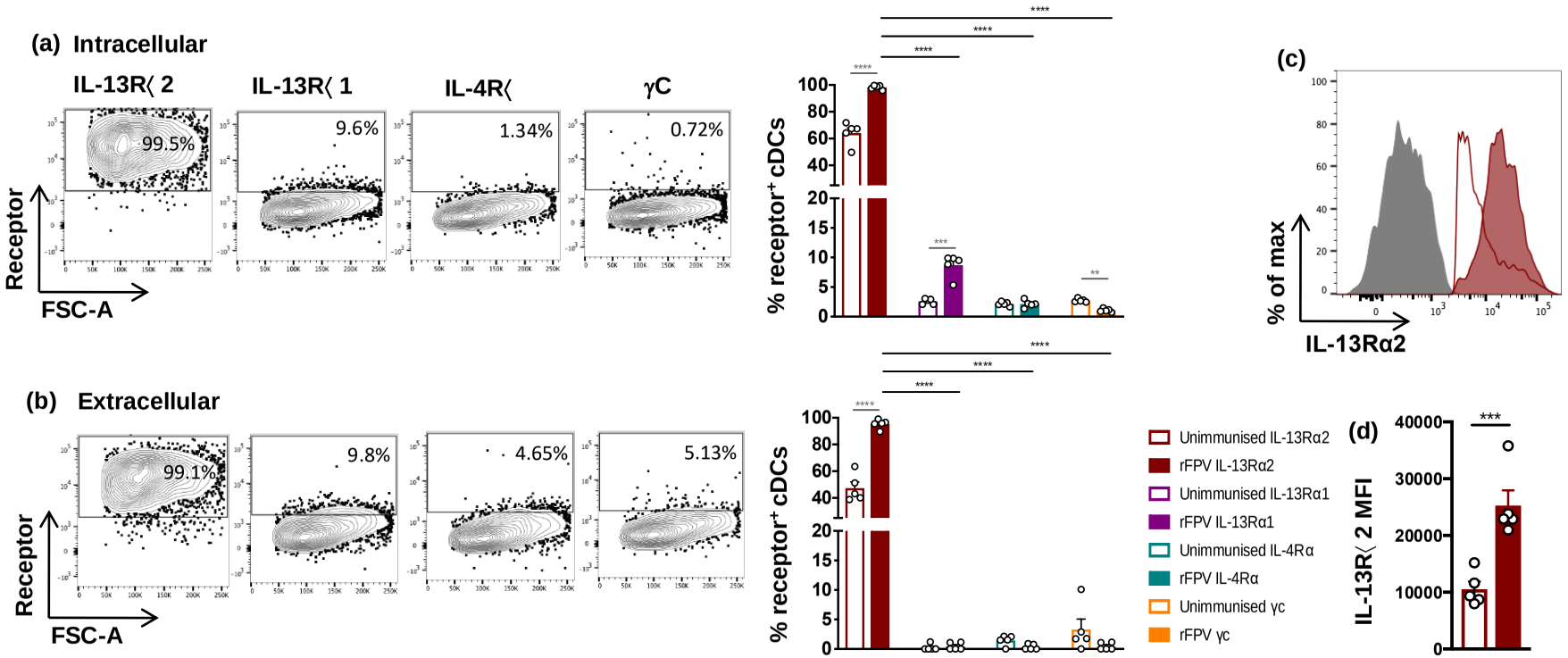
(a) Intracellular
IL-13R⟨ 2
IL-13R⟨ 1
IL-4R⟨
γC
99.5%
9.6%
1.34%
0.72%
Receptor
FSC-A
% receptor+ cDCs
(b) Extracellular
99.1%
9.8%
4.65%
5.13%
Receptor
FSC-A
% receptor+ cDCs
Unimmunised IL-13Rα2
rFPV IL-13Rα2
Unimmunised IL-13Rα1
rFPV IL-13Rα1
Unimmunised IL-4Rα
rFPV IL-4Rα
Unimmunised γc
rFPV γc
(c)
% of max
IL-13Rα2
(d)
IL-13R⟨ 2 MFI

Figure 4.5 (a-d). Evaluation of IL-4 and IL-13 receptors on lung cDCs 24 h post rFPV vaccination. BALB/c mice (n=5 per group) were intranasally (i.n.) immunised with rFPV. 24 h post vaccination, lungs were harvested and single cell suspensions were stained for MHC-II^{+} CD11c^{+} CD11b^{+} CD103^{-} cDCs to evaluate receptor expressions on lung cDCs using flow cytometry as described in methods. Representative flow cytometry plots (left panel) and bar graphs (right panel) show the percentage of cDCs expressing IL-13Rα2, IL-13Rα1, IL-4Rα and γc at the **(a)** intracellular and **(b)** extracellular levels compared between rFPV vaccinated and unimmunised mice. **(c)** FACS histogram plot and **(d)** bar graph show a comparative extracellular IL-13Rα2 expression density on lung cDCs from rFPV vaccinated (solid red) compared to unimmunised mice (red line) and isotype control (solid grey). In all graphs, error bars represent Standard Error of mean (SEM) and *p* values were calculated using One-way ANOVA followed by Tukey's multiple comparison test (black) for comparing any two conditions and paired Student's t-test (grey) for comparing a specific pair of dependent conditions (unimmunised and rFPV). *$p<0.05$, **$p<0.01$, ***$p<0.001$, ****$p<0.0001$. Experiments were repeated thrice.

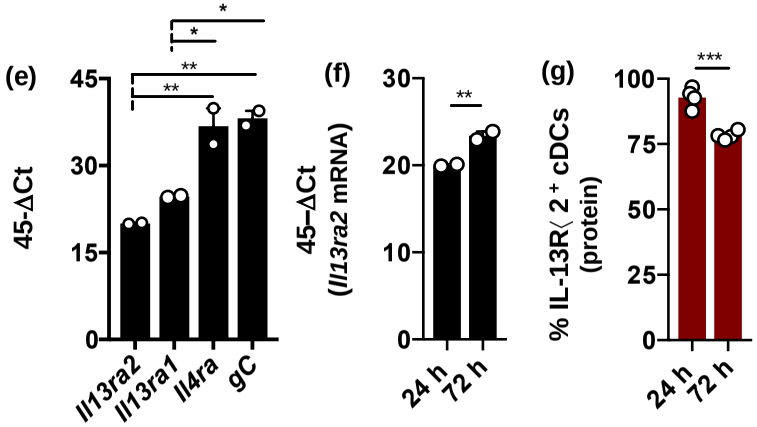

Figure 4.5 (e-g). Evaluation of mRNA expression of IL-4 and IL-13 receptors on sorted lung cDCs post rFPV vaccination. Bar graphs show mRNA expression level of **(e)** *Il13ra2*, *Il13ra1*, *Il4ra* and *gC* at 24 h and **(f)** *Il13ra2* at 24 and 72 h post rFPV vaccination, in 500 sorted lung cDCs, evaluated using qPCR, represented as 45-ΔCt, as described in materials and methods each dot represents one set of 500 cDCs. **(g)** Bar graph represents percentage of lung cDCs (n=4) expressing IL-13Rα2 at 24 and 72 h post rFPV vaccination measured using flow cytometry as described in methods. Error bars represent Standard Error of mean (SEM) and *p* values were calculated using One-way ANOVA followed by Tukey's multiple comparison test. *$p<0.05$, **$p<0.01$, ***$p<0.001$, ****$p<0.0001$. These experiments were repeated twice.

Interestingly, qPCR analysis of IL-4/IL-13 mRNA expression on lung cDCs at 24 h post rFPV vaccination revealed that *Il13ra2* mRNA expression was significantly lower (associated with high Ct) **(Figure 4.5e and 4.8)** compared to all the other receptors, where *Il4ra* and *gC* mRNA expression levels were much greater than *Il13ra1* and *Il13ra2* (*Il13ra2* vs *Il4ra* p=0.0034, *Il13ra2* vs *gC* p=0.0018), **(Figure 4.5e)**. However, in the context of IL-13Rα2, at 72 h post rFPV vaccination, elevated mRNA followed by reduced protein expression was observed (inverse to 24h) **(Figure 4.5f and g),** indicative of a non-linear mRNA-protein regulation of this receptor.

To further confirm the expression profiles of IL-13Rα2, IL-13Rα1 and IL-4Rα 24 h post rFPV vaccination on lung DCs, immunofluorescence staining was also performed as described in methods and **Figure 4.9a**. Data showed that elevated proportion of lung CD11c$^+$ DCs expressed IL-13Rα2, compared to IL-13Rα1 or IL-4Rα, (p<0.0001) in accordance with flow cytomtery data **(Figure 4.10a and b).**

4.4.2 IL-13 stimulation conditions lead to differential expression of IL-13Rα1 and IL-13Rα2 on CD11c$^+$ lung DCs

As different viral vector-based vaccines have shown to induce different levels of IL-13 at the lung mucosae, which influence DC activity [367], *in vitro* IL-13 stimulation was performed to mimic these vaccination conditions in order to study the effect of IL-13 on IL-4/IL-13 receptors. Flow cytometric analysis showed that when unimmunized lung cells from BALB/c mice were stimulated with a range of IL-13 concentrations, at different time intervals, IL-13Rα1 and IL-13Rα2 were differentially expressed. Within 30 minutes of low IL-13 (100

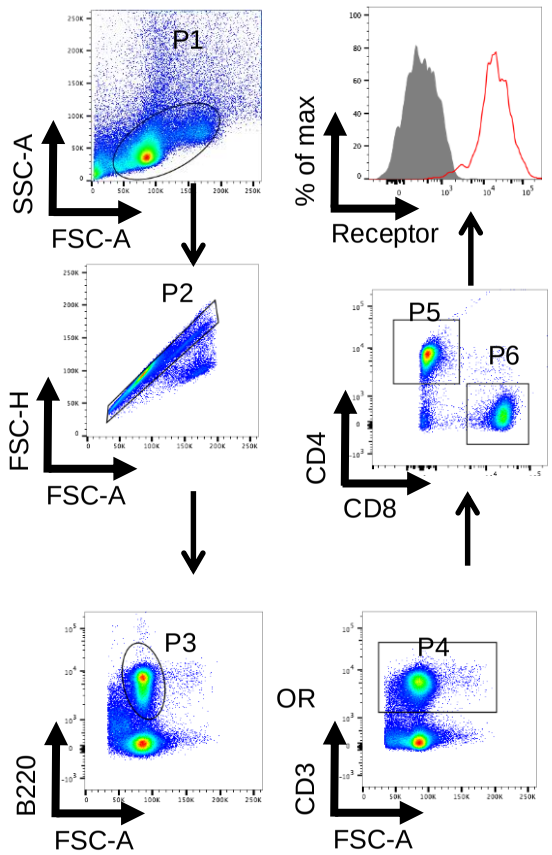
P1
SSC-A
FSC-A
P2
FSC-H
FSC-A
P3
B220
FSC-A
OR
P4
CD3
FSC-A
P5
P6
CD4
CD8
% of max
Receptor

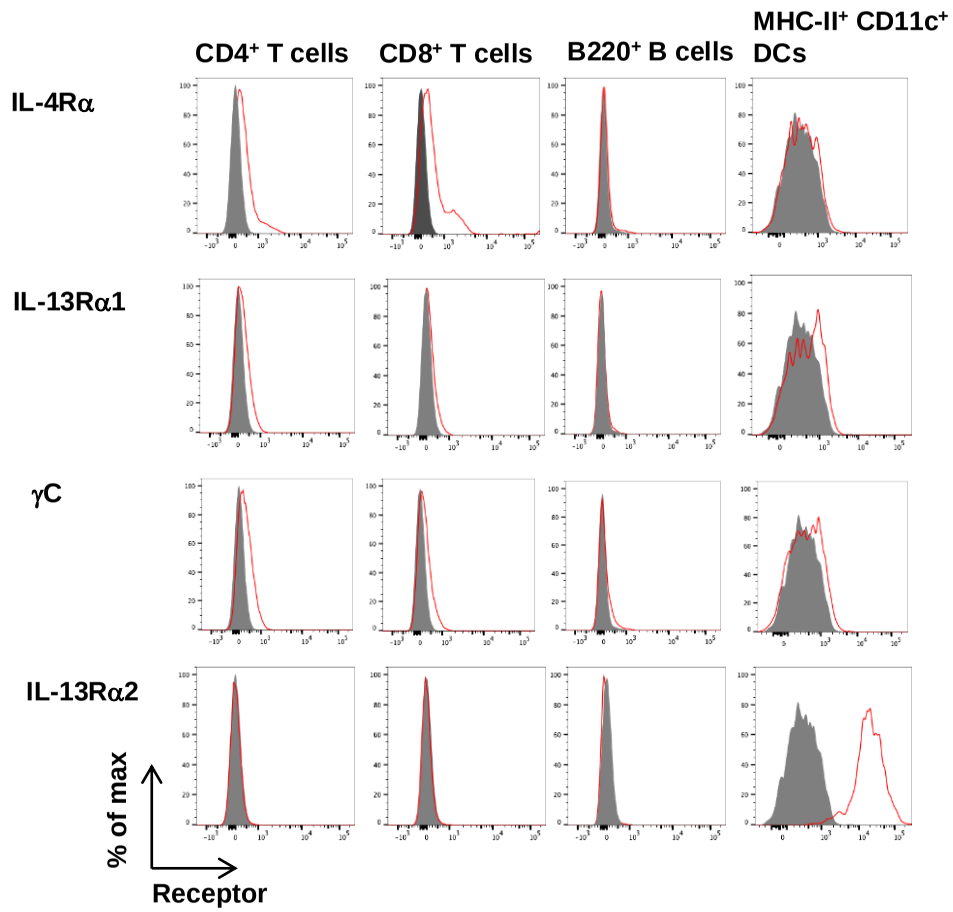
CD4+ T cells
CD8+ T cells
B220+ B cells
MHC-II+ CD11c+ DCs
IL-4Rα
IL-13Rα1
γC
IL-13Rα2
% of max
Receptor

Figure 4.6. Evaluation of IL-4 and IL-13 receptor expression on lung lymphocytes and DCs 24h following rFPV vaccination. BALB/c mice n=5 were i.n. vaccinated with rFPV and 24h post lungs were prepared as described in methods. (Left panel) B220$^+$ B cells (P3) were gated from Single lymphocytes (P2) and CD4$^+$ T cells (P5) and CD8$^+$ T cells (P6) were gated from CD3$^+$ T cells (P3), following gating on single lymphocytes (P2). MHC-II$^+$ CD11c$^+$ DCs were gated following strategy described in methods. (Right panel) Flow cytometry analysis was performed and representative histogram plots show geometric mean intensities for IL-4Rα, IL-13Rα1, γc and IL-13Rα2 (red line) against the isotype control (solid grey) on lung CD4$^+$ T cells, CD8$^+$ T cells, B220$^+$ B cells and MHC-II$^+$ CD11c$^+$ DCs.

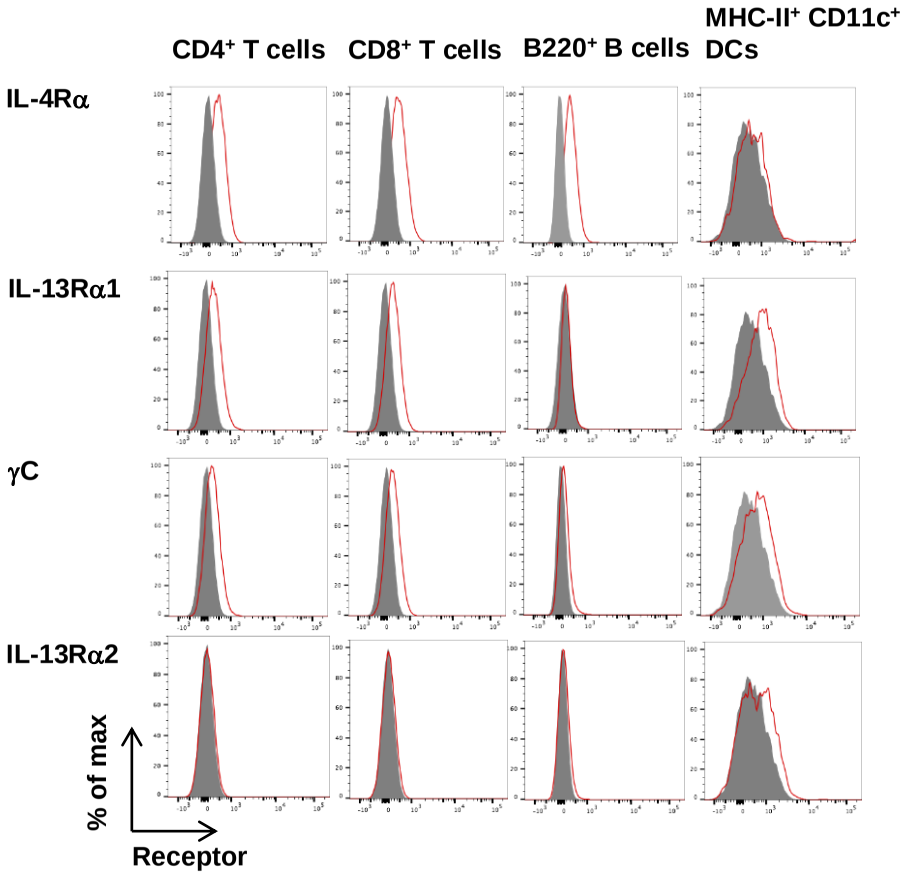

Figure 4.7. Evaluation of IL-4 and IL-13 receptor expression on splenic lymphocytes and DCs. Unimmunised BALB/c mice n=5 were used to obtain spleens and single cell suspensions were prepared to stain for lymphocytes and DCs as described in methods. $CD4^+$ T cells, $CD8^+$ T cells and $B220^+$ B cells were gated as shown in Figure 4.7 and MHC-II^+ $CD11c^+$ DCs were gated following strategy described in methods. Flow cytometry analysis was performed and representative histogram plots show geometric mean intensities for IL-4Rα, IL-13Rα1, γc and IL-13Rα2 (red line) against the isotype control (solid grey) on splenic $CD4^+$ T cells, $CD8^+$ T cells, $B220^+$ B cells and MHC-II^+ $CD11c^+$ DCs.

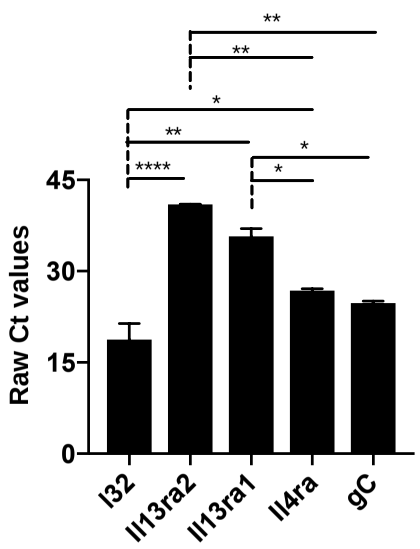

Figure 4.8. Evaluation of IL-4/ IL-13 receptor mRNA expression on lung cDCs at 24 h post rFPV vaccination. BALB/c mice lungs (n=3) were harvested at 24 h post rFPV vaccination and single cell suspensions were FACS sorted for 500 MHC-II^{+} CD11c^{+} CD11b^{+} CD103^{-} cDCs to evaluate IL-4 and IL-13 receptors at the mRNA level using qPCR as described in methods. Bar graphs represent raw Ct values for all receptors and house-keeping gene, Ribosomal protein L32 (*l32).* Note that high Ct indicates low mRNA expression. Error bars represent Standard Error of mean (SEM) and *p* values were calculated using One-way ANOVA followed by Tukey's multiple comparison test. **p*<0.05, ***p*<0.01, ****p*<0.001, *****p*<0.0001. Experiments was repeated two times.

(a) Representative images for DAPI only background control for confocal microscopy images

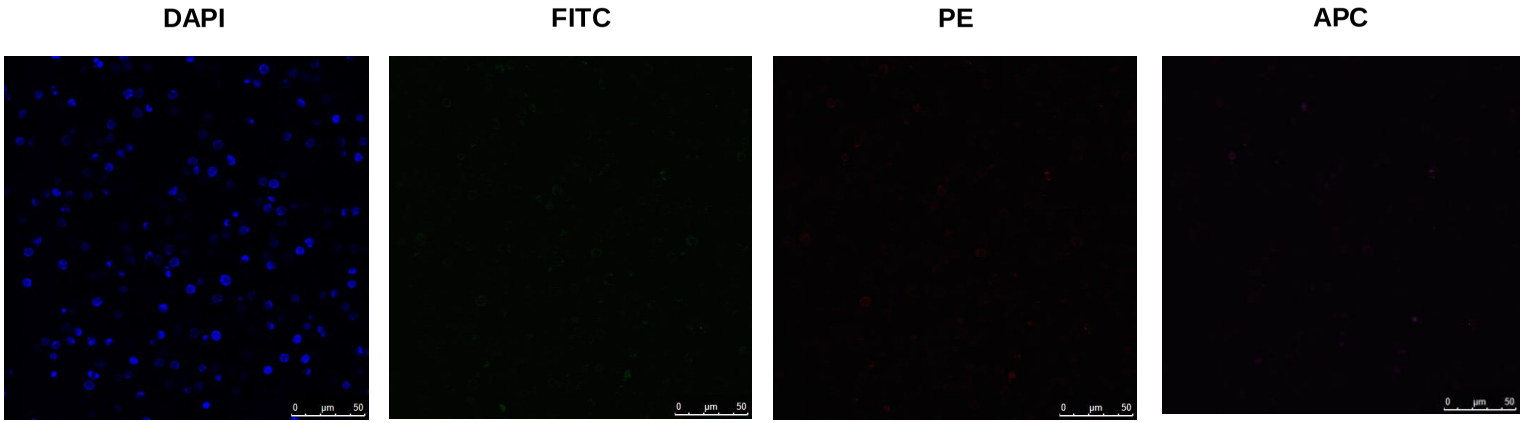

(b) DAPI only background control and unstained control for in vitro IL-13 stimulation studies

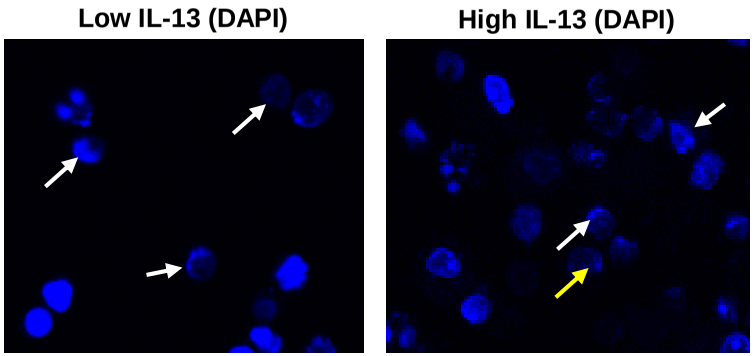

Figure 4.9. Immunofluorescence imaging of lung CD11c^{+} DC negative controls for receptors using confocal microscopy. (a) Representative confocal microscopy images of lung cells stained with DAPI to identify viable cells unstained for receptor antibodies, showing negative controls for the FITC, PE and APC channels. **(b)** Unimmunised lung cells showing DAPI^{lo} cells stimulated with, low (100pg/ml) and high (10000pg/ml) IL-13. White arrows indicate CD11c^{+} DCs co-expressing IL-13Rα2 and IL-13Rα1, whilst yellow arrows show expression of IL-13Rα1 only.

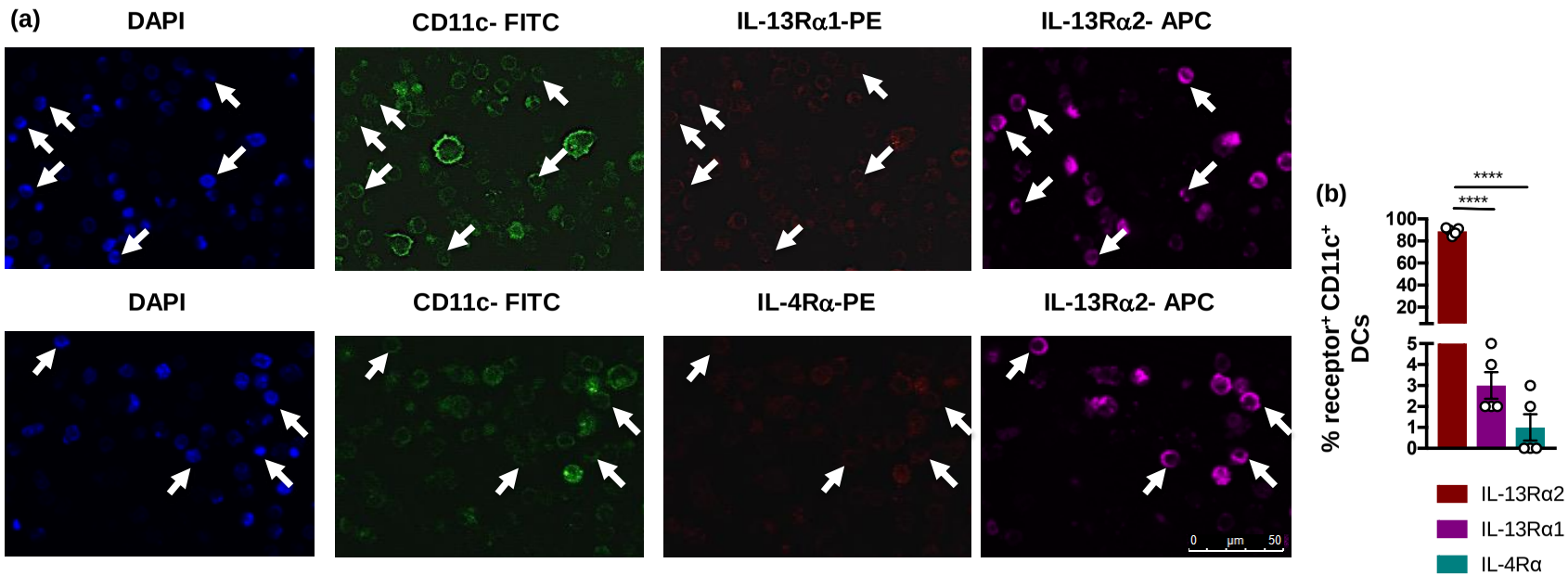
(a)
DAPI
CD11c- FITC
IL-13Rα1-PE
IL-13Rα2- APC
DAPI
CD11c- FITC
IL-4Rα-PE
IL-13Rα2- APC
0 µm 50
(b)
% receptor+ CD11c+ DCs
****
****
100
80
60
40
20
5
4
3
2
1
0
IL-13Rα2
IL-13Rα1
IL-4Rα

Figure 4.10. Evaluation of IL-4/IL-13 receptor expression on lung CD11c$^+$ DCs 24 h following rFPV vaccination using confocal microscopy. (a) Representative immunofluorescence images show lung cells from i.n. rFPV vaccinated BALB/c mice (n=5) 24 h post-delivery, expressing IL-13Rα2$^+$ and IL-13Rα1$^+$ (top panel) and IL-13Rα2$^+$ and IL-4Rα^+ (bottom panel) at magnification x60, as described in methods. White arrows indicate CD11c$^+$ DCs either IL-13Rα2$^+$ IL-13Rα1$^+$ or IL-13Rα2$^+$ IL-4Rα^+. **(b)** Bar graph shows the significant differences between percentage of cDCs expressing IL-13Rα2$^+$, IL-13Rα1$^+$, or IL-4Rα^+. Error bars represent Standard Error of mean (SEM) and *p* values were calculated using One-way ANOVA followed by Tukey's multiple comparison test. *$p<0.05$, **$p<0.01$, ***$p<0.001$, ****$p<0.0001$. All experiments were repeated three times.

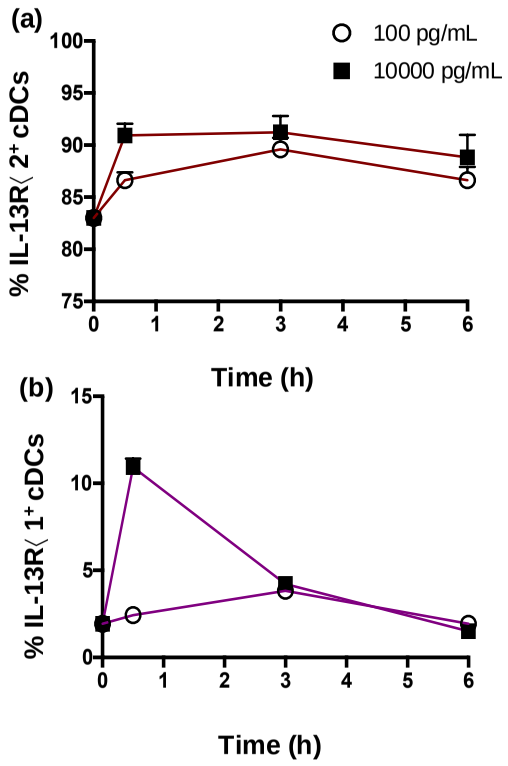

Figure 4.11 (a-b). Evaluation of relative IL-13Rα1 and IL-13Rα2 expression on lung DCs following low and high IL-13 stimulation *in vitro* using flow cytometry. Lung cells from unimmunised BALB/c (n=5 per group) were stimulated with 100 pg/ml (low) or 10000 pg/ml (high) IL-13 for 0.5, 3 and 6 h. Lung suspensions were stained for MHC-II$^+$ CD11c$^+$ DCs and IL-13 receptor expression was evaluated using flow cytometry. Line graphs show percentage of lung cDCs expressing **(a)** IL-13Rα2 and **(b)** IL-13Rα1 in response to low or high IL-13 concentrations over time. Error bars represent Standard Error of mean (SEM). Experiments were repeated thrice.

pg/ml) stimulation, IL-13Rα2 was expressed, and was sustained even at 10000 pg/ml (10 ng/ml) IL-13 concentration **(Figure 4.11a)**. In contrast, only very high IL-13 concentrations, 10000 pg/ml (10 ng/ml) lead to the expression of IL-13Rα1 and the expression was time dependent, where at 6h the expression level was similar to the baseline control, unlike IL-13Rα2 **(Figure 4.11b)**. Confocal imaging as described in methods further confirmed that very high IL-13 10000 pg/ml (10 ng/ml) can induce elevated expression of IL-13Rα1 on lung CD11c$^+$ DCs compared to no or low IL-13 (100 pg/ml) conditions (p<0.0001) **(Figure 4.11c** top and bottom panels**)**. In contrast, both high and low IL-13 conditions, showed no difference in IL-13Rα2 expression on lung CD11c$^+$ DCs, consistent with flow cytometry **(Figure 4.11c** top and middle panels**)**. Moreover, an average 77% and 15% of lung CD11c$^+$ DCs were found to co-express IL-13Rα2 and IL-13Rα1 under high and low IL-13 conditions respectively **(Figure 4.11d).** Confocal microscopy also further confirmed that there was no IL-4Rα activity following IL-13 stimulation (data not shown).

4.4.3 STAT3 inhibition significantly up-regulated IL-13Rα2 and down-regulated IL-13Rα1 on lung DCs

IL-13Rα1 signalling is known to activate STAT6 [278], and in some cases STAT3 [368,371], and IL-13Rα2 has shown to activate STAT3 and TGF-β1 [299,309]. Furthermore, our recent studies have shown *Stat3*, *Stat6* and *Tgfb1* gene expression on lung ILC2s, 24 h following viral vector vaccination (Jaeson *et al*. submitted). Knowing that ILC2-derived cytokines, especially IL-13, can impact DC recruitment [367], in this study, 12 regulatory genes were assessed by single

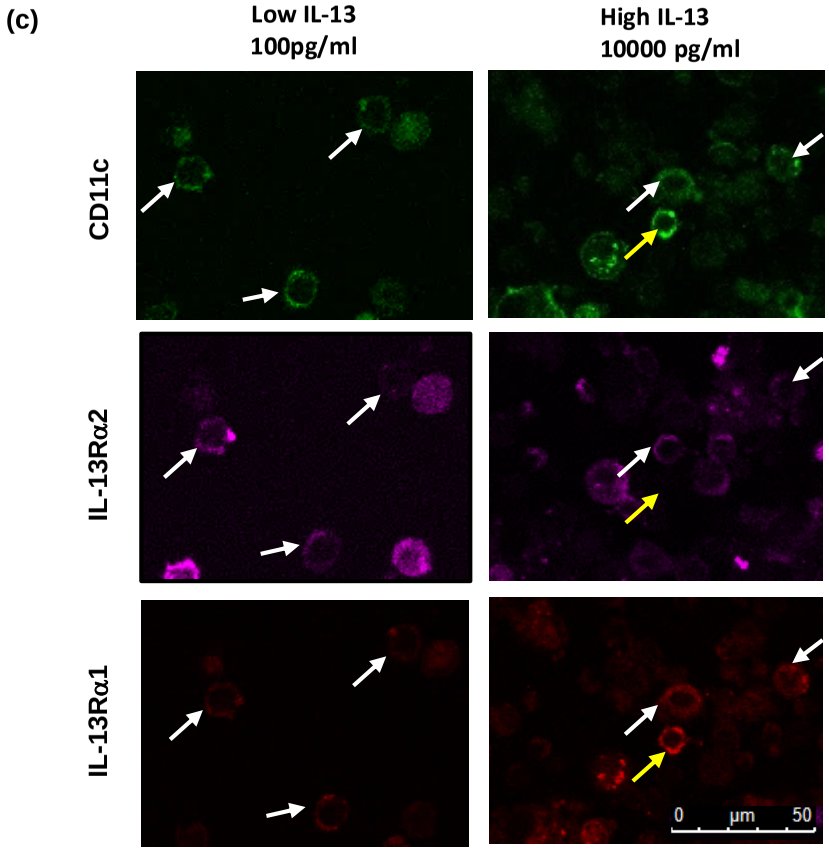
(c)
Low IL-13
100pg/ml
High IL-13
10000 pg/ml
CD11c
IL-13Rα2
IL-13Rα1
0 µm 50

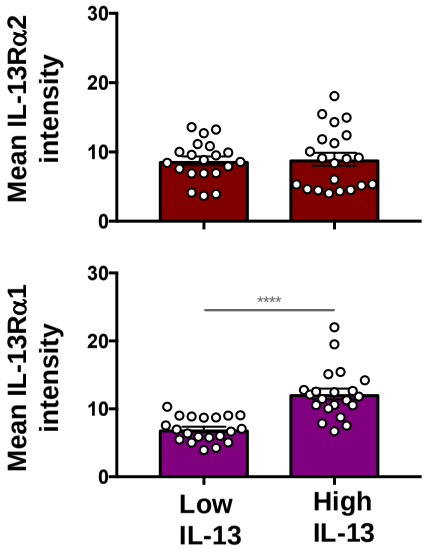
Mean IL-13Rα2 intensity
30
20
10
0
Mean IL-13Rα1 intensity
30
20
10
0
****
Low IL-13
High IL-13

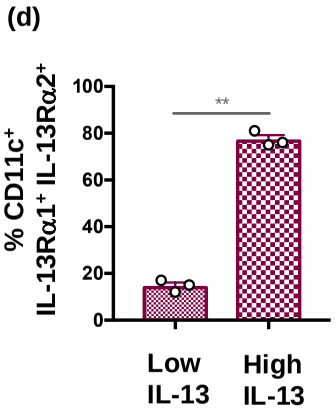
(d)
% CD11c+ IL-13Rα1+ IL-13Rα2+
100
80
60
40
20
0
**
Low IL-13
High IL-13

Figure 4.11 (c-d). Evaluation of relative IL-13Rα1 and IL-13Rα2 expression on lung DCs following low and high IL-13 stimulation *in vitro* using confocal microscopy. (c) Representative images at magnification x60 of $DAPI^{lo}$ cells as described in Figure 4.10b show corresponding CD11c (top), IL-13Rα2 (middle) and IL-13Rα1 (bottom) expression as well as quantified mean intensity for IL-13Rα2 (red bars) and IL-13Rα1 (magenta bars) at 10000 pg/ml (high) and 100 pg/ml (low) IL-13 conditions, stimulated for 0.5 h, as described in methods. White arrows indicate $CD11c^{+}$ DCs co-expressing IL-13Rα2 and IL-13Rα1, whilst yellow arrows show expression of IL-13Rα1 only. **(d)** Bar graph indicates the percentage of $CD11c^{+}$ DCs co-expressing IL-13Rα2 and IL-13Rα1 under low and high IL-13 stimulation conditions . Error bars represent Standard Error of mean (SEM) and *p* values were calculated using paired Student's t-test. *$p<0.05$, **$p<0.01$, ***$p<0.001$, ****$p<0.0001$ and these experiments were repeated three times.

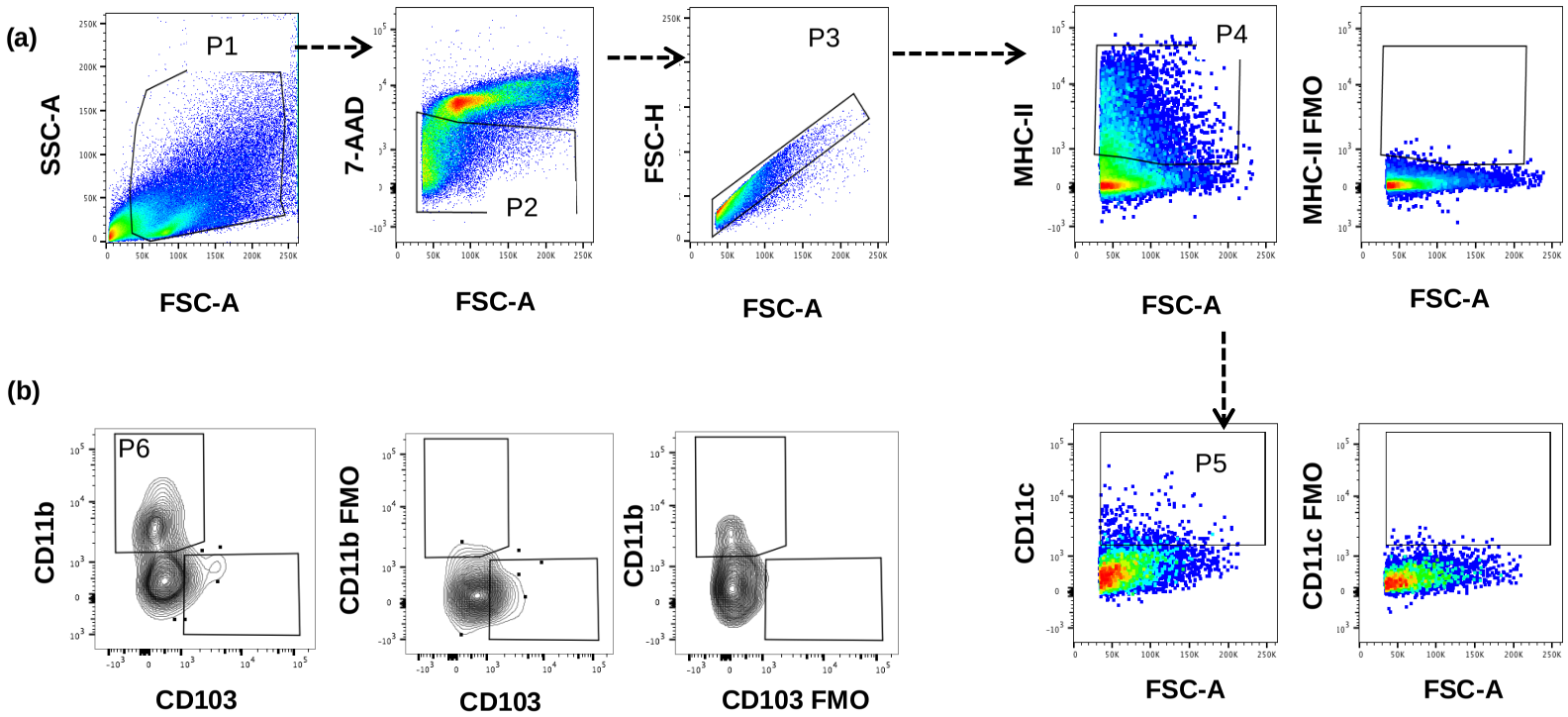
(a)
P1
SSC-A
FSC-A
P2
7-AAD
FSC-A
P3
FSC-H
FSC-A
P4
MHC-II
FSC-A
MHC-II FMO
FSC-A
(b)
P6
CD11b
CD103
CD11b FMO
CD103
CD11b
CD103 FMO
P5
CD11c
FSC-A
CD11c FMO
FSC-A

Figure 4.12. Flow cytometry gating strategy and Fluorescence minus one (FMO) controls used to identify lung cDCs for single cell cell sorting following i.n. viral vector immunisation. Pre-gated cells (P1) were used to gate on 7-AAD^{-} viable cells (P2), followed by doublet exclusion (P3) based on forward scatter (FSC-H and FSC-A). Cells were then gated on MHC-II-I-Ad^{+} (P4), followed by total DCs represented as (MHC-II-I-A^{d+} CD11c^{+} - P5). **(b)** Total lung DCs were further gated on CD11b^{+} CD103^{-} cDCs (P6) based on FMO controls as indicated.

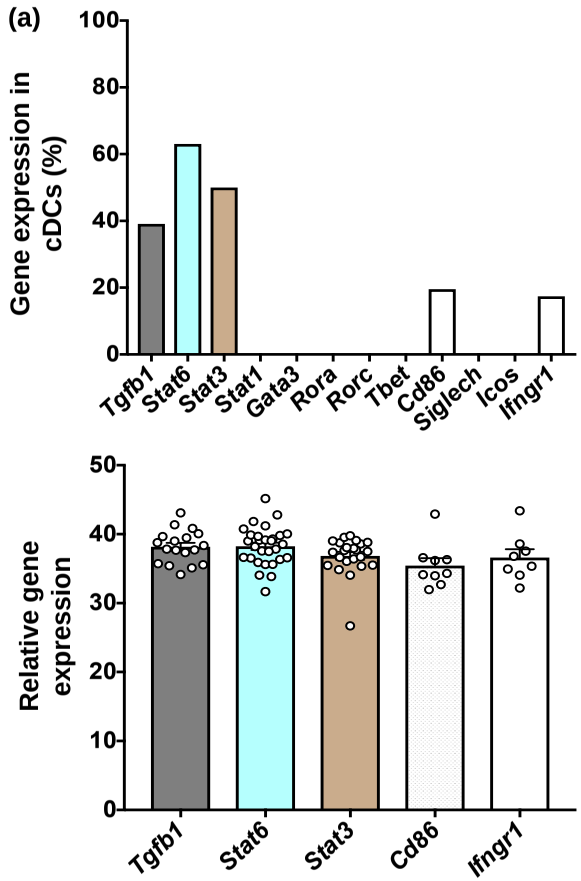
(a)
Gene expression in cDCs (%)
100
80
60
40
20
0
Tgfb1
Stat6
Stat3
Stat1
Gata3
Rora
Rorc
Tbet
Cd86
Siglech
Icos
Ifngr1
Relative gene expression
50
40
30
20
10
0
Tgfb1
Stat6
Stat3
Cd86
Ifngr1

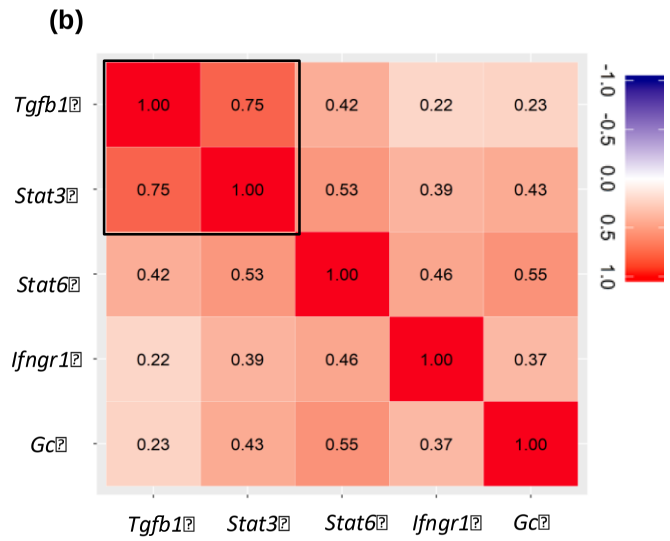
(b)
Tgfb1 1.00 0.75 0.42 0.22 0.23
Stat3 0.75 1.00 0.53 0.39 0.43
Stat6 0.42 0.53 1.00 0.46 0.55
Ifngr1 0.22 0.39 0.46 1.00 0.37
Gc 0.23 0.43 0.55 0.37 1.00
Tgfb1 Stat3 Stat6 Ifngr1 Gc
-1.0 -0.5 0.0 0.5 1.0

Figure 4.13. Expression of IL-4/IL-13 related molecules 24 h following rFPV vaccination. BALB/c mice (n=3) were vaccinated i.n. with rFPV and MHC-II^{+} CD11c^{+} CD11b^{+} CD103^{-} single cDCs were sorted for Fluidigm 48.48 Biomark assay to analyse the expression of 12 selected genes as described in methods. **(a)** Graphs represent the percentage of cDCs expressing the genes of interest (top) and the expression level for each gene represented as 40 – ΔCt (where 40 represent the maximum number of qPCR cycles) (bottom). **(b)** Principal Component Analysis (PC1 vs PC2) was performed on the genes of interest as described in methods. Correlation data indicate the level of expression where values closest to 1.00 represent the strongest correlation. Experiments were repeated two times.

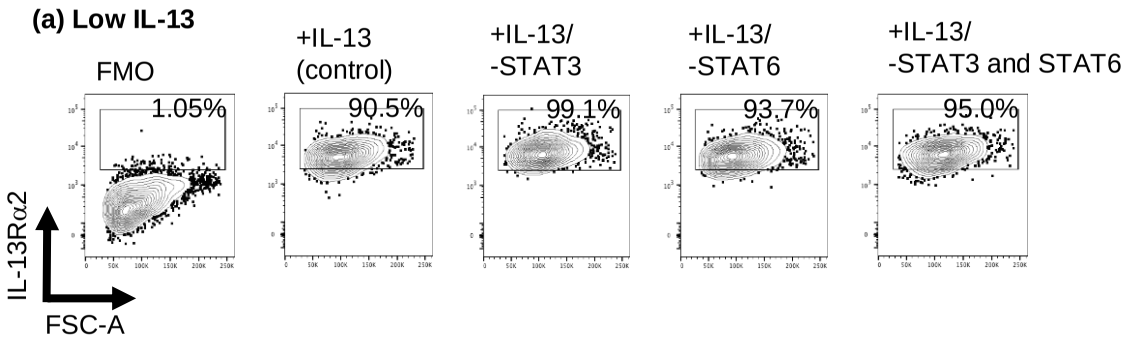
(a) Low IL-13
FMO
1.05%
+IL-13
(control)
90.5%
+IL-13/
-STAT3
99.1%
+IL-13/
-STAT6
93.7%
+IL-13/
-STAT3 and STAT6
95.0%
IL-13Rα2
FSC-A

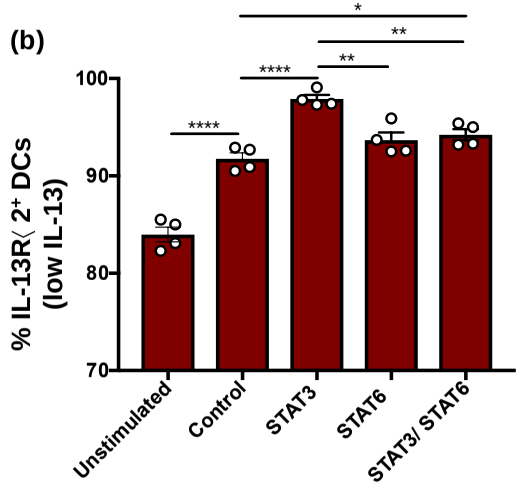
(b)
% IL-13R〈 2+ DCs
(low IL-13)
100
90
80
70
****
****
**
**
*
Unstimulated
Control
STAT3
STAT6
STAT3/ STAT6

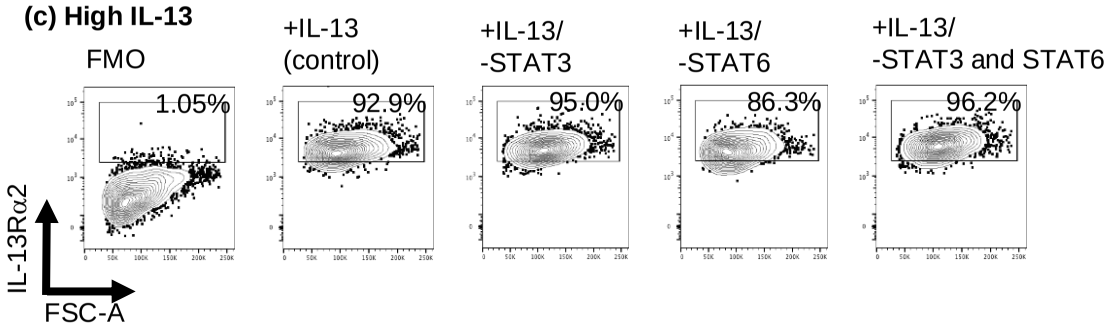
(c) High IL-13
FMO
1.05%
+IL-13
(control)
92.9%
+IL-13/
-STAT3
95.0%
+IL-13/
-STAT6
86.3%
+IL-13/
-STAT3 and STAT6
96.2%
IL-13Rα2
FSC-A

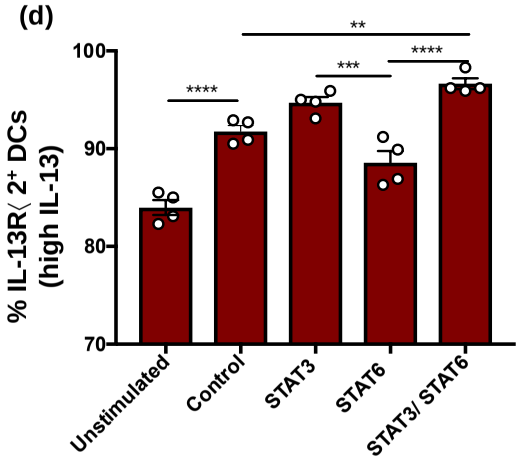
(d)
% IL-13R〈 2+ DCs
(high IL-13)
100
90
80
70
****
***
****
**
Unstimulated
Control
STAT3
STAT6
STAT3/ STAT6

Figure 4.14. Expression of IL-13Rα2 on lung DCs following *in vitro* IL-13 stimulation. Flow cytometry plots and bar graphs indicate expression of IL-13Rα2 on lung MHC-II^{+} CD11c^{+} DCs from BALB/c mice (n=4) following STAT3, STAT6 or combined STAT3/STAT6 inhibition **(a and b)** under 100 pg/ml (low IL-13) and **(c and d)** 10000 pg/ml (high IL-13) concentrations for 3 h, *in vitro* compared to no stimulation (unstimulated). Error bars represent Standard Error of mean (SEM) and *p* values were calculated using One-way ANOVA followed by Tukey's multiple comparison test. *$p<0.05$, **$p<0.01$, ***$p<0.001$, ****$p<0.0001$. Experiments were repeated three times.

cell Fluidigm 48.48 assay as described in materials and methods and **Figure 4.12**. Data revealed that, 40-60% of cDCs expressed *Tgfb1, Stat3* and *Stat6*, 24 h post rFPV vaccination **(Figure 4.13a)**. Also, 15-20% of cDCs were found to express *Ifngr1* and *cd86*. The *cd86* expression as opposed to *siglec-h* further confirmed that the sorted single cells were cDCs and not pDCs **(Figure 4.13a)**. Principal component Analysis (PCA) revealed that, the probability of co-expression of *Stat3* and *Tgfb1* on cDCs was much greater (75%) than *Tgfb1* and *Stat6* (42%) **(Figure 4.13b),** and co-expression of *Stat3* together with *Stat6* was (53%), 24 h post rFPV vaccination **(Figure 4.13b).** Furthermore, the probability of co-expression of *Ifngr1* with *Stat3* whilst being 39%, *Ifngr1 with Tgfb1* was 22%, which were much lower than co-expression of *Ifngr1* and *Stat6* (46%) **(Figure 4.13b).** Note that in these studies, Ribosomal protein L32 (*Rpl32*), Stratifin (*Ywhas*) and Eukaryote elongation factor 2 (*Eef2*) were used as endogenous positive control genes to validate the mRNA data **(Table 2.6)**.

To understand the relationship between STAT3, STAT6 and IL-13Rα2 at the protein level (by mimicking low and high IL-13 conditions at the vaccination site post different viral vector-based vaccination), when lung cells were treated with small-molecule inhibitors of STAT3 or STAT6 in the presence of low (100 pg/ml) and high (10000 pg/ml or 10ng/ml) IL-13, differential regulation of IL-13Rα2 was detected on lung DCs. These results clearly demonstrated that under low IL-13 stimulatory conditions, STAT3 inhibition caused significant up-regulation of IL-13Rα2 compared to the uninhibited control (p<0.001) **(Figure 4.14a-b)**. In contrast, under these conditions, although STAT6 inhibition showed some up-regulation of IL-13Rα2 **(Figure 4.14a-b)**, combined STAT3/STAT6 inhibition did

not show any change in IL-13Rα2 expression compared to STAT6 inhibition alone, although there was some up-regulation compared to the control (p=0.026) **(Figure 4.14a-b).** But surprisingly, under high IL-13, both STAT3 inhibition and combined STAT3/STAT6 inhibition induced elevated IL-13Rα2 expression on DCs **(Figure 4.14c-d)**. Under all inhibitory conditions tested, the profiles of IL-13Rα1 and IL-4Rα expression mimicked each other **(Figure 4.14a-d)**. Specifically, STAT6 inhibition caused significant up-regulation of these two receptors on DCs compared to the uninhibited control. In contrast, STAT3 and combined STAT3/STAT6 inhibition showed a significant down-regulation of IL-13Rα1 and IL-4Rα compared to the uninhibited control **(Figure 4.14a-d)**. Note that, STAT6 inhibition induced IL-13Rα1 up-regulation, further confirming the association of IL-13Rα1 with STAT6. Therefore, following STAT3 inhibition up-regulation of IL-13Rα2 was indicative of the IL-13Rα2 association with STAT3. It is also noteworthy that, IL-4 receptors (IL-4Rα and γc) were not regulated on DCs even upon IL-4 stimulation **(Figure 4.15a-b)**. This confirmed that the observed receptor regulation was triggered by IL-13 not IL-4.

4.4.4 STAT3 inhibition significantly down-regulated TGF-β1 on lung cDCs *in vivo*, associated with IL-13Rα2

Since Fluidigm 48.48 Biomark analysis of rFPV vaccinated lung cDCs revealed that *Stat3* and *Tgfb1* gene expression were strongly correlated, next association of STAT3 activation/phosphorylation with TGF-β1 at the protein level was evaluated. *In vitro* inhibition studies under low IL-13 (100 pg/ml) stimulation revealed revealed that STAT3 inhibition significantly down-regulated TGF-β1 expression in cDCs whilst STAT6 inhibition had no impact compared to the

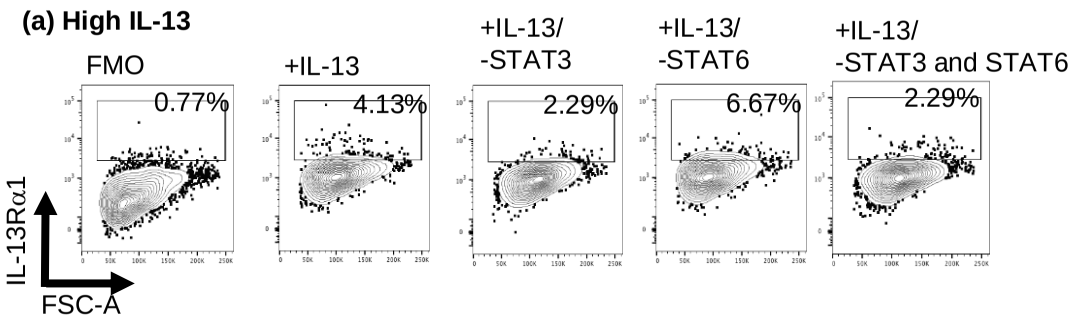
(a) High IL-13
FMO
+IL-13
+IL-13/
-STAT3
+IL-13/
-STAT6
+IL-13/
-STAT3 and STAT6
0.77%
4.13%
2.29%
6.67%
2.29%
IL-13Rα1
FSC-A

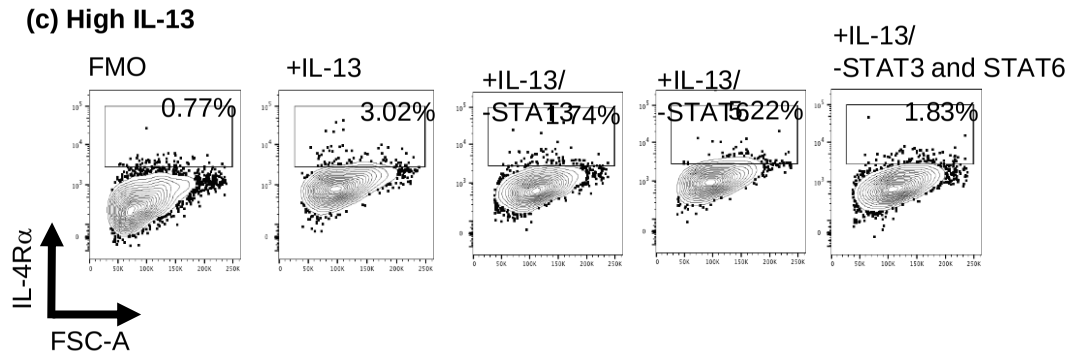
(c) High IL-13
FMO
+IL-13
+IL-13/
-STAT3
+IL-13/
-STAT6
+IL-13/
-STAT3 and STAT6
0.77%
3.02%
1.74%
5.22%
1.83%
IL-4Rα
FSC-A

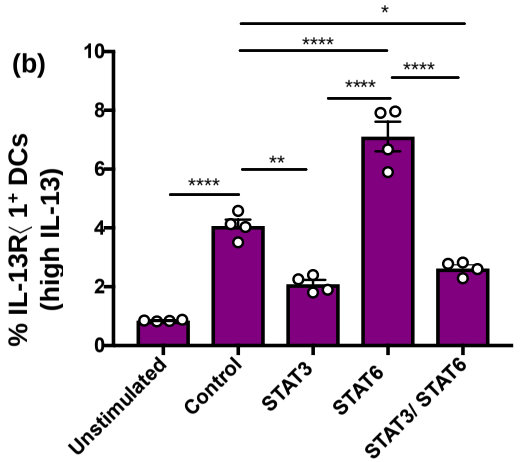
(b)
% IL-13Rα1+ DCs
(high IL-13)
Unstimulated
Control
STAT3
STAT6
STAT3/ STAT6

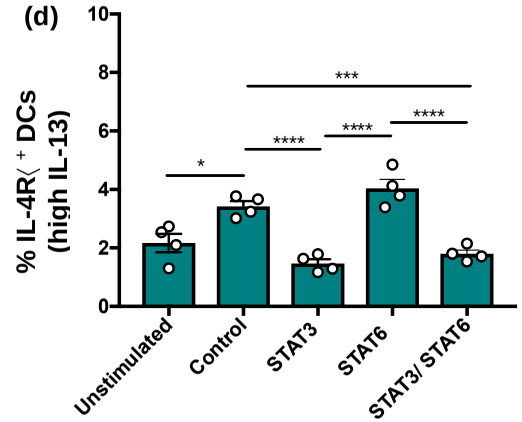
(d)
% IL-4Rα+ DCs
(high IL-13)
Unstimulated
Control
STAT3
STAT6
STAT3/ STAT6

Figure 4.15. Expression of IL-13Rα1 and IL-4Rα on lung DCs following *in vitro* IL-13 stimulation. Flow cytometry plots and bar graphs indicate expression of **(a and b)** IL-13Rα1 and **(c and d)** IL-4Rα on lung MHC-II^{+} CD11c^{+} DCs from BALB/c mice (n=4) following STAT3, STAT6 or combined STAT3/STAT6 inhibition under 10000 pg/ml (high IL-13) concentrations for 3 h *in vitro* compared to no stimulation (unstimulated). Error bars represent Standard Error of mean (SEM) and *p* values were calculated using One-way ANOVA followed by Tukey's multiple comparison test. *$p<0.05$, **$p<0.01$, ***$p<0.001$, ****$p<0.0001$. Experiments were repeated three times.

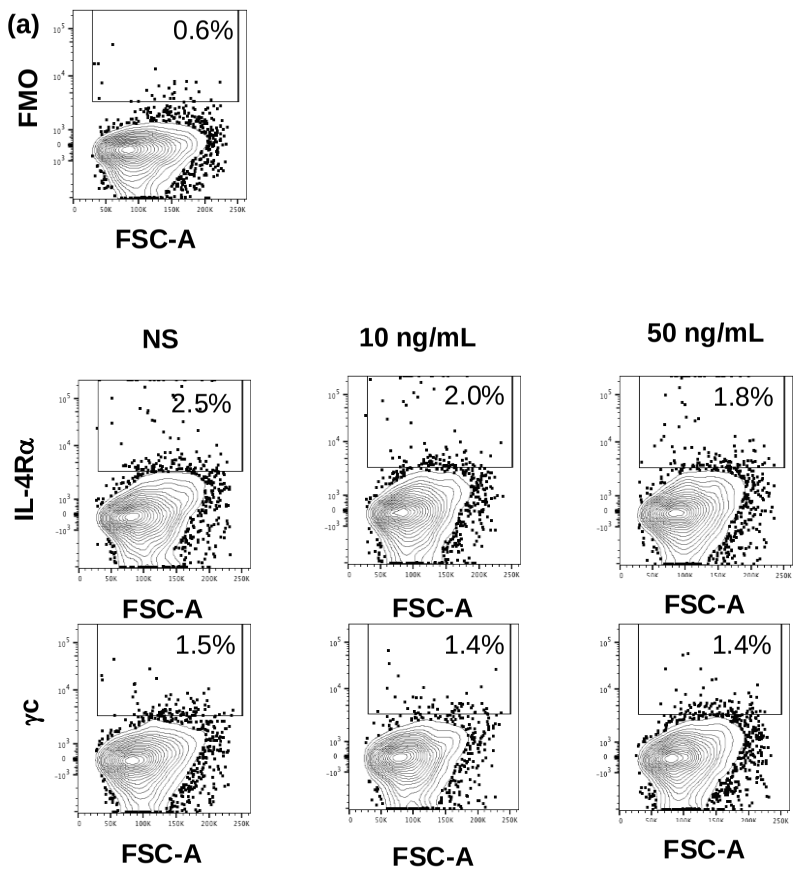

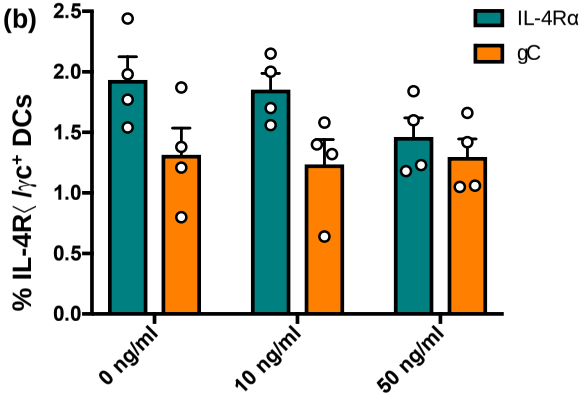

Figure 4.16. Expression of IL-4Rα and γc on lung cDCs following *in vitro* IL-13 stimulation. (a) Flow cytometry plots and (b) bar graphs indicate IL-4Rα and γc expression on unimmunised lung MHC-II$^+$ CD11c$^+$ DCs (n=4) following 0, 10 and 50 ng/ml of IL-4 stimulation for 0.5 h. Error bars represent Standard Error of mean (SEM) and *p* values were calculated using One-way ANOVA followed by Tukey's multiple comparison test. **p*<0.05, ***p*<0.01, ****p*<0.001, *****p*<0.0001. Experiments were repeated three times.

uninhibited control **(Figure 4.16a-b)**. To understand the relationship between IL-13, IL-13Rα2, STAT3 and TGF-β1, when STAT6$^{-/-}$ mice were vaccinated i.n. with rFPV (which induced low IL-13 at the vaccination site and enhanced IL-13Rα2 expression on lung cDCs, **(Figure 4.5)**) and lung cDCs were assessed 24 h post vaccination, phosphorylated STAT3 (pSTAT3) and TGF-β1 were both up-regulated on STAT6$^{-/-}$ cDCs compared to the wild type counterpart (p=0.0038 and 0.0003 respectively, **(Figure 4.17c-d)**), suggestive of IL-13Rα2 signalling. Moreover, significant up-regulation of IL-13Rα2 **(Figure 4.18a-b)** and down-regulation of TGF-β1 **(Figure 4.18c-d)** were also observed in unimmunised IL-13$^{-/-}$ cDCs compared to WT. Taken together these observations evoked the notion that the measured TGF-β1 and IL-13Rα2 expression profiles were linked to IL-13.

4.4.5 IL-13Rα2 and IFN-γR were co-expressed on lung cDCs 24 h following i.n. rFPV vaccination

Our previous studies have shown that 24 h post viral vector vaccination, ILC1/ILC3- derived IFN-γ expression was inversely associated with ILC2-derived IL-13 at the vaccination site, which significantly impacted cDC recruitment [99,367]. Knowing that IFN-γ is a potent IL-13 inhibitor and can also mobilise IL-13Rα2 from intracellular compartments to the cell surface [286,373,374], in this part of the study, the association of IFN-γR and IL-13Rα2 on lung cDCs, following i.n. rFPV vaccination was further investigated.

Data revealed that following i.n. rFPV vaccination, differential IL-13Rα2 and IFN-γR expression levels were observed on lung cDCs **(Figure 4.19a-d)**. Specifically,

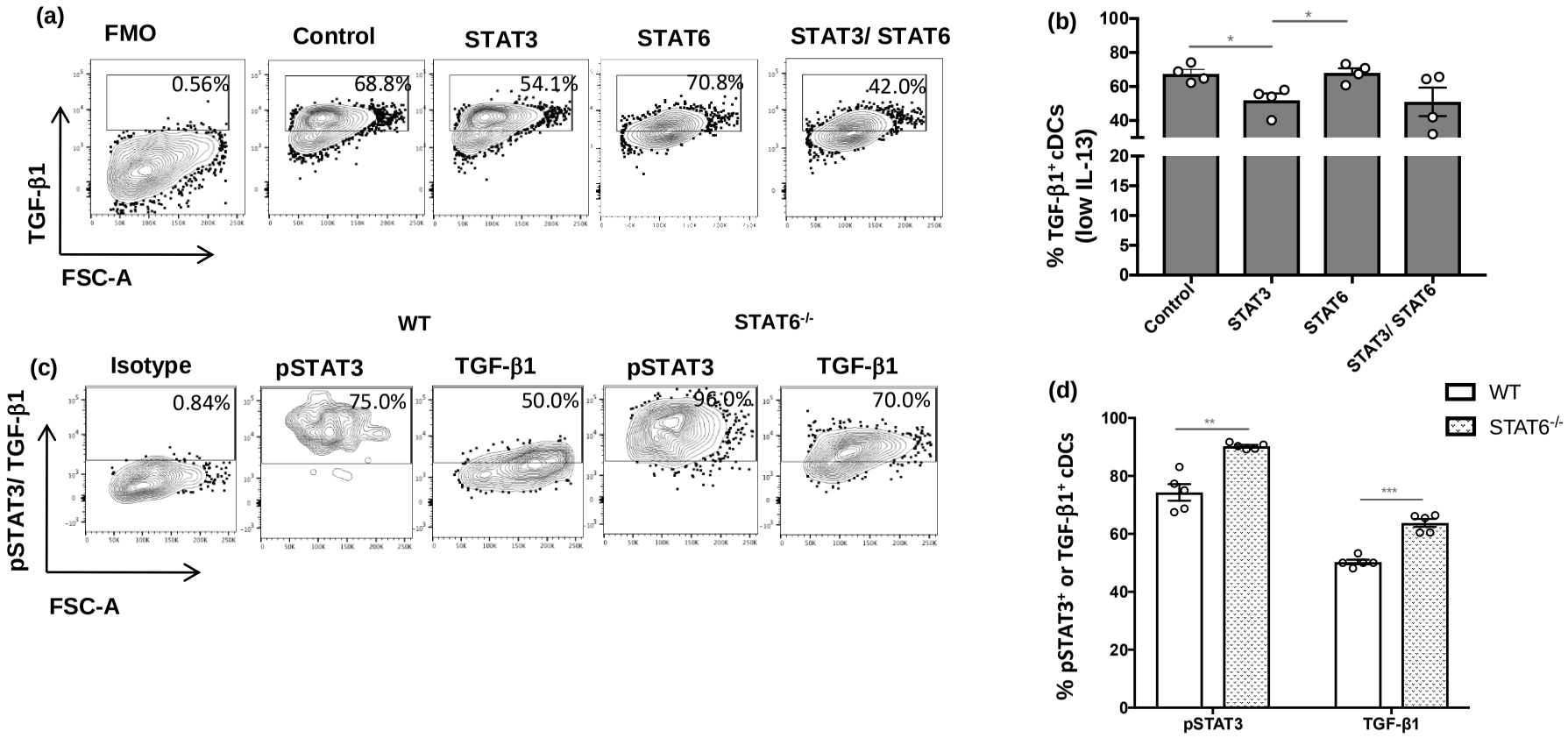
(a)
FMO
Control
STAT3
STAT6
STAT3/ STAT6
0.56%
68.8%
54.1%
70.8%
42.0%
TGF-β1
FSC-A
(b)
% TGF-β1+ cDCs (low IL-13)
Control
STAT3
STAT6
STAT3/ STAT6
(c)
WT
STAT6-/-
Isotype
pSTAT3
TGF-β1
pSTAT3
TGF-β1
0.84%
75.0%
50.0%
96.0%
70.0%
pSTAT3/ TGF-β1
FSC-A
(d)
WT
STAT6-/-
% pSTAT3+ or TGF-β1+ cDCs
pSTAT3
TGF-β1

Figure 4.17. Evaluation of pSTAT3 and TGF-β1 on lung cDCs upon IL-13 stimulation *in vitro*, in the presence of STAT3 and STAT6 inhibitors or 24 h post rFPV vaccination. Unimmunised BALB/c lungs (n=4) were treated with STAT3, STAT6 or combined STAT3/STAT6 inhibitors overnight, followed by 100 pg/ml of low IL-13 for 3 hours as described in methods. **(a and b)** Indicate representative FACS plots and graphs showing TGF-β1 expression in lung MHC-II^{+} CD11c^{+} CD11b^{+} cDCs following *in vitro* STAT3 and STAT6 inhibition. **(c and d)** Indicate lung cDCs expressing pSTAT3 and TGF-β1 24 h post i.n. rFPV vaccination of STAT6$^{-/-}$ and WT BALB/c mice (n=5). Error bars represent Standard Error of mean (SEM) and *p* values were calculated using paired Student's t-test. **p*<0.05, ***p*<0.01, ****p*<0.001, *****p*<0.0001. These experiments were repeated three times.

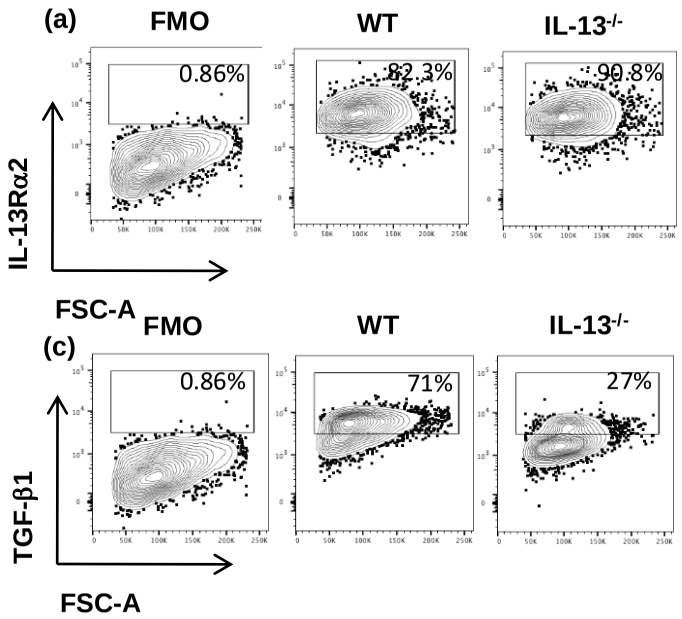

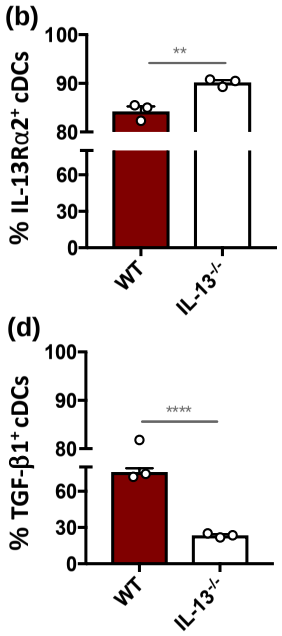

Figure 4.18. Evaluation of IL-13Ra2 and TGF-β1 on lung cDCs in IL-13$^{-/-}$ and WT mice. (a and b) indicate IL-13Rα2 and **(c and d)** indicate TGF-β1 expression on lung cDCs from unimmunised IL-13$^{-/-}$ and WT BALB/c mice (n=3 per group). Error bars represent Standard Error of mean (SEM) and *p* values were calculated using paired Student's t-test. **p*<0.05, ***p*<0.01, ****p*<0.001, *****p*<0.0001. These experiments were repeated two times.

the percentage of cDCs expressing intracellular IL-13Rα2 was significantly elevated compared to extracellular IFN-γR (p=0.0228) **(Figure 4.19a-b).** Alternatively, extracellular IL-13Rα2 was significantly elevated compared to intracellular IFN-γR (p<0.0001), demonstrating an inverse correlation of the two receptors **(Figure 4.19a-b).** When analysis was performed to evaluate whether lung cDCs co-expressed IL-13Rα2 together with IFN-γR following i.n. rFPV vaccination, flow cytometry data revealed that the majority of the cDCs were double positive for the two receptors (85%) **(Figures 4.20a-b)**. This was further substantiated by confocal imaging on lung CD11c$^+$ DCs where ~75% of cells co-expressed IL-13Rα2 and IFN-γR **(Figures 4.21a-b)**.

4.4.6 rFPV, rMVA and Adenovirus 5 (Ad5) vaccinations differentially regulated IL-13 receptors, STAT3/STAT6 and IFN-γR on cDC 24 h post vaccination

Knowing that different viral vectors can induce different ILC2-derived IL-13 levels and DC subsets at the vaccination site, which were associated with different vaccine specific adaptive immune outcomes [367], next the IL-4/IL-13 receptor expression and regulation on lung cDCs post i.n. rMVA and Ad5 delivery were compared to i.n. rFPV vaccination. Interestingly, even though all three vaccinations induced significantly elevated intracellular and extracellular expression of IL-13Rα2 on lung cDCs (95–98%), elevated IL13Rα1 and IL-4Rα (intracellular) were only detected in cDCs, following rMVA and Ad5 viral vector vaccination **(Figure 4.5a-b and 4.22a-b)**. It was noteworthy that, both intracellular and extracellular expression of the latter two receptors was significantly lower (rFPV 1-12%, rMVA 1-58% and Ad5 2-30% respectively) compared to IL-13Rα2 (95 – 100%) **(Figure 4.5a-b and 4.22a-b).**

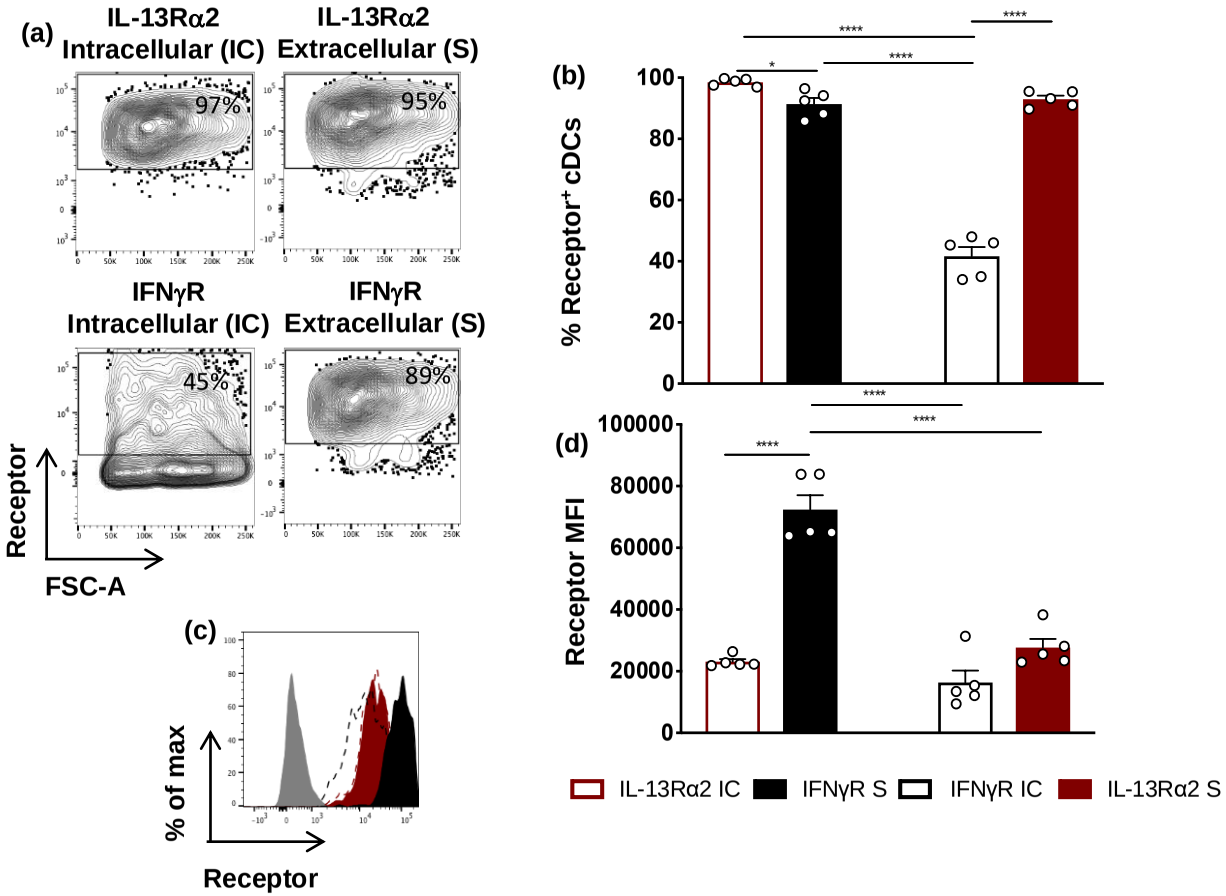
(a)
IL-13Rα2 Intracellular (IC)
IL-13Rα2 Extracellular (S)
97%
95%
IFNγR Intracellular (IC)
IFNγR Extracellular (S)
45%
89%
Receptor
FSC-A
(b)
% Receptor+ cDCs
100
80
60
40
20
0
*
****
(c)
% of max
Receptor
(d)
Receptor MFI
100000
80000
60000
40000
20000
0
IL-13Rα2 IC
IFNγR S
IFNγR IC
IL-13Rα2 S

Figure 4.19. Analysis of relative expression of IL-13Rα2 and IFN-γR on lung cDCs 24 h post rFPV vaccination. BALB/c mice (n=5 per group) were intranasally (i.n.) immunised with rFPV. 24 h post delivery, lung cells were stained for cDCs to evaluate receptor expressions using flow cytometry as described in methods. **(a and b)** Representative flow cytometry plots and bar graph show the percentage of cDCs expressing intracellular and extracellular IL-13Rα2 and IFN-γR on lung cDCs. **(c and d)** Representative histogram plots and bar graph show a comparative extracellular IL-13Rα2 (solid red), intracellular IL-13Rα2 (dotted red), extracellular IFN-γR (solid black) and intracellular IFN-γR (dotted black) expression densities on lung cDCs from rFPV vaccinated mice compared to an isotype control (solid black). Error bars represent Standard Error of mean (SEM) and *p* values were calculated using One-way ANOVA followed by Tukey's multiple comparison test and paired Student's t-test. **p*<0.05, ***p*<0.01, ****p*<0.001, *****p*<0.0001. These experiments were repeated three times.

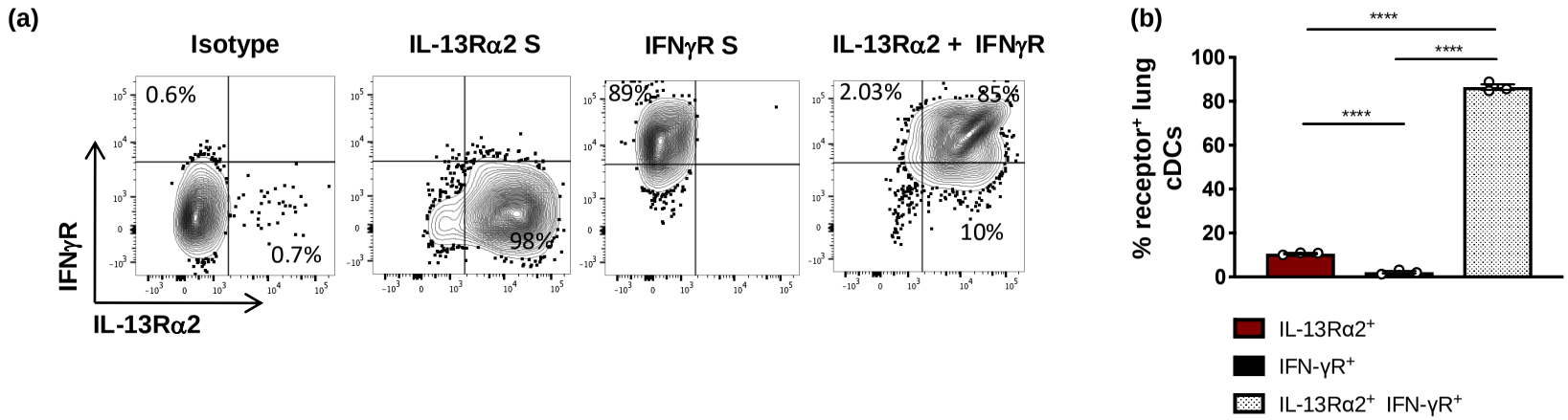

Figure 4.20. Evaluation of IL-13Rα2 and IFN-γR receptor co-expression on lung cDCs 24 h post rFPV vaccination using flow cytometry. BALB/c mice (n=3) were intranasally (i.n.) immunised with rFPV. 24 h post delivery, lung cells were stained for MHC-II$^+$ CD11c$^+$ CD11b$^+$ CD103$^-$ cDCs to evaluate receptor expressions using flow cytometry as described in methods **(a and b)** Representative flow cytometry plots and bar graph show single expression and co-expression of IL-13Rα2 and IFN-γR on lung cDCs. Standard Error of mean (SEM) and *p* values were calculated using One-way ANOVA followed by Tukey's multiple comparison test and paired Student's t-test. **p*<0.05, ***p*<0.01, ****p*<0.001, *****p*<0.0001. These experiments were repeated three times.

Interestingly, although lung cDCs obtained from rFPV, rMVA and Ad5 vaccine groups showed expression of *Stat6, Stat3, tgfb1 and Ifngr1* genes at a single cell level as well as at the protein level (pSTAT3, pSTAT6, TGF-β1 and IFN-γR) **(Figures 4.23 and 4.24)**, the expression profiles were significantly different between the three vaccine groups. Specifically, the expression of both pSTAT3 and pSTAT6 were found to be in the order of rFPV > rMVA > Ad5 **(Figure 4.23a-b)**. The expression of TGF-β1 was similar in rFPV and rMVA, but significantly lower in Ad5 **(Figure 4.23a-b)**. In contrast, in the context of IFN-γR expression, the order was found to be rMVA > rFPV > Ad5 **(Figure 4.23a-b)**. At the mRNA level, rMVA and Ad5 cDCs showed a greater probability of *Stat3* and *Stat6* co-expression (79% and 76% respectively) compared to the rFPV group **(Figures 4.24a-b)**. The probability of *Stat3* or *Stat6* co-expression together with *Ifngr1* was found to be in the order of rFPV (30%, 46%) < Ad5 (64%, 60%) < rMVA (71%, 83%) **(Figures 4.13b and 4.24a-b)**. The probability of *Stat3* and *Tgfb1* co-expression was found to be very similar between rFPV (75%) and Ad5 (77%) cDCs **(Figures 4.13b and 4.24b)**. However, *Stat6* and *tgfb1* co-expression profile was in the order of Ad5 > rMVA > rFPV (93%, 70%, 42% respectively) **(Fig. 4.13b and 4.24a-b)**.

To investigate differential regulation of *Stat3* and *Stat6* under different IL-13 conditions, a PCA was performed with respect to *Stat3, Stat6, Tgfb1* and *Ifngr1* **(Figures 4.3 and 4.24c)**. Distinct gene clusters with different combinations of the four genes were analysed as described in methods and **Figure 4.3**. The proportion of each co-expression combination was represented as a stacked bar graph for each vaccine vector **(Figure 4.24c)**, rFPV vaccination induced the highest proportion of cDCs expressing *Stat3* and *Stat6* together with *Tgfb1*

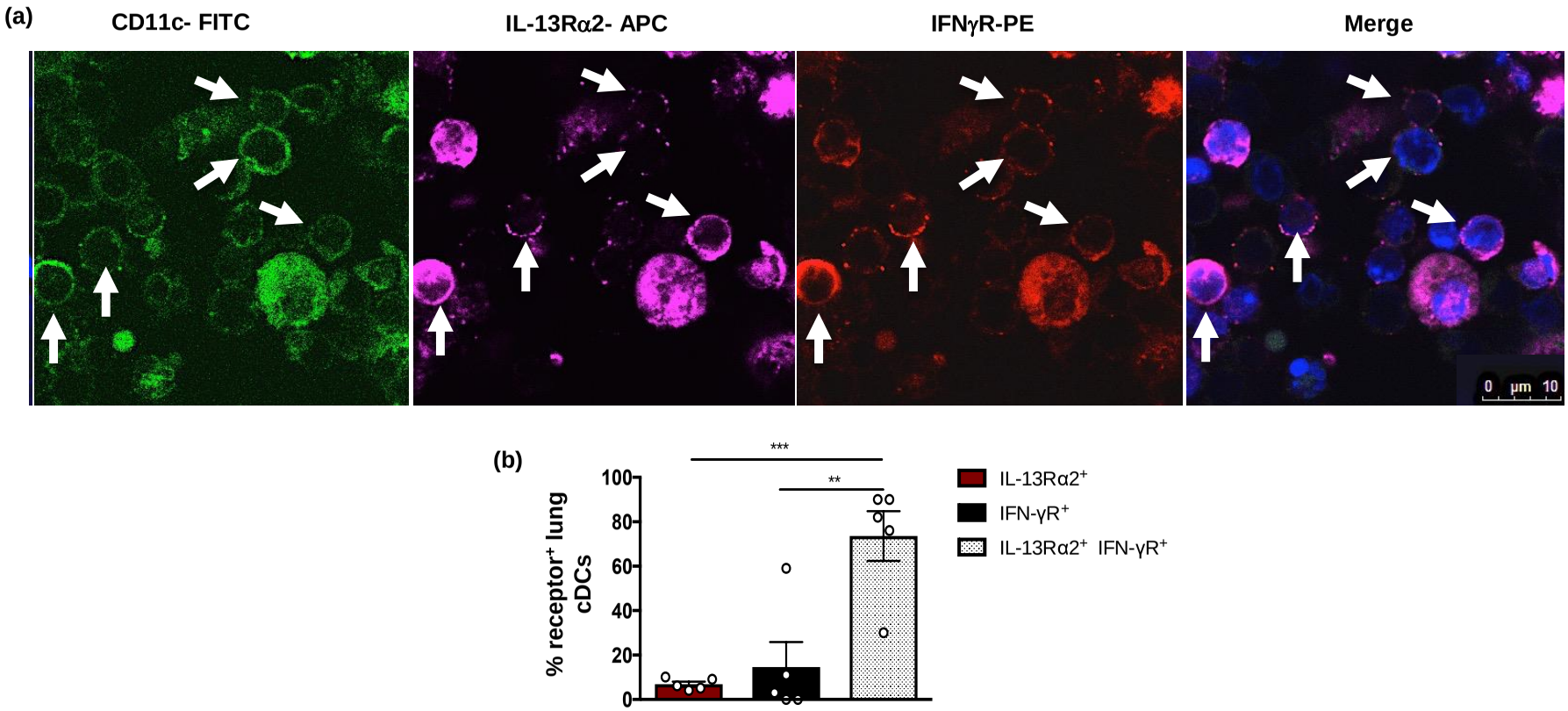
(a)
CD11c- FITC
IL-13Rα2- APC
IFNγR-PE
Merge
0 µm 10
(b)
% receptor+ lung cDCs
100
80
60
40
20
0
***
**
IL-13Rα2+
IFN-γR+
IL-13Rα2+ IFN-γR+

Figure 4.21. Evaluation of IL-13Rα2 and IFN-γR receptor co-expression on lung cDCs 24 h post rFPV vaccination using confocal microscopy. (a) Representative confocal microscopy images and **(b)** bar graph show i.n. rFPV vaccinated (n=5) lung cells expressing IL-13Rα2 and IFN-γR at magnification x60 as described in methods. Each white arrow indicates a single $CD11c^+$ DC across all channels as well as merge image, co-expressing IL-13Rα2 and IFN-γR. These experiments were repeated three times.

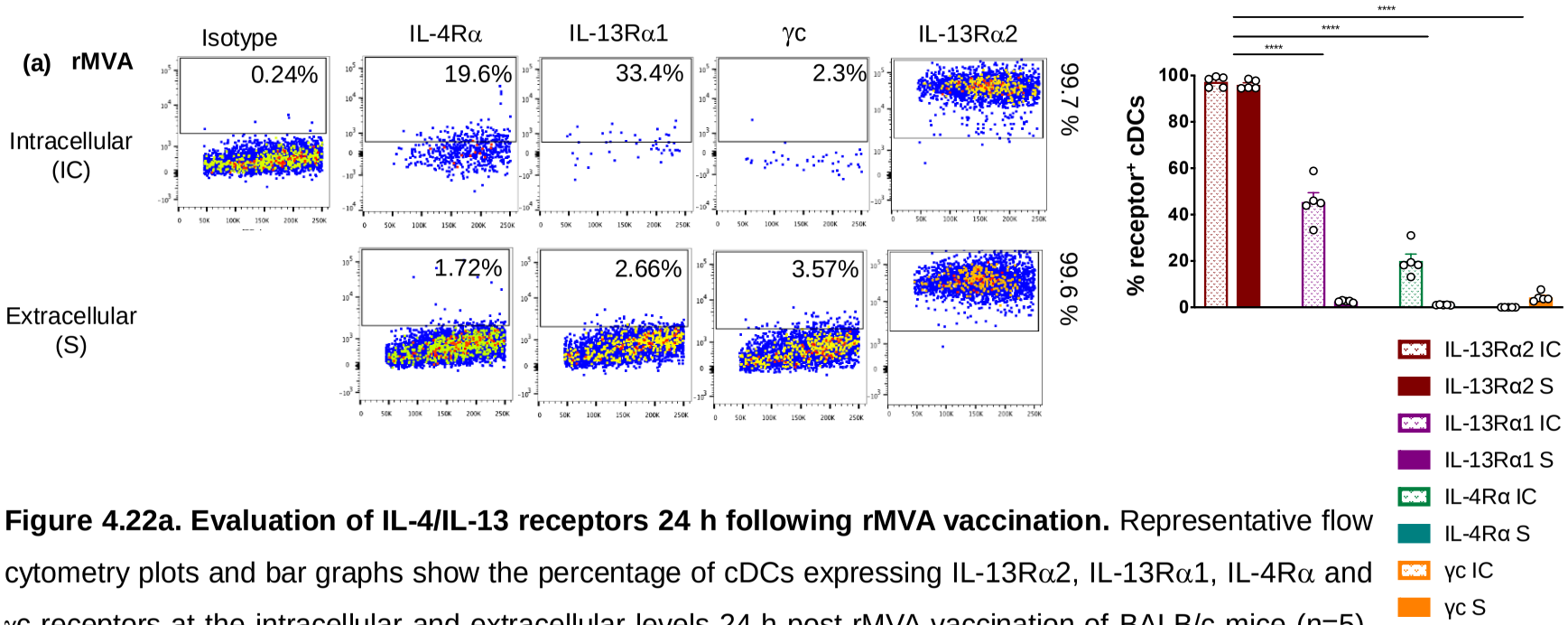

Figure 4.22a. Evaluation of IL-4/IL-13 receptors 24 h following rMVA vaccination. Representative flow cytometry plots and bar graphs show the percentage of cDCs expressing IL-13Rα2, IL-13Rα1, IL-4Rα and γc receptors at the intracellular and extracellular levels 24 h post rMVA vaccination of BALB/c mice (n=5). Error bars represent Standard Error of mean (SEM) and *p* values were calculated using One-way ANOVA followed by Tukey's multiple comparison test. **p*<0.05, ***p*<0.01, ****p*<0.001, *****p*<0.0001. These experiments were repeated three times.

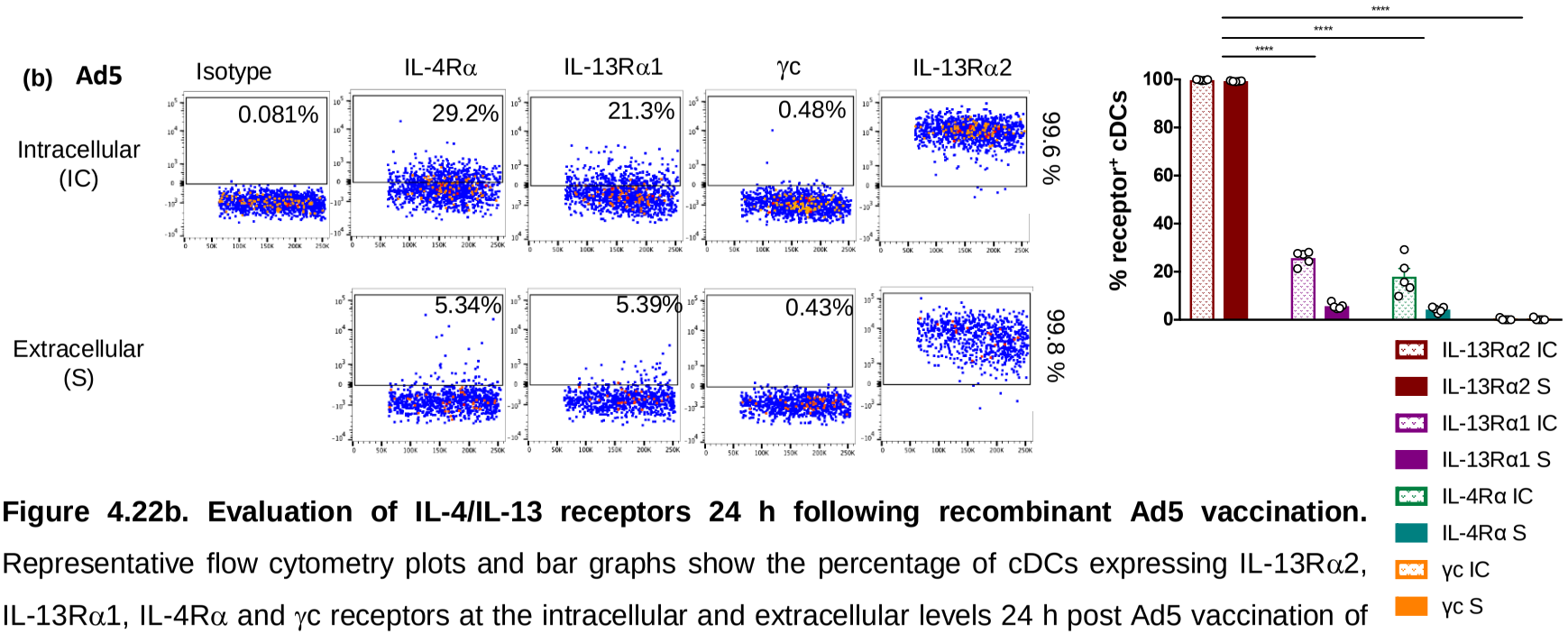

Figure 4.22b. Evaluation of IL-4/IL-13 receptors 24 h following recombinant Ad5 vaccination. Representative flow cytometry plots and bar graphs show the percentage of cDCs expressing IL-13Rα2, IL-13Rα1, IL-4Rα and γc receptors at the intracellular and extracellular levels 24 h post Ad5 vaccination of BALB/c mice (n=5). Error bars represent Standard Error of mean (SEM) and *p* values were calculated using One-way ANOVA followed by Tukey's multiple comparison test. **p*<0.05, ***p*<0.01, ****p*<0.001, *****p*<0.0001. These experiments were repeated three times.

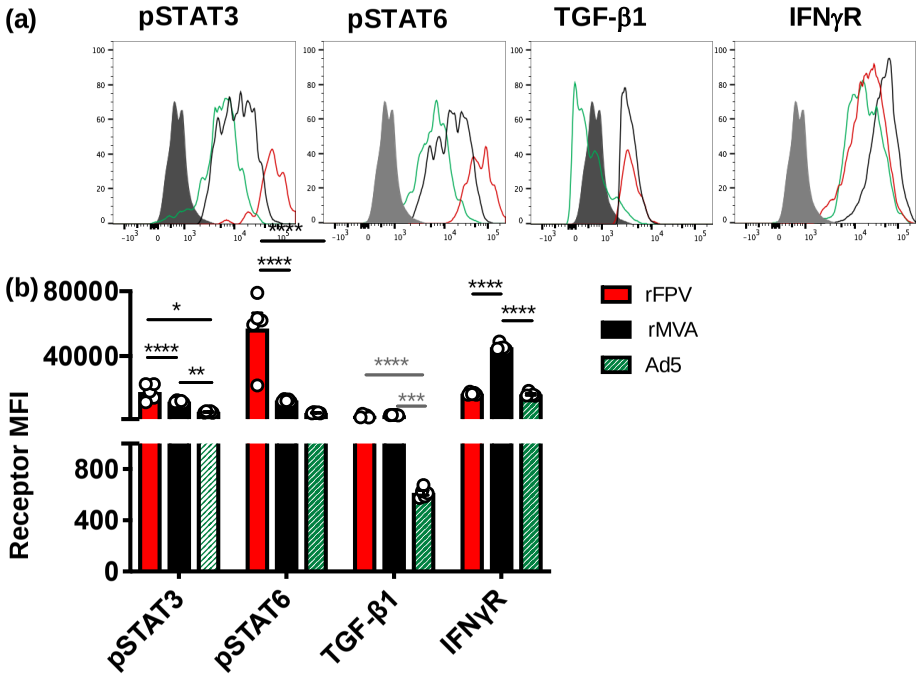

Figure 4.23. Evaluation of IL-4/IL-13 related molecules on lung cDCs following rFPV, rMVA and recombinant Ad5 vaccinations. (a) Representative histogram plots and **(b)** bar graph show comparative extracellular pSTAT3, pSTAT6, TGF-β1 and IFN-γR expression densities on lung cDCs (n=5) from rFPV vaccinated (red), rMVA (black), Ad5 vaccinated (green) compared to the FMO control (solid grey). Error bars represent Standard Error of mean (SEM) and *p* values were calculated using One-way ANOVA followed by Tukey's multiple comparison test (black) for comparing any two conditions and paired Student's t-test (grey) for comparing a specific pair of dependent conditions. **p*<0.05, ***p*<0.01, ****p*<0.001, *****p*<0.0001. These experiments were repeated three times.

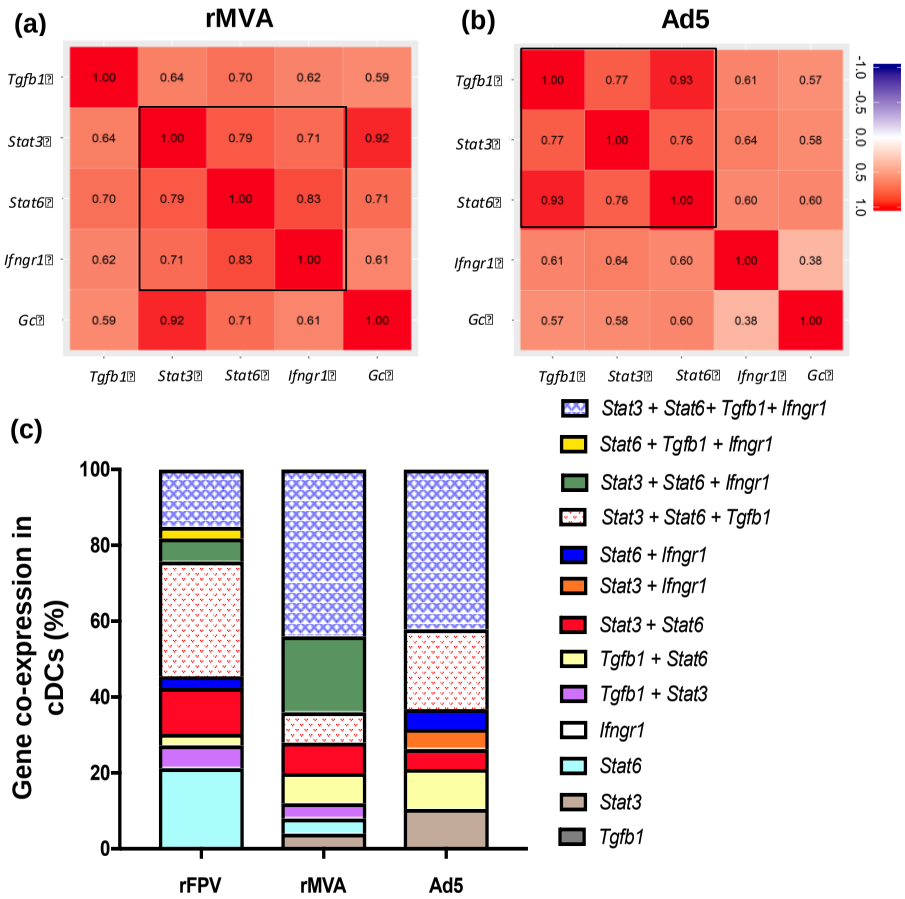

Figure 4.24. Evaluation of IL-4/IL-13 related genes on lung cDCs following rFPV, rMVA and recombinant Ad5 vaccinations. (a and b) PCA of *Tgfb1*, *Stat3*, *Stat6*, *Ifngr1* and *Gc* genes expressed on single lung cDCs following rMVA and Ad5 vaccination, post Fluidigm 48.48 Biomark analysis. **(c)** Stacked bar graphs represent viral vector dependent *Stat3*, *Stat6*, *Tgfb1* and *Ifngr1* gene *co*-expression on cDCs following rFPV, rMVA or Ad5 vaccination using PCA and K-means clustering analysis as described in methods**.** Each vaccine group represent 48 cells. These experiments were repeated two times.

(rFPV 30% vs rMVA 8%, Ad5 21%). Additionally, rFPV vaccinated cDCs expressing *Stat6* only (21%) and enhanced *Stat3* co-expression with other genes, indicated that the rFPV response was STAT3 dominant. Following rFPV vaccination, much lesser proportion of cDCs expressed *Stat3* and *Stat6* together with either *Ifngr1* (rFPV 6%, rMVA 20%, Ad5 0%) or *Tgfb1* and *Ifngr1* (rFPV 15%, Ad5 42%) **(Figure 4.24c)**. In contrast, rMVA induced the highest proportion of cells expressing *Stat3* and *Stat6* together with either *Tgfb1* and *Ifngr1* (44%) or *Ifngr1* only (rMVA 20%, rFPV 6%, Ad50%). Compared to rFPV, rMVA induced lower proportion of cDCs expressing *Stat3/Stat6* in combination with *Tgfb1* (rMVA 8%, rFPV 30%). Following Ad5 vaccination, the majority of the cDCs expressed *Stat3* as well as *Stat6* along with *Tgfb1* and *Ifngr1* (Ad5 42%, rFPV 15%), comparable to the response exhibited with rMVA (44%). However, the proportion of Ad5 cDCs expressing *Stat3* as well as *Stat6* together with *Tgfb1* expression was intermediary to that of rFPV and rMVA, however much higher proportion of Ad5 cDCs co-expressed *Stat6* and *Tgfb1* (Ad5 10%, rMVA 8%, rFPV 3%). Also, Ad5 vaccinated cDCs exhibited a more predominant co-expression of other genes with *Stat6* compared to *Stat3*, indicating that unlike rFPV, the Ad5 response was STAT6 dominant **(Figure 4.24c).**

4.5. Discussion

Asthma, allergy and vaccination studies have shown that lung cDCs are highly responsive to IL-13 [361,367,375]. Interestingly, this study demonstrated that, IL-13Rα1 and IL-13Rα2 were differentially regulated on lung DCs in an IL-13 concentration and time dependent manner. At the steady-state (prior to immunization) significantly higher percentage of lung cDCs expressed IL-13Rα2 compared to IL-13Rα1. Furthermore, both these receptors were rapidly up-

regulated on lung DCs upon IL-13 stimulation *in vitro* or 24h post viral vector-based vaccination. Specifically, IL-13Rα2 expression was maintained under both low and high IL-13, whilst IL-13Rα1 was only observed under high IL-13 conditions, suggesting, in lung cDCs IL-13Rα2 was the primary sensor and mediator (master regulator) of IL-13 responses. Moreover, this was further substantiated by the presence of elevated stable IL-13Rα2 protein and minimal mRNA expression at 24 h post rFPV vaccination, elucidating a distinct inverse protein-mRNA regulation, unlike IL-13 mediated inflammatory conditions [288,309,376-378]. Non-linear protein-mRNA regulation of other proteins [379,380], cytokines, including IL-13 [381] specifically, elevated protein and rapid mRNA degradation associated with protein stability have been previously documented [382-384]. Moreover, presence of minimal *Il13ra2* transcript levels in most mouse tissue types at steady-state [278,376-378,385] (NCBI Gene ID: 16165) and in human cancers post-transcriptional regulation of IL-13Rα2 by alternative epigenetic pathways have also been reported [386]. Knowing that lung is continuously exposed to many environmental invasions (pathogens and allergens), the elevated stable IL-13Rα2 protein on lung DC may support the notion that, at the first line of defence (the lung mucosae), high affinity IL-13 receptor, IL-13Rα2 acts as the primary IL-13 sensor to mediate early IL-13 regulation/homeostasis and dysregulation of IL-13Rα2 could most likely be the cause of IL-13 mediated inflammatory disease.

Previous studies in our laboratory have shown that transient inhibition of IL-4/IL-13 signalling via STAT6 (using an rFPV based IL-4R antagonist adjuvanted HIV recombinant viral i.n. rFPV prime/i.m. rMVA or rVV boost vaccination strategy) or transient sequestration of IL-13 at the vaccination site (using IL-13Rα2

adjuvanted HIV recombinant viral i.n. rFPV prime/i.m. rMVA or rVV boost vaccination strategy) can induce high avidity/poly-functional mucosal and systemic T cells with better protective efficacy [122,124], which was associated with elevated cDC recruitment [99,124]. These studies also showed that IL-13 was necessary for effective antibody differentiation [122], which was regulated via a STAT6 independent pathway [302]. When trying to unravel how IL-13 modulated these different vaccine-specific outcomes current study revealed that, i) under low IL-13 conditions /rFPV vaccination (which induced low IL-13 at the lung mucosa), IL-13Rα2 expression was up-regulated on DC; ii) under low IL-13/STAT3 inhibition IL-13Rα2 expression was up-regulated whilst TGF-β1 was down-regulated on lung DCs, as opposed to STAT6 inhibition; iii) Moreover, up-regulation of phosphorylated STAT3 and TGF-β1 was detected on STAT6$^{-/-}$ cDCs post rFPV vaccination. There findings collectively suggested that, under low IL-13 environments, cDCs most likely mediated IL-13 activity exclusively via IL-13Rα2 by promoting STAT3/TGF-β1 activation, which was consistent with other findings [299,309]. Also, the intriguing enhanced phosphorylated STAT6 expression on lung cDCs under low IL-13 signified a co-regulation of STAT3/STAT6 during this process. However, performing vaccination studies in IL-13Rα2$^{-/-}$ mice, to establish the 'direct' association of IL-13Rα2 signalling via STAT3 to induce TGF-β1 would have added great value to our findings and this warrants further investigation.

Under high IL-13, in addition to our study reconfirming the well-characterised IL-13Rα1/IL-4Rα signalling via STAT6 [278], we also showed regulation of IL-13Rα2 and co-expression of both IL-13Rα1 and IL-13Rα2 on lung DCs. These observations suggested that i) unlike low IL-13 conditions, DCs responded to high

IL-13 predominantly via IL-13Rα1/STAT6 pathway and ii) under high IL-13 conditions, IL-13Rα2 likely regulated IL-13 in a STAT3 dependent manner. Moreover, the unexpected up-regulation of IL-13Rα2 under high IL-13 and dual STAT3/STAT6 inhibition also suggested the possible involvement of STAT3-independent IL-13Rα2 signalling mechanisms, similar to IL-4 signalling via STAT1 and STAT5 [387] (redundancies built into the system to regulate IL-13). In inflammatory diseases and high IL-13 conditions, IL-13Rα2 is recognized to be a decoy receptor that sequesters excess IL-13 [376,377]. Interestingly, rMVA and Ad5 vaccination, which promoted high IL-13 [367], expressed *Stat6* mRNA and phosphorylated STAT6 on lung cDCs, associated with IL-13Rα1 signalling together with *Stat3* and phosphorylated STAT3 activation. Knowing that IL-13Rα2 can regulate IL-4Rα/STAT6 [388], promote TGF-β1 expression and latter can also regulate STAT6 [389], we propose that elevated IL-13 in the milieu post viral vector vaccination i) can activate IL-13Rα1/STAT6 signalling whilst promoting IL-13 sequestration by IL-13Rα2 in a STAT3 dependent manner on lung cDCs and ii) IL-13Rα2 can also regulate STAT6 in a STAT3 dependent manner, to prevent excessive IL-13 signalling on lung cDCs to maintain homeostasis at the lung mucosae **(Figure 4.25)**.

Studies have shown that STAT6 and STAT3 can be differentially regulated, according to the state of viral infection/vaccination. Specifically, in the context of viral vector-based vaccination whilst IL-13/STAT6 signalling has been shown to dampen effective antiviral immunity [132,302], however in acute and primary viral infections, it has shown to improve antiviral immunity [263,277]. This study showed that viral vector induced IL-13 “level” in the cell milieu significantly altered the

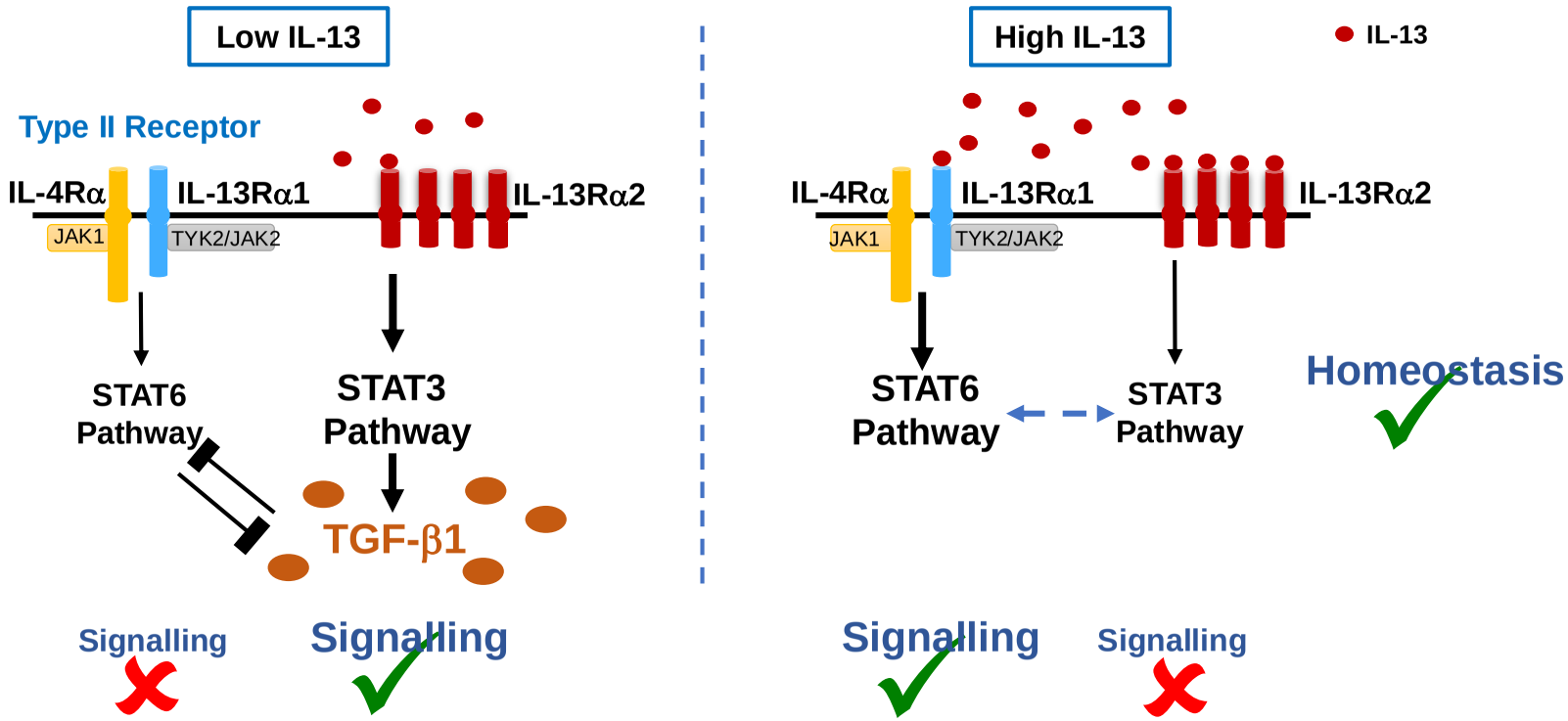
Low IL-13
Type II Receptor
IL-4Rα
IL-13Rα1
IL-13Rα2
JAK1
TYK2/JAK2
STAT6
Pathway
STAT3
Pathway
TGF-β1
Signalling
Signalling
High IL-13
IL-13
IL-4Rα
IL-13Rα1
IL-13Rα2
JAK1
TYK2/JAK2
STAT6
Pathway
STAT3
Pathway
Homeostasis
Signalling
Signalling

Figure 4.25. Proposed dual action of IL-13Rα2/STAT3 associated with IL-13 regulation following viral vector-based vaccination. Under low IL-13 conditions, IL-13Rα2 mediates IL-13 signalling via STAT3 to promote TGF-β1 expression. In contrast, under high IL-13 conditions, IL-13Rα1 mediates IL-13 signalling via STAT6, and IL-13Rα2 acts to sequester excess IL-13 in the milieu (does not signal) and activates STAT3, to maintain IL-13 homeostasis at the vaccination site. Findings in the literature and our current study indicate that STAT3 and STAT6 can co-regulate each other to prevent immune dysregulation under both these conditions.

STAT3/STAT6 equilibrium. Specifically, rFPV vaccination, associated with low ILC2-derived IL-13 at the vaccination site [366,390], exhibited enhanced STAT3 expression (both at mRNA protein levels), which correlated with TGF-β1 on lung cDCs, suggesting a positive regulation of IL-13Rα2/STAT3 by TGF-β1. In contrast, a negative association of *Stat3* with *Ifngr1*, was confirmed by the inverse correlation and co-expression pattern of IFN-γR with IL-13Rα2 on cDCs, suggesting that IL-13Rα2 could be negatively regulated by IFN-γ, under low IL-13 conditions, which is in agreement with studies by Daines *et al.* [286].

Data revealed that as opposed to rFPV vaccinated lung cDCs, rMVA vaccinated lung cDC (associated with high ILC2-derived IL-13 at the vaccination site [367]), exhibited both STAT3 and STAT6 expression, associated with an IFN-γR expression bias (both at the mRNA and protein levels). Interestingly, Ad5 vaccinated lung cDC, (associated with moderate ILC2-derived IL-13, intermediate of rFPV and rMVA [367]), showed higher association of STAT3 with IFN-γR compared to TGF-β1 (both the mRNA and protein levels). Knowing that IFN-γ can regulate IL-13 responses [371], these observations indicated that following viral vector-based vaccination, at the cDC level the differential environmental immune responses to IL-13 are not only determined/regulated by STAT3/STAT6, but also by TGF-β1 and IFN-γ either collaboratively or independently, which was consistent with cancer/inflammation studies [391-394]. Interestingly, rapid STAT3 activation has shown to control some viral infections [277,395,396] whilst, STAT6 independent mechanisms have also been associated with effective antibody differentiation [302]. Moreover, IL-13 mediated enhanced IFN-γ signalling has been shown to exacerbate respiratory viral infections [311,397]. Collectively, our findings propose the notion that in the context of viral vector-

based vaccination and recruitment of DCs, vectors that promote low ILC2-derived IL-13, induce IL-13Rα2 signalling and STAT3/TGF-β1 activation, are associated with effective T and B cell immune outcomes. In contrast, vectors that promote high ILC2-derived IL-13 induce IL-13Rα1/STAT6 signalling and elevated IFN-γ activity, lead to suboptimal vaccine-specific T cell outcomes. This may explain why in a prime-boost vaccine modality, choice of viral vector or adjuvant used in a 'prime' can crucially impact the vaccine-specific functional CD8 T cell avidity [133], (knowing that booster vaccination mainly expands the initial high or low avidity T cell subset generated during priming) [124].

In conclusion, our current study demonstrated a dual role of IL-13Rα2/STAT3 in IL-13 regulation of lung cDCs at the lung mucosae. Specifically, under viral vaccination-induced low IL-13, IL-13Rα2 functioned as a signalling receptor on lung cDCs, whilst, under high IL-13, mediated homeostasis by sequestration of excess IL-13 in the cell milieu, both involving STAT3 activation and co-regulation of STAT3 and STAT6 **(Figure 4.25)**. Hence, fully understanding these IL-13, STAT3/STAT6 regulatory paradigms, have high potential to help design more efficacious vaccines against chronic pathogens and also therapies against other IL-13 related diseases.

Chapter 5

Differential IL-13 receptor regulation on lung dendritic cells likely governs the unique pox viral vector-based vaccine immune outcomes. [4]

[4] Experiments related to ILCs was performed by Dr. Zheyi Li.

5.1 Abstract

Current study revealed that following intranasal poxviral vector-based vaccination, IL-13Rα2 and IL-13Rα1 were differentially regulated on lung DCs, in a viral vector and time dependent manner, where IL-13Rα2 was the immediate IL-13 sensor. Following recombinant fowlpox (rFPV) vaccination, known to induce low ILC2-derived IL-13 at the lung mucosae, IL-13Rα2 whilst being the immediate IL-13 mediator on lung cDCs, low affinity Type II receptor complex IL-13Rα1/ IL-4Rα regulated responses 48-72h post delivery. In contrast, replication competent recombinant vaccinia virus (rVV), which induced high ILC2-derived IL-13, exhibited sustained elevated expression of IL-13Rα2 together with IL-13Rα1/IL-4Rα on lung cDC. Latter indicating that, in the context of rVV vaccination, IL-13Rα2 likely was involved in sequestration of excess IL-13 in the milieu, whilst signalling via the low affinity IL-13Rα1/IL-4Rα complex, resembling IL-13 regulation under chronic inflammation conditions. Interestingly, cDC obtained from replication abortive, recombinant Modified Vaccinia Ankara (rMVA), known to induce moderate ILC2-derived IL-13, showed an intermediary IL-13 receptor regulation profile to rFPV and rVV. Moreover, the deletion variant of rMVA, rMVAΔIL-1βR vaccination depicted a unique IL-13 regulatory profile where IL-13Rα2/IL-4Rα antagonism was likely at play. These findings demonstrated that the host tropism, replication status and presence or absence of immunomodulatory genes in a viral vector considerably impacted IL-4/IL-13 receptor regulation on lung DCs. The differences observed may explain how and why despite encoding the same vaccine antigens, different viral vectors yield

vastly different immune outcomes (eg. rFPV priming induce highly poly-functional cytotoxic CD8 T cells compared to rVV and/or rMVA vaccination). Taken together our findings imply that fate of a vaccine is influenced by the balanced and timely regulation of IL-13 by IL-13Rα2 and IL-13Rα1 on lung DCs, at the early stages (24-72h) of vaccination.

5.2 Introduction

Cytokine IL-13 can be characterized as a double edge sword, as under different disease conditions the 'level' of IL-13 can promote vastly different immune outcomes. Specifically, although overproduction, has been associated with allergic asthma [255,269], fibrosis [264,265], tumor progression [267,268], atopic dermatitis [257,266], lack of IL-13 has been linked to susceptibility to helminth, parasitic and some bacterial infections (eg. *K. Pneumonia*) [252,275,276]. Moreover, in some acute and primary viral infections, whilst IL-13 has been associated with improved antiviral immunity [263,277], in the context of viral vector-based vaccination, presence of IL-13 has been detrimental for the induction of effective T cell immunity whilst being crucial for effective antibody formation [132,302].

Our recent studies have demonstrated that following viral vector vaccination Innate Lymphoid Cell 2 (ILC2) are the major source of IL-13 at the vaccination site 24 h post delivery [306] and ILC2-derived IL-13 level can significantly alter the DC recruitment [367], responsible for uniquely different immune outcomes [99]. Specifically, low ILC2-derived IL-13 induced by recombinant fowlpox virus (rFPV), preferentially recruited cDCs not pDC to the lung mucosae unlike recombinant modified vaccinia Ankara (rMVA) or Vaccinia Virus (rVV) [367] and, the specific nature of a virus also significantly modulated this activity (eg. rMVA vs rMVAΔIL-1βR) [367].

It is well established that during IL-13 signalling, low affinity receptor IL-13Rα1 (K_D = 30 nM) heterodimerizes with IL-4Rα to form the functional IL-13Rα1/IL-

4Rα Type II receptor complex, which signals via STAT6 [278]. However, the exact signalling mechanism of the high affinity IL-13Rα2, (K_D = 440 pM) [378,398], is currently not well characterized, although deemed functional in humans [278,293,399]. Interestingly, these two receptors have been defined to have unique functions under different IL-13 conditions. For example, whilst, increased IL-13 production following asthma and allergy has shown to be regulated by IL-13Rα1 [262], under reduced IL-13 conditions, IL-13Rα1 has also shown to maintain homeostasis and lung repair [312]. Interestingly, the lesser-known IL-13Rα2 has been implicated in promoting lung and intestinal fibrosis, secondary methicillin resistant during staphylococcus aureus (MRSA) infection and liver pathology during some chronic infections [309-311]. Moreover, over-expression of IL-13Rα2 has been associated with poor prognosis of several cancer types [288,293].

Our recent intranasal viral vector-based vaccine studies have revealed that on lung DCs IL-13Rα2 acts a major IL-13 sensor and plays a dual role at the lung mucosae (Roy *et al.* (submitted)). Specifically, under low IL-13, IL-13Rα2 performs as the primary signalling receptor, whilst under high IL-13, helps to maintain homeostasis. Knowing that different viral vectors can induce variable ILC2-derived IL-13 levels at the lung mucosae [367], in this study we have attempted to unravel how IL-4 and IL-13 receptors get regulated on cDCs and pDCs 24-72h post pox viral vector vaccination.

5.3 Materials and Methods

5.3.1 Mice.

Pathogen-free 6–8 weeks old female BALB/c mice were purchased from the Australian Phenomics Facility, The Australian National University (ANU). The mice were maintained, monitored daily and euthanized using Australian NHMRC guidelines within the Australian Code of Practice for the Care and Use of Animals for Scientific Purposes and in accordance with guidelines approved by the ANU Animal Experimentation and Ethics Committee (AEEC), protocol number A2014/14 and A2017/15.

5.3.2 Viral vector based vaccination.

BALB/c mice were intranasally immunised with 1 X 10^7 plaque forming units (pfu) of FPV-HIV, MVA-HIV, MVA-ΔIL-1βR-HIV, VV-HIV, as described previously [367]. rFPV, rMVA, rMVA-ΔIL-1βR and rVV were sonicated thrice for 15 seconds on ice at 50% capacity using Branson Sonifier 450 immediately prior to vaccination. Mice were vaccinated with a volume of 10 µl per nostril (total 20 µl) under mild isofluorane anaesthetic.

5.3.3 Evaluation of lung ILC2s and corresponding IL-13 expression using flow cytometry.

Lung tissues were harvested 24 h post vaccination in complete RPMI and single cell suspensions were prepared as described previously [306,367]. Briefly, lungs were cut into small pieces, enzymatically digested with digestion buffer containing

1 mg/ml collagenase (Sigma-Aldrich, St Louis, MO), 1.2 mg/ml Dispase (Gibco, Auckland, NZ), 5 Units/ml DNase (Calbiochem, La Jolla, CA) in complete RPMI. Samples were filtered using 100µm falcon cell strainers followed by red cell lysis and cells were re-suspended in complete RPMI, rested overnight at 37°C under 5% CO_2 as per our previous studies prior to staining [306,367]. Lung cells were stained with lineage markers (FITC-conjugated anti-mouse CD3 (clone 17A2), CD19 (clone 6D5), CD11b (clone M1/70), CD11c (clone N418), CD49b (clone HMα2), FcεRIα (clone MAR-1)), PE-conjugated anti-mouse ST2/IL-33R (clone DIH9), APC/Cy7-conjugated anti-mouse CD45 (clone 30-F11), Brilliant Violet 421-conjugated anti-mouse CD335 (NKp46) (clone 29A1.4) obtained from Biolegend and PE-eFluor 610-conjugated anti-mouse IL-13 (clone eBio13A) purchased from eBioscience as previously described [306]. Briefly, following treatment with Brefeldin A for 5 hours, cell surface staining was performed followed by intracellular staining after fixing and permeabilising the cells. All samples were fixed with 0.5% paraformaldehyde and 1.4 x 10^6 events from each lung sample were acquired on a BD LSR Fortessa. Data were analysed using Tree Star FlowJo software (version 10.0.7) using gating strategies previously described [306,367].

5.3.4 Evaluation of IL-4 and IL-13 receptor expression on lung cDCs and pDCs using flow cytometry.

Lung tissues were harvested and prepared into single cell suspensions from mice, following 24, 48 or 72h post vaccination in complete RPMI. 2 X 10^6 cells from each sample were blocked with anti-mouse CD16/CD32 Fc Block antibody

(BD Biosciences, USA) for 20 min at 4°C and cells were stained with DC markers, APC-conjugated anti-mouse MHCII I-Ad (e-Biosciences, USA), biotin-conjugated anti-mouse CD11c (N418 clone, Biolegend, USA), followed by streptavidin Brilliant violet 421 (Biolegend, USA), anti mouse CD11b AlexaFluor 700 (M1170 clone, Biolegend, USA), anti-mouse CD103 FITC (2E7 clone, e-Biosciences, USA) and anti-mouse B220 PercpCy5.5 (RA3-6B2 clone, e-Biosciences, USA) for 30 min on ice. To evaluate IL-4 and IL-13 receptors, cells were also extracellularly either stained with anti-mouse IL-4Rα (CD124) PE (I015F8 clone, Biolegend, USA), anti-mouse IL-13Rα1 (CD213a) PE (13MOKA clone, e-Biosciences, USA), Biotin-conjugated anti-mouse IL-13Rα2 (110815 clone, R&D systems, USA), followed by streptavidin PE (Biolegend, USA), anti mouse γc (CD132) PE (TUGm2 clone, Biolegend, USA). Cells were further fixed using 1.5% paraformaldehyde followed by resuspension in PBS and analysed using BD LSRII flow cytometer Becton Dickinson, San Diego, CA). 5 x10^5 events per sample were acquired and results were analyzed using FlowJo software v10.0.7 and gating strategies described in **Figure 5.1a-c**.

5.3.5 Statistics.

IL-4 and IL-13 receptor proportions were calculated as a percentage of parent MHC-II$^+$ CD11c$^+$ CD11b$^+$ CD103$^-$ cDC and MHC-II$^+$ CD11c$^+$ CD11b$^-$ B220$^+$ pDC population. Please note that less than 10 receptor expressing cells were reported as undetectable expression. The *p*-values were calculated using either unpaired non-parametric Student's t-test or Two-way ANOVA with Tukey's multiple comparison post-test. All experiments were repeated minimum 2-3 times.

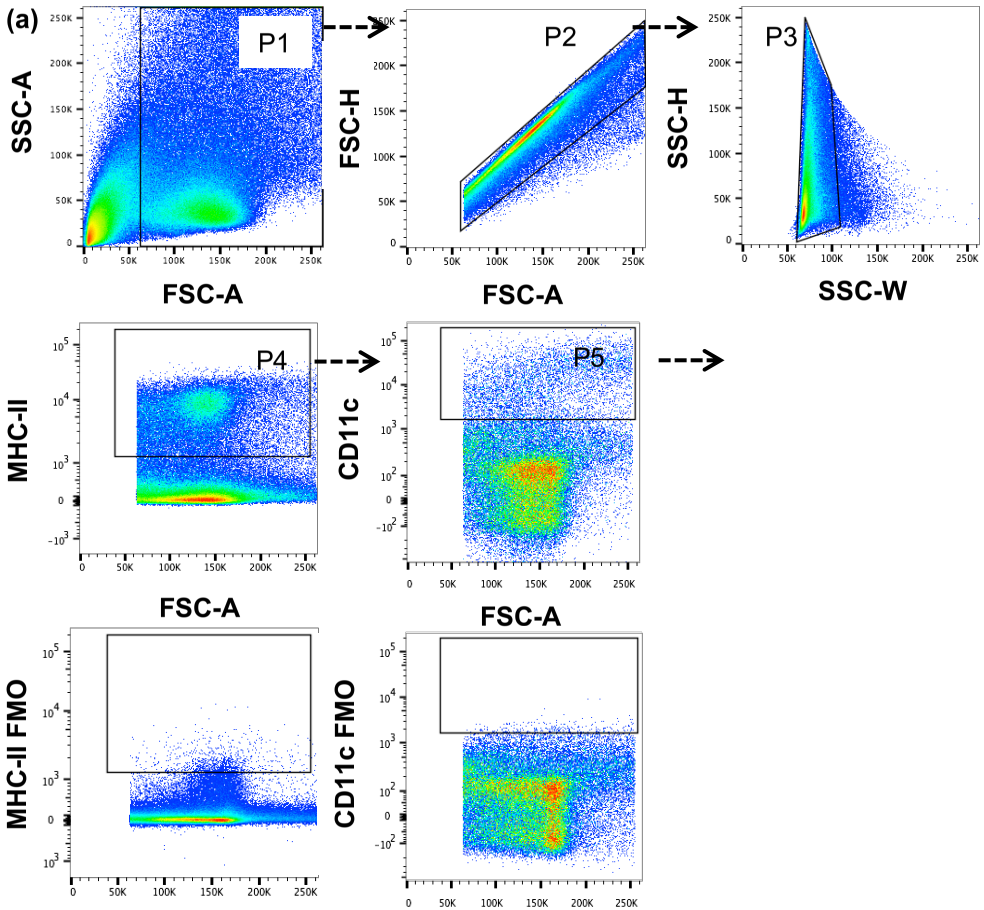

Figure 5.1a. Flow cytometry gating for evaluation of MHC-II$^+$ CD11c$^+$ DCs following i.n. viral vector based vaccination. Flow cytometry plots show viable cells (P1), followed by single cells based on forward scatter (FSC-H and FSC-A; P2) and side scatter (SSC-H and SSC-W; P3). Single cells were in turn gated on MHC-II-I-Ad$^+$ (P4) and CD11c (P5) compared to respective FMO controls to identify total DCs (MHC-II$^+$ CD11c$^+$ - P5).

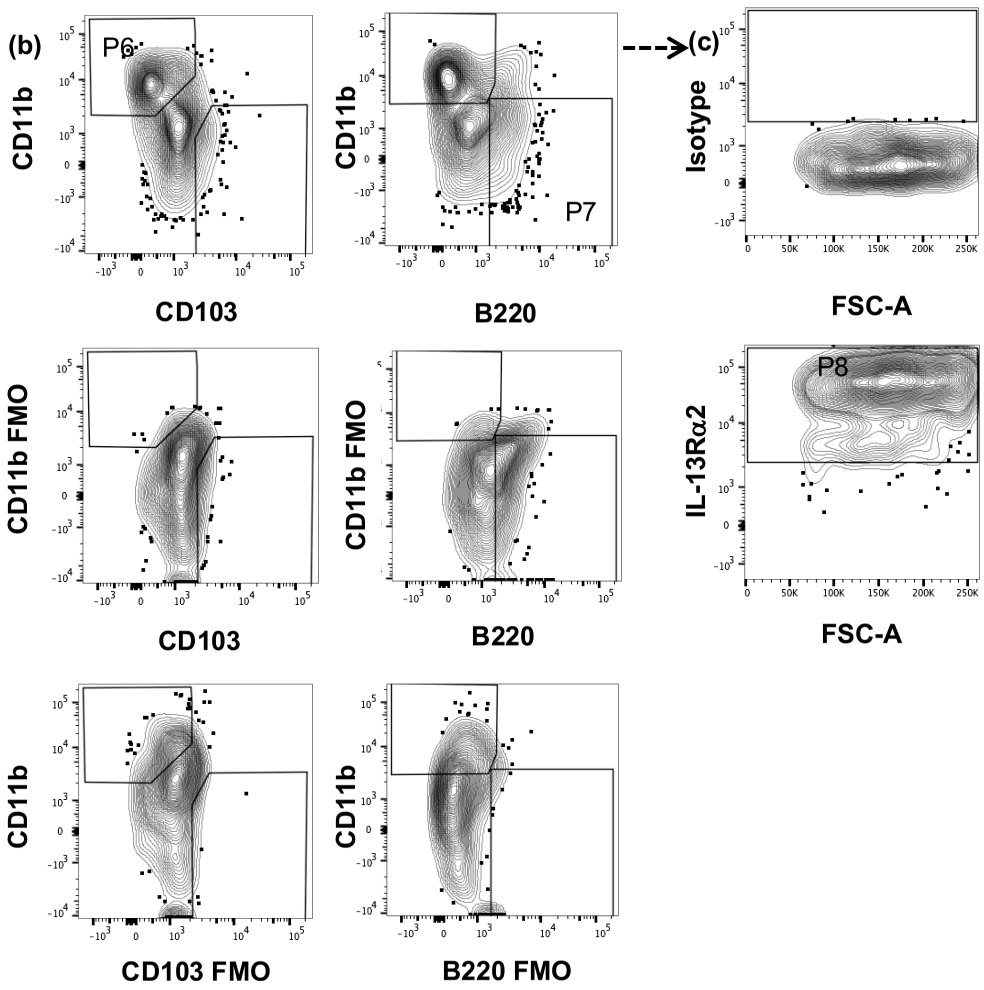

Figure 5.1 (b and c). Flow cytometry gating for evaluation of IL-4/IL-13 receptors on lung cDCs and pDCs following i.n. viral vector based vaccination. Following gating on total DCs (MHC-II$^+$ CD11c$^+$ - P5; as described in Figure 5.1a, these cells were further gated on CD11b$^+$ CD103$^-$ (P6) and CD11b$^-$ B220$^+$ (P7) using FMO controls for each marker as indicated. Receptor positive cells (P8) were further gated, based on isotype controls specific for the time point and viral vector.

5.4 Results

5.4.1. rFPV and rVV vaccinated lung cDCs exhibited uniquely differential IL-4/IL-13 receptor expression profiles 24h-72 h post delivery.

We have previously shown that the nature and replication status of a viral vector can significantly alter the ILC2-derived IL-13 level at the vaccination site [367]. Moreover, under low and high IL-13 conditions, IL-13 receptors can be differentially regulated (Roy *et al.* (submitted)), Therefore, in this study we have further evaluated the cDC associated IL-4/IL-13 receptor kinetics 24-72 h post rFPV and rVV vaccination as per described in methods. Results indicated that compared to rFPV which does not replicate in mammalian cells, replication competent rVV induced considerably elevated ILC2-derived IL-13 at the lung mucosae by an ST2/IL-33R$^-$ ILC subset at 24h post vaccination (p<0.0001) **(Figure 5.2).** Moreover, there was also a significant regulation of the different IL-4/IL-13 receptors on cDC where the number of cells that expressed IL-13Rα2 were much greater than IL-13Rα1 and IL-4Rα. Interestingly, although the percentage of cDCs expressing IL-13Rα2 was much greater at 24 - 48h (90%) compared to 72 h post rFPV delivery (~80%) (p<0.0001) **(Figure 5.3a),** the IL-4Rα and IL-13Rα1 on cDC were significantly up-regulated at 48 and 72 h (24 vs 48 h and 24 vs 72 h p<0.0001) **(Figure. 5.3b-c).** In contrast, post rVV vaccination significantly elevated and sustained IL-13Rα2 expression (99%) was detected over time **(Figure 5.4a),** whilst the IL-13Rα1/IL-4Rα expression trends were found to be very similar to rFPV vaccination **(Figure 5.4b-c)**. Unlike the other receptors, the expression of γc, which heterodimerises with IL-4Rα to form the

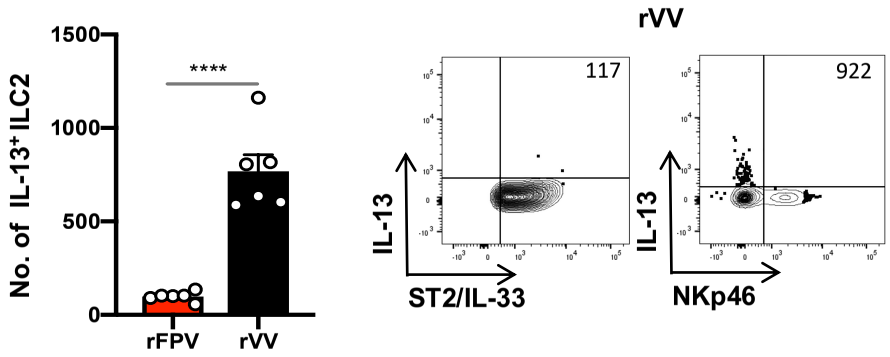

Figure 5.2. Evaluation of lung ILC2-derived IL-13 expression following intranasal rFPV and rVV vaccination. BALB/c mice (n=6 per group) were immunised i.n. with rFPV or rVV, 24 h post vaccination single cell suspensions from lungs were prepared and stained for Lin$^-$ ST2/IL-33R$^+$ and Lin$^-$ ST2/IL-33$^-$ NKp46$^-$ ILC2s and their IL-13 expression was assessed using flow cytometry**.** Graphs show the number of Lin$^-$ ST2/IL-33R$^+$ and Lin$^-$ ST2/IL-33$^-$ NKp46$^-$ ILC2s expressing IL-13, 24 h post rFPV and rVV vaccination (left panel). Representative FACS plots show average number of Lin$^-$ ST2/IL-33R$^+$ and Lin$^-$ ST2/IL-33$^-$ NKp46$^-$ ILC2s expressing IL-13 following rVV vaccination (right panel). Error bars represent Standard Error of mean (SEM) and *p* values were calculated using unpaired non-parametric student's t test. **p*<0.05, ***p*<0.01, ****p*<0.001, *****p*<0.0001. Experiments with each vector were repeated 3 times.

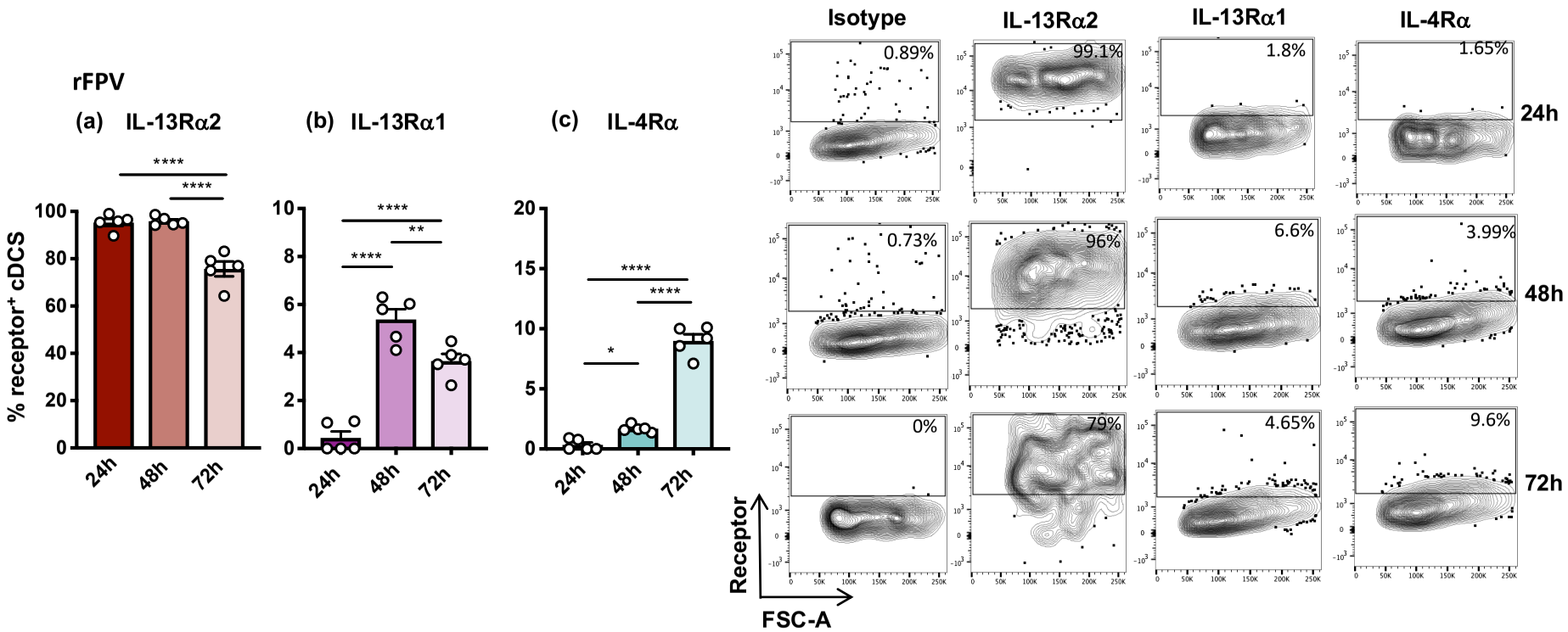
rFPV
(a) IL-13Rα2
(b) IL-13Rα1
(c) IL-4Rα
% receptor+ cDCS
24h
48h
72h
Isotype
IL-13Rα2
IL-13Rα1
IL-4Rα
0.89%
99.1%
1.8%
1.65%
0.73%
96%
6.6%
3.99%
0%
79%
4.65%
9.6%
Receptor
FSC-A

Figure 5.3. Evaluation of lung cDCs expressing IL-4/IL-13 receptors, following intranasal rFPV vaccination. BALB/c lungs (n=5 per vaccine group) were harvested at 24 h, 48 h or 72 h post rFPV delivery. Single cell suspensions were prepared and stained for MHC-II$^+$ CD11c$^+$ CD11b$^+$ CD103$^-$ cDCs and IL-4/IL-13 receptors and the expression on lung cDCs were assessed using flow cytometry as described in methods. Bar graphs (left panel) and representative flow cytometry plots (right panel) show IL-13Rα2, IL-13Rα1 and IL-4Rα expression following vaccination with (a-c) rFPV. Error bars represent Standard Error of mean (SEM) and *p* values were calculated using Two-way ANOVA followed by Tukey's multiple comparison test. *$p<0.05$, **$p<0.01$, ***$p<0.001$, ****$p<0.0001$. Experiments with each vector were repeated minimum 2-3 times.

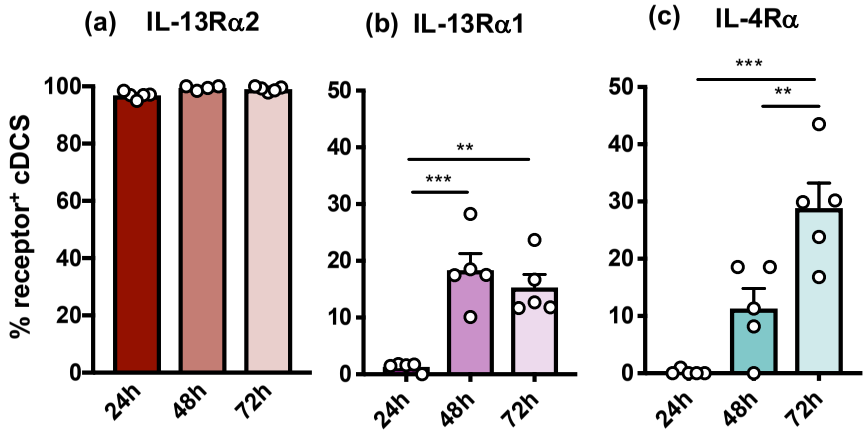
(a) IL-13Rα2
(b) IL-13Rα1
(c) IL-4Rα
% receptor+ cDCS
24h
48h
72h
***
**

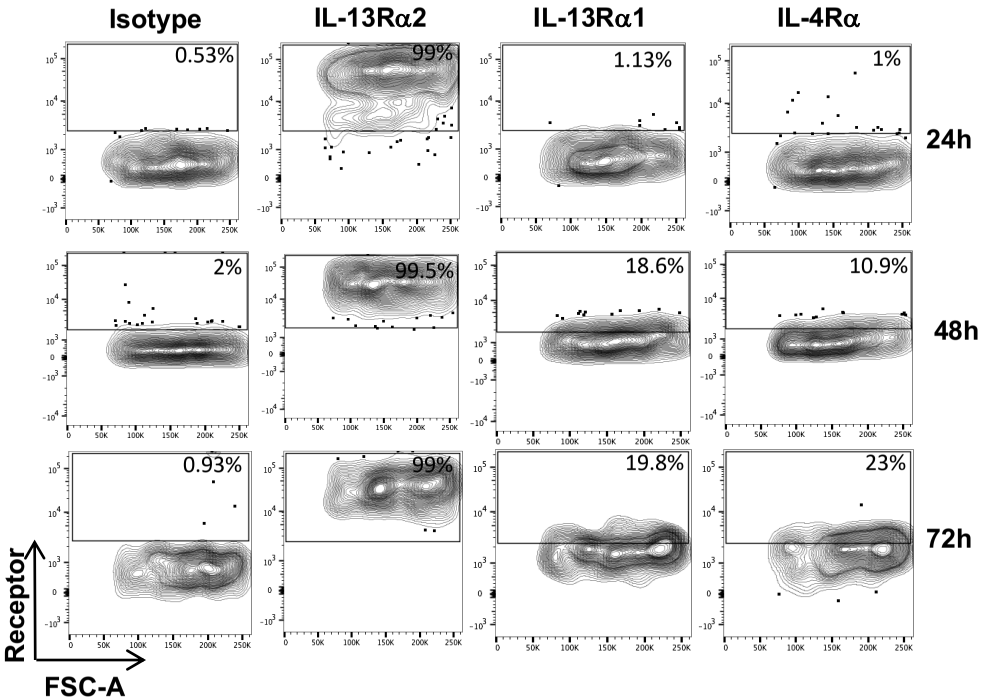
Isotype
IL-13Rα2
IL-13Rα1
IL-4Rα
24h
48h
72h
0.53%
99%
1.13%
1%
2%
99.5%
18.6%
10.9%
0.93%
99%
19.8%
23%
Receptor
FSC-A

Figure 5.4. Evaluation of lung cDCs expressing IL-4/IL-13 receptors, following intranasal rVV vaccination. BALB/c lungs (n=5 per vaccine group) were harvested at 24 h, 48 h or 72 h post rVV delivery. Single cell suspensions were prepared and stained for MHC-II^{+} CD11c^{+} CD11b^{+} CD103^{-} cDCs and IL-4/IL-13 receptors and the expression on lung cDCs were assessed using flow cytometry. Bar graphs (left panel) and representative flow cytometry plots (right panel) show IL-13Rα2, IL-13Rα1 and IL-4Rα expression following vaccination with (a-c) rVV vaccination. Error bars represent Standard Error of mean (SEM) and *p* values were calculated using Two-way ANOVA followed by Tukey's multiple comparison test. *$p<0.05$, **$p<0.01$, ***$p<0.001$, ****$p<0.0001$. Experiments with each vector were repeated minimum 2-3 times.

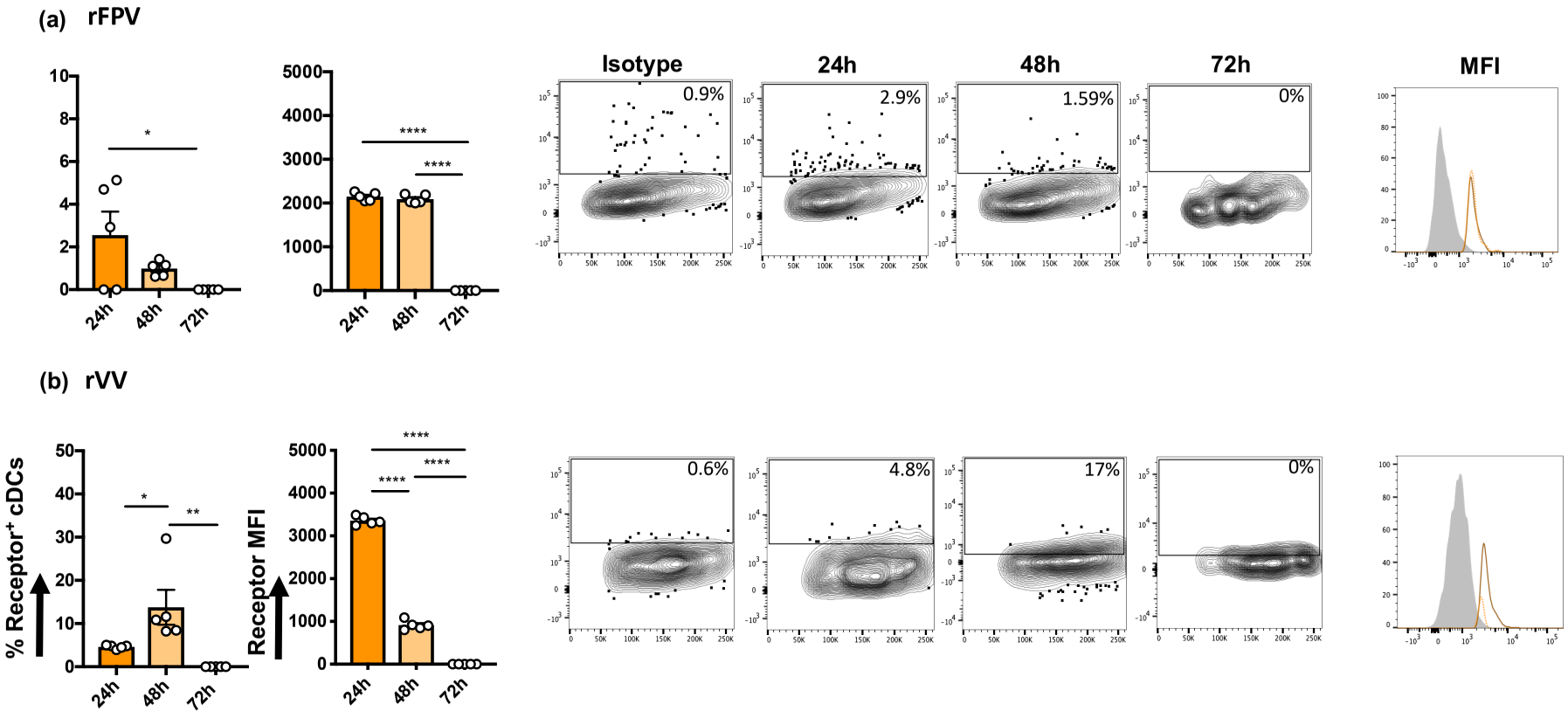
(a) rFPV
Isotype
24h
48h
72h
MFI
0.9%
2.9%
1.59%
0%
(b) rVV
% Receptor+ cDCs
Receptor MFI
0.6%
4.8%
17%
0%
24h
48h
72h

Figure 5.5. Evaluation of γc expression on lung cDCs at 24, 48 and 72 h following rFPV and rVV vaccination. BALB/c mice n=5 (per group) were i.n. vaccinated with rFPV and rVV, and lungs were harvested at 24, 48 or 72 h post delivery to evaluate γc expression on lung cDCs using flow cytometry as described in methods. Bar graphs (left panel) and representative plots (right panel) show percentage of cDCs expressing γc and the corresponding mean fluorescence intensities following **(a)** rFPV and **(b)** rVV vaccination. Histogram plots show γc expression densities at 24 h (solid orange line), 48 h (dotted orange line) and 72 h (tinted orange) compared to the isotype control (solid grey). Error bars represent Standard Error of mean (SEM) and *p* values were calculated using Two-way ANOVA followed by Tukey's multiple comparison test. *$p<0.05$, **$p<0.01$, ***$p<0.001$, ****$p<0.0001$. Experiments with each vector were repeated minimum 2-3 times.

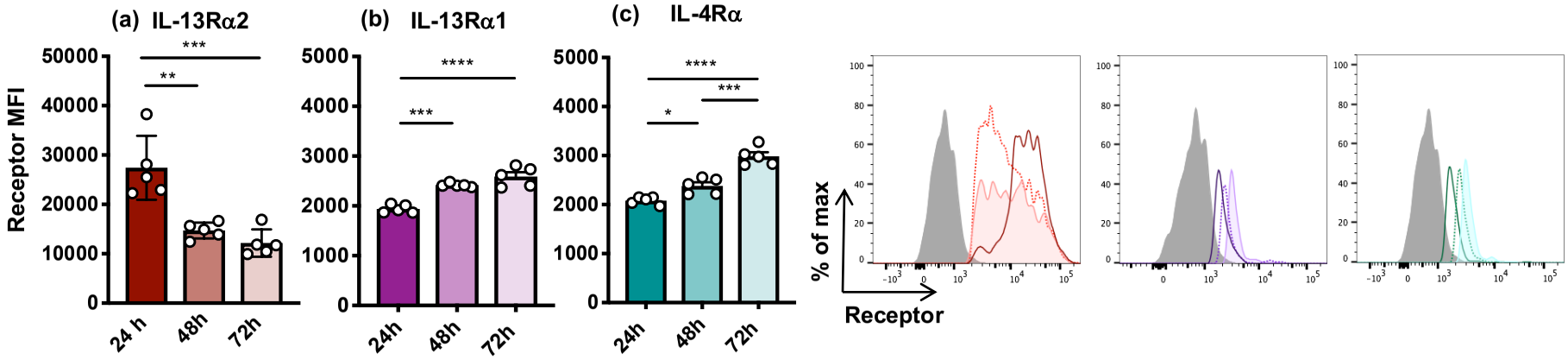

Figure 5.6. Evaluation of IL-4/IL-13 receptor mean fluorescence intensities following intranasal rFPV vaccination. BALB/c lungs (n=5 per vaccine group) were harvested at 24 h, 48 h or 72 h post rFPV delivery. Single cell suspensions were prepared and stained for MHC-II$^+$ CD11c$^+$ CD11b$^+$ CD103$^-$ cDCs and receptors to evaluate the IL-4/IL-13 receptor densities on lung cDCs using flow cytometry as described in methods**.** Bar graphs (left panel) and representative flow cytometry histogram plots (right panel) show IL-13Rα2, IL-13Rα1 and IL-4Rα expression at 24 h, 48 h and 72 h post **(a-c)** rFPV vaccination**.** Error bars represent Standard Error of mean (SEM) and *p* values were calculated using Two-way ANOVA followed by Tukey's multiple comparison test. **p*<0.05, ***p*<0.01, ****p*<0.001, *****p*<0.0001. Experiments with each vector were repeated minimum 2-3 times.

IL-4 type I receptor complex (IL-4Rα/γc), was not significantly expressed/regulated on cDC at 72 h post vaccination post vaccination **(Figure 5.5a-b).**

In the context of receptor densities (mean fluorescence intensity), 24 to 72 h post rFPV vaccination, the IL-13Rα2, showed a downward trend **(Figure 5.6a)**, where as an upward trend was observed with IL-13Rα1 and IL-4Rα **(Figure 5.6b-c)**. In contrast, post rVV vaccination down-regulation of both IL-13Rα2 and IL-13Rα1 densities were detected at 48h (24 vs 48 h $p<0.0001$), followed by an up-regulation at 72 h, comparable to 24 h was observed **(Figure 5.7a-b)**. However, IL-4Rα densities on rVV vaccinated cDC were gradually but significantly increased overtime (24 vs 48 h $p= 0.0127$, 48 vs 72 h and 24 vs 72 h $p<0.0001$) **(Figure 5.7c)**. In general, the IL-13Rα2 receptor densities on cDC following rFPV and rVV were approximately ten times greater than that of IL-13Rα1 and IL-4Rα.

5.4.2 rMVA and rMVAΔIL-1βR vaccination induced vastly different IL-13Rα2, IL-13Rα1 and IL-4Rα expression profiles on lung cDCs 24-72 h post delivery.

We have previously shown that a single deletion of virokine IL-1βR from rMVA (rMVAΔIL-1βR) could promote significantly lower ILC2-derived IL-13 expression and enhanced cDCs at the lung mucosae, compared to parental rMVA [367]. Thus, next the IL-4/IL-13 receptor expression profiles were assessed 24 - 72 h post delivery of these two vectors using flow cytometry as per indicated in methods.

Specifically, data revealed that compared to 24 and 48 h post rMVA vaccination significantly lower percentage of cDCs expressed IL-13Rα2 at 72 h (~95% vs ~50%) (p<0.0001) **(Figure 5.8a)**, where as IL-4Rα and IL-13Rα1 expression was significantly enhanced at 48h compared to 24h (~1 vs 3 and ~3 vs 6%) (p<0.0001) with no detectable expression at 72 h post delivery (48 vs 72 h p<0.0001) **(Figure 5.8b-c).** Although, with rMVAΔIL-1βR, similar IL-13Rα2 and IL-13Rα1 expression profiles to rMVA were detected **(Figure 5.9a-b)**, vastly different IL-4Rα expression profile was observed at 72 h, not only between the two vaccination groups (rMVA 0%, rMVAΔIL-1βR ~20%) but also during 24 - 72 h post rMVAΔIL-1βR delivery (24 vs 48 h and 24 vs 72 h p<0.0001) **(Figure 5.9c).** Once again the γc was not expressed on cDCs 72 h following rMVA and rMVAΔIL-1βR vaccination **(Figure 5.10a-b).**

In the context of receptor densities, IL-13Rα2 densities following rMVA and rMVAΔIL-1βR were also ~10 times greater than that of IL-13Rα1 and IL-4Rα. On rMVA and rMVAΔIL-1βR vaccinated cDC, although the IL-13Rα2 and IL-13Rα1 receptor densities tracked similar to that of the proportion of cDCs expressing each receptor **(Figure 5.11a-c and 5.12a-b)**, the IL-4Rα densities showed significant up-regulation at 72 h post rMVAΔIL-1βR vaccination, unlike rMVA, (rMVA vs rMVAΔIL-1βR p<0.0001) **(Figure 5.12c)**.

5.4.3 Following pox viral vaccination lung pDCs exhibited differential IL-13Rα2/IL-13Rα1 expression profiles to cDCs

Knowing that pDCs can modulate antibody differentiation by induction of type I interferons [336,400], plus our recent studies showing that IL-13 is necessary for effective antibody differentiation [122,257] and also viral vector induced ILC-derived IL-13 significantly impacted the pDC recruitment to the lung mucosae [367], we next evaluated the IL-4/IL-13 receptor regulation on pDCs post poxviral vaccination. Surprisingly, data revealed that although rFPV and rVV vaccinations showed regulation of IL- 13Rα2, IL-13Rα1, IL-4Rα and γc, post rMVA and rMVAΔIL-1βR vaccination no detectable expression of the latter three receptors was found on lung pDC even though elevated expression of IL-13Rα2 was detected 24 and 48 h post delivery (24 vs 48 h $p<0.0001$) **(Figure 5.13a-b)**. The IL-13Rα2 expression on pDCs post rFPV vaccination was found to be in the order of (24 > 48 < 72 h) (24 vs 48 h and 48 vs 72 h $p<0.0001$) **(Figure 5.14)**, where as rVV showed a significant up-regulation of IL-13Rα2, both at 48 and 72 h, compared to 24h post delivery (24 < 48 ≤ 72 h) (24 vs 48 h and 24 vs 72 h $p<0.0001$) **(Figure 5.15)**. Interestingly, very low number of rFPV vaccinated pDCs expressed IL-4Rα, IL-13Rα1 and γc at 24 h and 48 h (≥ 3%) and no detectable expression was observed at 72h post delivery **(Figure 5.14 and 5.16a).** In contrast, significant up regulation of IL-4Rα and IL-13Rα1 were detected on rVV vaccinated lung pDCs 48 to 72 h post delivery (20 - 80%) where very high proportion of pDCs expressed IL-13Rα1 (24 vs 48 and 24 vs 72 h $p<0.0001$) and IL-4Rα (24 vs 48 $p<0.0001$ and 24 vs 72 h $p=0.0003$) compared to 24h (≥ 2%) **(Figure 5.15).** Moreover, less than 2% of rVV vaccinated pDCs expressed γc at 24 h and no detectable expression was found at other time points **(Figure 5.15 and 5.16b).**

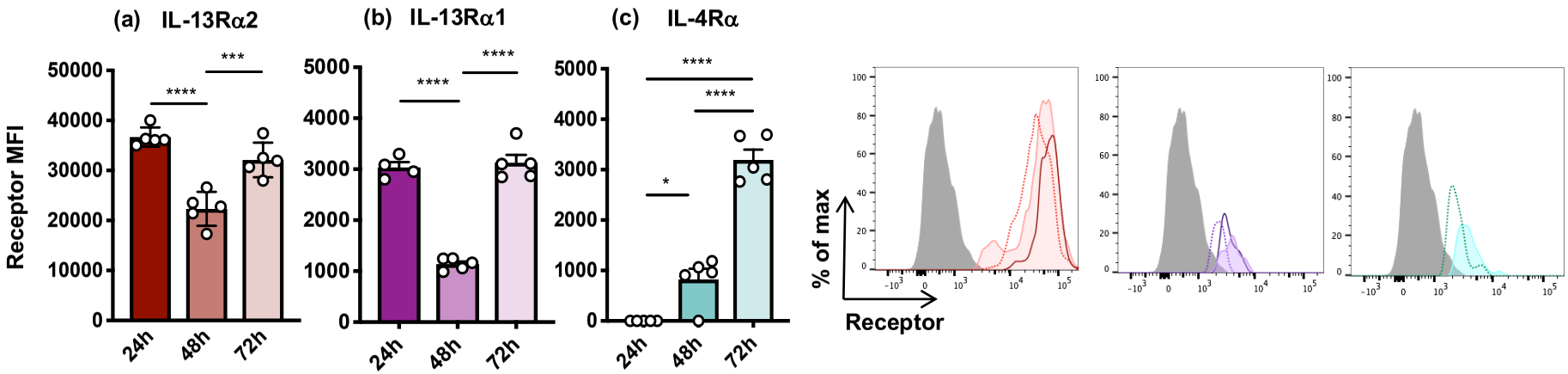

Figure 5.7. Evaluation of IL-4/IL-13 receptor mean fluorescence intensities following intranasal rVV vaccination. BALB/c lungs (n=5 per vaccine group) were harvested at 24 h, 48 h or 72 h post rVV delivery. Single cell suspensions were prepared and stained for MHC-II$^+$ CD11c$^+$ CD11b$^+$ CD103$^-$ cDCs and receptors to evaluate the IL-4/IL-13 receptor densities on lung cDCs using flow cytometry as described in methods**.** Bar graphs (left panel) and representative flow cytometry histogram plots (right panel) show IL-13Rα2, IL-13Rα1 and IL-4Rα expression at 24 h, 48 h and 72 h post **(a-c)** rVV vaccination**.** Error bars represent Standard Error of mean (SEM) and *p* values were calculated using Two-way ANOVA followed by Tukey's multiple comparison test. **p*<0.05, ***p*<0.01, ****p*<0.001, *****p*<0.0001. Experiments with each vector were repeated minimum 2-3 times.

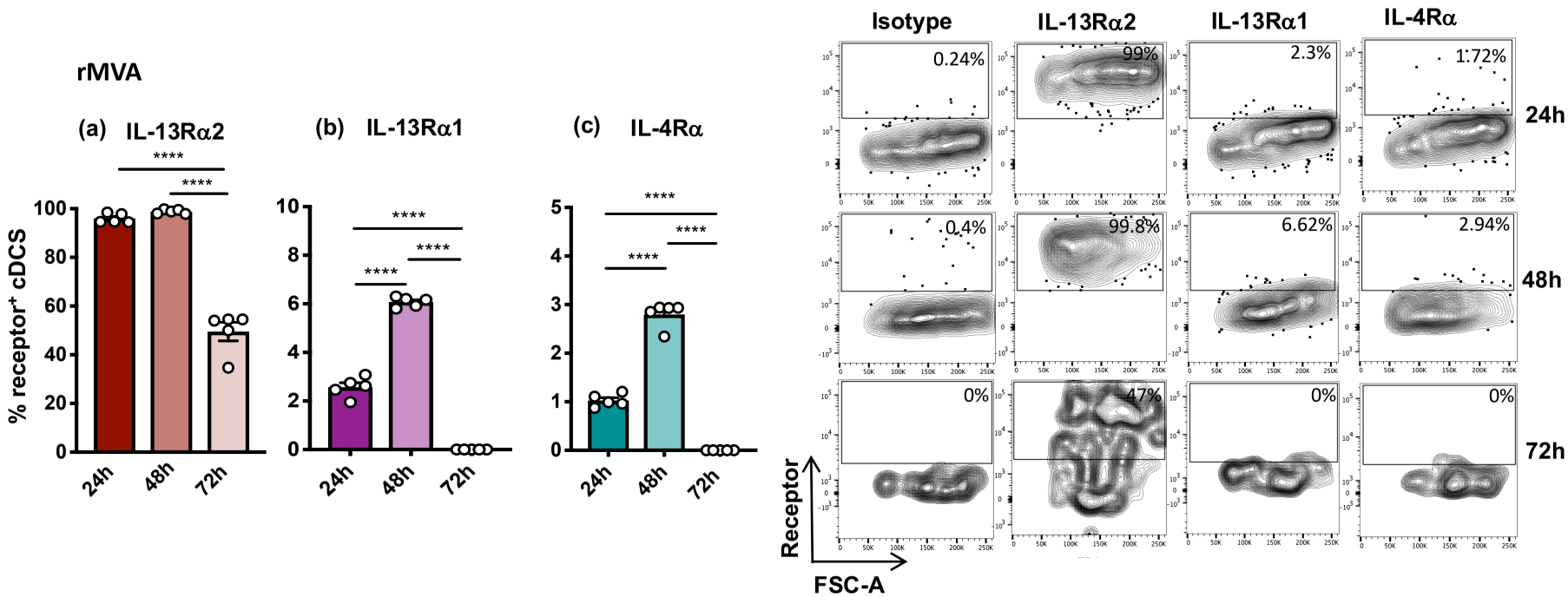
rMVA
(a) IL-13Rα2
(b) IL-13Rα1
(c) IL-4Rα
% receptor+ cDCS
****
24h
48h
72h
Isotype
IL-13Rα2
IL-13Rα1
IL-4Rα
0.24%
99%
2.3%
1.72%
0.4%
99.8%
6.62%
2.94%
0%
47%
0%
0%
Receptor
FSC-A

Figure 5.8. Evaluation of lung cDCs expressing IL-4/IL-13 receptors, following intranasal rMVA vaccination. BALB/c lungs (n=5 per vaccine group) were harvested at 24 h, 48 h or 72 h post rMVA delivery. Single cell suspensions were prepared and stained for MHC-II^{+} CD11c^{+} CD11b^{+} CD103^{-} cDCs and IL-4/IL-13 receptors and the expression on lung cDCs were assessed using flow cytometry. Bar graphs (left panel) and representative flow cytometry plots (right panel) show IL-13Rα2, IL-13Rα1 and IL-4Rα expression following vaccination with (a-c) rMVA vaccination. Error bars represent Standard Error of mean (SEM) and *p* values were calculated using Two-way ANOVA followed by Tukey's multiple comparison test. *$p<0.05$, **$p<0.01$, ***$p<0.001$, ****$p<0.0001$. Experiments with each vector were repeated minimum 2-3 times.

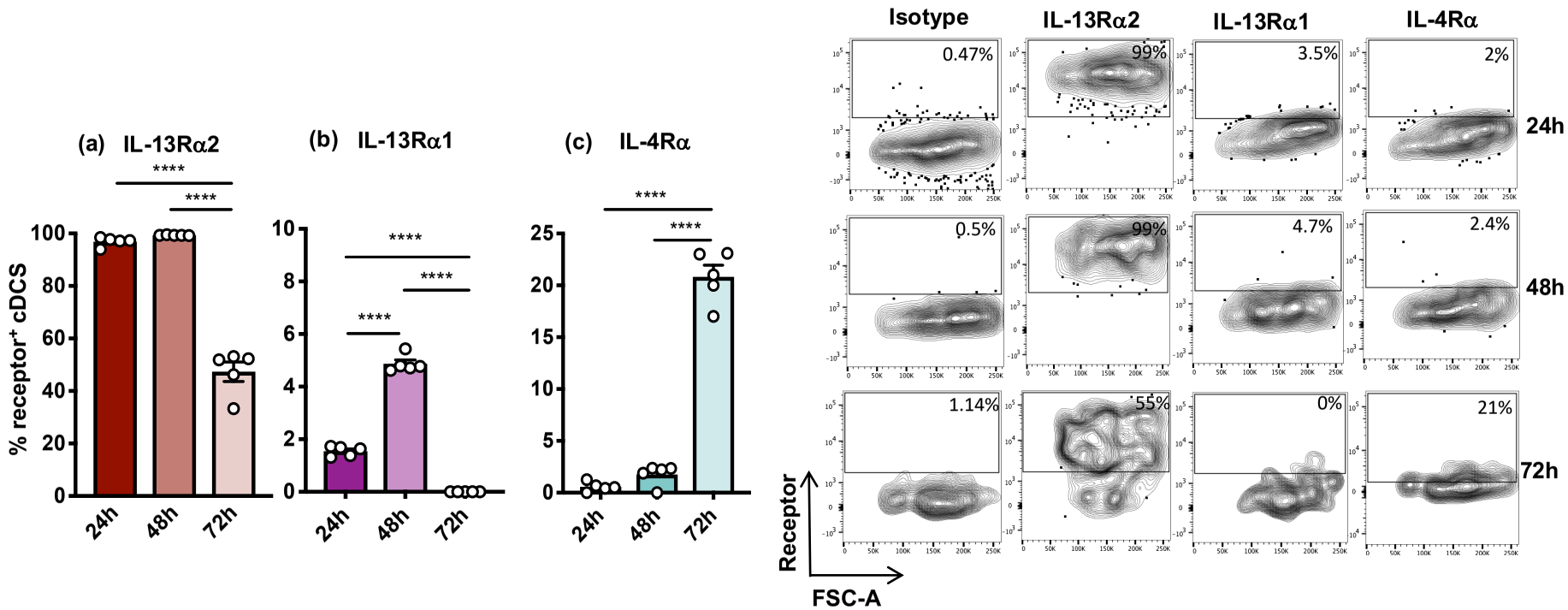
(a) IL-13Rα2
(b) IL-13Rα1
(c) IL-4Rα
% receptor+ cDCS
24h
48h
72h
****
Isotype
IL-13Rα2
IL-13Rα1
IL-4Rα
0.47%
99%
3.5%
2%
0.5%
99%
4.7%
2.4%
1.14%
55%
0%
21%
Receptor
FSC-A

Figure 5.9. Evaluation of lung cDCs expressing IL-4/IL-13 receptors, following intranasal rMVAΔIL-1βR vaccination. BALB/c lungs (n=5 per vaccine group) were harvested at 24 h, 48 h or 72 h post rMVAΔIL-1βR delivery. Single cell suspensions were prepared and stained for MHC-II^{+} CD11c^{+} CD11b^{+} CD103^{-} cDCs and IL-4/IL-13 receptors and the expression on lung cDCs were assessed using flow cytometry. Bar graphs (left panel) and representative flow cytometry plots (right panel) show IL-13Rα2, IL-13Rα1 and IL-4Rα expression following vaccination with (a-c) rMVAΔIL-1βR vaccination. Error bars represent Standard Error of mean (SEM) and *p* values were calculated using Two-way ANOVA followed by Tukey's multiple comparison test. *$p<0.05$, **$p<0.01$, ***$p<0.001$, ****$p<0.0001$. Experiments with each vector were repeated minimum 2-3 times.

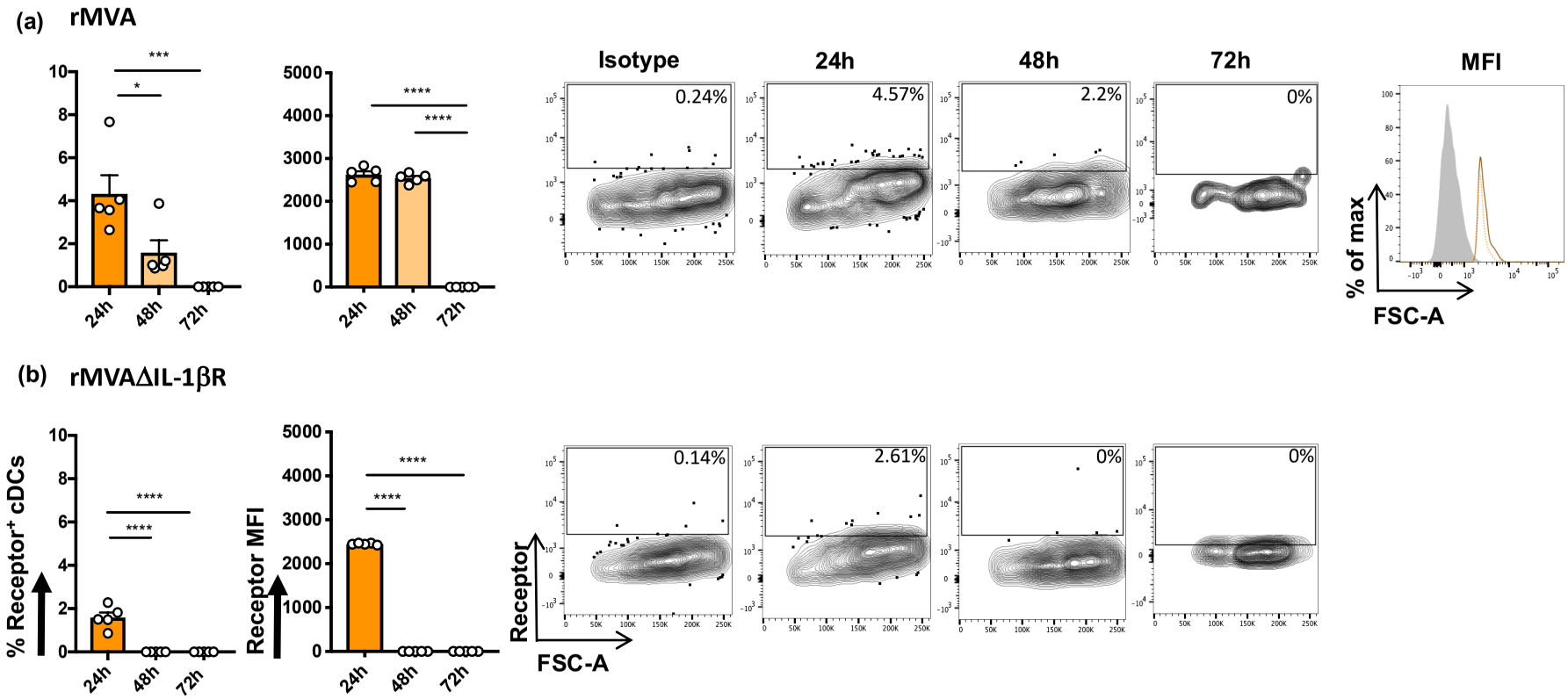
(a) rMVA
Isotype
24h
48h
72h
MFI
0.24%
4.57%
2.2%
0%
% of max
FSC-A
(b) rMVAΔIL-1βR
% Receptor+ cDCs
Receptor MFI
0.14%
2.61%
0%
0%
Receptor
FSC-A

Figure 5.10. Evaluation of γc expression on lung cDCs at 24, 48 and 72 h following rMVA and rMVAΔIL-1βR vaccination. BALB/c mice n=5 (per group) were i.n. vaccinated with rMVA or rMVAΔIL-1βR and lungs were harvested at 24, 48 or 72 h post delivery to evaluate γc expression on lung cDCs using flow cytometry as described in methods. Bar graphs (left panel) and representative plots (right panel) show percentage of cDCs expressing γc and the corresponding mean fluorescence intensities following **(a)** rMVA and **(b)** rMVAΔIL-1βR vaccination. Histogram plots show γc expression densities at 24 h (solid orange line), 48 h (dotted orange line) and 72 h (tinted orange) compared to the isotype control (solid grey). Error bars represent Standard Error of mean (SEM) and *p* values were calculated using Two-way ANOVA followed by Tukey's multiple comparison test. *$p<0.05$, **$p<0.01$, ***$p<0.001$, ****$p<0.0001$. Experiments with each vector were repeated minimum 2-3 times.

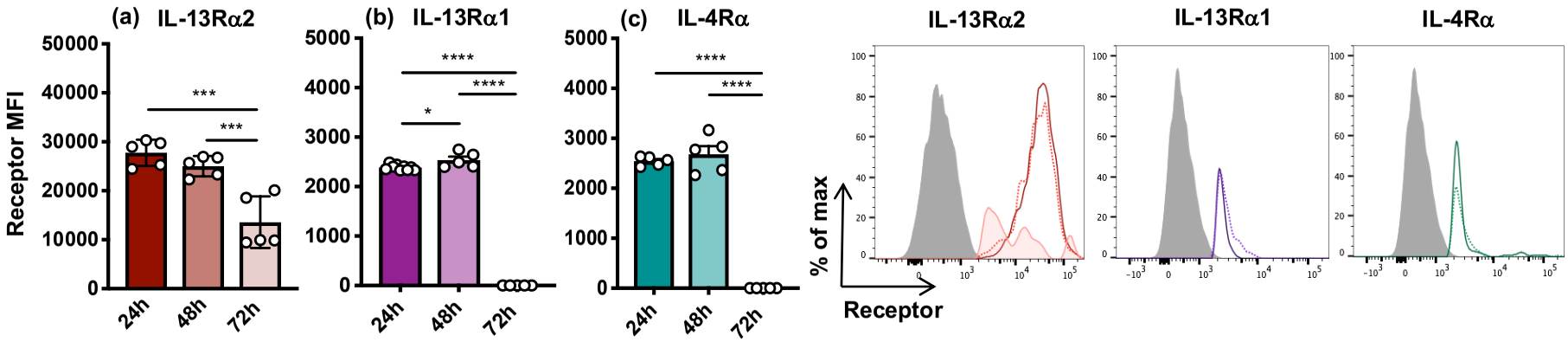

Figure 5.11. Evaluation of IL-4/IL-13 receptor mean fluorescence intensities following intranasal rMVA vaccination. BALB/c lungs (n=5 per vaccine group) were harvested at 24 h, 48 h or 72 h post rMVA delivery. Single cell suspensions were prepared and stained for MHC-II^{+} CD11c^{+} CD11b^{+} CD103^{-} cDCs and receptors to evaluate the IL-4/IL-13 receptor densities on lung cDCs using flow cytometry as described in methods**.** Bar graphs (left panel) and representative flow cytometry histogram plots (right panel) show IL-13Rα2, IL-13Rα1 and IL-4Rα expression at 24 h, 48 h and 72 h post **(a-c)** rMVA vaccination**.** Error bars represent Standard Error of mean (SEM) and *p* values were calculated using Two-way ANOVA followed by Tukey's multiple comparison test. **p*<0.05, ***p*<0.01, ****p*<0.001, *****p*<0.0001. Experiments with each vector were repeated minimum 2-3 times.

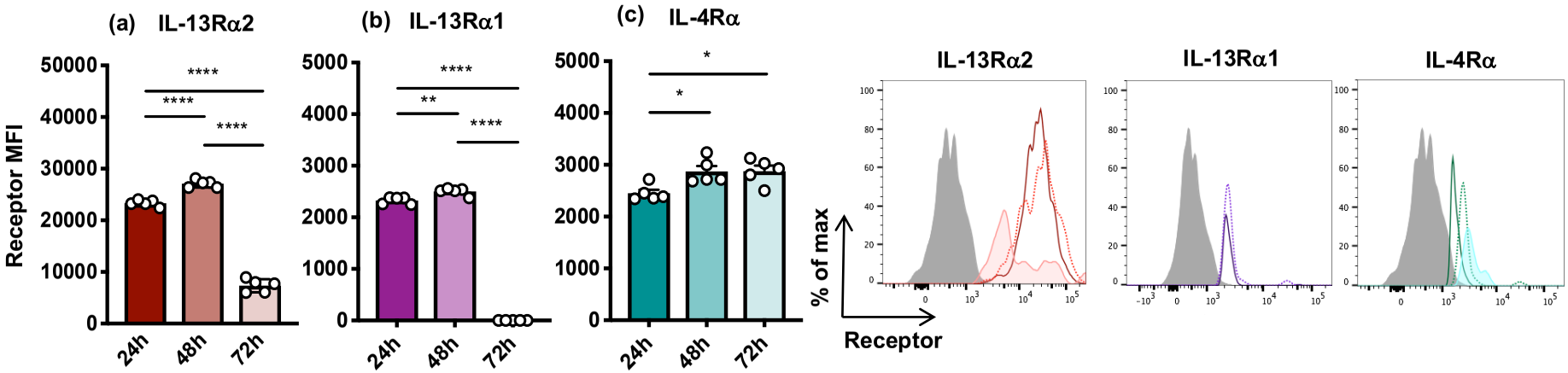

Figure 5.12. Evaluation of IL-4/IL-13 receptor mean fluorescence intensities following intranasal rMVAΔIL-1βR vaccination. BALB/c lungs (n=5 per vaccine group) were harvested at 24 h, 48 h or 72 h post rMVAΔIL-1βR delivery. Single cell suspensions were prepared and stained for MHC-II$^+$ CD11c$^+$ CD11b$^+$ CD103$^-$ cDCs and receptors to evaluate the IL-4/IL-13 receptor densities on lung cDCs using flow cytometry as described in methods**.** Bar graphs (left panel) and representative flow cytometry histogram plots (right panel) show IL-13Rα2, IL-13Rα1 and IL-4Rα expression at 24 h, 48 h and 72 h post **(a-c)** rMVAΔIL-1βR vaccination**.** Error bars represent Standard Error of mean (SEM) and *p* values were calculated using Two-way ANOVA followed by Tukey's multiple comparison test. **p*<0.05, ***p*<0.01, ****p*<0.001, *****p*<0.0001. Experiments with each vector were repeated minimum 2-3 times.

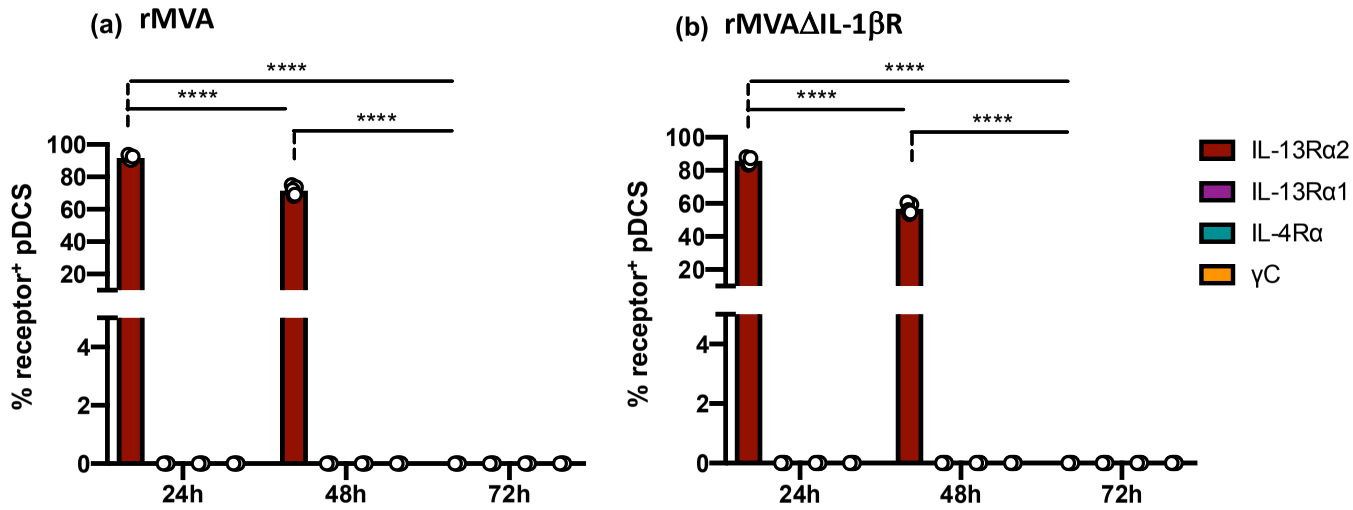

Figure 5.13. Evaluation of IL-4/ IL-13 receptor expression on lung pDCs at 24, 48 and 72 h following rMVA and rMVAΔIL-1βR vaccination. BALB/c mice n=5 (per group) were i.n. vaccinated with rMVA or rMVAΔIL-1βR and lungs were harvested at 24h 48 and 72 h post delivery to evaluate IL-4/IL-13 receptor expression on lung CD11b^{-} B220^{+} pDCs using flow cytometry as described in methods. Bar graphs show expression of IL-13Rα2, IL-13Rα1, IL-4Rα and γc on lung pDCs following **(a)** rMVA and **(b)** rMVAΔIL-1βR vaccination. Error bars represent Standard Error of mean (SEM) and *p* values were calculated using Two-way ANOVA followed by Tukey's multiple comparison test. *$p<0.05$, **$p<0.01$, ***$p<0.001$, ****$p<0.0001$. Experiments with each vector were repeated minimum 2-3 times.

rFPV vaccinated pDCs showed significant decrease in IL-13Rα2 (24 vs 48 h p = 0.0002; 24 vs 72 h p = 0.0003), IL-13Rα1 (24 vs 48 h and 24 vs 72 h p = 0.0284) and IL-4Rα densities (24 vs 48 h and 24 vs 72 h p = 0.0277) over time **(Figure 5.17)**. In contrast, rVV vaccinated pDCs showed significantly elevated IL-13Rα2 density at 72 h (24 vs 72 h p<0.0001), IL-13Rα1 (24 vs 48 h p=0.0002; 24 vs 72 h p<0.0001) and IL-4Rα densities (24 vs 48 h and 24 vs 72 h p<0.0001) over time **(Figure 5.18)**. Similar to cDCs, the expression/regulation of γc on pDCs were also not very significant **(Figure 5.16)**. Interestingly, the expression densities of IL-13Rα2 on rVV vaccinated pDC were also found to be approximately 10 times greater than that of IL-13Rα1 and IL-4Rα.

5.5. Discussion

The enhanced IL-13Rα2 expression unlike IL-13Rα1, detected on lung cDCs and pDCs 24 h following pox viral vector vaccination, have strengthened our previous findings that IL-13Rα2 may be the early sensor/mediator of IL-13 responses at the first line of defense, the lung mucosae (Roy *et al*. (submitted)). Moreover, the dissimilar expression of IL-4 Type I receptor complex (IL-4Rα and γC) on cDCs, further substantiated that at early stages of vaccination, IL-13 performed a more predominant role in shaping the vaccine-specific immune outcomes, than IL-4, which was also consistent with our previous findings [122,302]. Specifically, where, we have shown that pox viral vector-based vaccines, that have transiently inhibited IL-13 at the vaccination site by significantly dampening ILC2-derived IL-13 activity at the lung mucosae, 24h post delivery [306] have been associated with

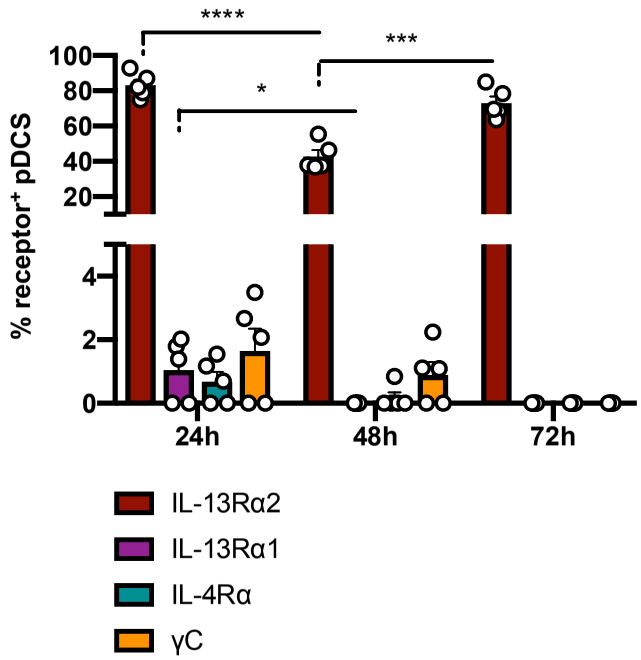
****
***
*
% receptor+ pDCS
100
80
60
40
20
4
2
0
24h
48h
72h
IL-13Rα2
IL-13Rα1
IL-4Rα
γC

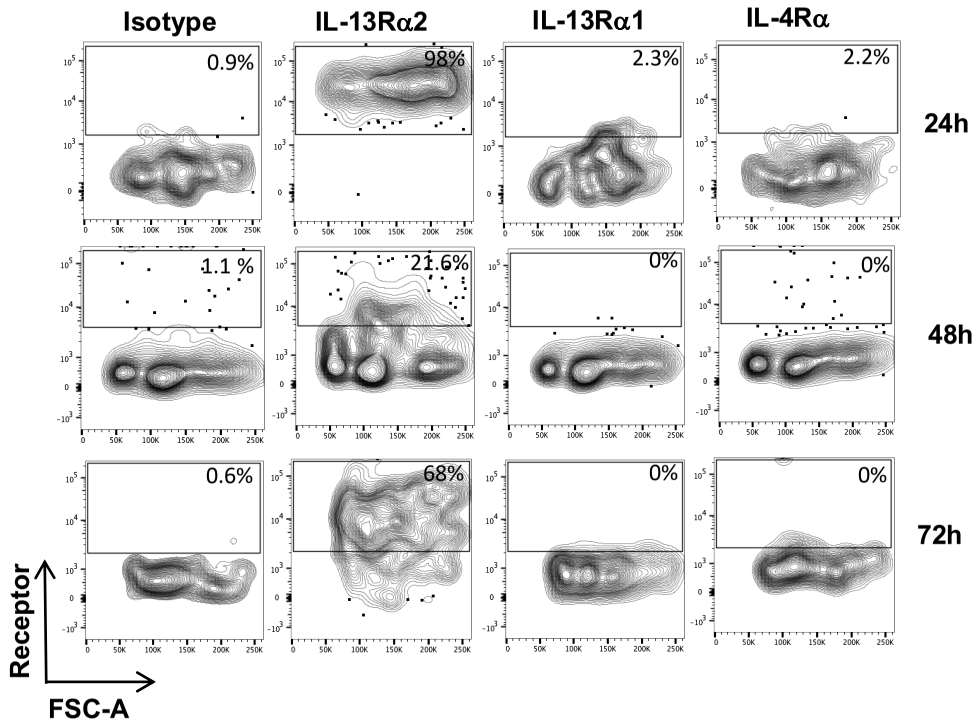
Isotype
IL-13Rα2
IL-13Rα1
IL-4Rα
0.9%
98%
2.3%
2.2%
24h
1.1 %
21.6%
0%
0%
48h
0.6%
68%
0%
0%
72h
Receptor
FSC-A

Figure 5.14. Evaluation of lung pDCs expressing IL-4/IL-13 receptors, following intranasal rFPV vaccination. BALB/c lungs (n=5 per vaccine group) were harvested at 24 h, 48 h or 72 h following vaccination with rFPV delivery. Single cell suspensions were prepared and stained for IL-4/IL-13 receptors on lung MHC-II^{+} CD11c^{+} CD11b^{-} B220^{+} pDCs using flow cytometry as described in methods**.** Bar graphs (left panel) and representative flow cytometry plots (right panel) show IL-13Rα2, IL-13Rα1, IL-4Rα and γc expression at 24 h, 48 h and 72 h, post rFPV vaccination**.** Error bars represent Standard Error of mean (SEM) and *p* values were calculated using Two-way ANOVA followed by Tukey's multiple comparison test. **p*<0.05, ***p*<0.01, ****p*<0.001, *****p*<0.0001. Experiments with each vector were repeated minimum 2-3 times.

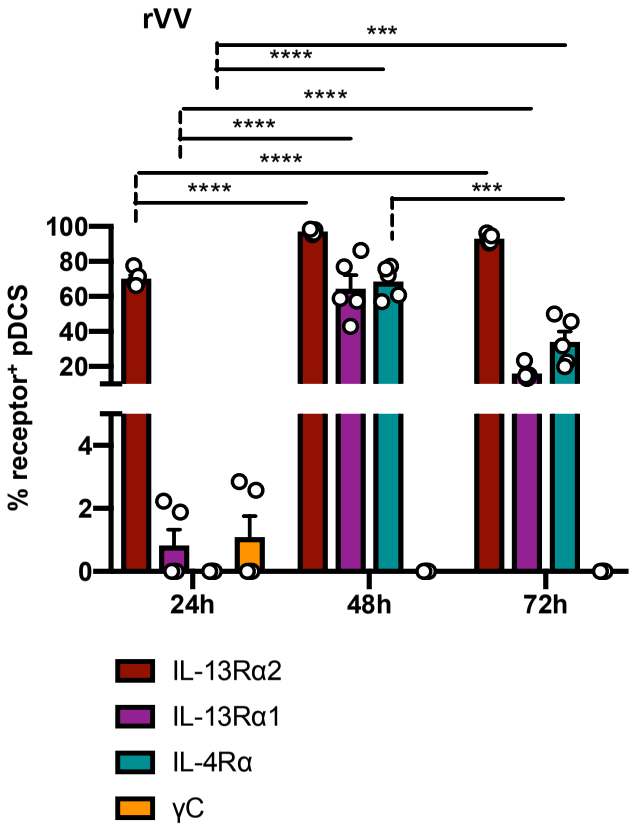
rVV
***
****
****
****
****
****
***
% receptor+ pDCS
100
80
60
40
20
4
2
0
24h
48h
72h
IL-13Rα2
IL-13Rα1
IL-4Rα
γC

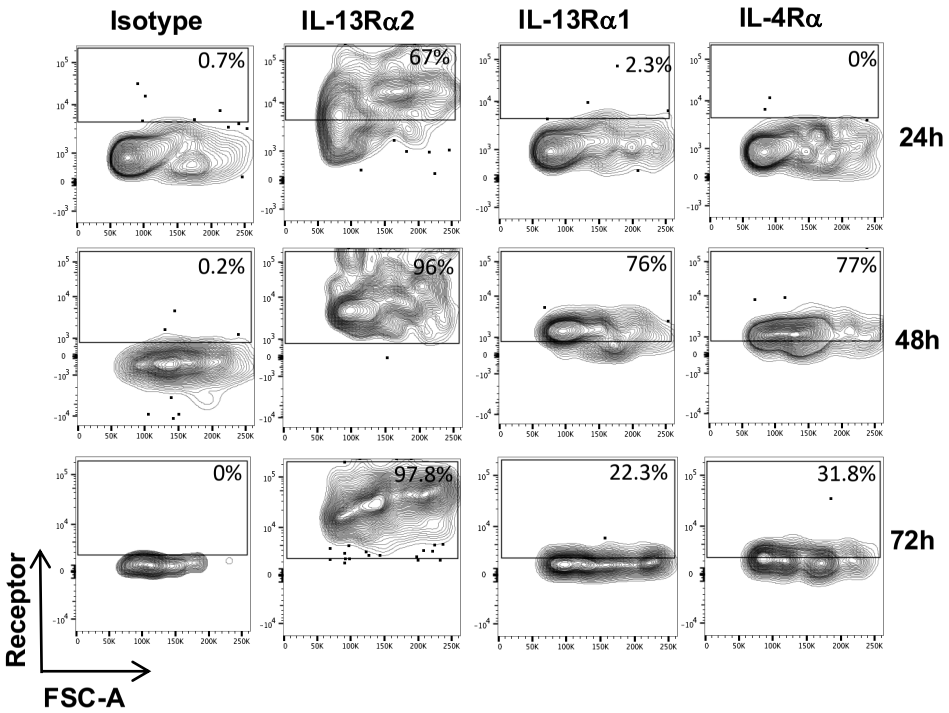
Isotype
IL-13Rα2
IL-13Rα1
IL-4Rα
0.7%
67%
2.3%
0%
24h
0.2%
96%
76%
77%
48h
0%
97.8%
22.3%
31.8%
72h
Receptor
FSC-A

Figure 5.15. Evaluation of lung pDCs expressing IL-4/IL-13 receptors, following intranasal rVV vaccination. BALB/c lungs (n=5 per vaccine group) were harvested at 24 h, 48 h or 72 h following vaccination with rVV delivery. Single cell suspensions were prepared and stained for IL-4/IL-13 receptors on lung MHC-II^{+} CD11c^{+} CD11b^{-} B220^{+} pDCs using flow cytometry as described in methods**.** Bar graphs (left panel) and representative flow cytometry plots (right panel) show IL-13Rα2, IL-13Rα1, IL-4Rα and γc expression at 24 h, 48 h and 72 h, post rVV vaccination**.** Error bars represent Standard Error of mean (SEM) and *p* values were calculated using Two-way ANOVA followed by Tukey's multiple comparison test. *$p<0.05$, **$p<0.01$, ***$p<0.001$, ****$p<0.0001$. Experiments with each vector were repeated minimum 2-3 times.

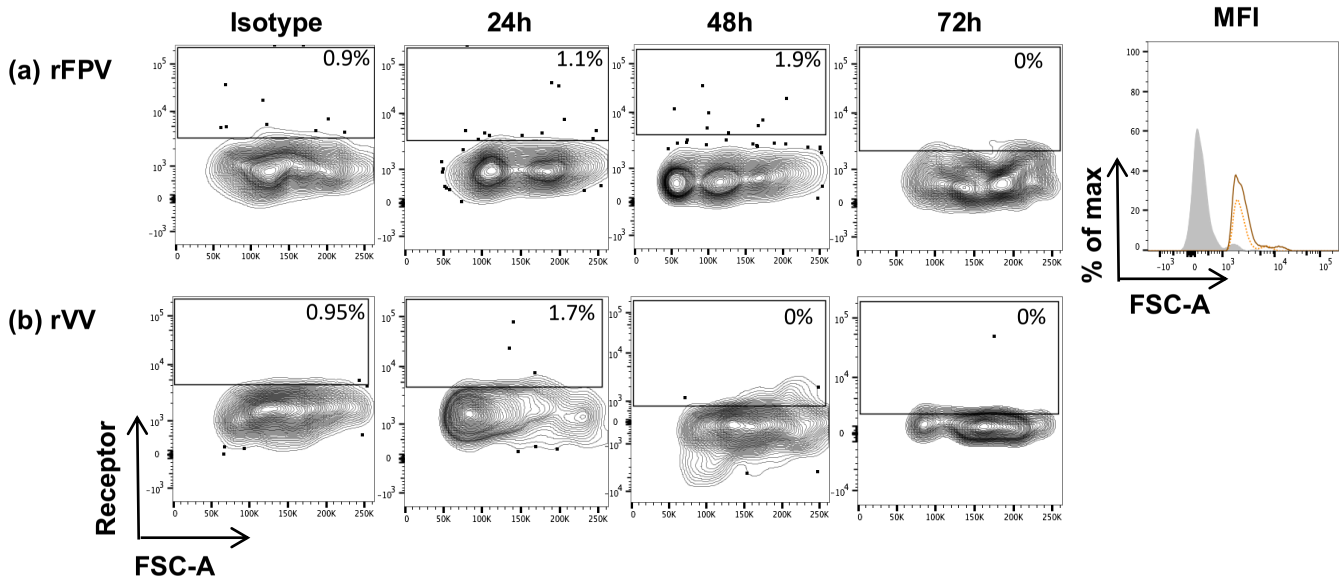

Figure 5.16. Evaluation of γc expression on lung pDCs at 24, 48 and 72 h following viral vector based vaccination. BALB/c mice n=5 (per group) were i.n. vaccinated with rFPV or rVV and lungs were harvested at 24, 48 or 72 h post delivery to evaluate γc expression on lung cDCs using flow cytometry as described in methods. Representative plots show percentage of $CD11b^{-}$ $B220^{+}$ pDCs expressing γc (left panel) following **(a)** rFPV and **(b)** rVV vaccination. Flow cytometry histogram plot(right panel) shows γc expression densities at 24 h (solid orange line), 48 h (dotted orange line) and 72 h (tinted orange) compared to the isotype control (solid grey) following rFPV vaccination.

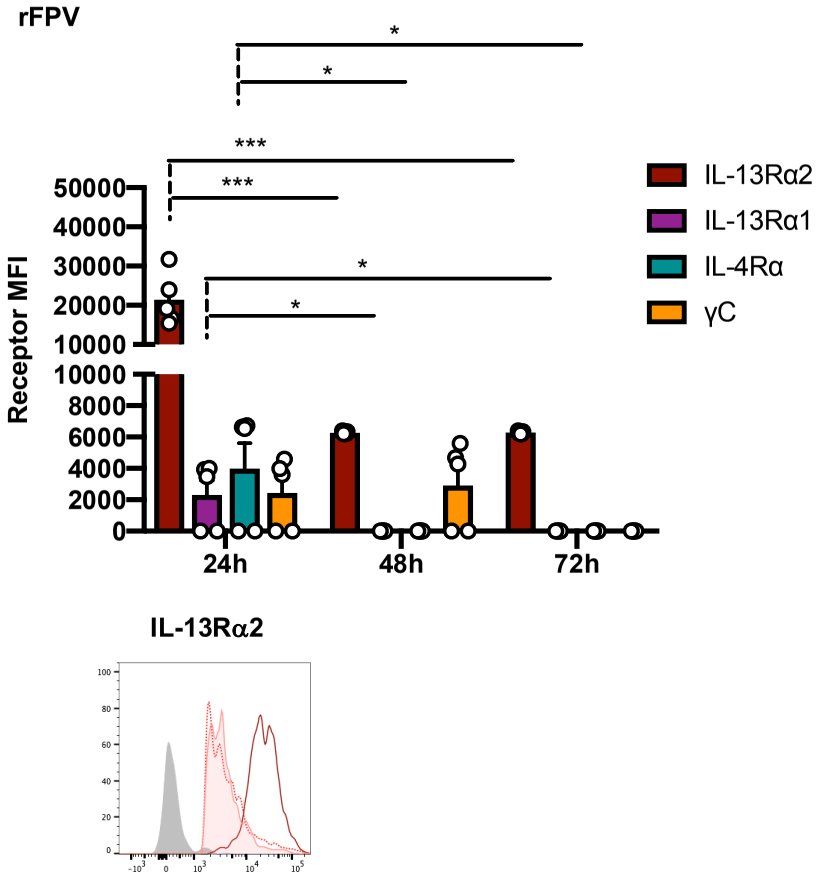

Figure 5.17. Evaluation of IL-4/IL-13 receptor mean fluorescence intensities on lung pDCs, following intranasal rFPV vaccination. BALB/c lungs (n=5 per vaccine group) were harvested at 24 h, 48 h or 72 h following rFPV vaccination with delivery. Single cell suspensions were prepared and stained for IL-4/IL-13 receptors on lung MHC-II^{+} CD11c^{+} CD11b^{-} B220^{+} pDCs to evaluate receptor densities using flow cytometry as described in methods. Bar graphs (top panel) and representative flow cytometry histogram plots (bottom panel) show IL-13Rα2, IL-13Rα1, IL-4Rα and γc expression over 24 - 72h post rFPV vaccination. Error bars represent Standard Error of mean (SEM) and *p* values were calculated using Two-way ANOVA followed by Tukey's multiple comparison test. **p*<0.05, ***p*<0.01, ****p*<0.001, *****p*<0.0001. Experiments with each vector were repeated minimum 2-3 times.

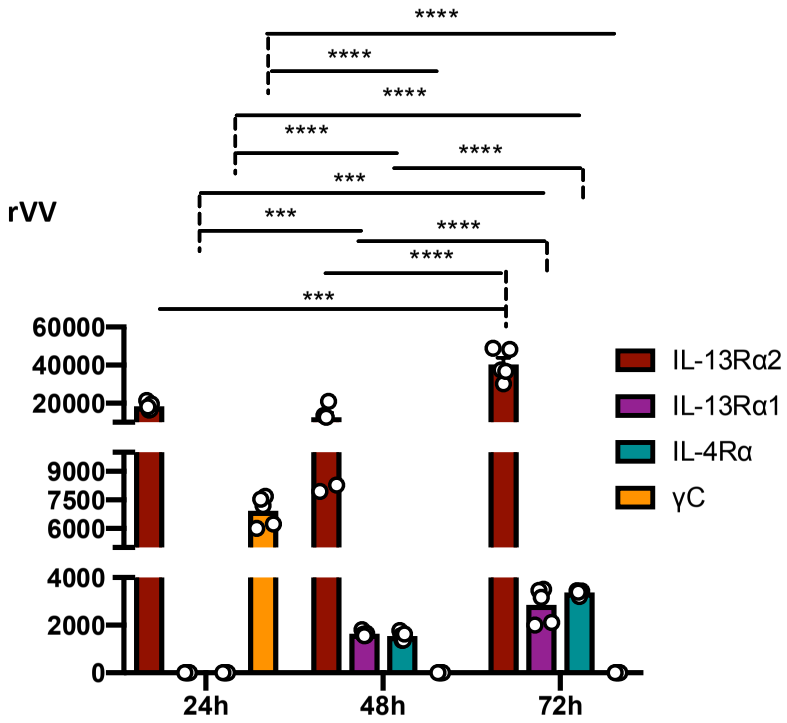
rVV
****
****
****
****
****
***
***
****
****
***
60000
40000
20000
9000
7500
6000
4000
2000
0
24h
48h
72h
IL-13Rα2
IL-13Rα1
IL-4Rα
γC

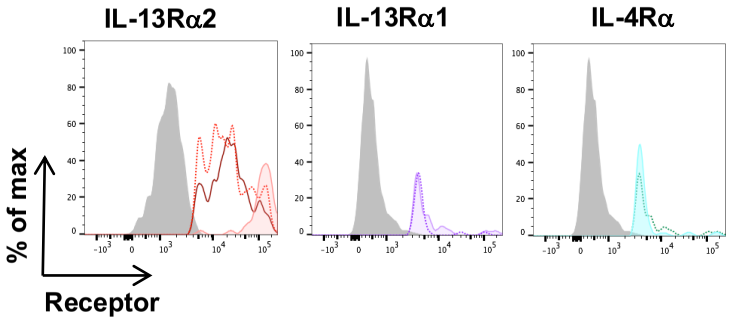
IL-13Rα2
IL-13Rα1
IL-4Rα
% of max
Receptor

Figure 5.18. Evaluation of IL-4/IL-13 receptor mean fluorescence intensities on lung pDCs, following intranasal rVV vaccination. BALB/c lungs (n=5 per vaccine group) were harvested at 24 h, 48 h or 72 h following rVV vaccination with delivery. Single cell suspensions were prepared and stained for IL-4/IL-13 receptors on lung MHC-II^{+} CD11c^{+} CD11b^{-} B220^{+} pDCs to evaluate receptor densities using flow cytometry as described in methods**.** Bar graphs (left panel) and representative flow cytometry histogram plots (right panel) show IL-13Rα2, IL-13Rα1, IL-4Rα and γc expression over 24 - 72h post rVV vaccination**.** Error bars represent Standard Error of mean (SEM) and *p* values were calculated using Two-way ANOVA followed by Tukey's multiple comparison test. *$p<0.05$, **$p<0.01$, ***$p<0.001$, ****$p<0.0001$. Experiments with each vector were repeated minimum 2-3 times.

enhanced lung cDC recruitment [99] and induction of high avidity T cells [123,367]. In this study the replication abortive (in mammalian cells) rFPV and replication competent rVV yielded uniquely different ILC2-derived IL-13 and IL-13 receptor regulation on lung cDCs. rFPV vaccination, which was linked to low ILC2-derived IL-13, showed up-regulation of IL-13Rα2 on cDC 24 h and down-regulation 72 h delivery, whist the opposing was observed with Type II receptor complex (IL-4Rα/IL-13Rα1) **(Figure 5.19)**. This once again indicated that on lung cDCs the high affinity IL-13Rα2 was most likely associated with IL-13 signalling at the early stages (24 h) of rFPV vaccination, whilst, low affinity IL-13Rα1 gained function at later stages of delivery. In contrast, post rVV vaccination (under high ILC2-derived IL-13), constantly elevated IL-13Rα2 expression 24-72 h **(Figure 5.19)** suggested that, under this condition IL-13Rα2 was likely involved in sequestration of the excess IL-13, produced by the replication competent vector (specifically 48-72 h) whilst signalling was mainly controlled by the low affinity Type II receptor complex (IL-4Rα /IL-13Rα1). These uniquely different early events may explain 'how and why' i) in a prime-boost vaccination modality, rFPV prime can generate high avidity T cells, unlike rVV [133] and ii) the order of vector delivery significantly impact vaccine-specific adaptive immune outcomes.

Recently, we have shown that rMVA vaccination can induce much higher IL-33R/ST2^{+}ILC2-derived IL-13 and reduced cDC recruitment at the lung mucosae compared to rFPV vaccination. [367]. Moreover, the level of IL-13 induced by these vectors were in the order of rFPV < rMVA < rVV (rMVA 2x higher and rVV 7x higher than rFPV) [367]. Interestingly, in this study early (24 to 48 h) post vaccination

IL-13/IL-4 receptor regulation was very similar between rMVA and rVV, indicative of the two vectors possessing similar IL-13 regulation mechanisms (sequestration of IL-13 by IL-13Rα2 and signaling via IL-13Rα1/IL-4Rα). Nevertheless, 72 h post rMVA delivery exhibited significantly reduced IL-4/IL-13 receptor activity compared to the replication competent rVV **(Figure 5.19)**, potentially associated with the continuous ILC2-derived IL-13 production at the vaccination site by rVV continuously activating IL-13Rα2, unlike the replication abortive rMVA.

Interestingly, unlike parental rMVA, the IL-1βR deletion variant rMVAΔIL-1βR vaccination, which showed similar ILC2-derived IL-13 levels and lung cDC activity at the lung mucosae to rFPV, [367] also exhibited down-regulation of IL-13Rα2 (and also IL-13Rα1) and an up-regulation of IL-4Rα, 72 h post vaccination (Figure 5.19). Given that, IL-13Rα2 can inhibit IL-4Rα activity [401], these observations inferred that, rMVAΔIL-1βR most likely regulated the vaccine-derived IL-13 responses 24 - 72 h post vaccination by IL-13Rα2 signalling and regulation of IL-4Rα by IL-13Rα2 antagonism, with no IL-4Rα/IL-13Rα1 (Type II receptor complex) signaling, unlike rFPV or rMVA. Interestingly, we have recently shown that compared to rFPV, rMVAΔIL-1βR vaccination generated not only significantly lower ILC2-derived IL-13 but also ILC1/ILC3-derived IFN-γ, (likely due to the residual viral IL-18 binding protein neutralizing host IL-18 preventing host IFN-γ production). Thus, in the context of rMVAΔIL-1βR, we postulate that the imbalance of IL-13/IFN-γ expression may be linked to the differential IL-13Rα1/IL-13Rα2 regulation compared to rFPV.

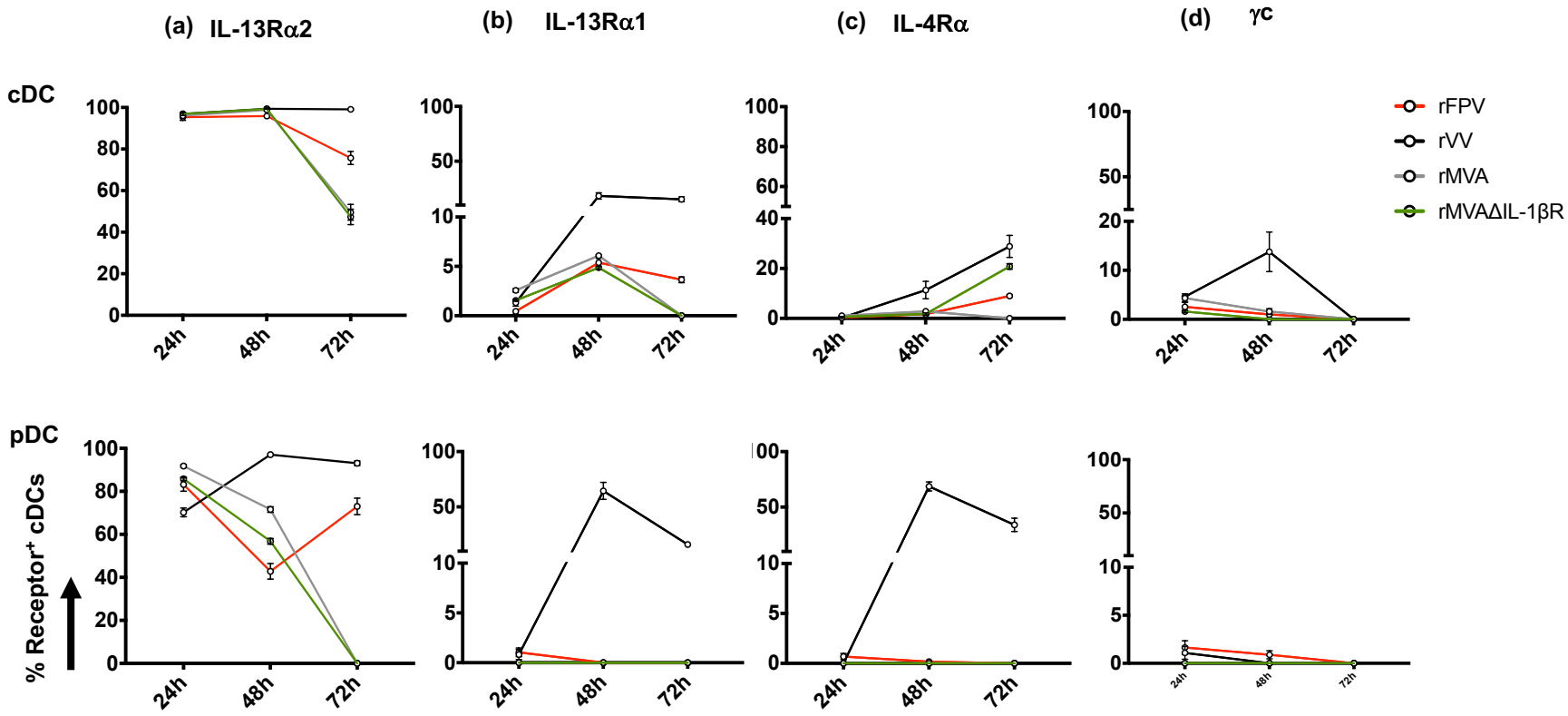
(a) IL-13Rα2
(b) IL-13Rα1
(c) IL-4Rα
(d) γc
cDC
pDC
% Receptor+ cDCs
24h
48h
72h
rFPV
rVV
rMVA
rMVAΔIL-1βR

Figure 5.19. Comparison of IL-4/ IL-13 receptor expression on lung cDCs and pDCs between 24 - 72 h following viral vector vaccination. IL-4/IL-13 receptor expression obtained from Fig 1-6 have been summarised to compare and contrast receptor expression between lung cDCs and pDCs between 24 – 72h hours post viral vector vaccination. Line graphs show **(a)** IL-13Rα2, **(b)** IL-13Rα1, **(c)** IL-4Rα and **(d)** γc on lung cDCs and pDCs following rFPV (red), rVV (black), rMVA (grey) or rMVAΔIL-1βR (green) vaccination.

Analogous to the cDCs, IL-13Rα2 and IL-13Rα1/IL-4Rα expression on lung pDCs were found to be significantly different 24 - 72 following different pox viral vector-based vaccination. Interestingly, rFPV, that induced low IL-13 at the vaccination site, showed significantly elevated cDC and moderate pDC recruitment to the lung mucosae, where as the opposing was true with rVV [306,367]. In the context of rFPV vaccinated lung pDC, enhanced IL-13Rα2 expression and no significant IL-13Rα1/IL-4Rα regulation over time **(Figure 5.19)**, once again highlighted an association of IL-13Rα2 signalling under low IL-13 unlike rVV. pDCs have long been associated with effective antibody maturation and development [336,400] and recently we have shown that following pox viral vaccination, the presence of IL-13 was crucial for effective antibody differentiation, via an STAT6 independent manner [302,402]. Intriguingly, our current findings further corroborate that in the context of pDC, IL-13 signaling/regulation via IL-13Rα2 may be involved in this process. Furthermore, rFPV primed pDCs, which exhibited enhanced IL-13Rα2 and minimal IL-13Rα1/IL-4Rα regulation on pDCs, has also shown to induce modest antibody responses in mice and macaques [122,123]. Whilst, rVV vaccination, which was associated with enhanced IL-13Rα2 and IL-13Rα1/IL-4Rα activity, has shown robust neutralizing antibodies in mice and humans [403-405]. In contrast, rMVA vaccination which has shown to induce much lower magnitude of antibody responses compared to rVV [137,266,406,407], interestingly, showed reduced lung pDCs compared to rVV, and down-regulation of IL-13Rα2 by 72 h post vaccination with no IL-13Rα1/IL-4Rα activity. These observations insinuate that, the ability of different viral vectors to

induce effective antibodies responses may also be governed by IL-13 regulation of IL-13Rα2 and IL-13Rα1/IL-4Rα on lung pDCs, at early stages of vaccination.

Moreover, rVV vaccination has shown to induce enhanced pDCs and cross-presenting DCs [367], associated with induction of greatly elevated VV-specific antibody as well as T cells responses both in mice and humans [403-405,408,409]. However, when rVV has been used as a vaccine vector, the quality of T cell responses induced to the encoded vaccine antigens have been much inferior compared to rFPV [133]. These observations, together with our current findings suggest that, in the context of viral vector-based vaccines, more attenuated and unrelated the vector to the host it may have the capacity to induce more efficacious and high quality vaccine-specific immune outcomes. This may also explain why, in a prime-boost vaccination modality, rFPV or canarypox vector prime have shown to induce more effective immune outcomes than other pox viral vectors [121,123,131,133], specifically, given that priming creates the initial antigen-specific T cell population, which gets expanded during the booster vaccination [122,124].

Collectively, our findings reveal that the host tropism, replication status as well as presence or absence of immunomodulatory genes in a viral vector can significantly impact the IL-4/IL-13 receptor regulation on lung DCs. These findings may elucidate why despite encoding the same vaccine antigens, different viral vectors yield vastly different vaccine-specific immune outcomes. Taken together our observations evoke the notion that efficacy/fate of a vaccine is likely governed

by the early effective regulation and balance of IL-13 by IL-13Rα2/IL-13Rα1 on DC at the vaccination site.

Chapter 6

General Discussion

6.1 Synopsis

Designing a successful vaccine against any chronic pathogen frequently poses many challenges. Specifically, in the context of HIV, high epitope variability, which leads to immune evasion and immune recognition [410,411], existence of different HIV clades in different geographic locations [412,413] have made designing an effective vaccine that can induce long lasting adaptive immunity, which recognizes the broad breadth of HIV antigens, extremely difficult. Whilst an HIV vaccine with cross-reactive or broadly neutralizing antibody responses remain elusive [414], studies have also established that cytotoxic $CD8^+$ T cells are crucial in preventing viral replication and pathogenecity [415-418]. Two decades of work in our laboratory have established that the route of vaccination, choice of viral vaccine vector and the vaccination induced cytokine milieu (IL-4/IL-13) critically influenced the fate of a vaccine [122-124,130-133]. Studies by Wijesundara *et al.* showed that in a heterologous poxvirus vector-based HIV prime-boost vaccination modality, the priming vector crucially impacted the functional avidity of HIV-specific $CD8^+$ T cells [133]. Specifically, rFPV prime was shown to induce $CD8^+$ T cells of higher functional avidity compared to rMVA or rVV [133]. Furthermore, novel recombinant poxviral vector-based HIV vaccines co-expressing IL-4/IL-13 inhibitors, which transiently blocked IL-13 or STAT6 signalling at the vaccination site, was shown to significantly influence cellular and humoral immune responses [122-124]. Specifically, i.n. rFPV/ i.m. rMVA or rVV poxvirus prime-boost vaccination strategy, that transiently inhibited STAT6 signalling at the lung mucosae was shown to induce both high avidity/poly-functional cytotoxic T cells as well as effective antibody responses in mice and

non-human primates [122,123] (Li *et al.* in preparation). In comparison, transient sequestration of IL-13 from the milieu only improved the functional avidity of T cells [124]. These studies clearly demonstrated that, IL-13 at the vaccination site, whilst being detrimental to functional avidity of T cells, was essential for effective humoral immunity. Trivedi *et al.* using these novel vaccines, also showed that reduced IL-13 levels at the vaccination site promoted cDC recruitment to the vaccination site associated with high avidity T cell induction [99]. Furthermore investigating which cells expressed IL-13 at the vaccination site 24h post viral vector, Li *et al.* for the first time established that ILC2 were the major producer of IL-13 [306]. This PhD project sought to unravel some of the fundamental mechanisms by which IL-13 modulated DC activity at the vaccination site. The major findings of this project were:

1. Viral vector-induced IL-13 levels at the vaccination site differentially regulated DC recruitment to the vaccination site, 24 h post delivery.
2. Enhanced expression of IL-13Rα2 detected on lung DCs was regulated in a vector-dependent manner (according to the level of IL-13 induced).
3. Following viral vector vaccination, low IL-13 conditions induced IL-13Rα2 signalling via STAT3 in lung cDCs, governed by TGF-β1 regulation, whilst high IL-13 conditions induced IL-13Rα1 signalling, where IL-13Rα2 regulated IL-13 homeostasis at the lung mucosae.
4. On lung cDCs, the densities of IL-13Rα2 and IFN-γR co-expression, 24 h post viral vector delivery, were found to be linked to different vaccine-specific T cell outcomes (observed in previous studies).

6.2. Viral vectors have not only their own ILC2-derived IL-13 profiles but also their own DC signature.

Findings in this thesis for the first time demonstrated that different viral vector-based vaccines expressing the same vaccine antigen can not only crucially impact the recruitment of different ILC and ILC2-derived IL-13 levels, but also the DC recruitment to the vaccination site, 24 h post delivery. Specifically, each viral vector exhibited its own ILC2-derived IL-13 profile as well as a DC signature. These findings further substantiated our previous findings, eliciting the importance of the priming vector, in a prime-boost modality. Previous studies have shown that the priming vaccination generates the initial vaccine-specific T cell pool, which gets expanded by the booster, responsible for the final T cell outcomes [122,124]. Specifically, in this study, i.n. rFPV priming which induced low ILC2-derived IL-13, showed enhanced cDC recruitment to the lung mucosae. Whilst i.n. rMVA and rVV priming which induced high ILC2-derived IL-13, recruited enhanced cross-presenting DCs. Using the novel IL-4/IL-13 inhibitor vaccines, adoptive transfer studies by Trivedi *et al.* have clearly shown that in a prime-boost modality, whilst cDCs were involved in the induction of high avidity T cells, cross-presenting DCs were associated with induction of low avidity T cells [133]. Moreover, recent studies by Li *et al*. have also shown that different ILC2-derived IL-13 levels in the lung and muscle correlated with varying T cell outcomes following viral vector-based vaccination [306]. Taken together, these current findings have further unravelled some of the fundamental IL-13 related mechanisms at the innate immune cell level, specifically how ILC-DC cross talk at the vaccination site shape the downstream adaptive immune outcomes.

Chapter 3 studies also demonstrated that manipulation of the inherent properties of the viral vector can significantly impact the ILC2-derived IL-13 as well as associated DC profiles at the vaccination site. For example, a single deletion of virokine IL-1βR from rMVA vector significantly reduced the ILC2-derived IL-13 levels at the vaccination site, compared to the parental rMVA and lead to enhanced cDC recruitment to the lung mucosae, similar to rFPV. In the context of rMVA, deletion mutants of immune evasive genes such as IL-18 binding protein or C6L and F1L have also been tested [183-185,419]. Interestingly, although the T cell outcomes of these mutant variants have been established, underlying mechanisms leading to the differential quality or magnitude of these T cell responses have not yet been characterized. These findings further lead into one of the major caveats in the current vector-based vaccine design, where the nature of the viral vector is often overlooked when designing vaccine against different pathogens. This study, for the first time, has demonstrated i) how a viral vector critically influenced the fate of a vaccine, and ii) how characterizing the IL-13 associated DC profiles, specifically unraveling the mechanisms of ILC-DC cross talk at the vaccination site may hold the key to better vector-based vaccine design in the future.

6.3. Viral vector-based vaccination, lung cDC and dual role of IL-13Rα2.

Chapter 4 and 5 studies for the first time unraveled one of the mechanisms by which lung DCs shape different cellular and humoral immune outcomes, 24 h post intranasal viral vector-based vaccination, where IL-13Rα2 was the main IL-

13 regulator on lung cDCs and pDCs. Specifically, how cDCs modulate high avidity T cells [99,124] and pDCs regulate antibody differentiation [97,420], via IL-13Rα2/STAT3. Interestingly, studies by Hamid *et al.* also pointed towards the involvement of a STAT6 independent mechanism (likely IL-13Rα2 related), involved in the latter process [302]. These finding clearly showed that according to the vector-specific IL-13 level, IL-13Rα2/STAT3 performed a dual role at the vaccination site (at the lung mucosae), where under low IL-13, IL-13Rα2/STAT3 lead to TGF-β1 activation, whilst, under high IL-13, the receptor performed a sequestration role to maintain homeostasis, similar to inflammatory conditions [295,296]. These observations were further corroborated by other vaccination studies where TGF-β1 was linked to enhanced protection associated with $CD4^+$ T cells [421,422], whilst, early STAT6 signalling was associated with poor vaccine-specific T cell outcomes [122,132]. Collectively, these observations, indicated that promoting low IL-13 production, leading to early enhanced IL-13Rα2/STAT3/TGF-β1 expression, as opposed to IL-13Rα1/STAT6/IFN-γR by cDCs may be a useful strategy when designing effective T cell-based vaccine strategies in the future.

One of the most unexpected findings of this thesis was the elevated expression of IL-13Rα2 not only on vaccinated cDCs, but also naïve lung cDCs (even though vaccination further up-regulated the expression). Knowing that the lung is constantly exposed to air-borne impurities and pathogens, and IL-13 is profoundly involved in lung inflammation, taken together these findings suggested that elevated IL-13Rα2 expression on lung cDCs could be an inherent mechanism by which lung DCs at the first of defence regulate IL-13 mediated

lung inflammation. Furthermore, given that IL-13Rα2 is known to play different roles in immune protection [295,296] as well as disease (cancer) progression [291], current findings suggested that this may occur via how effectively different environmental factors regulate cDC/IL-13Rα2. Findings of this thesis also advocated the notion that dysregulation of IL-13Rα2/IL-13Rα1 balance leading to STAT3/STAT6 malfunction may be the main cause of allergy/asthma, including exacerbation of certain IL-13 mediated disease conditions, specifically certain cancers.

6.4. Viral vector-specific IL-13Rα2/IFNγR co-expression profiles on lung cDCs likely influence vaccine-specific T cell outcomes.

Chapter 4 studies also revealed that each viral vector-specific IL-13 level can also influence the relative expression of IL-13Rα2 and IFN-γR on lung cDCs, 24 h post delivery. Interestingly, rFPV vaccination, which induced low ILC2-derived IL-13 and elevated ILC1/ILC3 derived IFN-γ at the lung mucosae, 24 h post delivery, was associated with co-expression of enhanced IL-13Rα2 and low IFN-γR on lung cDCs **(Figure 6.1)**. In contrast, rMVA, which induced opposing ILC-derived IL-13 and IFN-γ levels at the lung mucosae, showed elevated IL-13Rα2 expression and IFN-γR response bias on lung cDCs **(Figure 6.1)**. The moderate ILC-derived IL-13 and IFN-γ producer, rAd5 vector showed an intermediary IL-13Rα2/IFN-γR profile to rFPV and rMVA **(Figure 6.1)**. Remarkably, in this study the cDC recruitment to the lung mucosae was in the order of rFPV > Ad5 > rMVA. Ad5 showed reduced cDC and elevated pDC recruitment to the lung mucosae.

Interestingly, cDCs have been associated with high avidity T cell induction [99], and pDCs with effective antibody immunity [97,420]. Also, recent findings have shown that although rAd26 HIV vaccination induced enhanced HIV Env-specific antibody and ADCC responses in animal models and Phase 1 trials [232,233,423,424], did not induce effective HIV-specific $CD8^+$ T cell immunity. Knowing that i.n. rFPV/ i.m. rMVA vaccination can induce both high avidity/poly-functional mucosal/systemic $CD8^+$ T cells, ADCC and effective Env-specific antibody responses in non-human primates [123] (Li *et al*. in preparation), taken together the findings in this thesis, knowing that rFPV induced cDCs leading to high quality T cells [130-132], data suggested that in the future an i.n. rFPV/i.m.rAd26 booster strategy may have high potential to induce more effective balanced T and B cell vaccine outcomes . Collectively, these findings also propose the notion that the IL-13Rα2/IFN-γR co-expression patterns on lung cDCs may also reflect the different avidities/qualities of vaccine-specific T cells, following viral vector vaccination.

6.5. Viral vectors, IL-13 and DC profiles and how can these factors be modulated for better vaccine design.

Studies in our laboratory have shown that mucosal vaccination induced high avidity T cells associated with low IL-13 expression, whilst systemic vaccination induced low avidity T cells associated with high IL-13 expression by vaccine-specific T cells [130-132]. Li *et al.* have also shown that mucosal rFPV vaccination induced low ILC2-derived IL-13 compared to systemic vaccination [306]. Also, the chapter 3 related ILC studies substantiated Li *et al.*'s findings. Thus, extrapolating

the ILC-derived IL-13 and related DC profiles with different viral vectors 24h post i.n. delivery (low IL-13 associated with cDC, high IL-13 with cross presenting DC), data suggested that intramuscular vaccination which induced high IL-13 in the muscle, may have high potential to lead to recruitment of enhanced cross-presenting DCs, associated with low avidity T cell induction. Interestingly, this may explain why for over two decades, systemic HIV vector-based vaccination strategies have yielded extremely poor outcomes in HIV Phase I clinical trials [144,204].

For many years, immune potentiating adjuvants (4-1BBL), chemokines and cytokines (IL-2, IL-12, IL-18, type I and III interferons), have been co-expressed together with vaccine antigens, to improve vaccine-specific immunity [206-209,212,213,425-427]. Although majority of these vaccines have elicited "enhanced T cell immunity, measured by IFN-γ production", have not improved the "quality of T cell immunity" in animal models and most have shown poor immune outcomes in humans [204,214]. In contrast, vaccines antagonizing cytokine signaling at the vaccination site (such as IL-4R antagonist, IL-13Rα2), have shown to induce higher quality T cell immunity in mice and non-human primates [122-124,131]. Why sequestration of cytokines yield better quality T cells compared to overexpression were recently corroborated by Mahboob *et al.*, where they showed that overexpression of cytokines (e.g. IL-13, IFN-γ,) had no impact on the ILC2-derived IL-13 or ILC1/ILC3-derived IFN-γ expression at the vaccination site (Mahboob thesis 2016), whilst Li *et al.* showed that vaccines sequestering IL-25

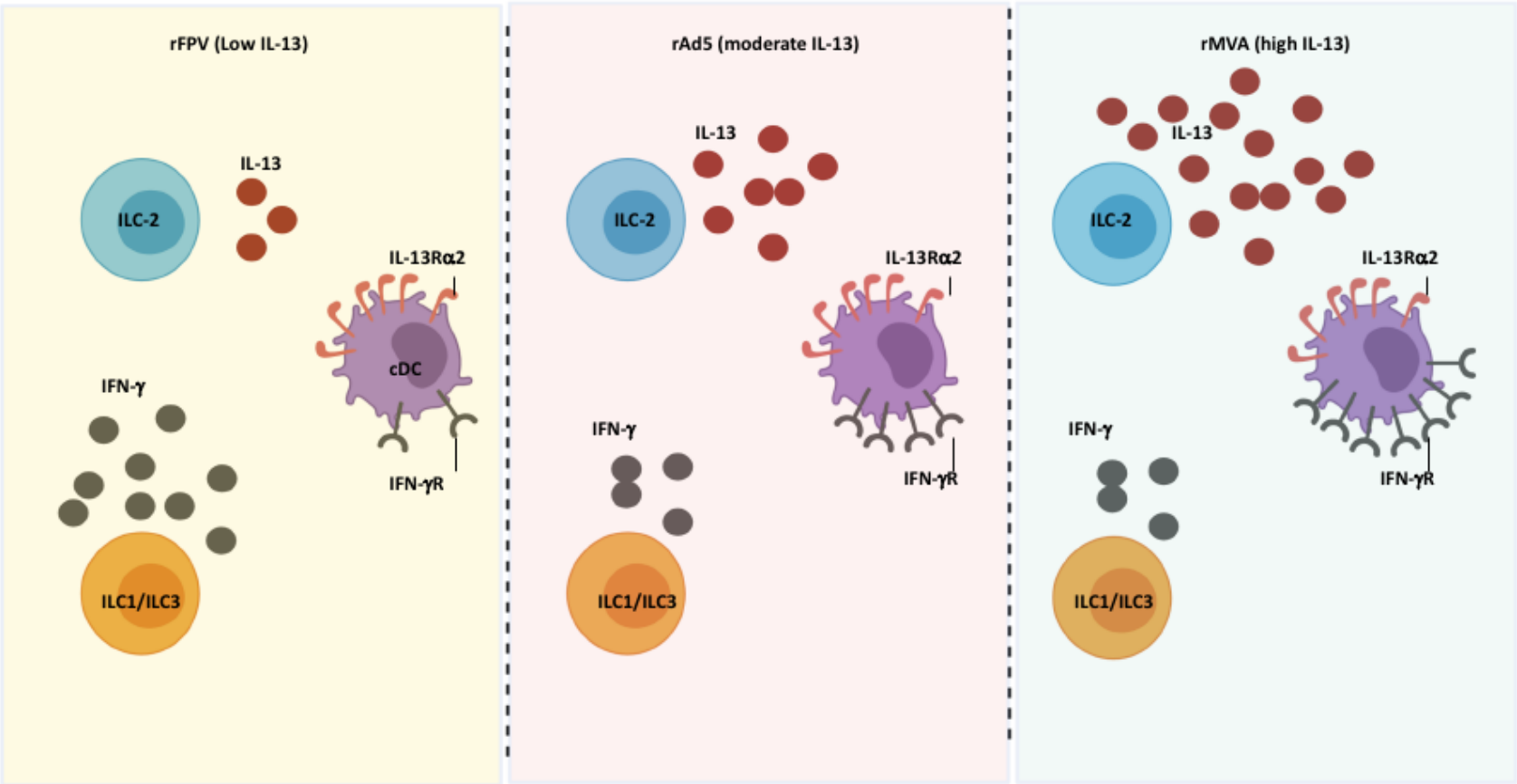
rFPV (Low IL-13)
IL-13
ILC-2
IL-13Rα2
cDC
IFN-γ
IFN-γR
ILC1/ILC3
rAd5 (moderate IL-13)
IL-13
ILC-2
IL-13Rα2
IFN-γ
IFN-γR
ILC1/ILC3
rMVA (high IL-13)
IL-13
ILC-2
IL-13Rα2
IFN-γ
IFN-γR
ILC1/ILC3

Figure 6.1. Schematic summary of thesis. Findings of the thesis revealed that 24 h following rFPV vaccination (left panel), low ILC2-derived IL-13 and high ILC1/ILC3-derived IFN-γ is secreted at the lung mucosae, associated with enhanced IL-13Rα2 and reduced IFN-γR expression on lung cDCs. Whilst, following rMVA vaccination (right panel), high ILC2-derived IL-13 and low ILC1/ILC3-derived IFN-γ profiles are induced, associated with elevated IL-13Rα2 expression and an enhanced IFN-γR response bias in lung cDCs. Moreover, post rAd5 delivery (middle panel), which induces moderate ILC2-derived IL-13 and low IFN-γ at the lung mucosae, also elicited an IL-13Rα2/IFN-γR profile intermediary to rFPV and rMVA.

at the vaccination site, which altered ILC activity can differentially modulate ILC2-derived IL-13 expression 24 h post i.n. or i.m. vaccination [428]. Taken together these findings indicated that, rather than over-expression of cytokines, antagonism (e.g. IL-4R antagonist, IL-13Rα2 and IL-25 binding protein) [122,124,428], which alters ILC/DC profiles at the vaccination site could be of more value in the context of inducing high quality T cells and protective efficacy against chronic viral pathogens. Knowing that IL-6, IL-10 and VEGF can alter DC function with respect to STAT3 activity in cancer therapy [429], co-expression of "DC targeted molecules" in viral vector-based vaccines, may warrant further investigation.

Unlike HIV-1 infection, in the context of bacterial pathogens such as *Mycobacterium tuberculosis* and *Chlamydia trachomatis*, $CD4^+$ T cells have been associated with host protection [430-436]. Studies have shown that cross-presenting DCs effectively present bacterial and fungal antigens to $CD4^+$ T cells [437,438]. Thus, taken together the findings of the current study, a prime-boost vaccination approach, using rMVA prime, which induces high ILC2-derived IL-13 and elevated cross-presenting DCs followed by a relevant booster (rFPV, rAd or protein), have high potential to yield effective antigen-specific $CD4^+$ T cell outcomes against these pathogens. In summary, these findings further highlighted that understanding the route and vector-specific ILC and DC profiles at the vaccination site may help tailor pathogen-specific vaccine design, to yield desired protective immune outcomes.

In conclusion, this study for the first time demonstrated that the viral vector-specific ILC2-derived IL-13 at the vaccination site crucially impacted the DC subsets recruited to the lung mucosae. The fate of a viral vector-based vaccine was determined by how the IL-13-driven IL-13Rα2 on lung cDCs was regulated, specifically by STAT3/TGF-β1 or STAT6/IFN-γR, where the former lead to high avidity T cell induction unlike the latter. Hence, not only the encoded antigens, but also the viral vector-associated IL-13 and DC regulation profiles should be carefully taken into consideration when designing viral vector-based vaccines against chronic pathogens. Vaccine strategies that can manipulate STAT3 and/or STAT6 activity may have high potential to yield exciting and different adaptive immune outcomes against different pathogens, in the future.

6.6 Limitations:

- One of the main limitations of this study was the unavailability of IL-13Rα2 and STAT3 knock out mice on the BALB/c background, which would have helped to confirm the 'direct relationship' of IL-13Rα2, STAT3 and TGF-β1 under low IL-13 conditions.
- Knowing that viral vector-based vaccination induced much greater ILC2-derived IL-13 in muscle than lung, a comparative study using i.m. delivery of different viral vectors to evaluate lung DC subsets recruited to the muscle, 24h post delivery would have added value to the work.
- Establishing the 'direct' cross-talk between ILC2-derived IL-13 and lung DCs using ILC2$^{-/-}$ mouse model on BALB/c background would have been useful to further confirm findings of the thesis.

6.7 Future directions:

- Designing a database denoting the ILC profiles (e.g. ILC2-derived IL-13, ILC1/ILC3-derived IFN-γ and IL-17 levels) and DC profiles with expression patterns of IL-13Rα2, STAT3, STAT6, TGF-β1, IFN-γR levels, 24h post delivery, for commonly used viral vectors as well as adjuvants following intranasal and intramuscular vaccination could be a powerful reference library/repository, which may help design more effective vector-based vaccine strategies, according to the pathogen of interest in the future. This may help restrain/prevent the current notion that, when designing vaccines "same vector or adjuvant would fit every pathogen".
- Knowing that in addition to DCs, macrophages and monocyte-derived DCs also polarize Th1 and Th2 immunity, it would be of value to test whether these cells have any association with the IL-13 levels at the vaccination site, or the observed outcomes are DC-specific.
- Now, knowing that in the context of viral vaccination DCs play a key role in governing the fate of the vaccine, it would be also of interest to further unravel other underlying mechanisms, specifically how different lung DCs selectively present antigens to activate specific T cell clones to induce mucosal homing.
- Perform pull-down assays to assess whether there are any other receptors that complex with IL-13Rα2 to initiate STAT3 signalling or IL-13Rα2 remodeling post IL-13 binding to initiate signalling.
- This study demonstrated that following viral vector vaccination, STAT3/ STAT6 play an important role in lung cDC regulation. Hence, it would be

of interest to characterize how these molecules also regulate cross-presenting DCs and pDCs following viral vector vaccination.

- In the future, following viral vector based vaccination, subjecting sorted DCs to parallel RNA single cell sequencing (MARS-seq) [439] may also help to generate a viral vector-specific genetic signature (find molecules other than the observed regulatory elements), which may help design better vaccines strategies in the future.

References

1 Spiering, M. J. Primer on the Immune System. *Alcohol Res* **37**, 171-175 (2015).

2 Riera Romo, M., Perez-Martinez, D. & Castillo Ferrer, C. Innate immunity in vertebrates: an overview. *Immunology* **148**, 125-139 (2016).

3 Janeway, C. A., Jr. & Medzhitov, R. Innate immune recognition. *Annu Rev Immunol* **20**, 197-216 (2002).

4 Kawai, T. & Akira, S. The role of pattern-recognition receptors in innate immunity: update on Toll-like receptors. *Nat Immunol* **11**, 373-384 (2010).

5 Medzhitov, R. Recognition of microorganisms and activation of the immune response. *Nature* **449**, 819-826 (2007).

6 Takeuchi, O. & Akira, S. Pattern recognition receptors and inflammation. *Cell* **140**, 805-820 (2010).

7 Brubaker, S. W., Bonham, K. S., Zanoni, I. & Kagan, J. C. Innate immune pattern recognition: a cell biological perspective. *Annu Rev Immunol* **33**, 257-290 (2015).

8 Topham, N. J. & Hewitt, E. W. Natural killer cell cytotoxicity: how do they pull the trigger? *Immunology* **128**, 7-15 (2009).

9 McGhee, J. R. & Fujihashi, K. Inside the mucosal immune system. *PLoS Biol* **10**, e1001397 (2012).

10 Pelaseyed, T. *et al.* The mucus and mucins of the goblet cells and enterocytes provide the first defense line of the gastrointestinal tract and interact with the immune system. *Immunol Rev* **260**, 8-20 (2014).

11 Nagler-Anderson, C. Man the barrier! Strategic defences in the intestinal mucosa. *Nat Rev Immunol* **1**, 59-67 (2001).

12 Sperandio, B., Fischer, N. & Sansonetti, P. J. Mucosal physical and chemical innate barriers: Lessons from microbial evasion strategies. *Semin Immunol* **27**, 111-118 (2015).

13 Gill, N., Wlodarska, M. & Finlay, B. B. The future of mucosal immunology: studying an integrated system-wide organ. *Nat Immunol* **11**, 558-560, doi:10.1038/ni0710-558 (2010).

14 Cesta, M. F. Normal structure, function, and histology of mucosa-associated lymphoid tissue. *Toxicol Pathol* **34**, 599-608 (2006).

15 Hathaway, L. J. & Kraehenbuhl, J. P. The role of M cells in mucosal immunity. *Cell Mol Life Sci* **57**, 323-332 (2000).

16 Kim, S. H. & Jang, Y. S. Antigen targeting to M cells for enhancing the efficacy of mucosal vaccines. *Exp Mol Med* **46**, e85 (2014).

17 Neutra, M. R., Pringault, E. & Kraehenbuhl, J. P. Antigen sampling across epithelial barriers and induction of mucosal immune responses. *Annu Rev Immunol* **14**, 275-300 (1996).

18 Gregson, R. L., Davey, M. J. & Prentice, D. E. The response of rat bronchus-associated lymphoid tissue to local antigenic challenge. *British journal of experimental pathology* **60**, 471-482 (1979).

19 Kawamata, N. *et al.* Expression of endothelia and lymphocyte adhesion molecules in bronchus-associated lymphoid tissue (BALT) in adult human lung. *Respiratory research* **10**, 97, doi:10.1186/1465-9921-10-97 (2009).

20 Woodland, D. L. & Randall, T. D. Anatomical features of anti-viral immunity in the respiratory tract. *Semin Immunol* **16**, 163-170, doi:10.1016/j.smim.2004.02.003 (2004).

21 Hwang, J. Y., Randall, T. D. & Silva-Sanchez, A. Inducible Bronchus-Associated Lymphoid Tissue: Taming Inflammation in the Lung. *Front Immunol* **7**, 258 (2016).

22 Kimura, S. *et al.* Airway M Cells Arise in the Lower Airway Due to RANKL Signaling and Reside in the Bronchiolar Epithelium Associated With iBALT in Murine Models of Respiratory Disease. *Front Immunol* **10**, 1323, doi:10.3389/fimmu.2019.01323 (2019).

23 Kretschmer, S. *et al.* Visualization of intrapulmonary lymph vessels in healthy and inflamed murine lung using CD90/Thy-1 as a marker. *PloS one* **8**, e55201, doi:10.1371/journal.pone.0055201 (2013).

24 Picker, L. J. Mechanisms of lymphocyte homing. *Current opinion in immunology* **4**, 277-286, doi:10.1016/0952-7915(92)90077-r (1992).

25 Richert, L. E. *et al.* Inducible bronchus-associated lymphoid tissue (iBALT) synergizes with local lymph nodes during antiviral CD4+ T cell responses. *Lymphatic research and biology* **11**, 196-202, doi:10.1089/lrb.2013.0015 (2013).

26 Shinoda, K. *et al.* Thy1+IL-7+ lymphatic endothelial cells in iBALT provide a survival niche for memory T-helper cells in allergic airway inflammation. *Proceedings of the National Academy of Sciences of the United States of America* **113**, E2842-2851, doi:10.1073/pnas.1512600113 (2016).

27 Banchereau, J. & Steinman, R. M. Dendritic cells and the control of immunity. *Nature* **392**, 245-252 (1998).

28 Engering, A. J. *et al.* The mannose receptor functions as a high capacity and broad specificity antigen receptor in human dendritic cells. *Eur J Immunol* **27**, 2417-2425 (1997).

29 Sallusto, F., Cella, M., Danieli, C. & Lanzavecchia, A. Dendritic cells use macropinocytosis and the mannose receptor to concentrate macromolecules in the major histocompatibility complex class II compartment: downregulation by cytokines and bacterial products. *J Exp Med* **182**, 389-400 (1995).

30 Tan, M. C. *et al.* Mannose receptor-mediated uptake of antigens strongly enhances HLA class II-restricted antigen presentation by cultured dendritic cells. *Eur J Immunol* **27**, 2426-2435 (1997).

31 Grogan, J. L. *et al.* Early transcription and silencing of cytokine genes underlie polarization of T helper cell subsets. *Immunity* **14**, 205-215 (2001).

32 Hsieh, C. S. *et al.* Development of TH1 CD4+ T cells through IL-12 produced by Listeria-induced macrophages. *Science* **260**, 547-549 (1993).

33 Mullen, A. C. *et al.* Role of T-bet in commitment of TH1 cells before IL-12-dependent selection. *Science* **292**, 1907-1910 (2001).

34 Zheng, W. & Flavell, R. A. The transcription factor GATA-3 is necessary and sufficient for Th2 cytokine gene expression in CD4 T cells. *Cell* **89**, 587-596 (1997).

35 Bhaumik, S. & Basu, R. Cellular and Molecular Dynamics of Th17 Differentiation and its Developmental Plasticity in the Intestinal Immune Response. *Front Immunol* **8**, 254, doi:10.3389/fimmu.2017.00254 (2017).

36 Shortman, K. & Naik, S. H. Steady-state and inflammatory dendritic-cell development. *Nat Rev Immunol* **7**, 19-30 (2007).

37 Watowich, S. S. & Liu, Y. J. Mechanisms regulating dendritic cell specification and development. *Immunol Rev* **238**, 76-92 (2010).

38 Kroger, C. J., Spidale, N. A., Wang, B. & Tisch, R. Thymic Dendritic Cell Subsets Display Distinct Efficiencies and Mechanisms of Intercellular MHC Transfer. *J Immunol* **198**, 249-256 (2017).

39 Steinman, R. M. & Hemmi, H. Dendritic cells: translating innate to adaptive immunity. *Curr Top Microbiol Immunol* **311**, 17-58 (2006).

40 Brandtzaeg, P. & Johansen, F. E. Mucosal B cells: phenotypic characteristics, transcriptional regulation, and homing properties. *Immunol Rev* **206**, 32-63 (2005).

41 Dieu, M. C. *et al.* Selective recruitment of immature and mature dendritic cells by distinct chemokines expressed in different anatomic sites. *J Exp Med* **188**, 373-386 (1998).

42 Iwasaki, A. Mucosal dendritic cells. *Annu Rev Immunol* **25**, 381-418 (2007).

43 Kraehenbuhl, J. P. & Neutra, M. R. Epithelial M cells: differentiation and function. *Annu Rev Cell Dev Biol* **16**, 301-332 (2000).

44 Pavli, P., Hume, D. A., Van De Pol, E. & Doe, W. F. Dendritic cells, the major antigen-presenting cells of the human colonic lamina propria. *Immunology* **78**, 132-141 (1993).

45 Tschernig, T. & Pabst, R. Bronchus-associated lymphoid tissue (BALT) is not present in the normal adult lung but in different diseases. *Pathobiology* **68**, 1-8 (2000).

46 Rescigno, M. *et al.* Dendritic cells express tight junction proteins and penetrate gut epithelial monolayers to sample bacteria. *Nat Immunol* **2**, 361-367 (2001).

47 Jang, M. H. *et al.* Intestinal villous M cells: an antigen entry site in the mucosal epithelium. *Proceedings of the National Academy of Sciences of the United States of America* **101**, 6110-6115 (2004).

48 McDole, J. R. *et al.* Goblet cells deliver luminal antigen to CD103+ dendritic cells in the small intestine. *Nature* **483**, 345-349, doi:10.1038/nature10863 (2012).

49 Yoshida, M. *et al.* Human neonatal Fc receptor mediates transport of IgG into luminal secretions for delivery of antigens to mucosal dendritic cells. *Immunity* **20**, 769-783 (2004).

50 Diehl, G. E. *et al.* Microbiota restricts trafficking of bacteria to mesenteric lymph nodes by CX(3)CR1(hi) cells. *Nature* **494**, 116-120, doi:10.1038/nature11809 (2013).

51 Jang, M. H. *et al.* CCR7 is critically important for migration of dendritic cells in intestinal lamina propria to mesenteric lymph nodes. *J Immunol* **176**, 803-810 (2006).

52 Chang, S. Y., Ko, H. J. & Kweon, M. N. Mucosal dendritic cells shape mucosal immunity. *Exp Mol Med* **46**, e84, doi:10.1038/emm.2014.16 (2014).

53 Mora, J. R. *et al.* Selective imprinting of gut-homing T cells by Peyer's patch dendritic cells. *Nature* **424**, 88-93 (2003).

54 Campbell, J. J. *et al.* Expression of chemokine receptors by lung T cells from normal and asthmatic subjects. *J Immunol* **166**, 2842-2848, doi:10.4049/jimmunol.166.4.2842 (2001).

55 Lobb, R. R., Pepinsky, B., Leone, D. R. & Abraham, W. M. The role of alpha 4 integrins in lung pathophysiology. *The European respiratory journal. Supplement* **22**, 104s-108s (1996).

56 Mikhak, Z., Strassner, J. P. & Luster, A. D. Lung dendritic cells imprint T cell lung homing and promote lung immunity through the chemokine receptor CCR4. *J Exp Med* **210**, 1855-1869 (2013).

57 Butcher, E. C., Williams, M., Youngman, K., Rott, L. & Briskin, M. Lymphocyte trafficking and regional immunity. *Advances in immunology* **72**, 209-253 (1999).

58 Lewis, M., Tarlton, J. F. & Cose, S. Memory versus naive T-cell migration. *Immunology and cell biology* **86**, 226-231, doi:10.1038/sj.icb.7100132 (2008).

59 Berlin, C. *et al.* Alpha 4 beta 7 integrin mediates lymphocyte binding to the mucosal vascular addressin MAdCAM-1. *Cell* **74**, 185-195, doi:10.1016/0092-8674(93)90305-a (1993).

60 Diamond, M. S. & Springer, T. A. The dynamic regulation of integrin adhesiveness. *Current biology : CB* **4**, 506-517, doi:10.1016/s0960-9822(00)00111-1 (1994).

61 Fabbri, M., Bianchi, E., Fumagalli, L. & Pardi, R. Regulation of lymphocyte traffic by adhesion molecules. *Inflammation research : official journal of the European Histamine Research Society ... [et al.]* **48**, 239-246, doi:10.1007/s000110050454 (1999).

62 Igietseme, J. U., Eko, F. O., He, Q. & Black, C. M. Antibody regulation of Tcell immunity: implications for vaccine strategies against intracellular pathogens. *Expert Rev Vaccines* **3**, 23-34 (2004).

63 Johnston, B. & Butcher, E. C. Chemokines in rapid leukocyte adhesion triggering and migration. *Semin Immunol* **14**, 83-92, doi:10.1006/smim.2001.0345 (2002).

64 Shacklett, B. L., Critchfield, J. W., Ferre, A. L. & Hayes, T. L. Mucosal T-cell responses to HIV: responding at the front lines. *J Intern Med* **265**, 58-66 (2009).

65 Vorkas, C. K. *et al.* Mucosal-associated invariant and gammadelta T cell subsets respond to initial Mycobacterium tuberculosis infection. *JCI Insight* **3**, 121899 (2018).

66 Wu, H. Y. & Russell, M. W. Nasal lymphoid tissue, intranasal immunization, and compartmentalization of the common mucosal immune system. *Immunol Res* **16**, 187-201 (1997).

67 Dominguez, P. M. & Ardavin, C. Differentiation and function of mouse monocyte-derived dendritic cells in steady state and inflammation. *Immunol Rev* **234**, 90-104 (2010).

68 Ginhoux, F. *et al.* The origin and development of nonlymphoid tissue CD103+ DCs. *J Exp Med* **206**, 3115-3130 (2009).

69 Kim, T. H. & Lee, H. K. Differential roles of lung dendritic cell subsets against respiratory virus infection. *Immune Netw* **14**, 128-137 (2014).

70 Reizis, B., Bunin, A., Ghosh, H. S., Lewis, K. L. & Sisirak, V. Plasmacytoid dendritic cells: recent progress and open questions. *Annu Rev Immunol* **29**, 163-183 (2011).

71 Belz, G. T. *et al.* Distinct migrating and nonmigrating dendritic cell populations are involved in MHC class I-restricted antigen presentation after lung infection with virus. *Proceedings of the National Academy of Sciences of the United States of America* **101**, 8670-8675 (2004).

72 Lukens, M. V., Kruijsen, D., Coenjaerts, F. E., Kimpen, J. L. & van Bleek, G. M. Respiratory syncytial virus-induced activation and migration of

respiratory dendritic cells and subsequent antigen presentation in the lung-draining lymph node. *J Virol* **83**, 7235-7243 (2009).

73 Jakubzick, C. *et al.* Lymph-migrating, tissue-derived dendritic cells are minor constituents within steady-state lymph nodes. *J Exp Med* **205**, 2839-2850, doi:10.1084/jem.20081430 (2008).

74 Desch, A. N., Henson, P. M. & Jakubzick, C. V. Pulmonary dendritic cell development and antigen acquisition. *Immunol Res* **55**, 178-186, doi:10.1007/s12026-012-8359-6 (2013).

75 Ho, A. W. *et al.* Lung CD103+ dendritic cells efficiently transport influenza virus to the lymph node and load viral antigen onto MHC class I for presentation to CD8 T cells. *J Immunol* **187**, 6011-6021, doi:10.4049/jimmunol.1100987 (2011).

76 Iborra, S. *et al.* The DC receptor DNGR-1 mediates cross-priming of CTLs during vaccinia virus infection in mice. *The Journal of clinical investigation* **122**, 1628-1643, doi:10.1172/jci60660 (2012).

77 Larsson, M. *et al.* Efficiency of cross presentation of vaccinia virus-derived antigens by human dendritic cells. *Eur J Immunol* **31**, 3432-3442, doi:10.1002/1521-4141(200112)31:12<3432::aid-immu3432>3.0.co;2-r (2001).

78 von Garnier, C. *et al.* Anatomical location determines the distribution and function of dendritic cells and other APCs in the respiratory tract. *J Immunol* **175**, 1609-1618, doi:10.4049/jimmunol.175.3.1609 (2005).

79 Desch, A. N. *et al.* CD103+ pulmonary dendritic cells preferentially acquire and present apoptotic cell-associated antigen. *J Exp Med* **208**, 1789-1797, doi:10.1084/jem.20110538 (2011).

80 Jakubzick, C., Helft, J., Kaplan, T. J. & Randolph, G. J. Optimization of methods to study pulmonary dendritic cell migration reveals distinct capacities of DC subsets to acquire soluble versus particulate antigen. *Journal of immunological methods* **337**, 121-131, doi:10.1016/j.jim.2008.07.005 (2008).

81 Allan, R. S. *et al.* Migratory dendritic cells transfer antigen to a lymph node-resident dendritic cell population for efficient CTL priming. *Immunity* **25**, 153-162, doi:10.1016/j.immuni.2006.04.017 (2006).

82 Hintzen, G. *et al.* Induction of tolerance to innocuous inhaled antigen relies on a CCR7-dependent dendritic cell-mediated antigen transport to the bronchial lymph node. *J Immunol* **177**, 7346-7354, doi:10.4049/jimmunol.177.10.7346 (2006).

83 Wakim, L. M. & Bevan, M. J. Cross-dressed dendritic cells drive memory CD8+ T-cell activation after viral infection. *Nature* **471**, 629-632, doi:10.1038/nature09863 (2011).

84 Furuhashi, K. *et al.* Mouse lung CD103+ and CD11bhigh dendritic cells preferentially induce distinct CD4+ T-cell responses. *American journal of respiratory cell and molecular biology* **46**, 165-172, doi:10.1165/rcmb.2011-0070OC (2012).

85 Misharin, A. V., Morales-Nebreda, L., Mutlu, G. M., Budinger, G. R. & Perlman, H. Flow cytometric analysis of macrophages and dendritic cell subsets in the mouse lung. *American journal of respiratory cell and molecular biology* **49**, 503-510, doi:10.1165/rcmb.2013-0086MA (2013).

86 GeurtsvanKessel, C. H. *et al.* Dendritic cells are crucial for maintenance of tertiary lymphoid structures in the lung of influenza virus-infected mice. *J Exp Med* **206**, 2339-2349, doi:10.1084/jem.20090410 (2009).

87 Jakubzick, C., Tacke, F., Llodra, J., van Rooijen, N. & Randolph, G. J. Modulation of dendritic cell trafficking to and from the airways. *J Immunol* **176**, 3578-3584, doi:10.4049/jimmunol.176.6.3578 (2006).

88 del Rio, M. L., Rodriguez-Barbosa, J. I., Kremmer, E. & Forster, R. CD103- and CD103+ bronchial lymph node dendritic cells are specialized in presenting and cross-presenting innocuous antigen to CD4+ and CD8+ T

cells. *J Immunol* **178**, 6861-6866, doi:10.4049/jimmunol.178.11.6861 (2007).

89 Kim, T. S. & Braciale, T. J. Respiratory dendritic cell subsets differ in their capacity to support the induction of virus-specific cytotoxic CD8+ T cell responses. *PloS one* **4**, e4204 (2009).

90 Ballesteros-Tato, A., Leon, B., Lund, F. E. & Randall, T. D. Temporal changes in dendritic cell subsets, cross-priming and costimulation via CD70 control CD8(+) T cell responses to influenza. *Nat Immunol* **11**, 216-224 (2010).

91 Cisse, B. *et al.* Transcription factor E2-2 is an essential and specific regulator of plasmacytoid dendritic cell development. *Cell* **135**, 37-48, doi:10.1016/j.cell.2008.09.016 (2008).

92 Merad, M., Sathe, P., Helft, J., Miller, J. & Mortha, A. The dendritic cell lineage: ontogeny and function of dendritic cells and their subsets in the steady state and the inflamed setting. *Annu Rev Immunol* **31**, 563-604, doi:10.1146/annurev-immunol-020711-074950 (2013).

93 Reizis, B. Regulation of plasmacytoid dendritic cell development. *Current opinion in immunology* **22**, 206-211, doi:10.1016/j.coi.2010.01.005 (2010).

94 Boogaard, I. *et al.* Respiratory syncytial virus differentially activates murine myeloid and plasmacytoid dendritic cells. *Immunology* **122**, 65-72 (2007).

95 Cella, M., Facchetti, F., Lanzavecchia, A. & Colonna, M. Plasmacytoid dendritic cells activated by influenza virus and CD40L drive a potent TH1 polarization. *Nat Immunol* **1**, 305-310 (2000).

96 Fonteneau, J. F. *et al.* Activation of influenza virus-specific CD4+ and CD8+ T cells: a new role for plasmacytoid dendritic cells in adaptive immunity. *Blood* **101**, 3520-3526 (2003).

97 Deal, E. M., Lahl, K., Narvaez, C. F., Butcher, E. C. & Greenberg, H. B. Plasmacytoid dendritic cells promote rotavirus-induced human and murine B cell responses. *The Journal of clinical investigation* **123**, 2464-2474 (2013).

98 Swiecki, M., Wang, Y., Gilfillan, S. & Colonna, M. Plasmacytoid dendritic cells contribute to systemic but not local antiviral responses to HSV infections. *PLoS pathogens* **9**, e1003728, doi:10.1371/journal.ppat.1003728 (2013).

99 Trivedi, S., Jackson, R. J. & Ranasinghe, C. Different HIV pox viral vector-based vaccines and adjuvants can induce unique antigen presenting cells that modulate CD8 T cell avidity. *Virology* **468-470**, 479-489 (2014).

100 Zhang, L., Wang, W. & Wang, S. Effect of vaccine administration modality on immunogenicity and efficacy. *Expert Rev Vaccines* **14**, 1509-1523, doi:10.1586/14760584.2015.1081067 (2015).

101 Su, F., Patel, G. B., Hu, S. & Chen, W. Induction of mucosal immunity through systemic immunization: Phantom or reality? *Hum Vaccin Immunother* **12**, 1070-1079 (2016).

102 Belyakov, I. M. & Ahlers, J. D. What role does the route of immunization play in the generation of protective immunity against mucosal pathogens? *J Immunol* **183**, 6883-6892 (2009).

103 Perrone, L. A. *et al.* Intranasal vaccination with 1918 influenza virus-like particles protects mice and ferrets from lethal 1918 and H5N1 influenza virus challenge. *J Virol* **83**, 5726-5734 (2009).

104 Taylor, G., Bruce, C., Barbet, A. F., Wyld, S. G. & Thomas, L. H. DNA vaccination against respiratory syncytial virus in young calves. *Vaccine* **23**, 1242-1250 (2005).

105 Yang, K. *et al.* Immune responses and protection obtained with rotavirus VP6 DNA vaccines given by intramuscular injection. *Vaccine* **19**, 3285-3291 (2001).

106 Kunkel, E. J. & Butcher, E. C. Plasma-cell homing. *Nat Rev Immunol* **3**, 822-829, doi:10.1038/nri1203 (2003).

107 Belyakov, I. M. *et al.* Mucosal immunization with HIV-1 peptide vaccine induces mucosal and systemic cytotoxic T lymphocytes and protective immunity in mice against intrarectal recombinant HIV-vaccinia challenge. *Proceedings of the National Academy of Sciences of the United States of America* **95**, 1709-1714 (1998).

108 Cheng, E., Souza, R. F. & Spechler, S. J. Tissue remodeling in eosinophilic esophagitis. *Am J Physiol Gastrointest Liver Physiol* **303**, G1175-1187 (2012).

109 Kaetzel, C. S., Robinson, J. K., Chintalacharuvu, K. R., Vaerman, J. P. & Lamm, M. E. The polymeric immunoglobulin receptor (secretory component) mediates transport of immune complexes across epithelial cells: a local defense function for IgA. *Proceedings of the National Academy of Sciences of the United States of America* **88**, 8796-8800, doi:10.1073/pnas.88.19.8796 (1991).

110 Neutra, M. R. & Kozlowski, P. A. Mucosal vaccines: the promise and the challenge. *Nat Rev Immunol* **6**, 148-158 (2006).

111 van Egmond, M. *et al.* IgA and the IgA Fc receptor. *Trends in immunology* **22**, 205-211 (2001).

112 Almeida, A. J. & Alpar, H. O. Nasal delivery of vaccines. *Journal of drug targeting* **3**, 455-467, doi:10.3109/10611869609015965 (1996).

113 Holmgren, J. & Czerkinsky, C. Mucosal immunity and vaccines. *Nature medicine* **11**, S45-53, doi:10.1038/nm1213 (2005).

114 Olszewska, W. & Steward, M. W. Nasal delivery of epitope based vaccines. *Advanced drug delivery reviews* **51**, 161-171 (2001).

115 Cuburu, N. *et al.* Intravaginal immunization with HPV vectors induces tissue-resident CD8+ T cell responses. *The Journal of clinical investigation* **122**, 4606-4620, doi:10.1172/jci63287 (2012).

116 Luci, C. *et al.* Dendritic cell-mediated induction of mucosal cytotoxic responses following intravaginal immunization with the nontoxic B subunit of cholera toxin. *J Immunol* **176**, 2749-2757, doi:10.4049/jimmunol.176.5.2749 (2006).

117 Poles, J., Alvarez, Y. & Hioe, C. E. Induction of intestinal immunity by mucosal vaccines as a means of controlling HIV infection. *AIDS research and human retroviruses* **30**, 1027-1040, doi:10.1089/aid.2014.0233 (2014).

118 Buchbinder, S. P. *et al.* Efficacy assessment of a cell-mediated immunity HIV-1 vaccine (the Step Study): a double-blind, randomised, placebo-controlled, test-of-concept trial. *Lancet* **372**, 1881-1893 (2008).

119 Gray, G. E. *et al.* Safety and efficacy of the HVTN 503/Phambili study of a clade-B-based HIV-1 vaccine in South Africa: a double-blind, randomised, placebo-controlled test-of-concept phase 2b study. *Lancet Infect Dis* **11**, 507-515 (2011).

120 Pitisuttithum, P. *et al.* Randomized, double-blind, placebo-controlled efficacy trial of a bivalent recombinant glycoprotein 120 HIV-1 vaccine among injection drug users in Bangkok, Thailand. *J Infect Dis* **194**, 1661-1671 (2006).

121 Rerks-Ngarm, S. *et al.* Vaccination with ALVAC and AIDSVAX to prevent HIV-1 infection in Thailand. *N Engl J Med* **361**, 2209-2220 (2009).

122 Jackson, R. J., Worley, M., Trivedi, S. & Ranasinghe, C. Novel HIV IL-4R antagonist vaccine strategy can induce both high avidity CD8 T and B cell immunity with greater protective efficacy. *Vaccine* **32**, 5703-5714 (2014).

123 Khanna, M. *et al.* Mucosal and systemic SIV-specific cytotoxic CD4(+) T cell hierarchy in protection following intranasal/intramuscular recombinant pox-viral vaccination of pigtail macaques. *Sci Rep* **9**, 5661 (2019).

124 Ranasinghe, C., Trivedi, S., Stambas, J. & Jackson, R. J. Unique IL-13Ralpha2-based HIV-1 vaccine strategy to enhance mucosal immunity, CD8(+) T-cell avidity and protective immunity. *Mucosal Immunol* **6**, 1068-1080 (2013).

125 Ahlers, J. D. *et al.* A push-pull approach to maximize vaccine efficacy: abrogating suppression with an IL-13 inhibitor while augmenting help with granulocyte/macrophage colony-stimulating factor and CD40L. *Proceedings of the National Academy of Sciences of the United States of America* **99**, 13020-13025 (2002).

126 Belshe, R. B. *et al.* Induction of immune responses to HIV-1 by canarypox virus (ALVAC) HIV-1 and gp120 SF-2 recombinant vaccines in uninfected volunteers. NIAID AIDS Vaccine Evaluation Group. *Aids* **12**, 2407-2415 (1998).

127 Belyakov, I. M. *et al.* Mucosal AIDS vaccine reduces disease and viral load in gut reservoir and blood after mucosal infection of macaques. *Nature medicine* **7**, 1320-1326 (2001).

128 Belyakov, I. M. *et al.* Impact of vaccine-induced mucosal high-avidity CD8+ CTLs in delay of AIDS viral dissemination from mucosa. *Blood* **107**, 3258-3264 (2006).

129 Kent, S. J. *et al.* Mucosally-administered human-simian immunodeficiency virus DNA and fowlpoxvirus-based recombinant vaccines reduce acute phase viral replication in macaques following vaginal challenge with CCR5-tropic SHIVSF162P3. *Vaccine* **23**, 5009-5021 (2005).

130 Ranasinghe, C. *et al.* Mucosal HIV-1 pox virus prime-boost immunization induces high-avidity CD8+ T cells with regime-dependent cytokine/granzyme B profiles. *The Journal of Immunology* **178**, 2370-2379 (2007).

131 Ranasinghe, C. *et al.* Evaluation of fowlpox-vaccinia virus prime-boost vaccine strategies for high-level mucosal and systemic immunity against HIV-1. *Vaccine* **24**, 5881-5895 (2006).

132 Ranasinghe, C. & Ramshaw, I. A. Immunisation route-dependent expression of IL-4/IL-13 can modulate HIV-specific CD8(+) CTL avidity. *Eur J Immunol* **39**, 1819-1830, doi:10.1002/eji.200838995 (2009).

133 Wijesundara, D. K. *et al.* Use of an in vivo FTA assay to assess the magnitude, functional avidity and epitope variant cross-reactivity of T cell responses following HIV-1 recombinant poxvirus vaccination. *PloS one* **9**, e105366 (2014).

134 Ahlers, J. D., Belyakov, I. M. & Berzofsky, J. A. Cytokine, chemokine, and costimulatory molecule modulation to enhance efficacy of HIV vaccines.

Current molecular medicine **3**, 285-301, doi:10.2174/1566524033479843 (2003).

135 Boyle, D. B., Anderson, M. A., Amos, R., Voysey, R. & Coupar, B. E. Construction of recombinant fowlpox viruses carrying multiple vaccine antigens and immunomodulatory molecules. *BioTechniques* **37**, 104-106, 108-111, doi:10.2144/04371rr02 (2004).

136 Crotty, S. *et al.* Mucosal immunization of cynomolgus macaques with two serotypes of live poliovirus vectors expressing simian immunodeficiency virus antigens: stimulation of humoral, mucosal, and cellular immunity. *J Virol* **73**, 9485-9495 (1999).

137 Garcia-Arriaza, J. & Esteban, M. Enhancing poxvirus vectors vaccine immunogenicity. *Hum Vaccin Immunother* **10**, 2235-2244, doi:10.4161/hv.28974 (2014).

138 Gherardi, M. M. *et al.* Prime-boost immunization schedules based on influenza virus and vaccinia virus vectors potentiate cellular immune responses against human immunodeficiency virus Env protein systemically and in the genitorectal draining lymph nodes. *J Virol* **77**, 7048-7057, doi:10.1128/jvi.77.12.7048-7057.2003 (2003).

139 Gherardi, M. M., Ramirez, J. C. & Esteban, M. Interleukin-12 (IL-12) enhancement of the cellular immune response against human

immunodeficiency virus type 1 env antigen in a DNA prime/vaccinia virus boost vaccine regimen is time and dose dependent: suppressive effects of IL-12 boost are mediated by nitric oxide. *J Virol* **74**, 6278-6286, doi:10.1128/jvi.74.14.6278-6286.2000 (2000).

140 Shiver, J. W. *et al.* Replication-incompetent adenoviral vaccine vector elicits effective anti-immunodeficiency-virus immunity. *Nature* **415**, 331-335, doi:10.1038/415331a (2002).

141 Abaitua, F., Rodriguez, J. R., Garzon, A., Rodriguez, D. & Esteban, M. Improving recombinant MVA immune responses: potentiation of the immune responses to HIV-1 with MVA and DNA vectors expressing Env and the cytokines IL-12 and IFN-gamma. *Virus Res* **116**, 11-20 (2006).

142 Choi, Y. & Chang, J. Viral vectors for vaccine applications. *Clin Exp Vaccine Res* **2**, 97-105 (2013).

143 Keefer, M. C. *et al.* A phase I trial of preventive HIV vaccination with heterologous poxviral-vectors containing matching HIV-1 inserts in healthy HIV-uninfected subjects. *Vaccine* **29**, 1948-1958, doi:10.1016/j.vaccine.2010.12.104 (2011).

144 Kelleher, A. D. *et al.* A randomized, placebo-controlled phase I trial of DNA prime, recombinant fowlpox virus boost prophylactic vaccine for HIV-1. *Aids* **20**, 294-297 (2006).

145 Rollier, C. S., Reyes-Sandoval, A., Cottingham, M. G., Ewer, K. & Hill, A. V. Viral vectors as vaccine platforms: deployment in sight. *Current opinion in immunology* **23**, 377-382 (2011).

146 Kim, S. H. *et al.* Clinical responses to smallpox vaccine in vaccinia-naive and previously vaccinated populations: undiluted and diluted Lancy-Vaxina vaccine in a single-blind, randomized, prospective trial. *J Infect Dis* **192**, 1066-1070, doi:10.1086/432765 (2005).

147 Qin, L., Liang, M. & Evans, D. H. Genomic analysis of vaccinia virus strain TianTan provides new insights into the evolution and evolutionary relationships between Orthopoxviruses. *Virology* **442**, 59-66, doi:10.1016/j.virol.2013.03.025 (2013).

148 Sanchez-Sampedro, L. *et al.* The evolution of poxvirus vaccines. *Viruses* **7**, 1726-1803, doi:10.3390/v7041726 (2015).

149 Khliabich, G. N., Sumarokov, A. A., Karinskaia, G. A., Shkol'nik, R. & Iaroslavskaia, N. V. [Comparative study of the smallpox vaccines from B-51, EM-63 and L-IVP in a controlled epidemiological experiment. II. The characteristiics of the immunogenicity of the smallpox vaccines]. *Zhurnal mikrobiologii, epidemiologii, i immunobiologii*, 37-42 (1978).

150 Qin, L., Upton, C., Hazes, B. & Evans, D. H. Genomic analysis of the vaccinia virus strain variants found in Dryvax vaccine. *J Virol* **85**, 13049-13060, doi:10.1128/jvi.05779-11 (2011).

151 Talbot, T. R. *et al.* Vaccination success rate and reaction profile with diluted and undiluted smallpox vaccine: a randomized controlled trial. *Jama* **292**, 1205-1212, doi:10.1001/jama.292.10.1205 (2004).

152 Bejon, P. *et al.* Extended follow-up following a phase 2b randomized trial of the candidate malaria vaccines FP9 ME-TRAP and MVA ME-TRAP among children in Kenya. *PloS one* **2**, e707 (2007).

153 Berthoud, T. K. *et al.* Potent CD8+ T-cell immunogenicity in humans of a novel heterosubtypic influenza A vaccine, MVA-NP+M1. *Clin Infect Dis* **52**, 1-7 (2011).

154 Cavenaugh, J. S. *et al.* Partially randomized, non-blinded trial of DNA and MVA therapeutic vaccines based on hepatitis B virus surface protein for chronic HBV infection. *PloS one* **6**, e14626 (2011).

155 Garcia, F. *et al.* Safety and immunogenicity of a modified pox vector-based HIV/AIDS vaccine candidate expressing Env, Gag, Pol and Nef proteins of HIV-1 subtype B (MVA-B) in healthy HIV-1-uninfected volunteers: A phase I clinical trial (RISVAC02). *Vaccine* **29**, 8309-8316 (2011).

156 Gomez, C. E. *et al.* The HIV/AIDS vaccine candidate MVA-B administered as a single immunogen in humans triggers robust, polyfunctional, and selective effector memory T cell responses to HIV-1 antigens. *J Virol* **85**, 11468-11478 (2011).

157 Sheehy, S. H. *et al.* Phase Ia clinical evaluation of the safety and immunogenicity of the Plasmodium falciparum blood-stage antigen AMA1 in ChAd63 and MVA vaccine vectors. *PloS one* **7**, e31208 (2012).

158 Bart, P. A. *et al.* EV01: a phase I trial in healthy HIV negative volunteers to evaluate a clade C HIV vaccine, NYVAC-C undertaken by the EuroVacc Consortium. *Vaccine* **26**, 3153-3161, doi:10.1016/j.vaccine.2008.03.083 (2008).

159 Harari, A. *et al.* An HIV-1 clade C DNA prime, NYVAC boost vaccine regimen induces reliable, polyfunctional, and long-lasting T cell responses. *J Exp Med* **205**, 63-77, doi:10.1084/jem.20071331 (2008).

160 Konishi, E. *et al.* A highly attenuated host range-restricted vaccinia virus strain, NYVAC, encoding the prM, E, and NS1 genes of Japanese encephalitis virus prevents JEV viremia in swine. *Virology* **190**, 454-458 (1992).

161 McCormack, S. *et al.* EV02: a Phase I trial to compare the safety and immunogenicity of HIV DNA-C prime-NYVAC-C boost to NYVAC-C alone. *Vaccine* **26**, 3162-3174, doi:10.1016/j.vaccine.2008.02.072 (2008).

162 Liu, Q. *et al.* HIV-1 vaccines based on replication-competent Tiantan vaccinia protected Chinese rhesus macaques from simian HIV infection. *Aids* **29**, 649-658, doi:10.1097/qad.0000000000000595 (2015).

163 Amara, R. R. *et al.* Control of a mucosal challenge and prevention of AIDS by a multiprotein DNA/MVA vaccine. *Science* **292**, 69-74 (2001).

164 Hochstein-Mintzel, V., Hanichen, T., Huber, H. C. & Stickl, H. [An attenuated strain of vaccinia virus (MVA). Successful intramuscular immunization against vaccinia and variola (author's transl)]. *Zentralblatt fur Bakteriologie, Parasitenkunde, Infektionskrankheiten und Hygiene. Erste Abteilung Originale. Reihe A: Medizinische Mikrobiologie und Parasitologie* **230**, 283-297 (1975).

165 Mayr, A., Stickl, H., Muller, H. K., Danner, K. & Singer, H. [The smallpox vaccination strain MVA: marker, genetic structure, experience gained with the parenteral vaccination and behavior in organisms with a debilitated defence mechanism (author's transl)]. *Zentralblatt fur Bakteriologie, Parasitenkunde, Infektionskrankheiten und Hygiene. Erste Abteilung Originale. Reihe B: Hygiene, Betriebshygiene, praventive Medizin* **167**, 375-390 (1978).

166 Mooij, P. *et al.* Differential CD4+ versus CD8+ T-cell responses elicited by different poxvirus-based human immunodeficiency virus type 1 vaccine candidates provide comparable efficacies in primates. *J Virol* **82**, 2975-2988 (2008).

167 Amara, R. R. *et al.* Different patterns of immune responses but similar control of a simian-human immunodeficiency virus 89.6P mucosal challenge by modified vaccinia virus Ankara (MVA) and DNA/MVA vaccines. *J Virol* **76**, 7625-7631 (2002).

168 Stevceva, L. *et al.* Both mucosal and systemic routes of immunization with the live, attenuated NYVAC/simian immunodeficiency virus SIV(gpe) recombinant vaccine result in gag-specific CD8(+) T-cell responses in mucosal tissues of macaques. *J Virol* **76**, 11659-11676, doi:10.1128/jvi.76.22.11659-11676.2002 (2002).

169 Blanchard, T. J., Alcami, A., Andrea, P. & Smith, G. L. Modified vaccinia virus Ankara undergoes limited replication in human cells and lacks several immunomodulatory proteins: implications for use as a human vaccine. *The Journal of general virology* **79 (Pt 5)**, 1159-1167, doi:10.1099/0022-1317-79-5-1159 (1998).

170 Meyer, H., Sutter, G. & Mayr, A. Mapping of deletions in the genome of the highly attenuated vaccinia virus MVA and their influence on virulence.

The Journal of general virology **72 (Pt 5)**, 1031-1038, doi:10.1099/0022-1317-72-5-1031 (1991).

171 Leung-Theung-Long, S. *et al.* A multi-antigenic MVA vaccine increases efficacy of combination chemotherapy against Mycobacterium tuberculosis. *PloS one* **13**, e0196815, doi:10.1371/journal.pone.0196815 (2018).

172 Rampling, T. *et al.* Safety and efficacy of novel malaria vaccine regimens of RTS,S/AS01B alone, or with concomitant ChAd63-MVA-vectored vaccines expressing ME-TRAP. *NPJ vaccines* **3**, 49, doi:10.1038/s41541-018-0084-2 (2018).

173 Kannanganant, S. *et al.* Local control of repeated-dose rectal challenges in DNA/MVA-vaccinated macaques protected against a first series of simian immunodeficiency virus challenges. *J Virol* **88**, 5864-5869 (2014).

174 Kwa, S. *et al.* CD40L-adjuvanted DNA/modified vaccinia virus Ankara simian immunodeficiency virus SIV239 vaccine enhances SIV-specific humoral and cellular immunity and improves protection against a heterologous SIVE660 mucosal challenge. *J Virol* **88**, 9579-9589 (2014).

175 Lai, L. *et al.* Prevention of infection by a granulocyte-macrophage colony-stimulating factor co-expressing DNA/modified vaccinia Ankara simian immunodeficiency virus vaccine. *J Infect Dis* **204**, 164-173 (2011).

176 Lai, L. *et al.* SIVmac239 MVA vaccine with and without a DNA prime, similar prevention of infection by a repeated dose SIVsmE660 challenge despite different immune responses. *Vaccine* **30**, 1737-1745 (2012).

177 Horton, H. *et al.* Immunization of rhesus macaques with a DNA prime/modified vaccinia virus Ankara boost regimen induces broad simian immunodeficiency virus (SIV)-specific T-cell responses and reduces initial viral replication but does not prevent disease progression following challenge with pathogenic SIVmac239. *J Virol* **76**, 7187-7202 (2002).

178 Vogel, T. U. *et al.* Multispecific vaccine-induced mucosal cytotoxic T lymphocytes reduce acute-phase viral replication but fail in long-term control of simian immunodeficiency virus SIVmac239. *J Virol* **77**, 13348-13360 (2003).

179 Hanke, T. *et al.* Effective induction of simian immunodeficiency virus-specific cytotoxic T lymphocytes in macaques by using a multiepitope gene and DNA prime-modified vaccinia virus Ankara boost vaccination regimen. *J Virol* **73**, 7524-7532 (1999).

180 Kent, S. J. *et al.* Enhanced T-cell immunogenicity and protective efficacy of a human immunodeficiency virus type 1 vaccine regimen consisting of consecutive priming with DNA and boosting with recombinant fowlpox virus. *J Virol* **72**, 10180-10188 (1998).

181 Otten, G. *et al.* Induction of broad and potent anti-human immunodeficiency virus immune responses in rhesus macaques by priming with a DNA vaccine and boosting with protein-adsorbed polylactide coglycolide microparticles. *J Virol* **77**, 6087-6092 (2003).

182 Gherardi, M. M., Perez-Jimenez, E., Najera, J. L. & Esteban, M. Induction of HIV immunity in the genital tract after intranasal delivery of a MVA vector: enhanced immunogenicity after DNA prime-modified vaccinia virus Ankara boost immunization schedule. *J Immunol* **172**, 6209-6220 (2004).

183 Falivene, J. *et al.* Improving the MVA vaccine potential by deleting the viral gene coding for the IL-18 binding protein. *PloS one* **7**, e32220, doi:10.1371/journal.pone.0032220 (2012).

184 Garber, D. A. *et al.* Deletion of specific immune-modulatory genes from modified vaccinia virus Ankara-based HIV vaccines engenders improved immunogenicity in rhesus macaques. *J Virol* **86**, 12605-12615, doi:10.1128/jvi.00246-12 (2012).

185 Garcia-Arriaza, J. *et al.* A candidate HIV/AIDS vaccine (MVA-B) lacking vaccinia virus gene C6L enhances memory HIV-1-specific T-cell responses. *PloS one* **6**, e24244, doi:10.1371/journal.pone.0024244 (2011).

186 Perdiguero, B. *et al.* Deletion of the viral anti-apoptotic gene F1L in the HIV/AIDS vaccine candidate MVA-C enhances immune responses against HIV-1 antigens. *PloS one* **7**, e48524, doi:10.1371/journal.pone.0048524 (2012).

187 Taylor, J. & Paoletti, E. Fowlpox virus as a vector in non-avian species. *Vaccine* **6**, 466-468 (1988).

188 Taylor, J. *et al.* Efficacy studies on a canarypox-rabies recombinant virus. *Vaccine* **9**, 190-193 (1991).

189 Weli, S. C. & Tryland, M. Avipoxviruses: infection biology and their use as vaccine vectors. *Virology journal* **8**, 49, doi:10.1186/1743-422x-8-49 (2011).

190 Coupar, B. E. *et al.* Fowlpox virus vaccines for HIV and SHIV clinical and pre-clinical trials. *Vaccine* **24**, 1378-1388, doi:10.1016/j.vaccine.2005.09.044 (2006).

191 Dale, C. J. *et al.* Efficacy of DNA and fowlpox virus priming/boosting vaccines for simian/human immunodeficiency virus. *J Virol* **78**, 13819-13828 (2004).

192 De Rose, R. *et al.* Comparative efficacy of subtype AE simian-human immunodeficiency virus priming and boosting vaccines in pigtail macaques. *J Virol* **81**, 292-300, doi:10.1128/jvi.01727-06 (2007).

193 De Rose, R. *et al.* Subtype AE HIV-1 DNA and recombinant Fowlpoxvirus vaccines encoding five shared HIV-1 genes: safety and T cell immunogenicity in macaques. *Vaccine* **23**, 1949-1956, doi:10.1016/j.vaccine.2004.10.012 (2005).

194 Pal, R. *et al.* ALVAC-SIV-gag-pol-env-based vaccination and macaque major histocompatibility complex class I (A*01) delay simian immunodeficiency virus SIVmac-induced immunodeficiency. *J Virol* **76**, 292-302, doi:10.1128/jvi.76.1.292-302.2002 (2002).

195 Pal, R. *et al.* Systemic immunization with an ALVAC-HIV-1/protein boost vaccine strategy protects rhesus macaques from CD4+ T-cell loss and reduces both systemic and mucosal simian-human immunodeficiency virus SHIVKU2 RNA levels. *J Virol* **80**, 3732-3742, doi:10.1128/jvi.80.8.3732-3742.2006 (2006).

196 Van Rompay, K. K. *et al.* Attenuated poxvirus-based simian immunodeficiency virus (SIV) vaccines given in infancy partially protect infant and juvenile macaques against repeated oral challenge with virulent SIV. *Journal of acquired immune deficiency syndromes (1999)* **38**, 124-134, doi:10.1097/00126334-200502010-00002 (2005).

197 Bonsignori, M. *et al.* Antibody-dependent cellular cytotoxicity-mediating antibodies from an HIV-1 vaccine efficacy trial target multiple epitopes and preferentially use the VH1 gene family. *J Virol* **86**, 11521-11532, doi:10.1128/jvi.01023-12 (2012).

198 de Souza, M. S. *et al.* The Thai phase III trial (RV144) vaccine regimen induces T cell responses that preferentially target epitopes within the V2 region of HIV-1 envelope. *J Immunol* **188**, 5166-5176, doi:10.4049/jimmunol.1102756 (2012).

199 Haynes, B. F. *et al.* Immune-correlates analysis of an HIV-1 vaccine efficacy trial. *N Engl J Med* **366**, 1275-1286, doi:10.1056/NEJMoa1113425 (2012).

200 Tomaras, G. D. *et al.* Vaccine-induced plasma IgA specific for the C1 region of the HIV-1 envelope blocks binding and effector function of IgG. *Proceedings of the National Academy of Sciences of the United States of America* **110**, 9019-9024, doi:10.1073/pnas.1301456110 (2013).

201 Zolla-Pazner, S. *et al.* Vaccine-induced IgG antibodies to V1V2 regions of multiple HIV-1 subtypes correlate with decreased risk of HIV-1 infection. *PloS one* **9**, e87572, doi:10.1371/journal.pone.0087572 (2014).

202 Skinner, M. A., Laidlaw, S. M., Eldaghayes, I., Kaiser, P. & Cottingham, M. G. Fowlpox virus as a recombinant vaccine vector for use in mammals

and poultry. *Expert Rev Vaccines* **4**, 63-76, doi:10.1586/14760584.4.1.63 (2005).

203 Leong, K. H., Ramsay, A. J., Boyle, D. B. & Ramshaw, I. A. Selective induction of immune responses by cytokines coexpressed in recombinant fowlpox virus. *J Virol* **68**, 8125-8130 (1994).

204 Hemachandra, A. *et al.* An HIV-1 clade A/E DNA prime, recombinant fowlpox virus boost vaccine is safe, but non-immunogenic in a randomized phase I/IIa trial in Thai volunteers at low risk of HIV infection. *Human vaccines* **6**, 835-840, doi:10.4161/hv.6.10.12635 (2010).

205 Ranasinghe, C. *et al.* A comparative analysis of HIV-specific mucosal/systemic T cell immunity and avidity following rDNA/rFPV and poxvirus-poxvirus prime boost immunisations. *Vaccine* **29**, 3008-3020 (2011).

206 Boyer, J. D. *et al.* SIV DNA vaccine co-administered with IL-12 expression plasmid enhances CD8 SIV cellular immune responses in cynomolgus macaques. *J Med Primatol* **34**, 262-270 (2005).

207 Chang, J. *et al.* IL-12 priming during in vitro antigenic stimulation changes properties of CD8 T cells and increases generation of effector and memory cells. *J Immunol* **172**, 2818-2826 (2004).

208 Day, S. L., Ramshaw, I. A., Ramsay, A. J. & Ranasinghe, C. Differential effects of the type I interferons alpha4, beta, and epsilon on antiviral activity and vaccine efficacy. *J Immunol* **180**, 7158-7166, doi:10.4049/jimmunol.180.11.7158 (2008).

209 Harrison, J. M. *et al.* 4-1BBL coexpression enhances HIV-specific CD8 T cell memory in a poxvirus prime-boost vaccine. *Vaccine* **24**, 6867-6874 (2006).

210 Kent, S. J. *et al.* A recombinant avipoxvirus HIV-1 vaccine expressing interferon-gamma is safe and immunogenic in macaques. *Vaccine* **18**, 2250-2256, doi:10.1016/s0264-410x(99)00559-9 (2000).

211 Ramsay, A. J. *et al.* Genetic vaccination strategies for enhanced cellular, humoral and mucosal immunity. *Immunol Rev* **171**, 27-44, doi:10.1111/j.1600-065x.1999.tb01341.x (1999).

212 Rodriguez, A. M. *et al.* IL-12 and GM-CSF in DNA/MVA immunizations against HIV-1 CRF12_BF Nef induced T-cell responses with an enhanced magnitude, breadth and quality. *PLoS One* **7**, e37801 (2012).

213 Xi, Y., Day, S. L., Jackson, R. J. & Ranasinghe, C. Role of novel type I interferon epsilon in viral infection and mucosal immunity. *Mucosal Immunol* **5**, 610-622, doi:10.1038/mi.2012.35 (2012).

214 Emery, S. *et al.* Influence of IFNgamma co-expression on the safety and antiviral efficacy of recombinant fowlpox virus HIV therapeutic vaccines following interruption of antiretroviral therapy. *Human vaccines* **3**, 260-267 (2007).

215 Hghihghi, H. R. *et al.* Characterization of host responses against a recombinant fowlpox virus-vectored vaccine expressing the hemagglutinin antigen of an avian influenza virus. *Clinical and vaccine immunology : CVI* **17**, 454-463, doi:10.1128/cvi.00487-09 (2010).

216 Hodge, J. W., Grosenbach, D. W., Aarts, W. M., Poole, D. J. & Schlom, J. Vaccine therapy of established tumors in the absence of autoimmunity. *Clinical cancer research : an official journal of the American Association for Cancer Research* **9**, 1837-1849 (2003).

217 Webster, D. P. *et al.* Safety of recombinant fowlpox strain FP9 and modified vaccinia virus Ankara vaccines against liver-stage P. falciparum malaria in non-immune volunteers. *Vaccine* **24**, 3026-3034, doi:10.1016/j.vaccine.2005.10.058 (2006).

218 Wild, F., Giraudon, P., Spehner, D., Drillien, R. & Lecocq, J. P. Fowlpox virus recombinant encoding the measles virus fusion protein: protection of mice against fatal measles encephalitis. *Vaccine* **8**, 441-442, doi:10.1016/0264-410x(90)90243-f (1990).

219 Barouch, D. H. Novel adenovirus vector-based vaccines for HIV-1. *Current opinion in HIV and AIDS* **5**, 386-390, doi:10.1097/COH.0b013e32833cfe4c (2010).

220 Tomusange, K. *et al.* Engineering human rhinovirus serotype-A1 as a vaccine vector. *Virus Res* **203**, 72-76 (2015).

221 Ura, T., Okuda, K. & Shimada, M. Developments in Viral Vector-Based Vaccines. *Vaccines (Basel)* **2**, 624-641 (2014).

222 Xiang, Z. Q., Pasquini, S. & Ertl, H. C. Induction of genital immunity by DNA priming and intranasal booster immunization with a replication-defective adenoviral recombinant. *J Immunol* **162**, 6716-6723 (1999).

223 Abe, S. *et al.* Adenovirus type 5 with modified hexons induces robust transgene-specific immune responses in mice with pre-existing immunity against adenovirus type 5. *J Gene Med* **11**, 570-579 (2009).

224 Gabitzsch, E. S. *et al.* Novel Adenovirus type 5 vaccine platform induces cellular immunity against HIV-1 Gag, Pol, Nef despite the presence of Ad5 immunity. *Vaccine* **27**, 6394-6398 (2009).

225 Liu, J. *et al.* Magnitude and phenotype of cellular immune responses elicited by recombinant adenovirus vectors and heterologous prime-boost regimens in rhesus monkeys. *J Virol* **82**, 4844-4852 (2008).

226 Sumida, S. M. *et al.* Neutralizing antibodies to adenovirus serotype 5 vaccine vectors are directed primarily against the adenovirus hexon protein. *J Immunol* **174**, 7179-7185 (2005).

227 Wohlfart, C. Neutralization of adenoviruses: kinetics, stoichiometry, and mechanisms. *J Virol* **62**, 2321-2328 (1988).

228 Yang, Y. *et al.* Cellular immunity to viral antigens limits E1-deleted adenoviruses for gene therapy. *Proceedings of the National Academy of Sciences of the United States of America* **91**, 4407-4411 (1994).

229 Roberts, D. M. *et al.* Hexon-chimaeric adenovirus serotype 5 vectors circumvent pre-existing anti-vector immunity. *Nature* **441**, 239-243 (2006).

230 Ura, T. *et al.* Designed recombinant adenovirus type 5 vector induced envelope-specific CD8(+) cytotoxic T lymphocytes and cross-reactive neutralizing antibodies against human immunodeficiency virus type 1. *J Gene Med* **11**, 139-149 (2009).

231 Zhang, C. & Zhou, D. Adenoviral vector-based strategies against infectious disease and cancer. *Hum Vaccin Immunother* **12**, 2064-2074, doi:10.1080/21645515.2016.1165908 (2016).

232 Baden, L. R. *et al.* First-in-human evaluation of the safety and immunogenicity of a recombinant adenovirus serotype 26 HIV-1 Env

vaccine (IPCAVD 001). *J Infect Dis* **207**, 240-247, doi:10.1093/infdis/jis670 (2013).

233 Barouch, D. H. *et al.* Characterization of humoral and cellular immune responses elicited by a recombinant adenovirus serotype 26 HIV-1 Env vaccine in healthy adults (IPCAVD 001). *J Infect Dis* **207**, 248-256, doi:10.1093/infdis/jis671 (2013).

234 Abbink, P. *et al.* Comparative seroprevalence and immunogenicity of six rare serotype recombinant adenovirus vaccine vectors from subgroups B and D. *J Virol* **81**, 4654-4663, doi:10.1128/jvi.02696-06 (2007).

235 Barouch, D. H. *et al.* Immunogenicity of recombinant adenovirus serotype 35 vaccine in the presence of pre-existing anti-Ad5 immunity. *J Immunol* **172**, 6290-6297, doi:10.4049/jimmunol.172.10.6290 (2004).

236 Fitzgerald, J. C. *et al.* A simian replication-defective adenoviral recombinant vaccine to HIV-1 gag. *J Immunol* **170**, 1416-1422, doi:10.4049/jimmunol.170.3.1416 (2003).

237 Lore, K. *et al.* Myeloid and plasmacytoid dendritic cells are susceptible to recombinant adenovirus vectors and stimulate polyfunctional memory T cell responses. *J Immunol* **179**, 1721-1729, doi:10.4049/jimmunol.179.3.1721 (2007).

238 Waddington, S. N. *et al.* Adenovirus serotype 5 hexon mediates liver gene transfer. *Cell* **132**, 397-409, doi:10.1016/j.cell.2008.01.016 (2008).

239 Gerlach, T., Elbahesh, H., Saletti, G. & Rimmelzwaan, G. F. Recombinant influenza A viruses as vaccine vectors. *Expert Rev Vaccines* **18**, 379-392 (2019).

240 Ashkenazi, S. *et al.* Superior relative efficacy of live attenuated influenza vaccine compared with inactivated influenza vaccine in young children with recurrent respiratory tract infections. *Pediatr Infect Dis J* **25**, 870-879 (2006).

241 de Goede, A. L. *et al.* Characterization of recombinant influenza A virus as a vector for HIV-1 p17Gag. *Vaccine* **27**, 5735-5739, doi:10.1016/j.vaccine.2009.07.032 (2009).

242 Ferko, B. *et al.* Hyperattenuated recombinant influenza A virus nonstructural-protein-encoding vectors induce human immunodeficiency virus type 1 Nef-specific systemic and mucosal immune responses in mice. *J Virol* **75**, 8899-8908, doi:10.1128/jvi.75.19.8899-8908.2001 (2001).

243 Gonzalo, R. M. *et al.* Enhanced CD8+ T cell response to HIV-1 env by combined immunization with influenza and vaccinia virus recombinants. *Vaccine* **17**, 887-892, doi:10.1016/s0264-410x(98)00274-6 (1999).

244 Nakaya, Y., Zheng, H. & Garcia-Sastre, A. Enhanced cellular immune responses to SIV Gag by immunization with influenza and vaccinia virus recombinants. *Vaccine* **21**, 2097-2106, doi:10.1016/s0264-410x(02)00781-8 (2003).

245 Tomusange, K. *et al.* Mucosal vaccination with a live recombinant rhinovirus followed by intradermal DNA administration elicits potent and protective HIV-specific immune responses. *Sci Rep* **6**, 36658 (2016).

246 Kimura, H., Yoshizumi, M., Ishii, H., Oishi, K. & Ryo, A. Cytokine production and signaling pathways in respiratory virus infection. *Frontiers in microbiology* **4**, 276, doi:10.3389/fmicb.2013.00276 (2013).

247 Ank, N. *et al.* Lambda interferon (IFN-lambda), a type III IFN, is induced by viruses and IFNs and displays potent antiviral activity against select virus infections in vivo. *J Virol* **80**, 4501-4509, doi:10.1128/jvi.80.9.4501-4509.2006 (2006).

248 Platanias, L. C. Mechanisms of type-I- and type-II-interferon-mediated signalling. *Nat Rev Immunol* **5**, 375-386, doi:10.1038/nri1604 (2005).

249 Pfeffer, K. Biological functions of tumor necrosis factor cytokines and their receptors. *Cytokine & growth factor reviews* **14**, 185-191 (2003).

250 Akdis, M. *et al.* Interleukins, from 1 to 37, and interferon-gamma: receptors, functions, and roles in diseases. *The Journal of allergy and clinical immunology* **127**, 701-721.e701-770, doi:10.1016/j.jaci.2010.11.050 (2011).

251 Liang, S. C. *et al.* Interleukin (IL)-22 and IL-17 are coexpressed by Th17 cells and cooperatively enhance expression of antimicrobial peptides. *J Exp Med* **203**, 2271-2279, doi:10.1084/jem.20061308 (2006).

252 Bancroft, A. J., McKenzie, A. N. & Grencis, R. K. A critical role for IL-13 in resistance to intestinal nematode infection. *J Immunol* **160**, 3453-3461 (1998).

253 Chapoval, S., Dasgupta, P., Dorsey, N. J. & Keegan, A. D. Regulation of the T helper cell type 2 (Th2)/T regulatory cell (Treg) balance by IL-4 and STAT6. *J Leukoc Biol* **87**, 1011-1018 (2010).

254 Corren, J. Role of interleukin-13 in asthma. *Curr Allergy Asthma Rep* **13**, 415-420 (2013).

255 Fallon, P. G., Emson, C. L., Smith, P. & McKenzie, A. N. IL-13 overexpression predisposes to anaphylaxis following antigen sensitization. *J Immunol* **166**, 2712-2716, doi:10.4049/jimmunol.166.4.2712 (2001).

256 Grunig, G. *et al.* Requirement for IL-13 independently of IL-4 in experimental asthma. *Science* **282**, 2261-2263, doi:10.1126/science.282.5397.2261 (1998).

257 Hamid, Q. *et al.* In vivo expression of IL-12 and IL-13 in atopic dermatitis. *The Journal of allergy and clinical immunology* **98**, 225-231 (1996).

258 Huang, S. K. *et al.* IL-13 expression at the sites of allergen challenge in patients with asthma. *J Immunol* **155**, 2688-2694 (1995).

259 Lawrence, R. A., Gray, C. A., Osborne, J. & Maizels, R. M. Nippostrongylus brasiliensis: cytokine responses and nematode expulsion in normal and IL-4-deficient mice. *Experimental parasitology* **84**, 65-73, doi:10.1006/expr.1996.0090 (1996).

260 Monick, M. M. *et al.* Respiratory syncytial virus synergizes with Th2 cytokines to induce optimal levels of TARC/CCL17. *J Immunol* **179**, 1648-1658, doi:10.4049/jimmunol.179.3.1648 (2007).

261 Moran, T. M., Isobe, H., Fernandez-Sesma, A. & Schulman, J. L. Interleukin-4 causes delayed virus clearance in influenza virus-infected mice. *J Virol* **70**, 5230-5235 (1996).

262 Munitz, A., Brandt, E. B., Mingler, M., Finkelman, F. D. & Rothenberg, M. E. Distinct roles for IL-13 and IL-4 via IL-13 receptor alpha1 and the type

II IL-4 receptor in asthma pathogenesis. *Proceedings of the National Academy of Sciences of the United States of America* **105**, 7240-7245 (2008).

263 Sakala, I. G., Chaudhri, G., Eldi, P., Buller, R. M. & Karupiah, G. Deficiency in Th2 cytokine responses exacerbate orthopoxvirus infection. *PloS one* **10**, e0118685, doi:10.1371/journal.pone.0118685 (2015).

264 Cheever, A. W. Pipe-stem fibrosis of the liver. *Transactions of the Royal Society of Tropical Medicine and Hygiene* **66**, 947-948 (1972).

265 Chiaramonte, M. G., Donaldson, D. D., Cheever, A. W. & Wynn, T. A. An IL-13 inhibitor blocks the development of hepatic fibrosis during a T-helper type 2-dominated inflammatory response. *The Journal of clinical investigation* **104**, 777-785, doi:10.1172/jci7325 (1999).

266 Jeong, C. W. *et al.* Differential in vivo cytokine mRNA expression in lesional skin of intrinsic vs. extrinsic atopic dermatitis patients using semiquantitative RT-PCR. *Clinical and experimental allergy : journal of the British Society for Allergy and Clinical Immunology* **33**, 1717-1724 (2003).

267 Miska, J. *et al.* Initiation of inflammatory tumorigenesis by CTLA4 insufficiency due to type 2 cytokines. *J Exp Med* **215**, 841-858, doi:10.1084/jem.20171971 (2018).

268 Terabe, M. *et al.* NKT cell-mediated repression of tumor immunosurveillance by IL-13 and the IL-4R-STAT6 pathway. *Nat Immunol* **1**, 515-520, doi:10.1038/82771 (2000).

269 Van der Pouw Kraan, T. C. *et al.* The role of IL-13 in IgE synthesis by allergic asthma patients. *Clinical and experimental immunology* **111**, 129-135, doi:10.1046/j.1365-2249.1998.00471.x (1998).

270 Wills-Karp, M. *et al.* Interleukin-13: central mediator of allergic asthma. *Science* **282**, 2258-2261, doi:10.1126/science.282.5397.2258 (1998).

271 McKenzie, G. J., Bancroft, A., Grencis, R. K. & McKenzie, A. N. A distinct role for interleukin-13 in Th2-cell-mediated immune responses. *Current biology : CB* **8**, 339-342, doi:10.1016/s0960-9822(98)70134-4 (1998).

272 Urban, J. F., Jr. *et al.* IL-13, IL-4Ralpha, and Stat6 are required for the expulsion of the gastrointestinal nematode parasite Nippostrongylus brasiliensis. *Immunity* **8**, 255-264, doi:10.1016/s1074-7613(00)80477-x (1998).

273 Woytschak, J. *et al.* Type 2 Interleukin-4 Receptor Signaling in Neutrophils Antagonizes Their Expansion and Migration during Infection and Inflammation. *Immunity* **45**, 172-184, doi:10.1016/j.immuni.2016.06.025 (2016).

274 Asquith, K. L. *et al.* Interleukin-13 promotes susceptibility to chlamydial infection of the respiratory and genital tracts. *PLoS pathogens* **7**, e1001339, doi:10.1371/journal.ppat.1001339 (2011).

275 Dulek, D. E. *et al.* Allergic airway inflammation decreases lung bacterial burden following acute Klebsiella pneumoniae infection in a neutrophil- and CCL8-dependent manner. *Infection and immunity* **82**, 3723-3739, doi:10.1128/iai.00035-14 (2014).

276 Finkelman, F. D., Wynn, T. A., Donaldson, D. D. & Urban, J. F. The role of IL-13 in helminth-induced inflammation and protective immunity against nematode infections. *Current opinion in immunology* **11**, 420-426, doi:10.1016/s0952-7915(99)80070-3 (1999).

277 Zhou, W. *et al.* IL-13 is associated with reduced illness and replication in primary respiratory syncytial virus infection in the mouse. *Microbes and infection* **8**, 2880-2889, doi:10.1016/j.micinf.2006.09.007 (2006).

278 Tabata, Y. & Khurana Hershey, G. K. IL-13 receptor isoforms: breaking through the complexity. *Curr Allergy Asthma Rep* **7**, 338-345 (2007).

279 Takeda, K., Kamanaka, M., Tanaka, T., Kishimoto, T. & Akira, S. Impaired IL-13-mediated functions of macrophages in STAT6-deficient mice. *J Immunol* **157**, 3220-3222 (1996).

280 Zurawski, G. & de Vries, J. E. Interleukin 13, an interleukin 4-like cytokine that acts on monocytes and B cells, but not on T cells. *Immunol Today* **15**, 19-26 (1994).

281 Kurowska-Stolarska, M. *et al.* IL-33 amplifies the polarization of alternatively activated macrophages that contribute to airway inflammation. *J Immunol* **183**, 6469-6477, doi:10.4049/jimmunol.0901575 (2009).

282 Rothenberg, M. E. *et al.* IL-13 receptor alpha1 differentially regulates aeroallergen-induced lung responses. *J Immunol* **187**, 4873-4880, doi:10.4049/jimmunol.1004159 (2011).

283 Amit, U. *et al.* New Role for Interleukin-13 Receptor alpha1 in Myocardial Homeostasis and Heart Failure. *Journal of the American Heart Association* **6**, doi:10.1161/jaha.116.005108 (2017).

284 Zhang, J. G. *et al.* Identification, purification, and characterization of a soluble interleukin (IL)-13-binding protein. Evidence that it is distinct from the cloned Il-13 receptor and Il-4 receptor alpha-chains. *J Biol Chem* **272**, 9474-9480 (1997).

285 Chiaramonte, M. G. *et al.* Regulation and function of the interleukin 13 receptor alpha 2 during a T helper cell type 2-dominant immune response. *J Exp Med* **197**, 687-701 (2003).

286 Daines, M. O. & Hershey, G. K. A novel mechanism by which interferon-gamma can regulate interleukin (IL)-13 responses. Evidence for intracellular stores of IL-13 receptor alpha -2 and their rapid mobilization by interferon-gamma. *J Biol Chem* **277**, 10387-10393 (2002).

287 Wood, N. *et al.* Enhanced interleukin (IL)-13 responses in mice lacking IL-13 receptor alpha 2. *J Exp Med* **197**, 703-709 (2003).

288 Barderas, R., Bartolome, R. A., Fernandez-Acenero, M. J., Torres, S. & Casal, J. I. High expression of IL-13 receptor alpha2 in colorectal cancer is associated with invasion, liver metastasis, and poor prognosis. *Cancer Res* **72**, 2780-2790 (2012).

289 Caput, D. *et al.* Cloning and characterization of a specific interleukin (IL)-13 binding protein structurally related to the IL-5 receptor alpha chain. *J Biol Chem* **271**, 16921-16926 (1996).

290 Fujisawa, T., Joshi, B. H. & Puri, R. K. IL-13 regulates cancer invasion and metastasis through IL-13Ralpha2 via ERK/AP-1 pathway in mouse model of human ovarian cancer. *Int J Cancer* **131**, 344-356 (2012).

291 Sengupta, S., Thaci, B., Crawford, A. C. & Sampath, P. Interleukin-13 receptor alpha 2-targeted glioblastoma immunotherapy. *Biomed Res Int* **2014**, 952128 (2014).

292 Zhao, Z., Wang, L. & Xu, W. IL-13Ralpha2 mediates PNR-induced migration and metastasis in ERalpha-negative breast cancer. *Oncogene* **34**, 1596-1607 (2015).

293 Nakashima, H., Husain, S. R. & Puri, R. K. IL-13 receptor-directed cancer vaccines and immunotherapy. *Immunotherapy* **4**, 443-451 (2012).

294 Verstockt, B. *et al.* Effects of Epithelial IL-13Ralpha2 Expression in Inflammatory Bowel Disease. *Front Immunol* **9**, 2983 (2018).

295 Andrews, A. L. *et al.* IL-13 receptor alpha 2: a regulator of IL-13 and IL-4 signal transduction in primary human fibroblasts. *The Journal of allergy and clinical immunology* **118**, 858-865 (2006).

296 Wilson, M. S. *et al.* IL-13Ralpha2 and IL-10 coordinately suppress airway inflammation, airway-hyperreactivity, and fibrosis in mice. *The Journal of clinical investigation* **117**, 2941-2951 (2007).

297 Mentink-Kane, M. M. *et al.* IL-13 receptor alpha 2 down-modulates granulomatous inflammation and prolongs host survival in schistosomiasis. *Proceedings of the National Academy of Sciences of the United States of America* **101**, 586-590 (2004).

298 Newman, J. P. *et al.* Interleukin-13 receptor alpha 2 cooperates with EGFRvIII signaling to promote glioblastoma multiforme. *Nature communications* **8**, 1913, doi:10.1038/s41467-017-01392-9 (2017).

299 Rahaman, S. O., Vogelbaum, M. A. & Haque, S. J. Aberrant Stat3 signaling by interleukin-4 in malignant glioma cells: involvement of IL-13Ralpha2. *Cancer Res* **65**, 2956-2963, doi:10.1158/0008-5472.can-04-3592 (2005).

300 Fichtner-Feigl, S. *et al.* Restoration of tumor immunosurveillance via targeting of interleukin-13 receptor-alpha 2. *Cancer Res* **68**, 3467-3475, doi:10.1158/0008-5472.can-07-5301 (2008).

301 Fichtner-Feigl, S. *et al.* IL-13 signaling via IL-13R alpha2 induces major downstream fibrogenic factors mediating fibrosis in chronic TNBS colitis. *Gastroenterology* **135**, 2003-2013, 2013 e2001-2007 (2008).

302 Hamid, M. A., Jackson, R. J., Roy, S., Khanna, M. & Ranasinghe, C. Unexpected involvement of IL-13 signalling via a STAT6 independent mechanism during murine IgG2a development following viral vaccination. *Eur J Immunol* **48**, 1153-1163, doi:10.1002/eji.201747463 (2018).

303 Berger, C. T. *et al.* High-functional-avidity cytotoxic T lymphocyte responses to HLA-B-restricted Gag-derived epitopes associated with relative HIV control. *J Virol* **85**, 9334-9345 (2011).

304 Ferre, A. L. *et al.* Mucosal immune responses to HIV-1 in elite controllers: a potential correlate of immune control. *Blood* **113**, 3978-3989, doi:10.1182/blood-2008-10-182709 (2009).

305 French, M. A. *et al.* Isotype-switched immunoglobulin G antibodies to HIV Gag proteins may provide alternative or additional immune responses to 'protective' human leukocyte antigen-B alleles in HIV controllers. *Aids* **27**, 519-528 (2013).

306 Li, Z., Jackson, R. J. & Ranasinghe, C. Vaccination route can significantly alter the innate lymphoid cell subsets: a feedback between IL-13 and IFN-gamma. *NPJ vaccines* **3**, 10, doi:10.1038/s41541-018-0048-6 (2018).

307 Townsend, D. G., Trivedi, S., Jackson, R. J. & Ranasinghe, C. Recombinant fowlpox virus vector-based vaccines: expression kinetics, dissemination and safety profile following intranasal delivery. *The Journal of general virology* **98**, 496-505 (2017).

308 Trivedi, S. *et al.* Identification of biomarkers to measure HIV-specific mucosal and systemic CD8(+) T-cell immunity using single cell Fluidigm 48.48 Dynamic arrays. *Vaccine* **33**, 7315-7327 (2015).

309 Fichtner-Feigl, S., Strober, W., Kawakami, K., Puri, R. K. & Kitani, A. IL-13 signaling through the IL-13alpha2 receptor is involved in induction of TGF-beta1 production and fibrosis. *Nature medicine* **12**, 99-106 (2006).

310 Mentink-Kane, M. M. & Wynn, T. A. Opposing roles for IL-13 and IL-13 receptor alpha 2 in health and disease. *Immunol Rev* **202**, 191-202, doi:10.1111/j.0105-2896.2004.00210.x (2004).

311 Rynda-Apple, A. *et al.* Regulation of IFN-gamma by IL-13 dictates susceptibility to secondary postinfluenza MRSA pneumonia. *Eur J Immunol* **44**, 3263-3272, doi:10.1002/eji.201444582 (2014).

312 Karo-Atar, D. *et al.* A protective role for IL-13 receptor alpha 1 in bleomycin-induced pulmonary injury and repair. *Mucosal Immunol* **9**, 240-253, doi:10.1038/mi.2015.56 (2016).

313 Ibanga, H. B. *et al.* Early clinical trials with a new tuberculosis vaccine, MVA85A, in tuberculosis-endemic countries: issues in study design. *Lancet Infect Dis* **6**, 522-528, doi:10.1016/s1473-3099(06)70552-7 (2006).

314 Ranasinghe, C. *et al.* Mucosal HIV-1 pox virus prime-boost immunization induces high-avidity CD8+ T cells with regime-dependent cytokine/granzyme B profiles. *J Immunol* **178**, 2370-2379 (2007).

315 Marthas, M. L. *et al.* Partial efficacy of a VSV-SIV/MVA-SIV vaccine regimen against oral SIV challenge in infant macaques. *Vaccine* **29**, 3124-3137, doi:10.1016/j.vaccine.2011.02.051 (2011).

316 Barouch, D. H. *et al.* Mosaic HIV-1 vaccines expand the breadth and depth of cellular immune responses in rhesus monkeys. *Nature medicine* **16**, 319-323, doi:10.1038/nm.2089 (2010).

317 Hansen, S. G. *et al.* Profound early control of highly pathogenic SIV by an effector memory T-cell vaccine. *Nature* **473**, 523-527, doi:10.1038/nature10003 (2011).

318 Kim, M. C. *et al.* Immunogenicity and efficacy of replication-competent recombinant influenza virus carrying multimeric M2 extracellular domains in a chimeric hemagglutinin conjugate. *Antiviral research* **148**, 43-52, doi:10.1016/j.antiviral.2017.10.018 (2017).

319 Garber, D. A. *et al.* Expanding the repertoire of Modified Vaccinia Ankara-based vaccine vectors via genetic complementation strategies. *PloS one* **4**, e5445, doi:10.1371/journal.pone.0005445 (2009).

320 Garcia-Arriaza, J., Najera, J. L., Gomez, C. E., Sorzano, C. O. & Esteban, M. Immunogenic profiling in mice of a HIV/AIDS vaccine candidate (MVA-B) expressing four HIV-1 antigens and potentiation by specific gene deletions. *PloS one* **5**, e12395, doi:10.1371/journal.pone.0012395 (2010).

321 Artis, D. & Spits, H. The biology of innate lymphoid cells. *Nature* **517**, 293-301, doi:10.1038/nature14189 (2015).

322 Neill, D. R. *et al.* Nuocytes represent a new innate effector leukocyte that mediates type-2 immunity. *Nature* **464**, 1367-1370, doi:10.1038/nature08900 (2010).

323 Klose, C. S. N. *et al.* Differentiation of type 1 ILCs from a common progenitor to all helper-like innate lymphoid cell lineages. *Cell* **157**, 340-356, doi:10.1016/j.cell.2014.03.030 (2014).

324 Gladiator, A., Wangler, N., Trautwein-Weidner, K. & LeibundGut-Landmann, S. Cutting edge: IL-17-secreting innate lymphoid cells are essential for host defense against fungal infection. *J Immunol* **190**, 521-525, doi:10.4049/jimmunol.1202924 (2013).

325 Spencer, S. P. *et al.* Adaptation of innate lymphoid cells to a micronutrient deficiency promotes type 2 barrier immunity. *Science* **343**, 432-437, doi:10.1126/science.1247606 (2014).

326 Lim, A. I. *et al.* IL-12 drives functional plasticity of human group 2 innate lymphoid cells. *J Exp Med* **213**, 569-583, doi:10.1084/jem.20151750 (2016).

327 Silver, J. S. *et al.* Inflammatory triggers associated with exacerbations of COPD orchestrate plasticity of group 2 innate lymphoid cells in the lungs. *Nat Immunol* **17**, 626-635, doi:10.1038/ni.3443 (2016).

328 Braciale, T. J. & Hahn, Y. S. Immunity to viruses. *Immunol Rev* **255**, 5-12, doi:10.1111/imr.12109 (2013).

329 Heath, W. R. & Carbone, F. R. Dendritic cell subsets in primary and secondary T cell responses at body surfaces. *Nat Immunol* **10**, 1237-1244, doi:10.1038/ni.1822 (2009).

330 Helft, J. *et al.* Cross-presenting CD103+ dendritic cells are protected from influenza virus infection. *The Journal of clinical investigation* **122**, 4037-4047 (2012).

331 Ingulli, E., Funatake, C., Jacovetty, E. L. & Zanetti, M. Cutting edge: antigen presentation to CD8 T cells after influenza A virus infection. *J Immunol* **182**, 29-33 (2009).

332 Waithman, J. *et al.* Resident CD8(+) and migratory CD103(+) dendritic cells control CD8 T cell immunity during acute influenza infection. *PloS one* **8**, e66136, doi:10.1371/journal.pone.0066136 (2013).

333 Hildner, K. *et al.* Batf3 deficiency reveals a critical role for CD8alpha+ dendritic cells in cytotoxic T cell immunity. *Science* **322**, 1097-1100, doi:10.1126/science.1164206 (2008).

334 GeurtsvanKessel, C. H. *et al.* Clearance of influenza virus from the lung depends on migratory langerin+CD11b- but not plasmacytoid dendritic cells. *J Exp Med* **205**, 1621-1634, doi:10.1084/jem.20071365 (2008).

335 Yoneyama, H. *et al.* Plasmacytoid DCs help lymph node DCs to induce anti-HSV CTLs. *J Exp Med* **202**, 425-435, doi:10.1084/jem.20041961 (2005).

336 Cerutti, A., Qiao, X. & He, B. Plasmacytoid dendritic cells and the regulation of immunoglobulin heavy chain class switching. *Immunology and cell biology* **83**, 554-562, doi:10.1111/j.1440-1711.2005.01389.x (2005).

337 Hamid, M. A., Jackson, R. J., Roy, S., Khanna, M. & Ranasinghe, C. Unexpected involvement of IL-13 signalling via a STAT6 independent mechanism during murine IgG2a development following viral vaccination. *Eur J Immunol* (2018).

338 Li, Z., Jackson, R. J. & Ranasinghe, C. Vaccination route can significantly alter the innate lymphoid cell subsets: A feedback between IL-13 and IFN-γ. *NPJ vaccines* (2018).

339 Huang, Y. *et al.* IL-25-responsive, lineage-negative KLRG1(hi) cells are multipotential 'inflammatory' type 2 innate lymphoid cells. *Nat Immunol* **16**, 161-169 (2015).

340 Huang, Y. *et al.* Inflammatory ILC2: An IL-25-activated circulating ILC population with a protective role during helminthic infection. *Journal of Immunology* **198** (2017).

341 Kim, B. S. *et al.* TSLP elicits IL-33-independent innate lymphoid cell responses to promote skin inflammation. *Sci Transl Med* **5**, 170ra116 (2013).

342 Bernink, J. H. *et al.* Interleukin-12 and -23 Control Plasticity of CD127(+) Group 1 and Group 3 Innate Lymphoid Cells in the Intestinal Lamina Propria. *Immunity* **43**, 146-160 (2015).

343 Gasteiger, G., Fan, X., Dikiy, S., Lee, S. Y. & Rudensky, A. Y. Tissue residency of innate lymphoid cells in lymphoid and nonlymphoid organs. *Science* **350**, 981-985 (2015).

344 Tan, H. X. *et al.* Recombinant influenza virus expressing HIV-1 p24 capsid protein induces mucosal HIV-specific CD8 T-cell responses. *Vaccine* **34**, 1172-1179 (2016).

345 Belyakov, I. M. & Ahlers, J. D. Comment on "trafficking of antigen-specific CD8+ T lymphocytes to mucosal surfaces following intramuscular vaccination". *J Immunol* **182**, 1779; author reply 1779-1780 (2009).

346 Belyakov, I. M., Isakov, D., Zhu, Q., Dzutsev, A. & Berzofsky, J. A. A novel functional CTL avidity/activity compartmentalization to the site of mucosal immunization contributes to protection of macaques against simian/human immunodeficiency viral depletion of mucosal CD4+ T cells. *J Immunol* **178**, 7211-7221 (2007).

347 Newcomb, D. C. *et al.* Human TH17 cells express a functional IL-13 receptor and IL-13 attenuates IL-17A production. *The Journal of allergy and clinical immunology* **127**, 1006-1013 e1001-1004 (2011).

348 Ravichandran, J., Jackson, R. J., Trivedi, S. & Ranasinghe, C. IL-17A expression in HIV-specific CD8 T cells is regulated by IL-4/IL-13 following HIV-1 prime-boost immunization. *J Interferon Cytokine Res* **35**, 176-185 (2015).

349 Lee, J. *et al.* Adenovirus Serotype 5 Vaccination Results in Suboptimal CD4 T Helper 1 Responses in Mice. *J Virol* **91**, 01132-01116 (2017).

350 Provine, N. M. *et al.* Longitudinal requirement for CD4+ T cell help for adenovirus vector-elicited CD8+ T cell responses. *J Immunol* **192**, 5214-5225 (2014).

351 Yang, T. C. *et al.* On the role of CD4+ T cells in the CD8+ T-cell response elicited by recombinant adenovirus vaccines. *Mol Ther* **15**, 997-1006 (2007).

352 Ashok, D. *et al.* Cross-presenting dendritic cells are required for control of Leishmania major infection. *Eur J Immunol* **44**, 1422-1432, doi:10.1002/eji.201344242 (2014).

353 Jirmo, A. C., Nagel, C. H., Bohnen, C., Sodeik, B. & Behrens, G. M. Contribution of direct and cross-presentation to CTL immunity against herpes simplex virus 1. *J Immunol* **182**, 283-292, doi:10.4049/jimmunol.182.1.283 (2009).

354 Staib, C., Kisling, S., Erfle, V. & Sutter, G. Inactivation of the viral interleukin 1beta receptor improves CD8+ T-cell memory responses elicited upon immunization with modified vaccinia virus Ankara. *The Journal of general virology* **86**, 1997-2006, doi:10.1099/vir.0.80646-0 (2005).

355 Erbel, C. *et al.* IL-17A influences essential functions of the monocyte/macrophage lineage and is involved in advanced murine and human atherosclerosis. *J Immunol* **193**, 4344-4355, doi:10.4049/jimmunol.1400181 (2014).

356 Novick, D. *et al.* Interleukin-18 binding protein: a novel modulator of the Th1 cytokine response. *Immunity* **10**, 127-136 (1999).

357 Gordon, S. & Martinez, F. O. Alternative activation of macrophages: mechanism and functions. *Immunity* **32**, 593-604 (2010).

358 McCormick, S. M. & Heller, N. M. Commentary: IL-4 and IL-13 receptors and signaling. *Cytokine* **75**, 38-50 (2015).

359 Webb, D. C. *et al.* Integrated signals between IL-13, IL-4, and IL-5 regulate airways hyperreactivity. *J Immunol* **165**, 108-113 (2000).

360 Oeser, K., Maxeiner, J., Symowski, C., Stassen, M. & Voehringer, D. T cells are the critical source of IL-4/IL-13 in a mouse model of allergic asthma. *Allergy* **70**, 1440-1449 (2015).

361 Morse, M. A., Lyerly, H. K. & Li, Y. The role of IL-13 in the generation of dendritic cells in vitro. *J Immunother* **22**, 506-513 (1999).

362 Pope, S. M. *et al.* IL-13 induces eosinophil recruitment into the lung by an IL-5- and eotaxin-dependent mechanism. *The Journal of allergy and clinical immunology* **108**, 594-601 (2001).

363 Halim, T. Y. *et al.* Group 2 innate lymphoid cells are critical for the initiation of adaptive T helper 2 cell-mediated allergic lung inflammation. *Immunity* **40**, 425-435 (2014).

364 Zhu, Z. *et al.* Pulmonary expression of interleukin-13 causes inflammation, mucus hypersecretion, subepithelial fibrosis, physiologic abnormalities, and eotaxin production. *The Journal of clinical investigation* **103**, 779-788 (1999).

365 Dalessandri, T., Crawford, G., Hayes, M., Castro Seoane, R. & Strid, J. IL-13 from intraepithelial lymphocytes regulates tissue homeostasis and protects against carcinogenesis in the skin. *Nature communications* **7**, 12080 (2016).

366 Li, Z., Jackson, R. J. & Ranasinghe, C. Vaccination route can significantly alter the innate lymphoid cell subsets: a feedback between IL-13 and IFN-gamma. *NPJ Vaccines* **3**, 10 (2018).

367 Roy, S. *et al.* Viral vector and route of administration determine the ILC and DC profiles responsible for downstream vaccine-specific immune outcomes. *Vaccine* **37**, 1266-1276, doi:10.1016/j.vaccine.2019.01.045 (2019).

368 Amit, U. *et al.* New Role for Interleukin-13 Receptor alpha1 in Myocardial Homeostasis and Heart Failure. *J Am Heart Assoc* **6**, 005108 (2017).

369 Miloux, B. *et al.* Cloning of the human IL-13R alpha1 chain and reconstitution with the IL4R alpha of a functional IL-4/IL-13 receptor complex. *FEBS Lett* **401**, 163-166 (1997).

370 Fujisawa, T., Joshi, B., Nakajima, A. & Puri, R. K. A novel role of interleukin-13 receptor alpha2 in pancreatic cancer invasion and metastasis. *Cancer Res* **69**, 8678-8685 (2009).

371 Ford, J. G. *et al.* IL-13 and IFN-gamma: interactions in lung inflammation. *J Immunol* **167**, 1769-1777 (2001).

372 Schust, J., Sperl, B., Hollis, A., Mayer, T. U. & Berg, T. Stattic: a small-molecule inhibitor of STAT3 activation and dimerization. *Chem Biol* **13**, 1235-1242 (2006).

373 Wynn, T. A., Eltoum, I., Oswald, I. P., Cheever, A. W. & Sher, A. Endogenous interleukin 12 (IL-12) regulates granuloma formation induced by eggs of Schistosoma mansoni and exogenous IL-12 both inhibits and prophylactically immunizes against egg pathology. *J Exp Med* **179**, 1551-1561 (1994).

374 Wynn, T. A. *et al.* IL-12 exacerbates rather than suppresses T helper 2-dependent pathology in the absence of endogenous IFN-gamma. *J Immunol* **154**, 3999-4009 (1995).

375 Webb, D. C., Cai, Y., Matthaei, K. I. & Foster, P. S. Comparative roles of IL-4, IL-13, and IL-4Ralpha in dendritic cell maturation and CD4+ Th2 cell function. *J Immunol* **178**, 219-227 (2007).

376 Badalyan, V. *et al.* TNF-alpha/IL-17 synergy inhibits IL-13 bioactivity via IL-13Ralpha2 induction. *The Journal of allergy and clinical immunology* **134**, 975-978 e975 (2014).

377 Chandriani, S. *et al.* Endogenously expressed IL-13Ralpha2 attenuates IL-13-mediated responses but does not activate signaling in human lung fibroblasts. *J Immunol* **193**, 111-119 (2014).

378 Donaldson, D. D. *et al.* The murine IL-13 receptor alpha 2: molecular cloning, characterization, and comparison with murine IL-13 receptor alpha 1. *J Immunol* **161**, 2317-2324 (1998).

379 Greenbaum, D., Colangelo, C., Williams, K. & Gerstein, M. Comparing protein abundance and mRNA expression levels on a genomic scale. *Genome biology* **4**, 117, doi:10.1186/gb-2003-4-9-117 (2003).

380 Moritz, C. P., Muhlhaus, T., Tenzer, S., Schulenborg, T. & Friauf, E. Poor transcript-protein correlation in the brain: negatively correlating gene products reveal neuronal polarity as a potential cause. *Journal of neurochemistry* **149**, 582-604, doi:10.1111/jnc.14664 (2019).

381 Shebl, F. M. *et al.* Comparison of mRNA and protein measures of cytokines following vaccination with human papillomavirus-16 L1 virus-like particles. *Cancer epidemiology, biomarkers & prevention : a publication of the American Association for Cancer Research, cosponsored by the American Society of Preventive Oncology* **19**, 978-981, doi:10.1158/1055-9965.epi-10-0064 (2010).

382 Moss Bendtsen, K., Jensen, M. H., Krishna, S. & Semsey, S. The role of mRNA and protein stability in the function of coupled positive and negative feedback systems in eukaryotic cells. *Sci Rep* **5**, 13910 (2015).

383 Shao, W. *et al.* Comparative analysis of mRNA and protein degradation in prostate tissues indicates high stability of proteins. *Nature communications* **10**, 2524, doi:10.1038/s41467-019-10513-5 (2019).

384 Wu, X. & Brewer, G. The regulation of mRNA stability in mammalian cells: 2.0. *Gene* **500**, 10-21 (2012).

385 Tabata, Y. *et al.* Allergy-driven alternative splicing of IL-13 receptor alpha2 yields distinct membrane and soluble forms. *J Immunol* **177**, 7905-7912, doi:10.4049/jimmunol.177.11.7905 (2006).

386 Wu, A. H. & Low, W. C. Molecular cloning and identification of the human interleukin 13 alpha 2 receptor (IL-13Ra2) promoter. *Neuro-oncology* **5**, 179-187, doi:10.1215/s1152851702000510 (2003).

387 Acacia de Sa Pinheiro, A. *et al.* IL-4 induces a wide-spectrum intracellular signaling cascade in CD8+ T cells. *J Leukoc Biol* **81**, 1102-1110 (2007).

388 Andrews, A. L. *et al.* The association of the cytoplasmic domains of interleukin 4 receptor alpha and interleukin 13 receptor alpha 2 regulates interleukin 4 signaling. *Mol Biosyst* **9**, 3009-3014 (2013).

389 Heath, V. L., Murphy, E. E., Crain, C., Tomlinson, M. G. & O'Garra, A. TGF-beta1 down-regulates Th2 development and results in decreased IL-4-induced STAT6 activation and GATA-3 expression. *Eur J Immunol* **30**, 2639-2649 (2000).

390 Roy, S. *et al.* Viral vector and route of administration determine the ILC and DC profiles responsible for downstream vaccine-specific immune outcomes. *Vaccine* (submitted).

391 Cao, H. *et al.* IL-13/STAT6 signaling plays a critical role in the epithelial-mesenchymal transition of colorectal cancer cells. *Oncotarget* **7**, 61183-61198 (2016).

392 Huang, Z., Xin, J., Coleman, J. & Huang, H. IFN-gamma suppresses STAT6 phosphorylation by inhibiting its recruitment to the IL-4 receptor. *J Immunol* **174**, 1332-1337 (2005).

393 Qing, Y. & Stark, G. R. Alternative activation of STAT1 and STAT3 in response to interferon-gamma. *J Biol Chem* **279**, 41679-41685 (2004).

394 Tang, L. Y. *et al.* Transforming Growth Factor-beta (TGF-beta) Directly Activates the JAK1-STAT3 Axis to Induce Hepatic Fibrosis in Coordination with the SMAD Pathway. *J Biol Chem* **292**, 4302-4312 (2017).

395 Ching, C. B. *et al.* Interleukin-6/Stat3 signaling has an essential role in the host antimicrobial response to urinary tract infection. *Kidney Int* **93**, 1320-1329 (2018).

396 Ivashkiv, L. B. STAT activation during viral infection in vivo: where's the interferon? *Cell Host Microbe* **8**, 132-135 (2010).

397 Ansar, M., Komaravelli, N., Ivanciuc, T., Casola, A. & Garofalo, R. P. Detrimental role of type I interferon signaling in respiratory syncytial virus infection. *The Journal of Immunology* **200**, 60.66-60.66 (2018).

398 Kawakami, K., Kawakami, M., Snoy, P. J., Husain, S. R. & Puri, R. K. In vivo overexpression of IL-13 receptor alpha2 chain inhibits tumorigenicity of human breast and pancreatic tumors in immunodeficient mice. *J Exp Med* **194**, 1743-1754, doi:10.1084/jem.194.12.1743 (2001).

399 Kawakami, K., Taguchi, J., Murata, T. & Puri, R. K. The interleukin-13 receptor alpha2 chain: an essential component for binding and internalization but not for interleukin-13-induced signal transduction through the STAT6 pathway. *Blood* **97**, 2673-2679 (2001).

400 Le Bon, A. *et al.* Type i interferons potently enhance humoral immunity and can promote isotype switching by stimulating dendritic cells in vivo. *Immunity* **14**, 461-470 (2001).

401 Rahaman, S. O. *et al.* IL-13R(alpha)2, a decoy receptor for IL-13 acts as an inhibitor of IL-4-dependent signal transduction in glioblastoma cells. *Cancer Res* **62**, 1103-1109 (2002).

402 Herrick, C. A., Xu, L., McKenzie, A. N., Tigelaar, R. E. & Bottomly, K. IL-13 is necessary, not simply sufficient, for epicutaneously induced Th2 responses to soluble protein antigen. *J Immunol* **170**, 2488-2495 (2003).

403 Davies, D. H. *et al.* Vaccinia virus H3L envelope protein is a major target of neutralizing antibodies in humans and elicits protection against lethal challenge in mice. *J Virol* **79**, 11724-11733, doi:10.1128/jvi.79.18.11724-11733.2005 (2005).

404 Graham, B. S. *et al.* Determinants of antibody response after recombinant gp160 boosting in vaccinia-naive volunteers primed with gp160-recombinant vaccinia virus. The National Institute of Allergy and Infectious Diseases AIDS Vaccine Clinical Trials Network. *J Infect Dis* **170**, 782-786 (1994).

405 He, Y. *et al.* Antibodies to the A27 protein of vaccinia virus neutralize and protect against infection but represent a minor component of Dryvax vaccine--induced immunity. *J Infect Dis* **196**, 1026-1032, doi:10.1086/520936 (2007).

406 Fouda, G. G. *et al.* Mucosal immunization of lactating female rhesus monkeys with a transmitted/founder HIV-1 envelope induces strong Env-specific IgA antibody responses in breast milk. *J Virol* **87**, 6986-6999 (2013).

407 Gomez, C. E., Perdiguero, B., Sanchez-Corzo, C., Sorzano, C. O. S. & Esteban, M. Immune Modulation of NYVAC-Based HIV Vaccines by Combined Deletion of Viral Genes that Act on Several Signalling Pathways. *Viruses* **10** (2017).

408 Munier, C. M. L. *et al.* The primary immune response to Vaccinia virus vaccination includes cells with a distinct cytotoxic effector CD4 T-cell phenotype. *Vaccine* **34**, 5251-5261 (2016).

409 Precopio, M. L. *et al.* Immunization with vaccinia virus induces polyfunctional and phenotypically distinctive CD8(+) T cell responses. *J Exp Med* **204**, 1405-1416 (2007).

410 McMichael, A. J. & Phillips, R. E. Escape of human immunodeficiency virus from immune control. *Annu Rev Immunol* **15**, 271-296 (1997).

411 Phillips, R. E. *et al.* Human immunodeficiency virus genetic variation that can escape cytotoxic T cell recognition. *Nature* **354**, 453-459 (1991).

412 Hemelaar, J. Implications of HIV diversity for the HIV-1 pandemic. *J Infect* **66**, 391-400 (2013).

413 Hemelaar, J., Gouws, E., Ghys, P. D. & Osmanov, S. Global trends in molecular epidemiology of HIV-1 during 2000-2007. *Aids* **25**, 679-689 (2011).

414 Kumar, R., Qureshi, H., Deshpande, S. & Bhattacharya, J. Broadly neutralizing antibodies in HIV-1 treatment and prevention. *Ther Adv Vaccines Immunother* **6**, 61-68 (2018).

415 Bailey, J. R. *et al.* Transmission of human immunodeficiency virus type 1 from a patient who developed AIDS to an elite suppressor. *J Virol* **82**, 7395-7410 (2008).

416 Blankson, J. N. *et al.* Isolation and characterization of replication-competent human immunodeficiency virus type 1 from a subset of elite suppressors. *J Virol* **81**, 2508-2518 (2007).

417 Buckheit, R. W., 3rd *et al.* Host factors dictate control of viral replication in two HIV-1 controller/chronic progressor transmission pairs. *Nature communications* **3**, 716 (2012).

418 Walker-Sperling, V. E. *et al.* Factors Associated With the Control of Viral Replication and Virologic Breakthrough in a Recently Infected HIV-1 Controller. *EBioMedicine* **16**, 141-149 (2017).

419 Perdiguero, B. *et al.* Deletion of the vaccinia virus gene A46R, encoding for an inhibitor of TLR signalling, is an effective approach to enhance the immunogenicity in mice of the HIV/AIDS vaccine candidate NYVAC-C. *PloS one* **8**, e74831, doi:10.1371/journal.pone.0074831 (2013).

420 Jego, G. *et al.* Plasmacytoid dendritic cells induce plasma cell differentiation through type I interferon and interleukin 6. *Immunity* **19**, 225-234 (2003).

421 Liao, H. *et al.* Protective Regulatory T Cell Immune Response Induced by Intranasal Immunization With the Live-Attenuated Pneumococcal Vaccine SPY1 via the Transforming Growth Factor-beta1-Smad2/3 Pathway. *Front Immunol* **9**, 1754, doi:10.3389/fimmu.2018.01754 (2018).

422 Wang, B. *et al.* Induction of TGF-beta1 and TGF-beta1-dependent predominant Th17 differentiation by group A streptococcal infection. *Proceedings of the National Academy of Sciences of the United States of America* **107**, 5937-5942, doi:10.1073/pnas.0904831107 (2010).

423 Barouch, D. H. *et al.* Protective efficacy of adenovirus/protein vaccines against SIV challenges in rhesus monkeys. *Science* **349**, 320-324, doi:10.1126/science.aab3886 (2015).

424 Corey, L. *et al.* Immune correlates of vaccine protection against HIV-1 acquisition. *Science translational medicine* **7**, 310rv317-310rv317 (2015).

425 Khalil, D. N., Smith, E. L., Brentjens, R. J. & Wolchok, J. D. The future of cancer treatment: immunomodulation, CARs and combination immunotherapy. *Nat Rev Clin Oncol* **13**, 394 (2016).

426 Lee, Y. S. *et al.* Enhanced antitumor effect of oncolytic adenovirus expressing interleukin-12 and B7-1 in an immunocompetent murine model. *Clinical cancer research : an official journal of the American Association for Cancer Research* **12**, 5859-5868 (2006).

427 Parker, J. N. *et al.* Enhanced inhibition of syngeneic murine tumors by combinatorial therapy with genetically engineered HSV-1 expressing CCL2 and IL-12. *Cancer Gene Ther* **12**, 359-368 (2005).

428 Li, Z., Jackson, R. J. & Ranasinghe, C. A hierarchical role of IL-25 in ILC development and function at the lung mucosae following viral-vector vaccination. *Vaccine X* **2**, 100035 (2019).

429 Li, H. S. *et al.* Bypassing STAT3-mediated inhibition of the transcriptional regulator ID2 improves the antitumor efficacy of dendritic cells. *Science signaling* **9**, ra94, doi:10.1126/scisignal.aaf3957 (2016).

430 Agrawal, T. *et al.* Protective or pathogenic immune response to genital chlamydial infection in women--a possible role of cytokine secretion profile of cervical mucosal cells. *Clinical immunology (Orlando, Fla.)* **130**, 347-354, doi:10.1016/j.clim.2008.10.004 (2009).

431 Flory, C. M., Hubbard, R. D. & Collins, F. M. Effects of in vivo T lymphocyte subset depletion on mycobacterial infections in mice. *J Leukoc Biol* **51**, 225-229, doi:10.1002/jlb.51.3.225 (1992).

432 Gupta, R., Vardhan, H., Srivastava, P., Salhan, S. & Mittal, A. Modulation of cytokines and transcription factors (T-Bet and GATA3) in CD4 enriched cervical cells of Chlamydia trachomatis infected fertile and infertile women upon stimulation with chlamydial inclusion membrane proteins B and C. *Reproductive biology and endocrinology : RB&E* **7**, 84, doi:10.1186/1477-7827-7-84 (2009).

433 Leveton, C. *et al.* T-cell-mediated protection of mice against virulent Mycobacterium tuberculosis. *Infection and immunity* **57**, 390-395 (1989).

434 Muller, I., Cobbold, S. P., Waldmann, H. & Kaufmann, S. H. Impaired resistance to Mycobacterium tuberculosis infection after selective in vivo

depletion of L3T4+ and Lyt-2+ T cells. *Infection and immunity* **55**, 2037-2041 (1987).

435 O'Garra, A. *et al.* The immune response in tuberculosis. *Annu Rev Immunol* **31**, 475-527, doi:10.1146/annurev-immunol-032712-095939 (2013).

436 Orme, I. M. Characteristics and specificity of acquired immunologic memory to Mycobacterium tuberculosis infection. *J Immunol* **140**, 3589-3593 (1988).

437 Backer, R., van Leeuwen, F., Kraal, G. & den Haan, J. M. CD8- dendritic cells preferentially cross-present Saccharomyces cerevisiae antigens. *Eur J Immunol* **38**, 370-380, doi:10.1002/eji.200737647 (2008).

438 Yrlid, U. & Wick, M. J. Antigen presentation capacity and cytokine production by murine splenic dendritic cell subsets upon Salmonella encounter. *J Immunol* **169**, 108-116, doi:10.4049/jimmunol.169.1.108 (2002).

439 Jaitin, D. A. *et al.* Massively parallel single-cell RNA-seq for marker-free decomposition of tissues into cell types. *Science* **343**, 776-779, doi:10.1126/science.1247651 (2014).

-

Chapter 3 Appendix

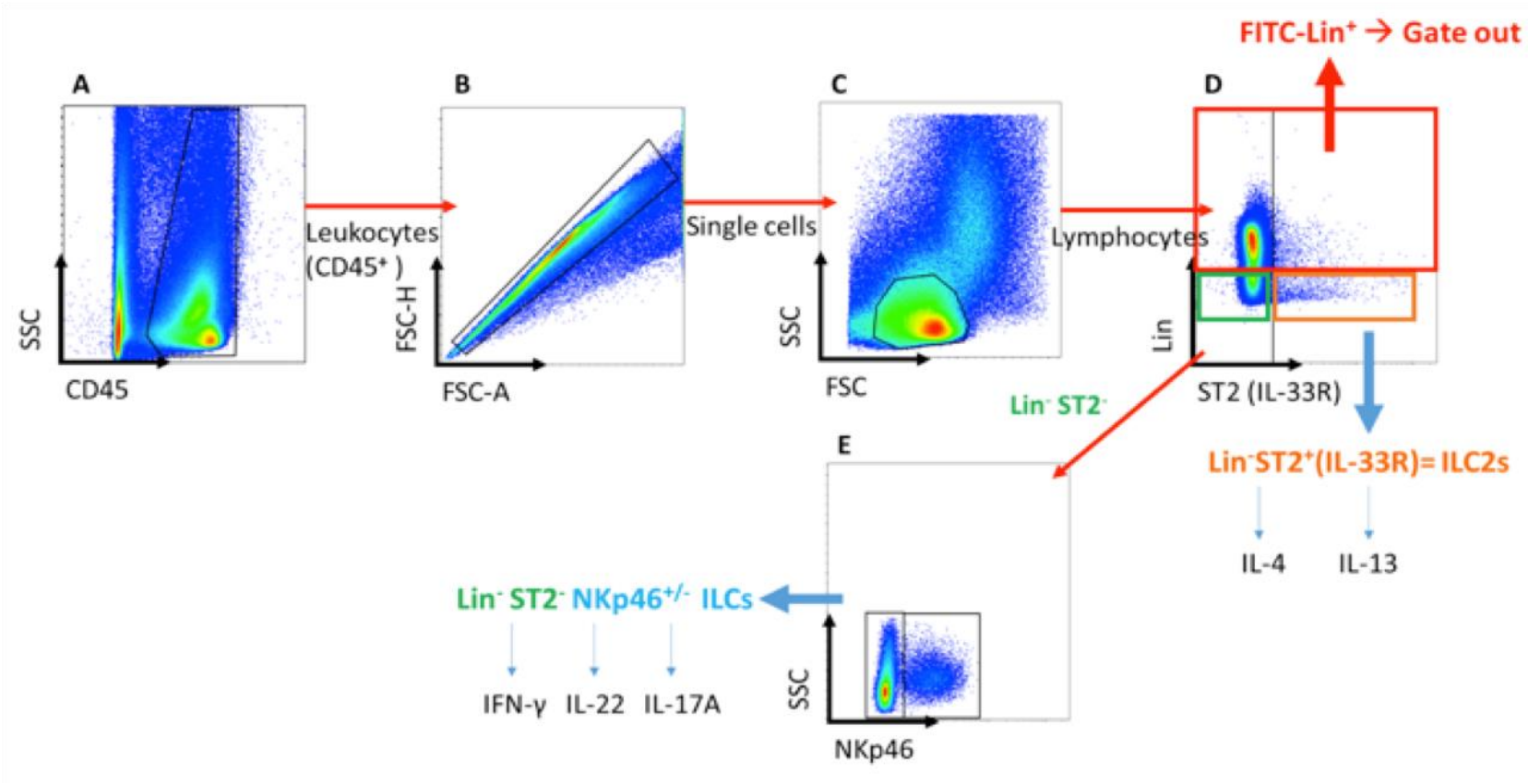
FITC-Lin⁺ → Gate out
A
B
C
D
SSC
CD45
Leukocytes
(CD45⁺)
FSC-H
FSC-A
Single cells
SSC
FSC
Lymphocytes
Lin
ST2 (IL-33R)
Lin⁻ ST2⁻
Lin⁻ST2⁺(IL-33R)= ILC2s
IL-4
IL-13
E
Lin⁻ ST2⁻ NKp46⁺/⁻ ILCs
IFN-γ
IL-22
IL-17A
SSC
NKp46

Chapter 3 Appendix Figure 1. Flow cytometry gating strategy of Lung ILC subsets. Lung ILCs from BALB/c mice were evaluated 24 hours post intranasal immunization with each viral vector based vaccine as per described in Methods. Firstly, from lung $CD45^+$ cells, lymphocytes were gated, following doublet discrimination. Next within the lymphocyte gate, lung ILC2 subset was identified as $lineage^-$ $ST2^+$/IL-$33R^+$ cells. $Lineage^-$ $ST2^-$ cells were further evaluated for NKp46 expression to analyse Lin^- $ST2^-$ $NKp46^+$ and Lin^- $ST2^-$ $NKp46^-$ cells (ILC1s and ILC3s). IL-13 expression was evaluated on ILC2s and IFN-γ, IL-17A and IL-22 expression was evaluated on ILC1s and ILC3s. Note that i) According to the micro environment/cell milieu, high plasticity of ILC1 and ILC3 has been observed and classifying ILC1 and ILC3 according to their cell surface marker expression has been a difficult task. Thus, in this viral vector-based vaccination study, for better clarity the ILC subsets (ILC1 and ILC3) were identified as $lineage^-$ $NKp46^+$ ILC and $lineage^-$ $NKp46^-$ ILC and assessed according to their cytokines production; ii) No granzyme B expression was detected on $lineage^-$ cells, unlike $lineage^+$ cells ($NKp46^+$ and $NKp46^-$), confirming the absence of NK cells in the $lineage^-$ subset and iii) None of the $lineage^+$ cells expressed IL-13 or IL-4, establishing that the ILC2 cells were not contaminated with any $lineage^+$ cells. These factors were clearly demonstrated in Li *et al.* 2018.

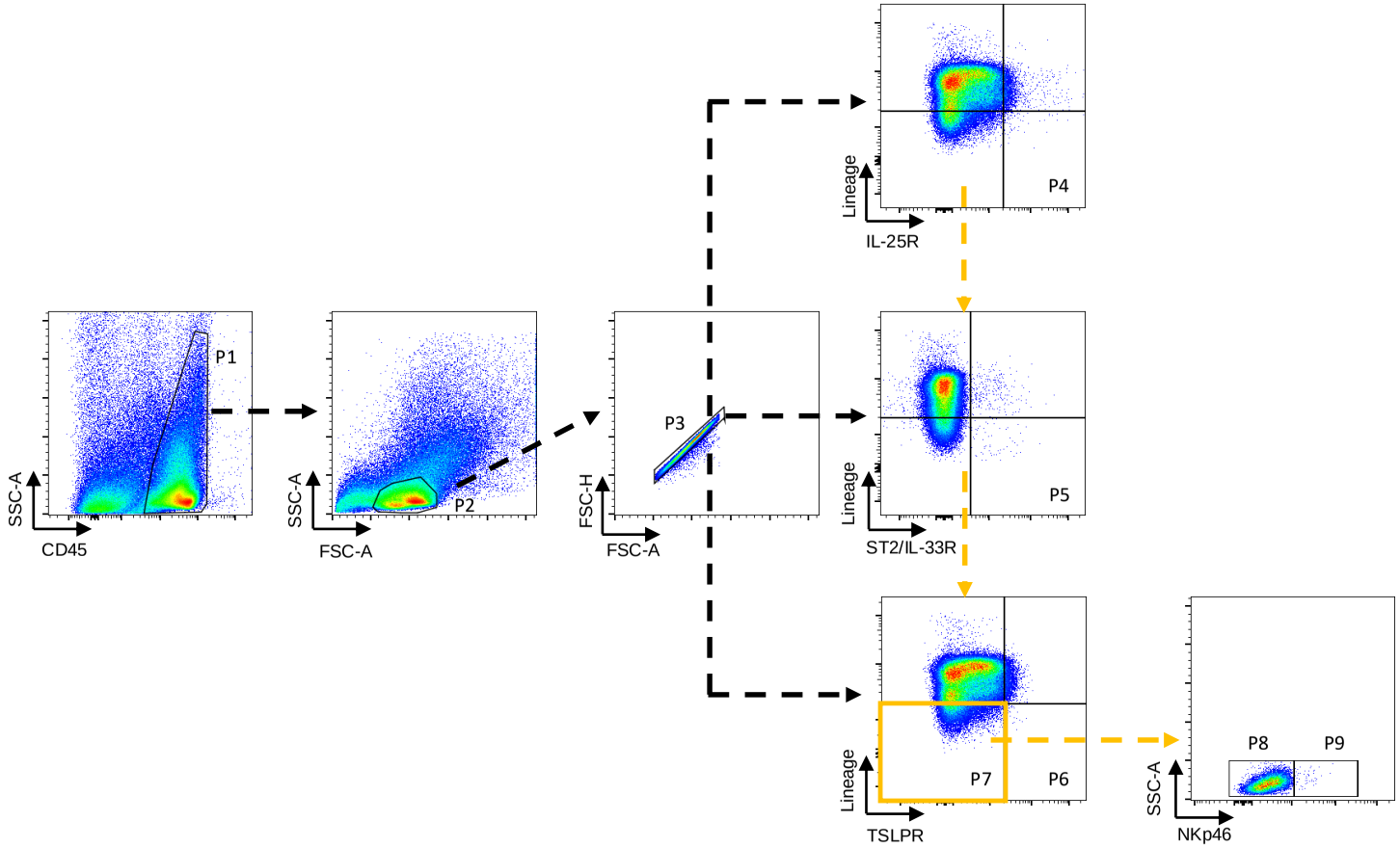
P1
SSC-A
CD45
P2
SSC-A
FSC-A
P3
FSC-H
FSC-A
P4
Lineage
IL-25R
P5
Lineage
ST2/IL-33R
P7
P6
Lineage
TSLPR
P8
P9
SSC-A
NKp46

Chapter 3 Appendix Figure 2. Flow cytometry gating strategy of muscle ILC subsets. Flow cytometry gating strategy used to evaluate ILC receptor subsets. Cells were pre-gated on $CD45^+$ leukocytes (P1), then FSC^{low} SSC^{low} lymphocytes (P2), followed by doublet discrimination (P3). Lin^- IL-$25R^+$ (P4), Lin^- $ST2^+$/IL-$33R^+$ (P5) and Lin^- $TSLPR^+$ (P6) were subsequently gated and analysed for IL-13 expression (indicated by the black arrows). Lin^- IL-$25R^-$ $ST2^-$/IL-$33R^-$ $TSLPR^-$ ILCs were also gated (P7); indicated by the yellow arrows and box) and IL-13 expression was assessed. $NKp46^-$ (P8) and $NKp46^+$ (P9) ILCs were gated from the Lin^- IL-$25R^-$ $ST2^-$/IL-$33R^-$ $TSLPR^-$ subset and IFN-γ and IL-17A expression was assessed.

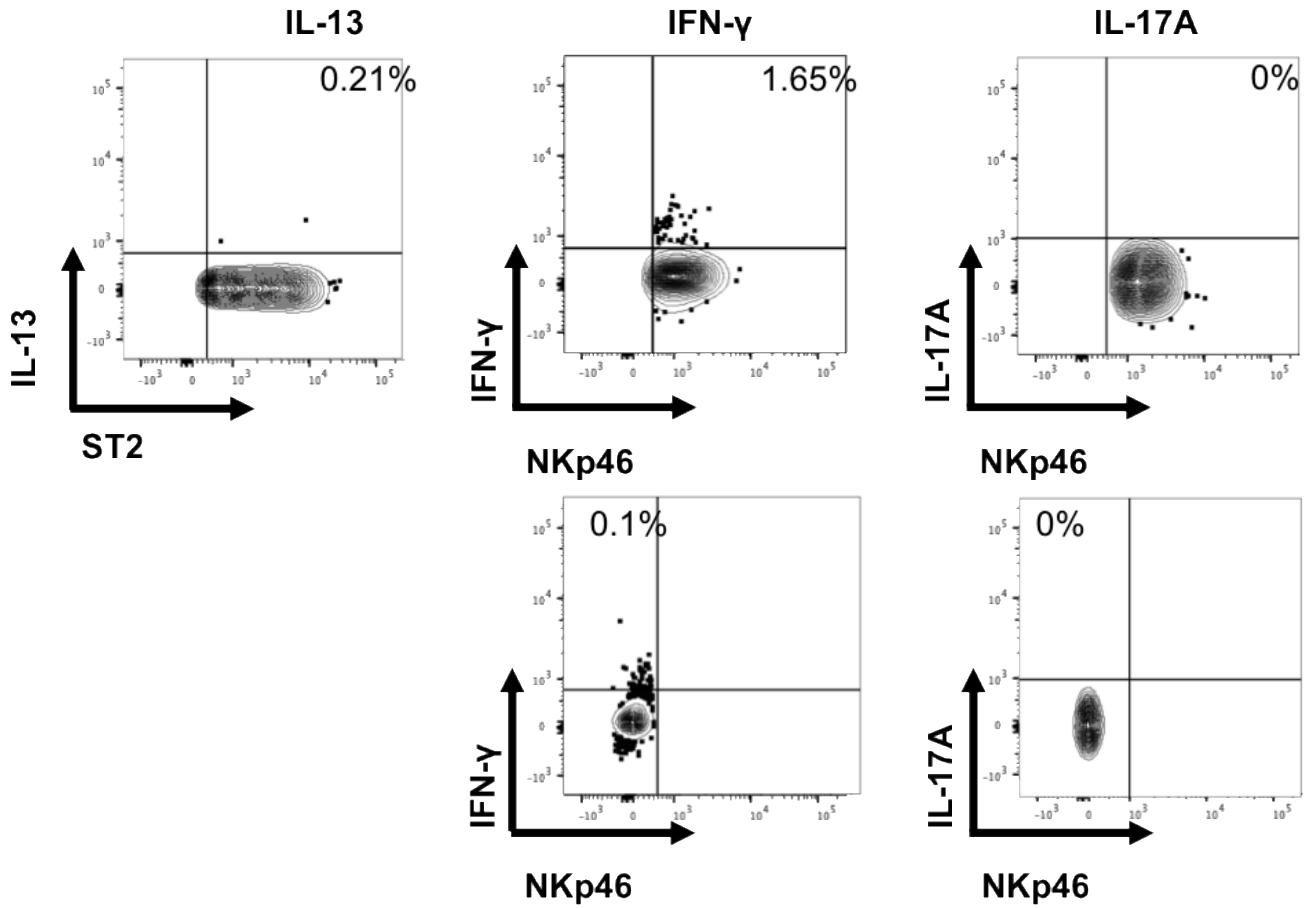
IL-13
IFN-γ
IL-17A
0.21%
1.65%
0%
IL-13
ST2
IFN-γ
NKp46
IL-17A
NKp46
0.1%
0%
IFN-γ
NKp46
IL-17A
NKp46

Chapter 3 Appendix Figure 3. Cytokine expression profiles in unimmunised lung ILCs. Lungs were harvested from unimmunized BALB/c mice and cytokine expressions were evaluated by flow cytometry as per in Methods. Lineage$^-$ ST2/IL-33R$^+$ cells were pre-gated to evaluate IL-13 expression. Lin$^-$ ST2$^-$ NKp46$^+$ and Lin$^-$ ST2$^-$ NKp46$^-$ ILC subsets were pre-gated for analysis of IFN-γ, IL-17A and IL-22 expression. Data from unimmunized control were utilised to assess the differences in cytokines expression at steady-state and following vaccination by each vector. Note that in this study, ILC subsets were measured both as percentage of parent population, as well as absolute numbers normalised to the CD45$^+$ subset as per in Li et al (submitted). Both ILC profiles were similar and hence in this study data were represented as percentage.

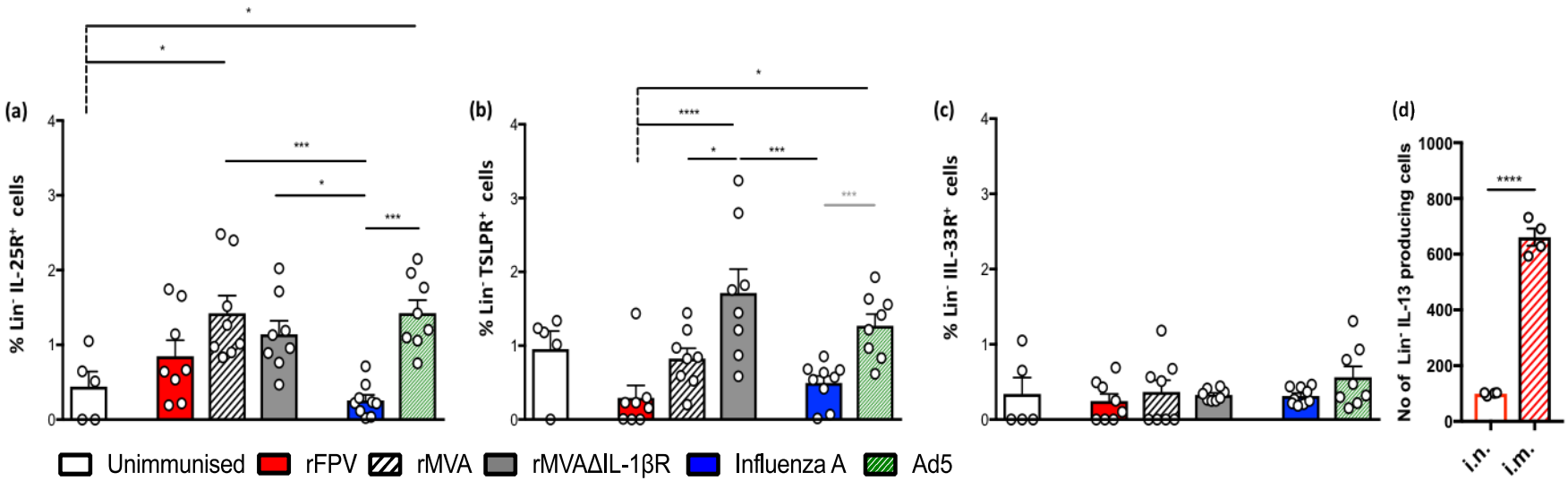
(a)
% Lin⁻ IL-25R⁺ cells
(b)
% Lin⁻ TSLPR⁺ cells
(c)
% Lin⁻ IIL-33R⁺ cells
(d)
No of Lin⁻ IL-13 producing cells
i.n.
i.m.
Unimmunised
rFPV
rMVA
rMVAΔIL-1βR
Influenza A
Ad5

Chapter 3 Appendix Figure 4. Evaluation of muscle ILC2 and corresponding IL-13 expression following intramuscular viral vaccination. BALB/c mice (n=5-9 per group) were i.m. immunised with rFPV, rMVA, rMVA-ΔIL-1βR, Influenza A, RV or Ad5. 24 h post vaccination single cell suspensions of muscles were stained for ILC2s and their IL-13 expression and analysed using flow cytometry as described in **Chapter 3 Appendix Figure 2**. ILC2 graphs show percentage of **(a)** IL-25R^{+} ILC2s, **(b)** TSLPR^{+} ILC2s and **(c)** ST2^{+}/IL-33R^{+} ILC2s in the muscle. To compare and contrast lung and muscle ILC2-derived IL-13, **(d)** bar graph represents IL-13 expression by Lin^{-} ST2/IL-33R^{+} ILC2 (i.n.) and Lin^{-} IL-25^{-} TSLPR^{-} ST2/IL-33R^{-} ILC2 (i.m.) following rFPV vaccination. Error bars represent Standard Error of mean (SEM) and p values were calculated using One-way ANOVA followed by Tukey's multiple comparison test (black lines) and paired student's t test (grey lines). *p<0.05, **p<0.01, ***p<0.001, ****p<0.0001. Experiments with each vector were repeated minimum 2-3 times.

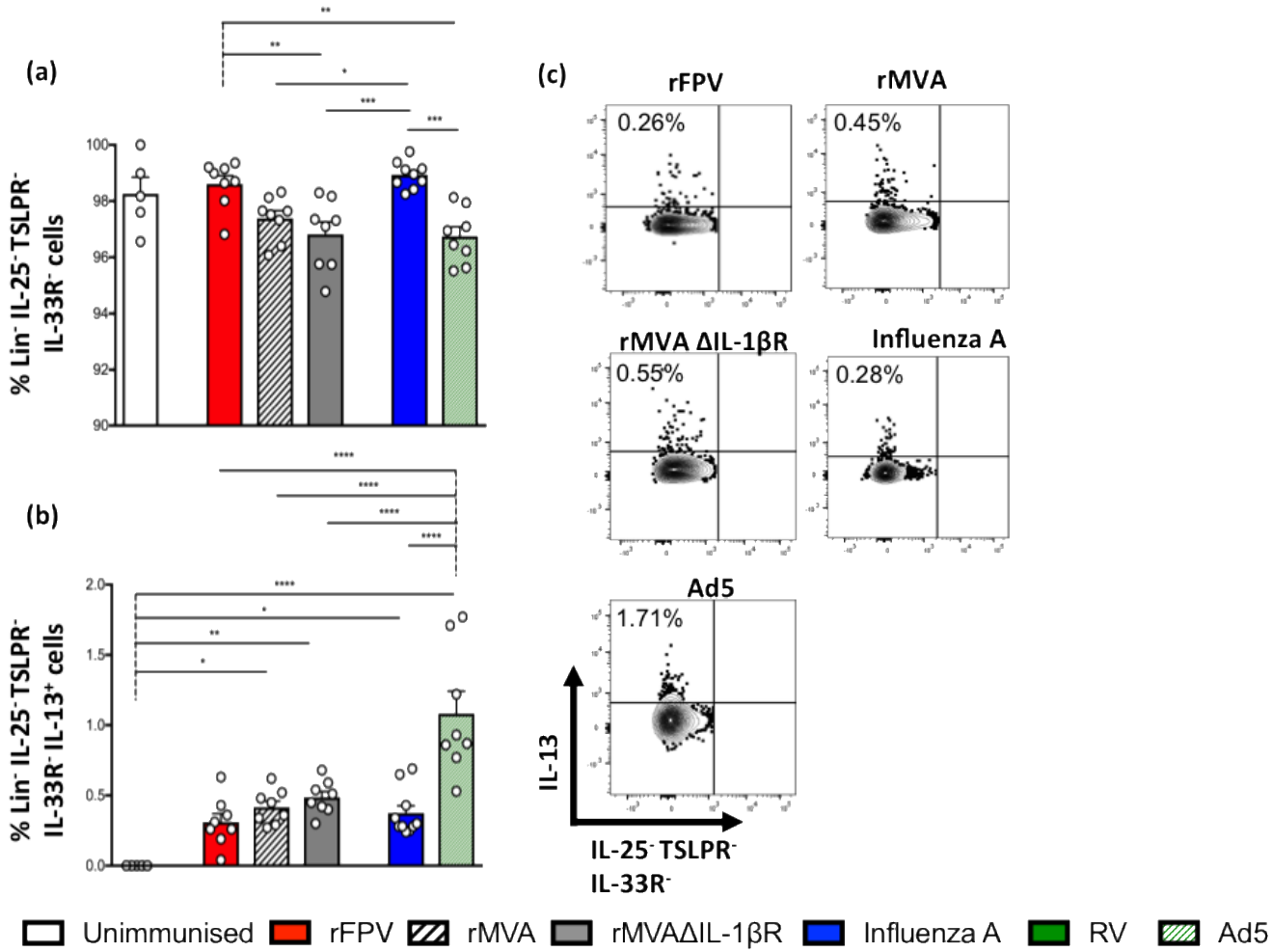
(a)
% Lin⁻ IL-25⁻ TSLPR⁻ IL-33R⁻ cells
100
98
96
94
92
90
(b)
% Lin⁻ IL-25⁻ TSLPR⁻ IL-33R⁻ IL-13⁺ cells
2.0
1.5
1.0
0.5
0.0
(c)
rFPV
0.26%
rMVA
0.45%
rMVA ΔIL-1βR
0.55%
Influenza A
0.28%
Ad5
1.71%
IL-13
IL-25⁻ TSLPR⁻ IL-33R⁻
Unimmunised
rFPV
rMVA
rMVAΔIL-1βR
Influenza A
RV
Ad5

Chapter 3 Appendix Figure 5. Evaluation of muscle ILC2 and corresponding IL-13 expression following intramuscular viral vaccination. BALB/c mice (n=5-9 per group) were i.m. immunised with rFPV, rMVA, rMVA-ΔIL-1βR, Influenza A, RV or Ad5. 24 h post vaccination muscles were harvested and single cell suspensions were stained for ILC2s and their IL-13 expression and analysed using flow cytometry. Cells were pre-gated on $CD45^{+}$ FSC^{low} SSC^{low} cells using FlowJo software as described in Materials and Methods and **Chapter 3 Appendix Figure 2**. Bar graphs show percentage of **(a)** Lin^{-} IL-25R^{-} TSLPR^{-} ST2/IL-33R^{-} ILC2 and **(b)** IL-13 expression by this novel ILC2 subset. **(c)** Representative FACS plots show percentage of Lin^{-} IL-25R^{-} TSLPR^{-} ST2^{-}/IL-33R^{-} ILC2 expressing IL-13. Error bars represent Standard Error of mean (SEM) and p values were calculated using One-way ANOVA followed by Tukey's multiple comparison test (black lines) and paired student's t test (grey lines). *p<0.05, **p<0.01, ***p<0.001, ****p<0.0001. Experiments with each vector were repeated minimum 2-3 times.

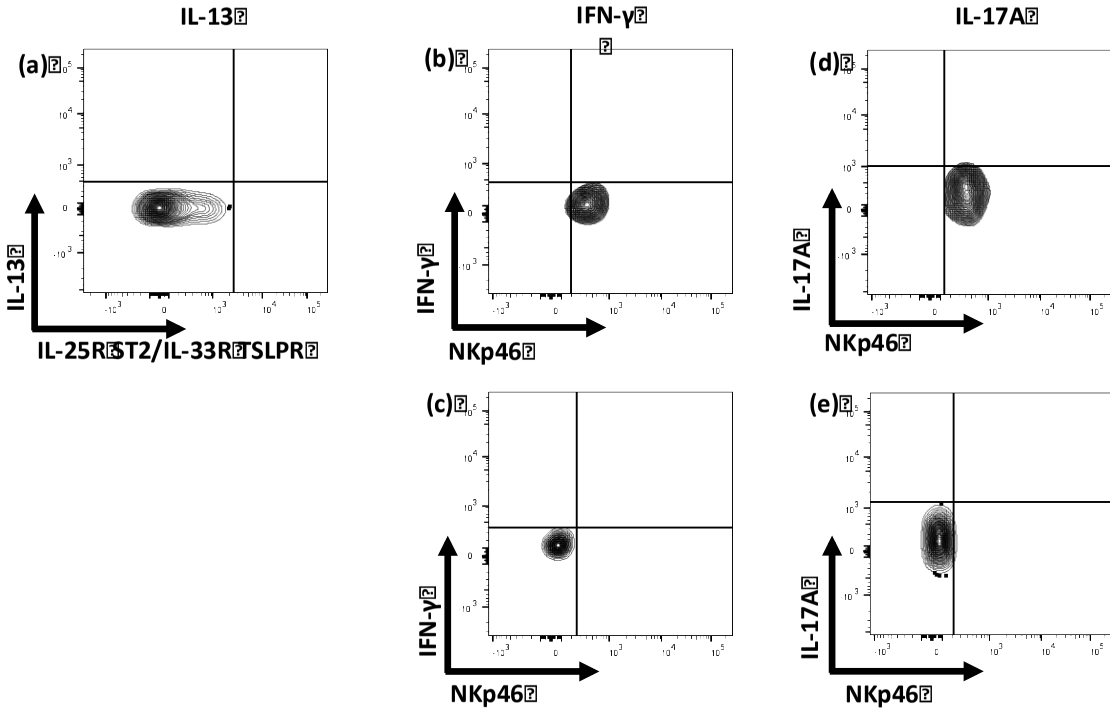

Chapter 3 Figure 6. Cytokine expression in unimmunised muscle ILCs. Muscles were harvested from unimmunised BALB/c mice, samples were processed and analysed using flow cytometry. IL-13 expression from the IL-25R$^-$ ST2/IL-33R$^-$ TSLPR$^-$ ILC2s **(a)**, IFN-γ expression from the NKp46$^+$ **(b)** and NKp46$^-$ **(c)** ILC1/ILC3s, and IL-17A expression from the NKp46$^+$ **(d)** and NKp46$^-$ **(e)** ILC1/ILC3s were evaluated.

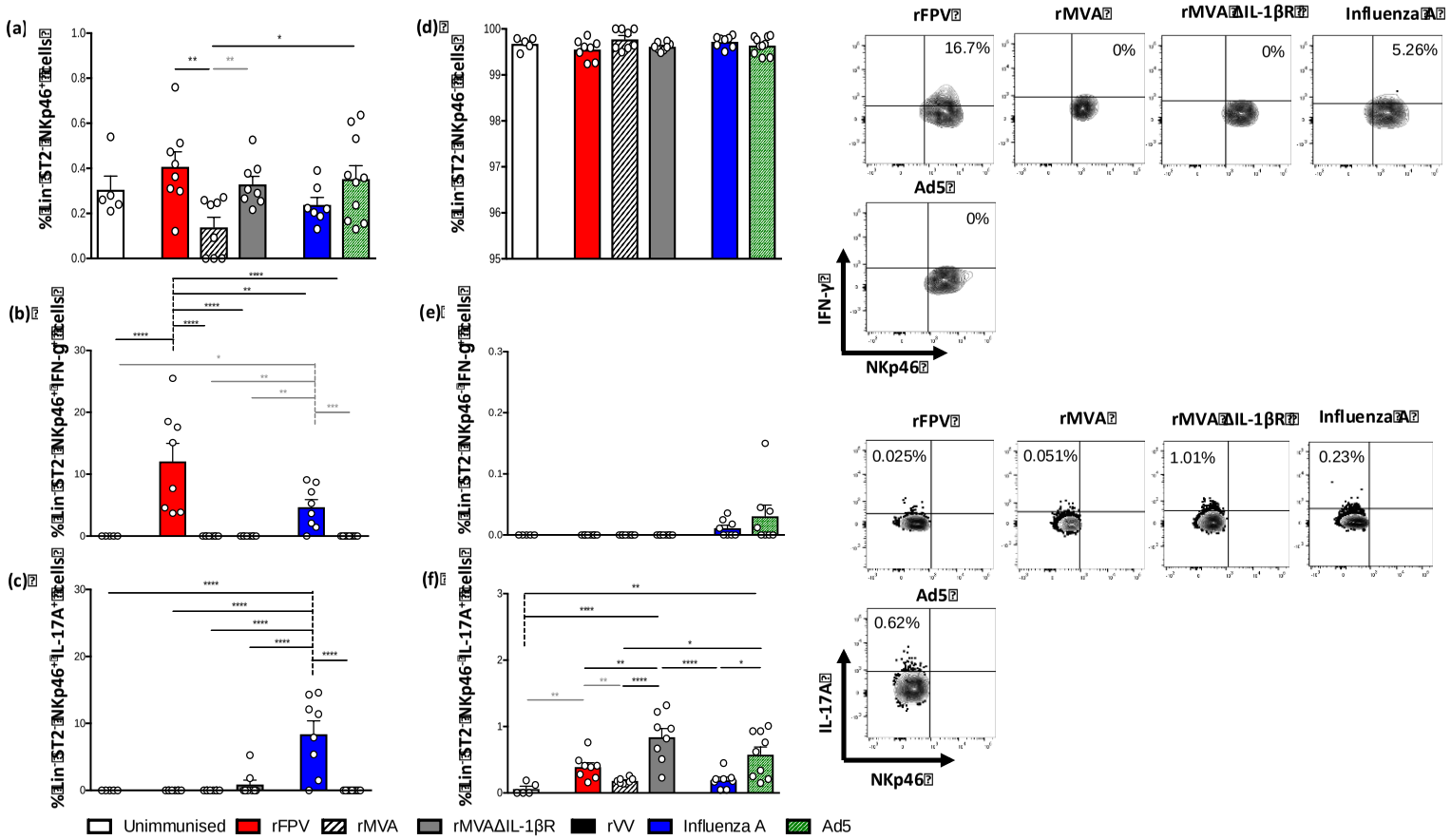
(a)
(b)
(c)
(d)
(e)
(f)
rFPV
rMVA
rMVAΔIL-1βR
Influenza A
Ad5
16.7%
0%
0%
5.26%
0%
0.025%
0.051%
1.01%
0.23%
0.62%
IFN-γ
IL-17A
NKp46
Unimmunised
rFPV
rMVA
rMVAΔIL-1βR
rVV
Influenza A
Ad5

Chapter 3 Appendix Figure 7. Evaluation of muscle Lin$^-$ ST2$^-$ NKp46$^+$ and NKp46$^-$ ILC-derived IFN-γ and IL-17A profiles post intramuscular viral vector vaccination. BALB/c mice (n=5-9) were i.m. immunised with rFPV, rMVA, rMVA-ΔIL-1βR, Influenza A or Ad5. 24h post vaccination muscles were harvested and cell suspensions were stained for Lin$^-$ ST2/IL-33R$^-$ NKp46$^+$ and NKp46$^-$ ILC and their cytokine expression. Cells were pre-gated on CD45$^+$ FSC^{low} SSC^{low} cells as described in Materials and Methods and **Chapter 3 Appendix Figure 2**. **(a)** Graphs show percentage of Lin$^-$ ST2/IL-33R$^-$ NKp46$^+$ ILCs and **(b)** corresponding IFN-γ and **(c)** IL-17A expression by theses cells, **(d)** percentage of Lin$^-$ ST2$^-$ NKp46$^-$ ILCs and **(e)** their corresponding IFN-γ and **(f)** IL-17A expression. Error bars represent SEM and *p* values were calculated using One-way ANOVA followed by Tukey's multiple comparison test (black lines) and paired student's t test (grey lines). **p*<0.05, ***p*<0.01, ***p<0.001, *****p*<0.0001. Representative FACS plots show IFN-γ and IL-17A expression by Lin$^-$ ST2/IL-33R$^-$ NKp46$^+$ (top) and NKp46$^-$ (bottom) ILC. Experiments for each group was repeated minimum 2-3 times.